METHODS FOR SYSTEMATIC PROCESS INTENSIFICATION

A Dissertation

by

SALIH EMRE DEMIREL

Submitted to the Office of Graduate and Professional Studies of
Texas A&M University
in partial fulfillment of the requirements for the degree of

DOCTOR OF PHILOSOPHY

Chair of Committee,	M. M. Faruque Hasan
Committee Members,	Mahmoud El-Halwagi
	Costas Kravaris
	A. Rashid Hasan
Head of Department,	Arul Jarayaman

August 2020

Major Subject: Chemical Engineering

ABSTRACT

Process intensification (PI) addresses the development of new equipment and processing techniques resulting in substantially smaller, cleaner, safer, and more energy-efficient technologies. It is a novel design concept suggesting an innovative outlook towards chemical processes. Incorporation of PI principles into the conceptual process design stage, where the initial layout of the plant is decided, can be beneficial not only in terms of economics, but it can also help to mitigate the industrial footprint on global warming and environmental pollution. However, identification of such intensified solutions at the conceptual design stage is a challenging task as there can be myriad of candidate process configurations. While optimization-based process synthesis approaches provide methodical tools for process design, they request pre-postulated superstructures with fixed connectivity and equipment types. This limits the scope for the discovery of unconventional design solutions. In this work, we present a new representation method for chemical processes based on building blocks which enables an optimization-based approach for systematic intensification of chemical processes. Building block-based representation does not require a priori postulation of equipment types and configurations and allows for a systematic representation, identification and generation of intensification alternatives at the equipment and flowsheet levels. The proposed approach not only identifies different intensified/traditional process equipment, but also automatically generates the corresponding flowsheet. Overall problem is formulated as a Mixed-Integer Nonlinear Optimization Problem (MINLP) where discrete variables are used in selection of the phenomena and enabling materials. Proposed superstructure representation is also generalized into a unified framework for solving different process synthesis and integration problems with a single superstructure eliminating the need for postulating new superstructures whenever a new problem is addressed. Several solution strategies are devised to address the solution of the MINLP model by exploiting the special structure of the representation. The capabilities of the proposed method are demonstrated through a wide range of examples.

DEDICATION

To my parents and sisters.

ACKNOWLEDGMENTS

I would like to express my sincere gratitude to Professor M. M. Faruque Hasan who introduced me to the process systems engineering, taught me the art and science of this exciting field, and constantly shared his wisdom and expertise with me. He always kept his door open for long hour discussions and impressed me with his "out-of-the-box" thinking. It was a privilege for me to work with him and I am deeply grateful for his support and encouragement during my Ph.D. study.

Besides my advisor, I would like to also express my sincere appreciations for the members of my thesis committee, Professor Mahmoud El-Halwagi, Professor Kostas Kravaris, and Professor A. Rashid Hasan, who devoted their valuable time to read and comment on my research proposal and thesis, spared time for answering my questions, provided insights and guidance, and motivated me to achieve more during the course of my study.

I would like to also thank the late Professor Christodoulos Floudas. Without his phone call during the admission process, I might not have joined Texas A&M University. I will always remember him with sincere gratitude and the deepest respect. I would like to offer my special thanks to Professor Stratos Pistikopoulos for his support during my study. Working with him on RAPID SYNOPSIS project provided me invaluable experience toward my future career and insights on the area of process systems engineering and process intensification. I am also particularly grateful for the assistance given by Professor Rafiqul Gani from PSE for SPEED who shared his wisdom and expertise on process intensification during his visits at Texas A&M University.

Last but not the least, I want to thank my dear parents, Ayşe and Cemal Demirel, who have always supported and encouraged me during my studies. Also, I thank my beloved sisters, Zeynep Merve Demirel and Elif Demirel who have been and will always be in my heart. I would like to also thank to my grandfather Selahattin Olcay and grandmother Semiha Olcay for their encouragement and praying during my studies. Without their moral support, it would be impossible to complete this work.

CONTRIBUTORS AND FUNDING SOURCES

Contributors

This work was supported by a dissertation committee consisting of Professor M. M. Faruque Hasan [advisor], Professor Mahmoud El-Halwagi and Professor Costas Kravaris of the Department of Chemical Engineering and Professor A. Rashid Hasan of the Department of Petroleum Engineering.

All the work conducted for the dissertation was completed by the student independently.

Funding Sources

Graduate study was supported by U.S. National Science Foundation (award number CBET-1606027), the American Chemical Society Petroleum Research Fund (ACS PRF 58764-DNI9), DOE RAPID Institute SYNOPSIS Project (DE-EE0007888-09-03), Texas A&M College of Engineering Graduate Teaching Fellowship and Texas A&M Energy Institute Fellowship.

TABLE OF CONTENTS

Page

LIST OF FIGURES

FIGURE Page

LIST OF TABLES

TABLE Page

1. INTRODUCTION*

Chemical industry has been one of the major contributors to the betterment of standard of living throughout the 20th century. Currently, more than 96% of manufactured products are linked to the chemical industrial production [1]. Increasing global population and urbanization are expected to soar the demand for chemical products. These projections emphasize the role of chemical industry for the future wellbeing of our modern society. However, with great power comes great responsibility and there exists many challenges before the chemical industry. As global warming reaches to critical levels and effects of environmental pollution becomes more pervasive, environmental sustainability considerations have become a major concern for the society. The chemical sector has the largest share in both oil and gas consumption. The overall demand of the industry constitutes 14% of the demand for oil and 8% of the natural gas [2]. For a long time, chemical process design activities has adopted the economic performance as the primary objective. Environmental regulations have been typically considered as a constraint while selecting the ultimate design. While new capital investments might be needed and existing plants need to be renovated to satisfy the increasing and shifting trends in the demand, these projects need to aim higher energy efficiency and reduced environmental footprint besides economics.

These economic and environmental objectives often exhibit significant trade-offs. During the conceptual design stage, these trade-offs can be addressed through multi-objective optimization [3, 4] considering sustainability metrics [5, 6], and/or incorporating explicit constraints for sustainability [7]. In the scope of optimization, this can be illustrated through optimal Pareto fronts, which describe the limits of the technology at hand. This is depicted by Pareto curve I in Fig-

*Parts of this chapter were adapted with permission from (S. E. Demirel, J. Li, and M. M. F. Hasan, "Systematic process intensification using building blocks," Computers & Chemical Engineering, vol. 105, pp. 2 - 38, 2017.) Copyright (2017) Elsevier, (S. E. Demirel, J. Li, and M. F. Hasan, "Systematic process intensification" Current Opinion in Chemical Engineering, vol. 22, pp. 108 - 113, 2019.) Copyright (2019) Elsevier, (Y. Tian, S. E. Demirel, , M. M. F. Hasan, and E. N. Pistikopoulos, "An overview of process systems engineering approaches for process intensification: State of the art," Chemical Engineering and Processing: Process Intensification, vol. 133, pp. 160 - 210, 2018.) Copyright (2018) Elsevier and (S. E. Demirel, J. Li and M. M. F. Hasan, "A general framework for process synthesis, integration, and intensification," Industrial & Engineering Chemistry Research," vol. 58, no. 15, pp. 5950 - 5967, 2019.) Copyright (2019) American Chemical Society.

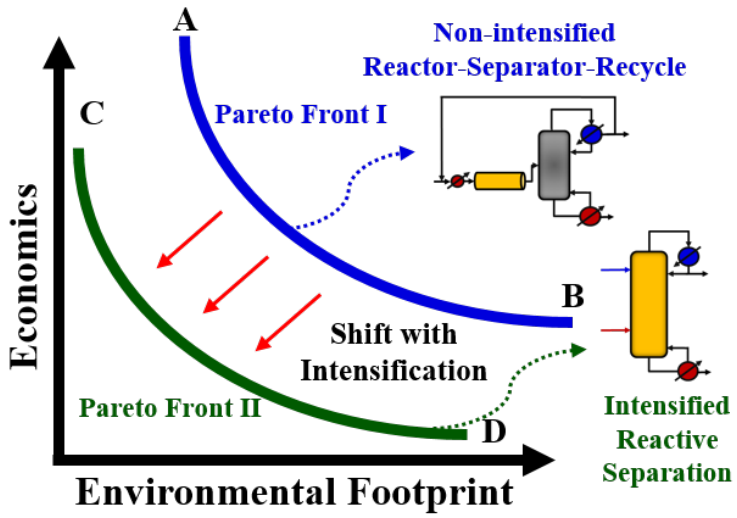

Figure 1.1: Effect of process intensification on the economics and sustainability. Process Intensification offers drastic improvements in process performance and can result in more environmental friendly and at the same time more economical designs.

ure 1.1. Here, Point A belongs to a process with minimal environmental footprint, yet it incurs a high cost burden. The design alternative shown in point B has the minimum cost, but it results in significantly larger environmental footprint. Traditional sustainable design methodologies strive for a 'middle ground' between the extreme points among pre-determined alternatives [8]. As long as our designs adhere to the same design principles, these trade-offs cannot be overcome. It is also possible that such solutions may not even exist within the traditional design search space and these trade-offs cannot be surpassed. Non-traditional and novel designs might be the only way to succeed and obtain both more economic and environmentally benign designs.

Furthermore, the time needed for developing new projects need to be reduced to facilitate a more robust production environment against drastic changes in the global supply chain. As the recent COVID-19 outbreak reveals, demand for certain chemicals might suddenly surge necessitating fast response for the changes in the societal needs. Navigating through these challenges require to adopt new design paradigms, implement innovative process solutions and develop systematic process design methodologies that can help to identify these innovations and decrease the

project durations. One attractive strategy towards countering these challenges is to utilize a rather new concept in chemical engineering: Process intensification (PI). PI is a novel design concept offering an innovative outlook towards chemical processes. It is defined as any design activity that secures substantial improvement in energy efficiency, processing volume, economics, environmental footprint, safety, etc. [9, 10, 11, 12, 13]. If the new design projects can adopt the principles of PI and the existing plants can be retrofitted with this innovative mindset, chemical industry can further extend its role in the welfare of our modern society.

This work aims to develop a systematic design methodology for process intensification through which this can be made possible. In what follows, first a brief introduction on the definition and principles of process intensification is provided. These PI principles are crucial in terms of developing a systematic framework towards PI as they provide hints for how to approach systematic process intensification problem. Then, a review on the existing works on the design and synthesis of chemical processes with a special focus on the PI systems is discussed. This is followed by a list of current research gaps and challenges which form the basis of this work.

1.1 Process Intensification

Process intensification has been introduced into the chemical engineering in the 1970s by the researchers in industrial laboratories of Imperial Chemical Industries' New Science Group. [9, 14]. It aimed "devising exceedingly compact plant which reduces both the main plant item and the installation costs." [15]. With defiance against the prevailing chemical engineering design paradigm, this meant larger plants are not necessarily better [16]. According to this early definition, PI is mainly focused on volume reduction and the benefit comes from the decrease in costs associated with the plant installation. However, with time, definition of PI has evolved to cover a wider range of activities. Stankiewicz and Moulijn, in their seminal paper published in 2000, defined PI as "... the development of innovative apparatuses and techniques that offer drastic improvements in chemical manufacturing and processing, substantially decreasing equipment volume, energy consumption, or waste formation, and ultimately leading to cheaper, safer, sustainable technologies" [9]. This provided the recognition of wider range of design activities within the realm of process

intensification, not only the ones resulting in drastic reduction in plant sizes. There are also more holistic perspectives towards PI activities. From an industrial point of view, Becht et al. further extended the scope of PI by defining it as "... an integrated approach for process and product innovation in chemical research and development, and chemical engineering in order to sustain profitability even in the presence of increasing uncertainties" which recognizes flexibility and robustness as also major PI outcomes [17]. Ponce-Ortega et al. (2012) realizes PI as an extension of process integration activities and emphasizes the importance of plant intensification over the unit intensification [18]. They defined the following design targets as PI: (i) smaller equipment size for a given throughput, (ii) higher throughput for a given equipment size or a given process, (iii) less holdup for equipment or less inventory for process of a certain material for the same throughput, (iv) less usage of utility materials and feedstock for a given throughput, and (v) higher performance for a given unit size [18].

These definitions are based on the evaluation criteria that we use to select the best candidate among alternatives. But how can we achieve these outcomes? According to Stankiewicz and Moulijn, PI as a practice-driven discipline aims the following principles [11]: i) Maximize the effectiveness of intermolecular and intramolecular events, ii) give each molecule the same processing experience, iii) optimize the driving forces, iv) maximize the synergistic effects of partial processes. These principles can be achieved through four different approaches operating within spatial, thermodynamic, functional and temporal domains. Spatial domain emphasizes the reducing the randomness in a process by using structured devices. Examples include using microchannels and monoliths for reactions. Thermodynamic domain relates to the optimal transfer of energy in an efficient form and through an optimal transfer mechanism. Use of microvawes for heating can be an example for PI within this domain. Functional domain emphasizes the combination of different operations so as to maximize the synergy in between. Reactive distillation equipment are the most prevalent examples of this form of intensification. Finally, in temporal domain, time is manipulated to either induce unsteady state conditions for a steady-state process or to control the duration of a process. One example of PI that operates in this domain is cyclic distillation

[14, 11]. Lutze et al. proposed a more practical set of principles for PI: i) integration of operations, ii) integration of functions, iii) integration of phenomena and/or iv) targeted enhancement of a phenomenon of a given operation [19]. This outlook toward PI introduces the concept of phenomena into process intensification. This is very crucial in terms of systematic design and screening of intensified alternatives as it will be described in the next section. Based on these principles, we can propose at least seven activities as a path for intensifying a process [13]. These are listed below with several examples:

1. combining multiple process tasks or equipment into a single unit (e.g., membrane reactors [20], sorption-enhanced reaction processes [21], reactive distillation [22, 23, 24, 25], dividing wall columns [26, 27, 28, 29], hybrid reactive and membrane assisted separations [30]),
2. discovery of novel multifunctional materials (e.g., ionic liquids, metal organic frameworks, zeolites) [31, 32],
3. tight process integration (i.e., material and/or energy integration) [18],
4. changing of operation modes (e.g., simulated moving bed reactors) [33],
5. miniaturization of process equipment (e.g., microreactors [34, 35]),
6. application of enhanced driving forces (e.g., rotating packed beds, ultrasonic mixing) [36],
7. advanced operational strategies (e.g., periodic operation, dynamic modes) [37, 38].

Several of these technologies are already adopted by the industry. A classic example of process intensification is the production of methyl acetate using task-integrated columns developed by researchers at Eastman Chemical Company [39, 40, 41]. In this task-integrated column, extractive and reactive distillation take place at separate regions of a single distillation column which results in five times lower energy requirements and capital expenditure when compared to the classical process in which reaction and separation tasks take place in isolated units [42]. There are several other successful industrial applications of reactive distillation technology for selective hydrogenation of mixed hydrocarbons, selective desulfurization of mid catalytic naphta, isomerization of

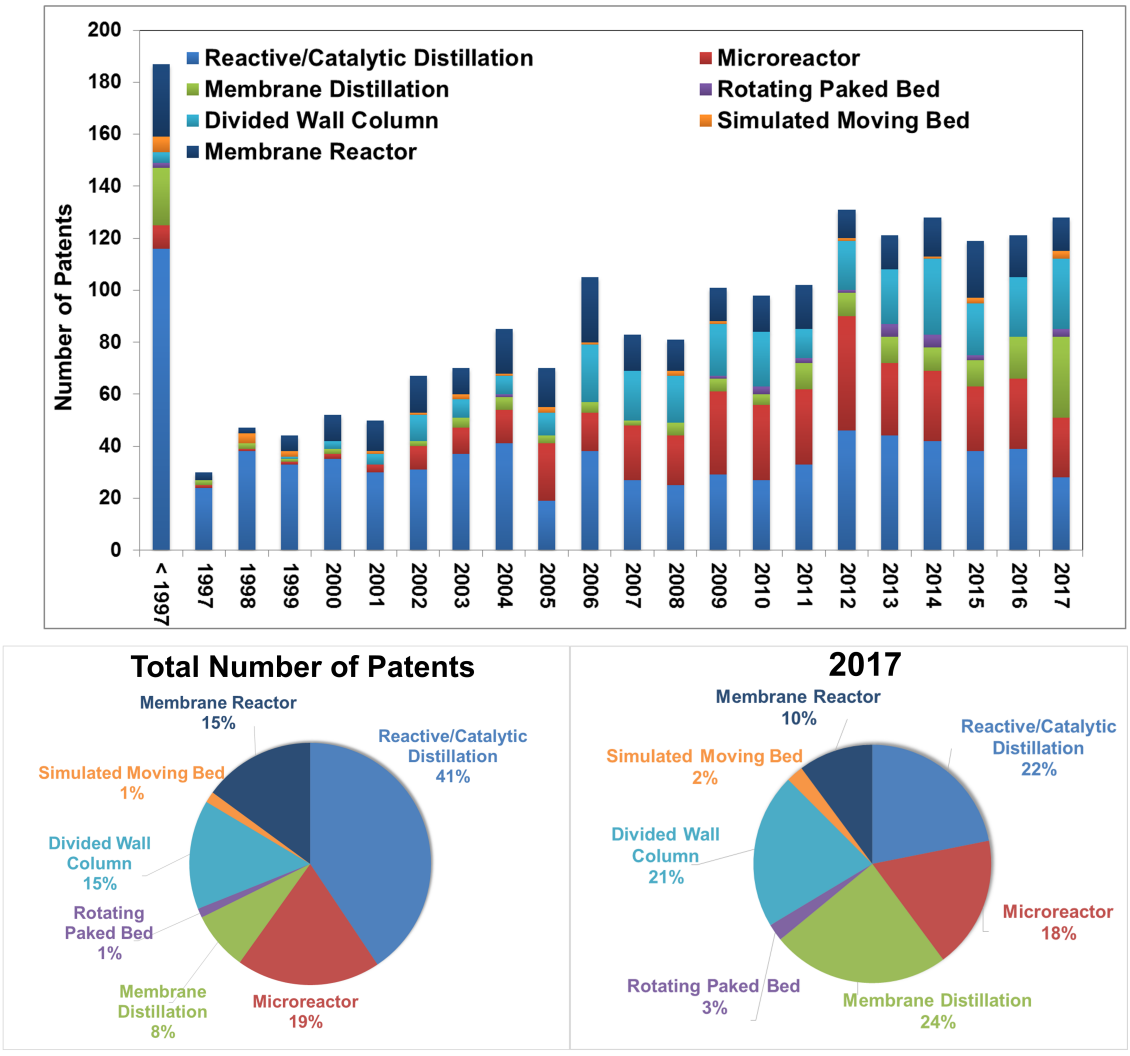

Figure 1.2: Patents granted on PI technologies. Number of patents granted on seven selected PI technologies until 2017 (top figure) (Adapted with permission from [13]). Distribution of each technology in the total number of patents (bottom left chart) and distribution of patents granted in 2017 (bottom right chart).

n-olefins to iso-olefins, etc. [25]. It is reported in 2007 that there are more than 150 reactive distillation columns operating in the industry. Dividing wall column (DWC) distillation is another intensified technology which has attracted significant attention. DWCs enable production of multiple products with high purity from a single distillation column which offer significant reduction in capital and energy costs. First reported industrial application of DWC was from BASF in 1985

[43]. After this, it is applied with an increased pace and more than 125 industrial installations are reported until 2011 by several companies including ExxonMobil and Chevron [44]. Other adopted technologies include static mixers (> 30 commercial models) [45] and reverse flow reactors (> 100 installations) [46, 13].

To investigate the interest toward different intensification technologies, we performed a patent search on seven indicative PI technologies [13]: reactive/catalytic distillation, membrane distillation, divided wall column, membrane reactor, microreactors, rotating packed beds and simulated moving beds. Search is conducted using Google Patents (updated on March 3rd, 2018) and the number of US, EP, and WO patents granted each year are shown in Figure 1.2. It is evident that the interest toward PI is increasing in a nearly constant pace judging from the total number of patents granted each year. The percentage of the patents on reactive distillation technology is by far the highest within the total number of patents granted until the end of 2017. Microreactors, membrane reactors and divided wall column are the other technologies that have high contribution. However, in recent years, interest toward membrane distillation technology seem to be increasing. In 2017, 24% of the total number of patents granted were on this technology. Combined with membrane reactors, they constitute more than one third of the patents granted in 2017. Similarly, although the patents on microreactors had a much smaller proportion in the earlier years, they seem to increase in a remarkable pace especially after 2005. This highlights the momentum towards the use of membrane-based and micro-processing technologies in the (bio)chemical processing industry.

There are several extensive reviews on the industrial applications of process intensification technologies. Harmsen reviews the industrial applications and currently available design tools for reactive distillation [42]. Yildirim et al. (2011) discusses different DWC configurations, industrial applications and control issues encountered in implementation of DWCs [44]. Powell (2017) gives an overview on intensification of multi-phase reactors and opportunities in methane conversion, biomass upgrading to fuels and carbon capture processes [47]. Richardson et al. (2012) discusses intensification of purification and conditioning processes for biomass-based syngas [48]. Pohar and Plazl (2009) give an overview on microreactor applications that has the potential to replace

existing technologies. Drioli et al. (2011) discusses several successful membrane-based process intensification technology applications and challenges toward wider application [49]. Recently, Tian et al. [13] also published a comprehensive review on PI technologies with industrial examples while also providing an extensive list of previous works on the modeling, simulation, synthesis and control of these PI technologies.

These PI technologies promise many benefits for developing sustainable chemical production schemes. However, identification of such intensified solutions at the conceptual design stage is a challenging task as there can be myriad of candidate process configurations. A wider application of PI in the chemical industry requires systematic tools that could suggest novel design alternatives at the early design stage [12]. Accordingly, systematic design methods that can be utilized for identifying these innovative solutions and help screening the most promising ones would be highly useful. In the next section, synthesis methods that were developed to this end are reviewed.

1.2 Process Intensification through Process Systems Engineering

Process design is more than of an art than science of obtaining process flowsheets that are capable of converting a set of feedstocks into a set of chemical products while meeting the product specifications in terms of both quality and quantity. Process systems engineering (PSE), as a separate discipline focused on process design and control, was coined in 1982 [50], around the same time with the process intensification. Since then, many achievements have taken place including development of process simulators, e.g. ASPEN Plus, gPROMS, and systematic methods for process synthesis and integration. With the recent advances in PI technologies, process intensification has also emerged as an important aspect of process design (Figure 1.3). With its systematic outlook, PSE tools have a lot to offer for process intensification and there have been significant efforts in the community to incorporate PI into the conceptual process design. These efforts are crucial in terms of reaping the full benefits of process intensification [10]. Here, we first provide an overview on the traditional process synthesis and integration methods and highlight their benefits and shortcomings in terms of process intensification. Then, we provide an overview on the PSE approaches for systematic process intensification.

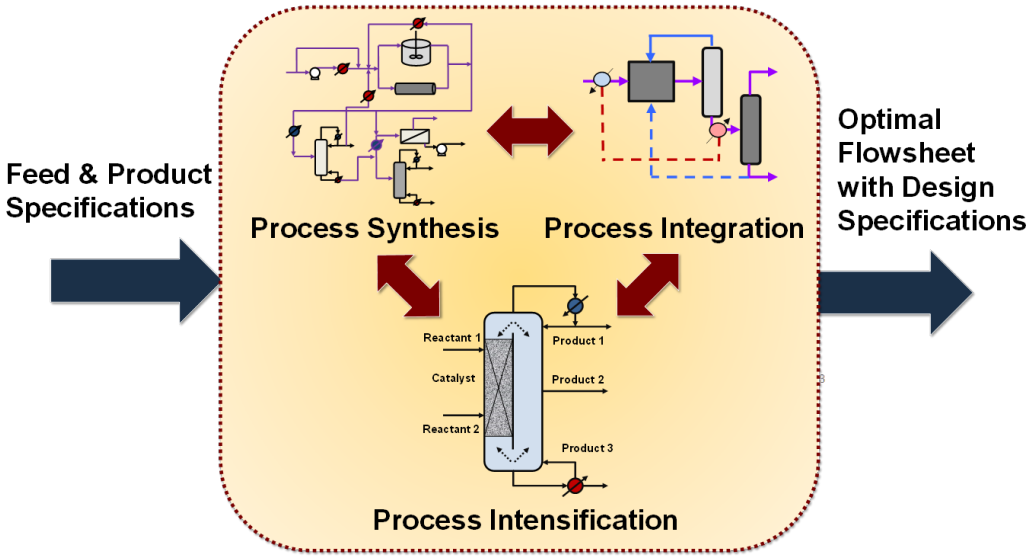

Figure 1.3: Conceptual process design methods for chemical processes. Process synthesis and integration are the pillars of conceptual process design. Incorporation of process intensification into conceptual process design is a recent development in process systems engineering (Reprinted with permission from [51]).

Process synthesis aims at screening flowsheet variants, equipment types, operating conditions and equipment connectivity under several design and operational constraints to come up with the optimal flowsheet structure and operating conditions. While early works on process synthesis utilized heuristics and hierarchical synthesis steps to generate flowsheet variants[52], superstructure optimization-based synthesis approaches gained more attention owing to their systematic nature and the ability to screen numerous process configurations [53].

Heuristics and hierarchical design methods decompose the problem into several decision steps and employ a set of rules to generate the flowsheet variants and decide on the final structure. Siirola and Rudd [54] proposed a methodology based on pure heuristics which is used in, for instance, separation sequence synthesis [55]. Later on, these heuristics are incorporated in a hierarchical framework in which rules are applied at different decision levels of the process design for the synthesis of whole flowsheet structures [56]. The hierarchical framework proposed by Douglas comprised of the following steps:

1. Batch vs. continuous,

2. Input - output structure of the flowsheet,

3. Recycle structure of the flowsheet,

4. Separation system synthesis,

5. Heat recovery network.

This method was demonstrated on hydrodealkylation of toluene example in great detail [57]. The onion model proposed by Smith [58, 59] is also based on hierarchical decision levels to generate complete flowsheets. According to this model, design starts with deciding on the reactors which dictate the structure of the separation system along with the necessary recycles. Heat exchange network design follows the design of separation systems. This level is followed by deciding on the external heating and cooling utilities (cooling water, refrigeration, furnace heating, etc.) for the process heating and cooling duties that cannot be satisfied within the process through heat recovery. Final step involves the decisions over the design of water and waste treatment networks. These early methods are based on unit operations concept and utilize short-cut models in deciding on the final flowsheet. While this can be useful for getting fast solutions, a critical shortcoming is that as the decisions are made in a sequential manner, the interactions between different decision levels are not accounted for. This leads to suboptimal process structures [52]. Several heuristic-based methodologies are also proposed to identify the process limitations and to incorporate process intensification alternatives into the search space [60]. Although merits of these methods in conceptual design should not be underestimated, including process intensification principles in hierarchical design procedures requires a high level of expertise on the problem at hand and generation of novel process solutions are limited to the known equipment types.

Optimization-based approaches are highly beneficial in terms of eliminating the disadvantages of heuristics and hierarchical approaches as they attempt to solve design problems by simultaneous consideration of design alternatives and their operating conditions. Superstructure-based process synthesis is comprised of three steps [53]:

1. Postulation of a superstructure that includes all the known alternatives,

2. Formulation of a mathematical programming model describing the superstructure,

3. Solution of the mathematical programming model with an optimization algorithm to decide on the optimal structure.

This provides a systematic approach for deciding on the optimal flowsheet structure among the known feasible alternatives. This approach has been applied to synthesis of several subsystems of chemical processes including heat recovery networks [61, 62], distillation network synthesis [63], reaction network synthesis [64, 65], etc. Total flowsheet synthesis and simultaneous synthesis of subnetworks along with the corresponding flowsheet have been also demonstrated for different applications. Examples include simultaneous heat exchanger network synthesis [66, 67], heat integrated distillation column networks [68], simultaneous heat, power and network synthesis [69] and total flowsheet synthesis for biomass to liquid transportation fuels [70] and ammonia production processes [7].

While these numerous applications of superstructure-based synthesis shows its utility, there exists several limitations [13, 71]. Representation method utilized in formulating the optimization problem is crucial as it determines the extent of the solution space. If a promising alternative is not included in the initial superstructure, it will not be suggested as a result of the problem solution. The solutions from superstructure-based methods are as good as the initial superstructure. Furthermore, the structure of the representation affects the solution quality. Same number of alternatives can be represented with different superstructures and the quality of the final solution might differ. Finally, the efficiency of the overall method in terms of its ability to be translated into computer algorithms is also crucial. Eventually, these methods are intended for obtaining systematic computer aided programs to guide process design activities. When a superstructure-based problem is solved, results suggest a vector of optimal variables which correspond to some structural and operational decisions. These need to be interpreted by the users (designers) to decide on the final design. The superstructure representation method affects how easy it is to visualize the final optimal results. These shortcomings are also valid when these approaches are utilized in process intensification.

Before proceeding with the applications for intensified systems, we first provide a review on the common superstructure-based representations.

Yeomans and Grossmann described two different representations based on three chemical process components (i.e., states, tasks, and equipment): State-Task-Network representation (STN) and State-Equipment-Network (SEN). In these representations, states were regarded as physico-chemical properties defining the streams, tasks were transformations between adjacent states (i.e., streams), and equipment were where tasks were carried out. In STN representation, task nodes were used to connect two different states while the equipment assignment was handled by the mathematical model. In SEN, on the other hand, states and equipment were defined while the assignment of tasks to equipment was determined via the model. Different implications of these representations in terms of modeling were also discussed [72] and also shown for distillation distillation column synthesis [73]. Friedler et al. [74] proposed Process graph (Pgraph) as a representation method with material and operation nodes connected with arcs representing connections between the nodes. Based on P-graph, a polynomial algorithm was devised for generating maximal superstructure [75]. Farkas et al. [76] proposed R-graph in which nodes constituted the input and output ports of the possible units. While the output port nodes were regarded as stream splitters input nodes were used as stream mixers, and connections from output to input nodes represented the process streams. They also investigated the structural multiplicity and redundancy in process network superstructures and proposed efficient MINLP and GDP models to tackle with these issues [76, 77]. Manousiouthakis and coworkers proposed a state-space representation that included a distribution network for mass and energy interconnections, and an operator network for equipment representations [78, 79]. Maravelias and coworkers proposed the unit-port conditioning stream (UPCS) framework for superstructure representation and developed connectivity rules to generate fully connected minimal superstructures with all feasible routes [80].

In terms of process intensification, when the intensified alternatives known beforehand, these common representations can be utilized for the synthesis of intensified systems. For instance, Mixed Integer Nonlinear Programming (MILNP)-type models are proposed for the synthesis of

equilibrium limited as well as kinetically controlled reactive distillation systems [81, 82]. These models and representations are used to decide on several design decisions including number of stages, reflux ratio, reaction volumes, feed locations. Several MINLP models are also proposed for the synthesis of dividing wall columns[28] and rotating packed beds [36].

Closely related with the process synthesis, process integration activities take a holistic approach and aim at reducing the consumption of resources by increasing the internal recycling and reuse of energy and materials [83, 84]. Process integration activities cover the following: (i) Task Identification: which refers the transformation of the design goals into actionable tasks, (ii) Targeting: which refers to the benchmarking activities that help set targets for the detailed design, (iii) Generation and selection of alternatives (Synthesis): which refers to the generation of process configurations with a rich-enough representation similar to process synthesis as described earlier, and (iv) Analysis of Selected Alternative(s): which includes using assessment tools to understand and determine the performance of process alternatives [85]. Pinch analysis and optimization-based methods are two common approaches for process integration [84]. There also exist hybrid approaches for process integration [86] as well as for process synthesis[87, 88] that combine hierarchical decision-making with mathematical optimization to enable efficient screening of alternatives at multiple stages. These methodologies strive for overcoming the challenges posed by the inherent combinatorial complexity in process design [89].

By judging from the traditional approaches for process synthesis and integration, we can summarize the relationship and scope of these methods along with the needs for process intensification as in Table 1.1. Traditional process synthesis activities operate at the equipment and flowsheet scales to find the optimal conditions and configurations. Process integration deals with plant-scale decisions, material/energy redistribution and utility networks. Process Intensification, on the other hand, seeks for enhancements at the fundamental physicochemical phenomena scale to generate novel equipment and flowsheet alternatives and seeks for multi-tasking units [91] (Figure 1.4). These differences in scales are also reflected in the mathematical models used in these methods. Process integration pivots around material and energy flows and source-sink connec-

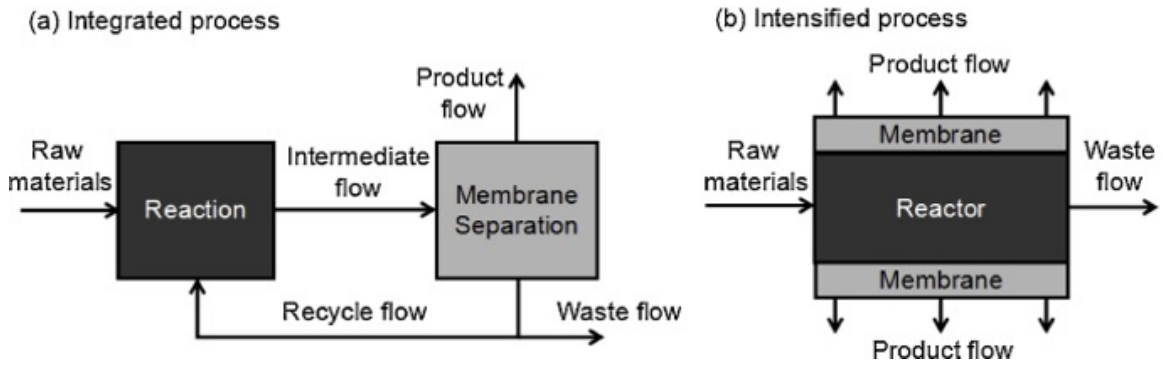

Figure 1.4: Process integration vs. process intensification. (a) Integrated reaction-separation process, b) Intensified process (using a membrane reactor as an example). Process intensification enables "multi-tasking" by combining reaction, separation and other operations in a single unit (Reprinted with permission from [90]).

tivity. These models are sometimes simplistic [92]. In traditional process synthesis, equipment sizing and connectivity can be fairly represented using short-cut methods[57, 80] and surrogate models[93, 94, 95]. Process intensification needs a more detailed description of physicochemical phenomena that are governed by the fundamental material/energy/momentum transport and thermodynamic constraints [10]. The aim of all these design activities, however, is to design energy efficient, sustainable and cost-effective chemical processes and the available methodologies can be utilized to create a symbiotic relationship among each other. Baldea[96], for instance, showed that intensification could be regarded as a limiting case of tight material integration. This relationship is also highlighted by Ponce-Ortega et al. [18] who suggested intensification at both the unit operations and the plant levels. Tight integration together with process synthesis can increase the sustainability and profitability, and in some cases, even lead to intensification through eliminating costly equipment, or utility streams [97, 98]. This signifies the importance of considering them in tandem at the early stage of a design activity. The challenge, however, lies in formulating a general method that can combine process synthesis, integration and intensification in a single framework capturing the different scales they operate.

This generalization, most crucially, requires a common representation method that is amenable to relate the fundamental process constituents (phenomena) with the equipment and flowsheet con-

Table 1.1: Aspects of process synthesis, integration and intensification (Adapted with permission from [51]).

	Process Synthesis	Process Integration	Process Intensification
Scale	Process equipment and flowsheet	Overall plant	Underlying phenomena, enabling materials
Focus	Flowsheet structure, equipment performance	Material and energy redistribution	Phenomena combination, enhancements
Emphasis	Equipment type and connectivity	Utility network connectivity	Phenomena, material type and connectivity
Models	High level, short-cut models	High level, short-cut models	Detailed models
Representation	Equipment network	Source-Sink network	Phenomena aggregations
Systematic Methods	Heuristic/ hierarchical, optimization-based	Pinch analysis, heuristics, optimization-based	Knowledge-based, optimization-based

figurations by capturing the synergies at different scales. One of the earliest works emphasizing this aspect came from Siirola [41], who proposed means-end analysis that is based on the elimination of property differences between the raw materials and the products through task-based operators. The methodology is able to systematically transform a traditional methyl acetate process with standalone reactor and separation columns into an intensified process that simultaneously performs reaction, extraction and distillation operations in a single task-integrated column.

There are several works that depart from unit operation-based representation of process alternatives and employ a set of processing tasks, phenomena, or functions to identify new designs [12, 19, 99, 100, 101, 102, 103, 104, 105]. Systematic efforts toward process intensification can be categorized based on their focus at different levels of the processes: plant, unit operation, functional (tasks) and phenomena levels [18, 19]. As design activities become less focused on unit operation and plant levels, which stand for the current process design approaches, and go deeper into task and phenomena levels, thinking becomes more fundamental and identification of intensification opportunities and novel process alternatives becomes possible (Figure 1.5). For instance, unit operation level is the classical approach in chemical engineering and activities toward design and optimization of single intensified equipment can be included in this level. As aforementioned,

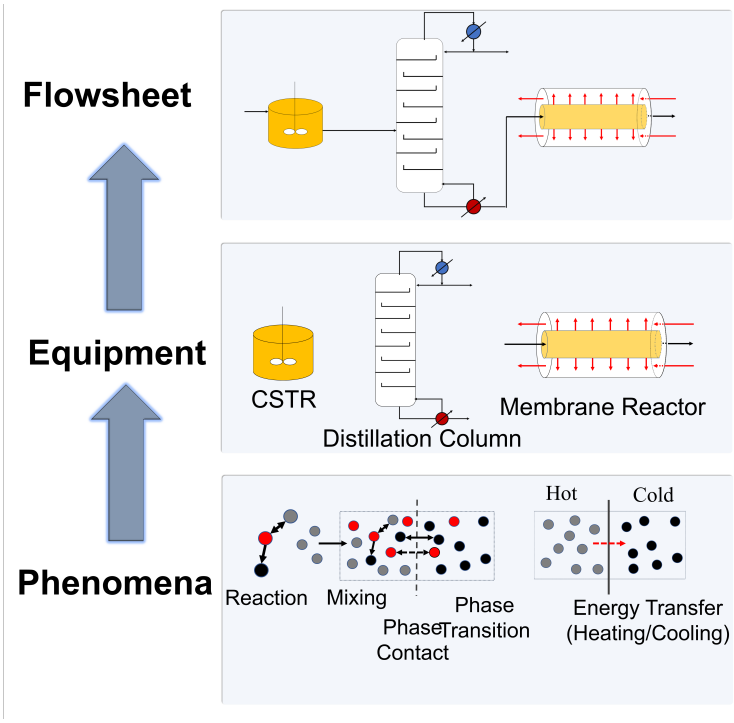

Figure 1.5: Phenomena-based approaches for process design. While unit operations has been the modus operandi for process design, observing chemical processes as combination of phenomena can open up many opportunities in terms of systematic process intensification (Adapted with permission from [12]).

these methods can be used to synthesis and optimization of standalone intensified equipment. Yet, as the equipment to operate with is fixed beforehand, the scope of the design activities which involve thinking in terms of unit operations is limited. Also, the design decisions made at the equipment level can have an affect on the overall process which is not taken into account if one only focuses on pre-specified equipment. Most promising methods for systematic design/synthesis of intensified processes have been developed at the phenomena level. According to Lutze et al. (2010), operating at phenomena level has an advantage over other approaches in that phenomena descriptions can be directly translated into mathematical equations [19]. Hence, several methods have emerged for chemical process synthesis incorporating intensification by operating at this level. Observing chemical processes as combination of phenomena can open up many opportunities in terms of systematic process intensification.

Several different approaches exist that utilize these bottom-approach for process design and enable systematic process intensification. Manousiouthakis and co-workers proposed the Infinite DimEnsionAl State Space (IDEAS) [106] approach as a representation and synthesis tool for process intensification. The method was built on a state-space representation [78] of processing routes where a set of process operators (OP), i.e. unit operations, were connected to each other with a distribution network (DN), i.e. flow operations, to consider all inlet outlet possibilities. IDEAS allows the formulation of general process network synthesis problems as infinite convex (linear) programs whose local solutions are guaranteed to be globally optimal. The IDEAS approach has been applied to the synthesis of heat/power integrated distillation processes [107], azeotropic distillation processes [108], non-ideal reactor network synthesis [109], reactive distillation processes [110, 111], and energetic intensification of a hydrogen production process [97].

Papalexandri and Pistikopoulos [112] developed a Generalized Modular Representation Framework (GMF) for the representation of chemical processes. Built on aggregated multifunctional mass/heat exchange modules and pure heat exchange modules, GMF disclosed intensification possibilities by optimizing mass and heat transfer performances based on Gibbs free energy. Conventional or even unconventional process flowsheets were generated via the solution of an superstructure-based optimization problem with MINLP formulation. Herein, the synthesis alternatives were not pre-postulated as process units, but explored as mass/heat-exchange feasibilities. The proposed representation/modeling framework has been demonstrated for combined separation/reaction systems [113, 114, 115], azeotropic separation systems [113, 116], multicomponent separation systems [117, 118], and heat-integrated distillation systems [119]. More recently, this approach has been also extended for considering safety and operability aspects of the suggested intensified designs [120, 121].

Sundmacher and co-workers [101, 122, 123] suggested an equipment independent process flowsheet representation based on “functional modules”. They decomposed a chemical process to be comprised of different “functional modules” such as pre-processing, contacting, activating, reaction, heat supply/removal, separating, and product formation. According to this concept, change

in the state of a volume element going through a functional module can be described via the active fluxes in that module, e.g. diffusion flux, and the corresponding components in the basis vectors, i.e. elementary process functions, which indicate a certain direction in thermodynamic state-space. They showed the applicability of their approach on the design of novel reactor concepts where the optimal design is realized by tracking a fluid element on its way through the reactor and optimizing the fluxes into it. The optimization of the fluxes is based on dynamic optimization with orthogonal collocation and according to the choice of which fluxes are investigated, whether selective removal of some reactant species are beneficial or not, might be also investigated which can suggest different reactive separation operations.

Very significant contributions to the available methods for process synthesis and intensification at the phenomena level have been made by Gani and coworkers. Lutze et al. [91] presented a comprehensive methodology for process synthesis/intensification to address the large search space formed by phenomena-based building blocks (PBBs). The proposed method was decomposed into several steps, supported by a pool of sub-algorithms and computational tools. In the first step, design objectives were defined and a base-case design was analyzed to identify the candidate PBBs. Nine major classes of PBBs were selected to represent the basic structures for process alternatives: Reaction (R), Mixing (M), 2-phase mixing (2phM), phase contact (PC), phase transition (PT), phase separation (PS), heating (H), cooling (C), and dividing (D). Identified candidate phenomena from Step 1 were then connected to form process options, which are screened for feasibility using heuristic rules and the most promising phenomena-based ones were transformed into unit operations. This methodology was firstly applied to the production of isopropyl acetate. Babi et al. [124] later extended it for membrane-based processes with sustainability considerations. Babi et al. [125] introduced superstructure-based process synthesis and detailed design for the base-case design selection which was then further improved with the phenomena-based methodology introduced by the previous works. Kuhlmann and Skiborowski [126, 127] used similar PBBs and proposed a state-space superstructure for the systematic generation of flowsheet variants.

There also exist other approaches for process intensification. Carrasco and Lima (2016) em-

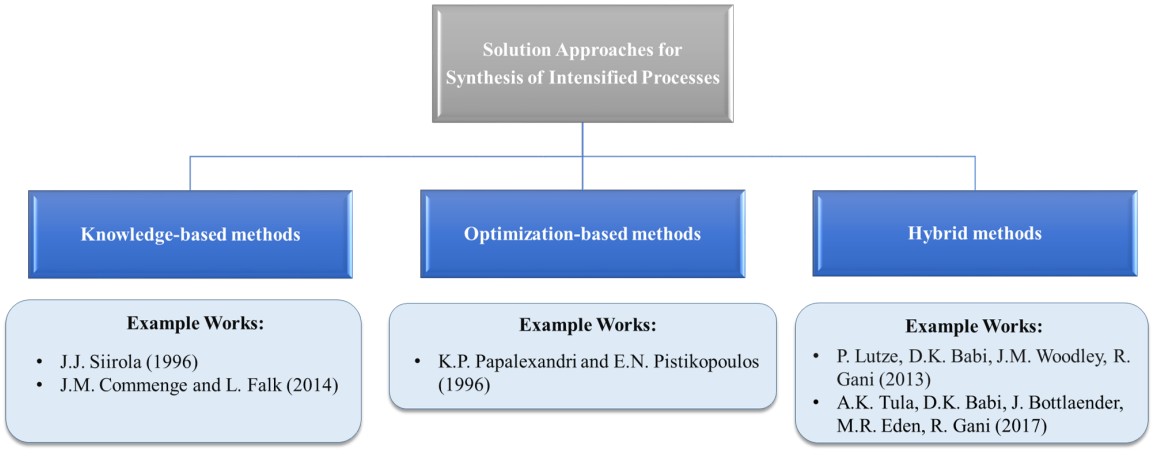

Figure 1.6: Classification of the solution strategies for systematic process intensification (Adapted with permission from [13]).

ployed an operability-based approach for the intensification of a membrane reactor for hydrogen production [128, 129]. Recker et al. (2015) proposed a sequential procedure which involved candidate flowsheet generation, flowsheet screening using shortcut methods and model-based process optimization for the design of reaction-separation processes [130]. Commenge and Falk (2014) proposed a 3-step sequential technique for process intensification. The first step is to identify the process limitation among a list of 16 possibilities that cover a large spectrum of cases. Then, the methodology relates the identified limitations to a set of intensification strategies. Finally, identified strategies are related to technologies that apply these strategies. The proposed method supplies a short list of appropriate solutions to be considered in technical design and economic evaluations together with a list of innovation strategies [60]. Arizmendi-Sanchez and Sharratt (2008) used abstract or equipment independent functional, structural and behavioral modules and phenomena, and proposed causal graphs to design and intensify a chemical process [131]. Rong et al. (2008) suggested a multiscale methodology based on manipulation of the identified key process phenomena to obtain intensified process alternatives [132]. Lakerveld et al. (2010) employed a modular task-based design which enabled the use of intensification principles for design of intensified crystallizers with flexibility over product purity [133]. Gopalakrishnan et al. (2012) suggested process simplification as a way of process intensification. Specifically, they proposed to synthesize process

configurations with the least number of processing steps while yielding a certain product from a set of raw materials [134].

All these methods can be also grouped according to their solution approaches. Similar to process synthesis and integration, process intensification methods can be divided into three categories based on the solution approaches as follows: i) knowledge-based methods [41, 60], ii) optimization-based approaches [111, 112], and iii) hybrid approaches [91] (Figure 1.6). Systematic screening of feasible solutions is an integral part of obtaining intensified processes. Heuristic methods rely on identification of hotspots and use of a set of guidelines to eliminate process bottlenecks. Hybrid methods use multi-step frameworks that combine heuristics and combination rules with optimization to sequentially reduce the search space for intensified alternatives. For instance, the phenomena-based methodology proposed by Gani and co-workers [91, 125, 135] performs both process synthesis and intensification in a hierarchical manner. The approach is able to identify the necessary and desirable phenomena and generate and screen various phenomena-based flowsheet options using a decomposition based solution strategy. The superstructure optimization-based approaches employ non-traditional representations which can be converted into mixed-integer nonlinear optimization (MINLP) formulations to simultaneously identify optimal intensification routes and process flowsheets. GMF approach [112], for instance, seeks for promising intensified flowsheets through thermodynamically feasible mass/heat exchange modules.

1.3 Research Gaps and Challenges

Despite the past research, the potential of process intensification is not fully explored yet. The current methods are mostly sequential and employ ad hoc design considerations and heuristics, which often result in suboptimal intensification solutions. A drawback of the superstructure-based approach for process synthesis incorporating process intensification is that the intensification alternatives need to be postulated a priori. In fact, no methods currently exist which can automatically generate all plausible intensification alternatives at the flowsheet level. Unless the connectivity between units and/or phenomena are explicitly defined within the superstructure, any non-intuitive intensification opportunity is left out without consideration. Therefore, it remains a challenge

to systematically identify, incorporate and screen all plausible intensification alternatives without exhaustive or sequential enumeration. It also remains a challenge to perform process synthesis and intensification within a single optimization framework that can capture the effect of decisions made at one level on the other levels of the processes. Key challenges toward systematic process intensification can be summarized as follow:

1. how to systematically select and combine multiple phenomena to create new opportunities and obtain "out-of-the-box" design solutions,

2. how to systematically identify intensified equipment and, at the same time, generate process flowsheets containing these equipment,

3. how to select optimal conditions and configurations of intensified equipment and process flowsheets,

4. how to incorporate process intensification into process synthesis and integration without a priori postulation of intensification alternatives.

1.4 Research Objectives

In this work, an original method for systematic process design, synthesis and intensification, which does not depend on a priori postulation of process alternatives will be sought for. Primary objectives of the current work can be summarized as:

1. Develop a systematic method for the identification and incorporation of intensification alternatives in process design.

2. Develop a unified method for process design, synthesis, integration and intensification.

3. Develop an automated flowsheet generation methodology that does not request intensification alternatives beforehand.

In order to address these objectives, a new representation for chemical processes is proposed. Proposed method does not rely on classical unit operation-based representation of process units, flowsheets and superstructures; yet, it is based on building blocks which can represent different phenomena, tasks and enabling materials. The systematic arrangement of these building blocks enables incorporation of all plausible design and intensification pathways within a general block-based superstructure. As building blocks operate at lower aggregation levels, novel equipment alternatives can be realized without specifying their existence. It also enables a mathematical programming-based method to simultaneously identify the best design, synthesis and intensification routes at the equipment and flowsheet levels. In doing so, trade-offs between design decisions made at different levels of process design can be captured.

This work is structured as follows. In Chapter 2, the proposed representation is introduced and how different phenomena, tasks, unit operations and superstructures can be represented is explained in detail. In Chapter 3, a generic MINLP problem allowing an automated process intensification method is provided. In Chapter 4, the proposed method is demonstrated on a wide range of process design and intensification problems. In Chapter 5, the contributions of the current work are summarized and future directions are provided.

2. BUILDING BLOCK REPRESENTATION OF CHEMICAL PROCESSES*

At the heart of the proposed systematic intensification methodology lies a new representation for chemical processes. This novel representation is based on abstract building blocks which provide a generic bottom-up approach towards chemical process design. It also enables an optimization-based approach for automated generation of chemical processes. The method is summarized in Figure 2.1. Given the available raw materials, reaction data, physical and thermodynamic data, material properties, available utilities and product requirements, the aim is to generate the corresponding flowsheet with intensified/traditional equipment types while screening according to the specified evaluation criteria, i.e. objective function for the optimization formulation. This flowsheet generation is performed through a generic optimization model which describes the abstract building blocks. Once the solutions are obtained with respect to building block representation, they can be converted to classical flowsheet representations.

In this chapter, we will describe this representation in detail. We first start by describing what an abstract building stands for. These abstract building blocks serve as the basic design elements for systematic process intensification. Then how these basic building block definitions can be used to represent different physiochemical phenomena, processing tasks and unit operations is explained. Following this, how these building blocks can be emulated for a generic superstructure representation is discussed. This superstructure representation is crucial for systematic process intensification as it enables an automated approach toward generating and screening intensified/traditional solutions at phenomena, equipment and flowsheet levels. Finally, we describe how resulting building block structure is interpreted and converted into classical process representations.

*Parts of this chapter were adapted with permission from (S.E. Demirel, J., Li, and M. M. F. Hasan, "Systematic process intensification using building blocks," Computers & Chemical Engineering, vol. 105, pp. 2 - 38, 2017.) Elsevier, from (S. E. Demirel, J. Li and M. M. F. Hasan, "A general framework for process synthesis, integration, and intensification," Industrial & Engineering Chemistry Research," vol. 58, no. 15, pp. 5950 - 5967, 2019.) Copyright (2019) American Chemical Society, and from (M. M. F. Hasan, S. E. Demirel and J. Li, "A building block approach to process intensification," Chemical Engineering Progress, vol. 115, no. 3, pp. 35 - 43, 2019.) Copyright (2019) American Institute of Chemical Engineers.

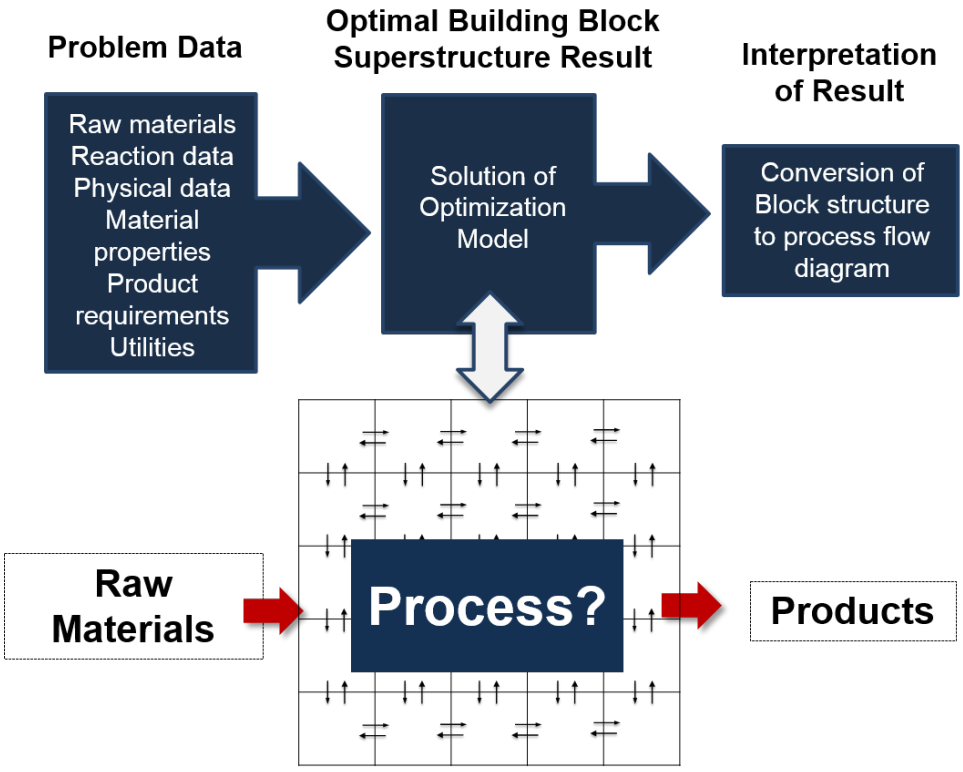

Figure 2.1: Summary of the proposed systematic process intensification method. Given the problem specifications, a generic building block-based superstructure representation is used to automatically generate different flowsheet variants. After the optimal building block results are obtained, they can be converted to classical flowsheet representations.

2.1 Building Block Concept

A building block is a two-dimensional abstract module characterized by its interior, four boundaries and the material(s) used inside or at the boundaries of it (Figure 2.2). Block interior and surrounding four boundaries serve as the fundamental design elements. The interior of a block can be either empty or filled with a functional material such as a catalyst or an adsorbent. Furthermore, permeation-related phenomena such as membrane separations can be represented using a barrier material at the boundary or interphase of two adjacent blocks, where one block would emulate the permeate side and the other block would emulate the retentate side of the membrane module. Hence, most physiochemical phenomena and processing tasks can be represented using building blocks. In this sense, the proposed building blocks capture a lower aggregation level than that of

phenomena and task-based approaches (See Figure 2.3).

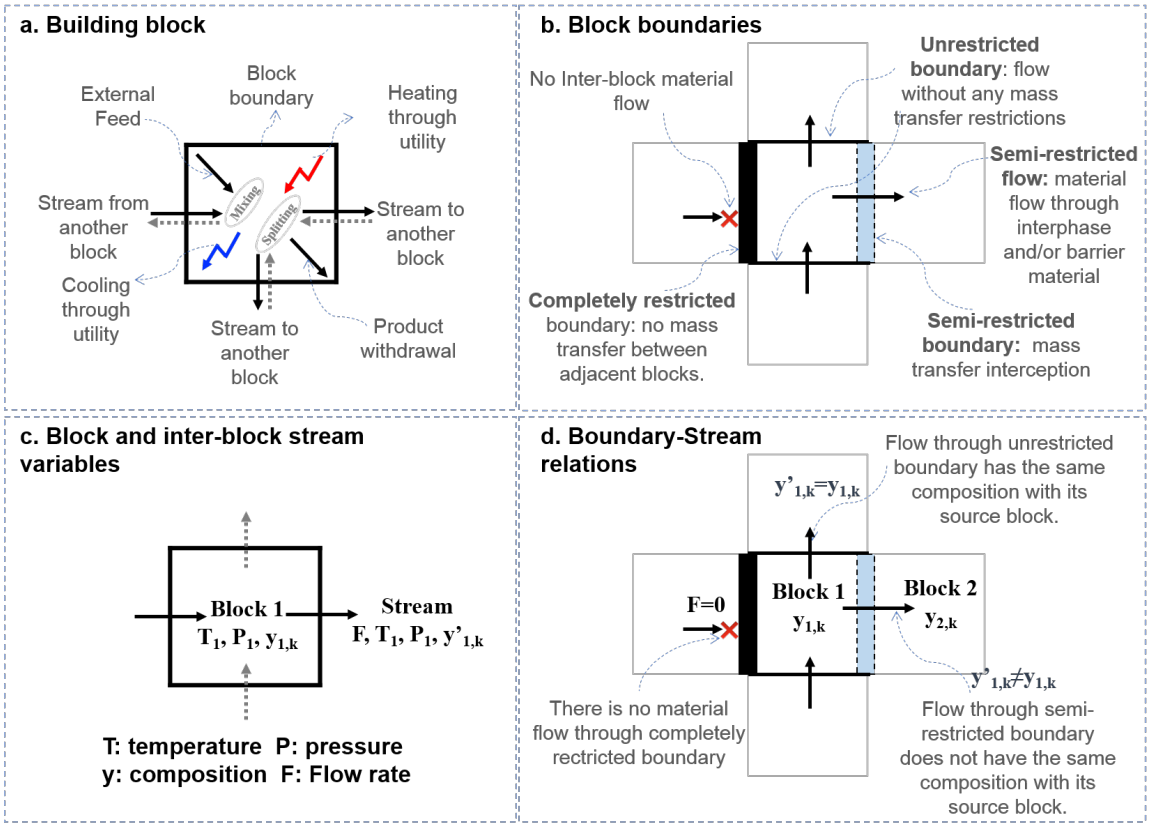

Figure 2.2: Basic design elements. Each building block has two basic design elements: a) building blocks, and b) building block boundaries. Each block has entering and exiting streams through block boundaries in addition to external feed and product streams (Adapted with permission from [136]). Each boundary is classified as unrestricted, semi-restricted or completely restricted. c) Each block has temperature, composition and pressure attributes. d) Attributes of the outlet streams and the interaction between building blocks depend on the boundary types.

In describing different elements of the chemical processes multiple blocks might be required. In this case, the interaction of the building blocks between each other becomes important. These interactions are enabled through the boundary separating two blocks from each other (Figure 2.2b). Each boundary between two neighboring blocks is classified as either unrestricted, semirestricted or completely restricted to capture different patterns of interactions in chemical processes. Unrestricted boundary indicates that the flow through it has the same composition with its source

block. There is no mass transfer interception between the neighboring blocks sharing a common unrestricted boundary. Completely restricted boundary is used to describe zero-flow conditions, i.e. wall in a divided wall column distillation. This type of boundary can be used to consider conduction for heat transfer (See Li et al. (2019) for an example [137]). Semirestricted boundary designates that the stream leaving through this boundary has a different composition than the source block itself. Two neighboring blocks with a common semirestricted boundary may represent a separation operation. If one block is in vapor phase and the other is in liquid phase, then a semirestricted boundary indicates a phase boundary between these phases.

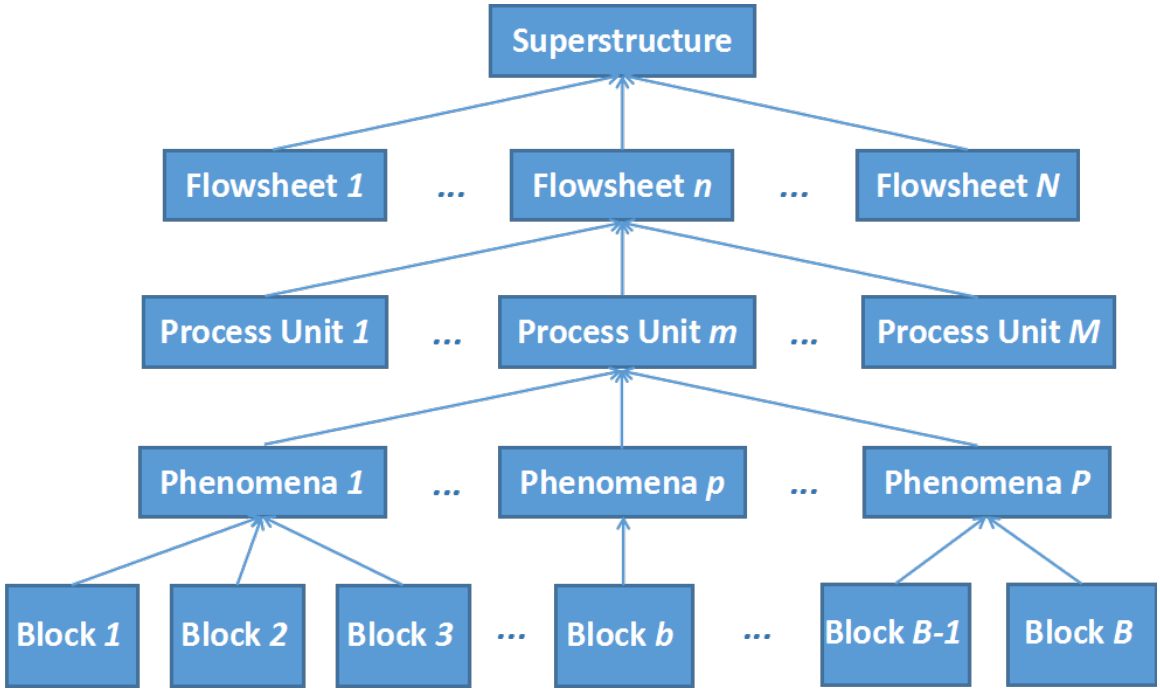

Figure 2.3: Forming a superstructure of design and intensification alternatives using building blocks. We introduce a building block concept which can be used to represent different phenomena encountered in chemical processes. These phenomena when combined can be used to represent different process units. Multiple process units lead to a process flowsheet. When multiple blocks that can represent different flowsheet alternatives combined in a certain fashion, a superstructure with all plausible design and intensification alternatives is obtained (Reprinted with permission from [90]).

Each building block has temperature, pressure and composition attributes, denoted by T, P, and y, respectively (Figure 2.2c). Based on these attributes, phase is also determined. Each block represents a single phase. This does not imply that multiphase flow cannot be achieved. When two neighboring blocks with different phases co-exist with a common semi-restricted boundary, we achieve a two-phase flow. Therefore, an interphase is represented by a semi-restricted boundary between the blocks representing two distinct phases. Phase assignment can be accomplished according to the specified thermodynamic relations. Our goal is to identify the optimal values of these physical qualities while considering appropriate thermodynamic relations between the attributes. There can be multiple incoming and outgoing streams through the block boundaries which are described by their flow rate, temperature, pressure and composition. All outgoing streams from a block share the same temperature and pressure. Chemical transformations and changes in the component qualities are represented inside the block. This means that incoming material streams to a building block are assumed to be mixed before getting involved in a transformation. This mixing is based on linear relationships in terms of the material flows, but other mixing rules can be applied as well. Representing chemical transformations within the block implies that the stream composition stays the same after it leaves the source block.

Although all outgoing streams from a block share the same temperature and pressure, its composition is determined by the boundary type (Figure 2.2d). If the boundary is unrestricted, then the stream composition is equal to the block composition itself. If the boundary is completely restricted, on the other hand, this stream might have a different composition dictated by the nature of the semi-restricted boundary and the corresponding mass transfer operation.

We can use building blocks to represent all the phenomena in different process units. Since a process flowsheet is a collection of multiple units, we can also use a finite number of blocks $\{1, ..., |B|\}$ to represent an entire process flowsheet and even a superstructure which stands for all plausible processing alternatives. The simple flowchart that can be followed to develop a process superstructure using building blocks is illustrated in Figure 2.3. We do not need to postulate different superstructures for different process intensification problems, but a single block superstructure

suffices. This marks a significant advantage of using a block superstructure over the classical superstructures of chemical process networks. Next, we continue with describing how different physiochemical phenomena can be represented by using these basic building block definitions.

2.2 Representing Chemical Phenomena

In our building block-based approach, a physiochemical phenomenon, a processing task or a function can be represented using a single block or using two neighboring blocks and their boundaries. Examples of these phenomena are reaction, phase contact and transition, mixing, splitting, heating, cooling, etc. [91]. This is illustrated in Figure 2.4.

Mixing, cooling, heating and reaction phenomena are represented by a single block, while separation phenomena, splitting and pressure changing tasks (pressurizing or depressurizing) require two interacting blocks. Splitting, phase change and pressure changing tasks are represented by two blocks sharing a common unrestricted boundary. Separation phenomena, on the other hand,require two neighboring blocks separated by a semi-restricted boundary. Phase dividing requires two blocks with two distinct phases separated by a completely restricted boundary. A summary of different physiochemical phenomena and tasks and the number of building blocks required to represent these phenomena are provided in Table 2.1.

Mixing: When multiple streams enter into a block and only one exit stream exists, then the block serves as a mixer. The block representation for mixing is shown in Figure 2.4a.

Splitting: A block with multiple outlets serves as a splitter (Figure 2.4b). Note that both the splitting and mixing phenomena can occur if multiple streams enter and exit at the boundaries of the same block.

Cooling and Heating: We model cooling and heating phenomena with the help of utility streams supplied externally as shown in Figures 2.4c-d. Each block has its associated variables to quantify the heating or cooling duty (Q^c or Q^h). Additionally, we also consider stream heaters/coolers to introduce additional flexibility in representation (Figure 2.4f). While block heat duty variables can be also used for representing heaters and coolers, they can also serve to represent phenomena that occur within the same space, e.g. reactor cooling/heating. Stream heaters and coolers, on the

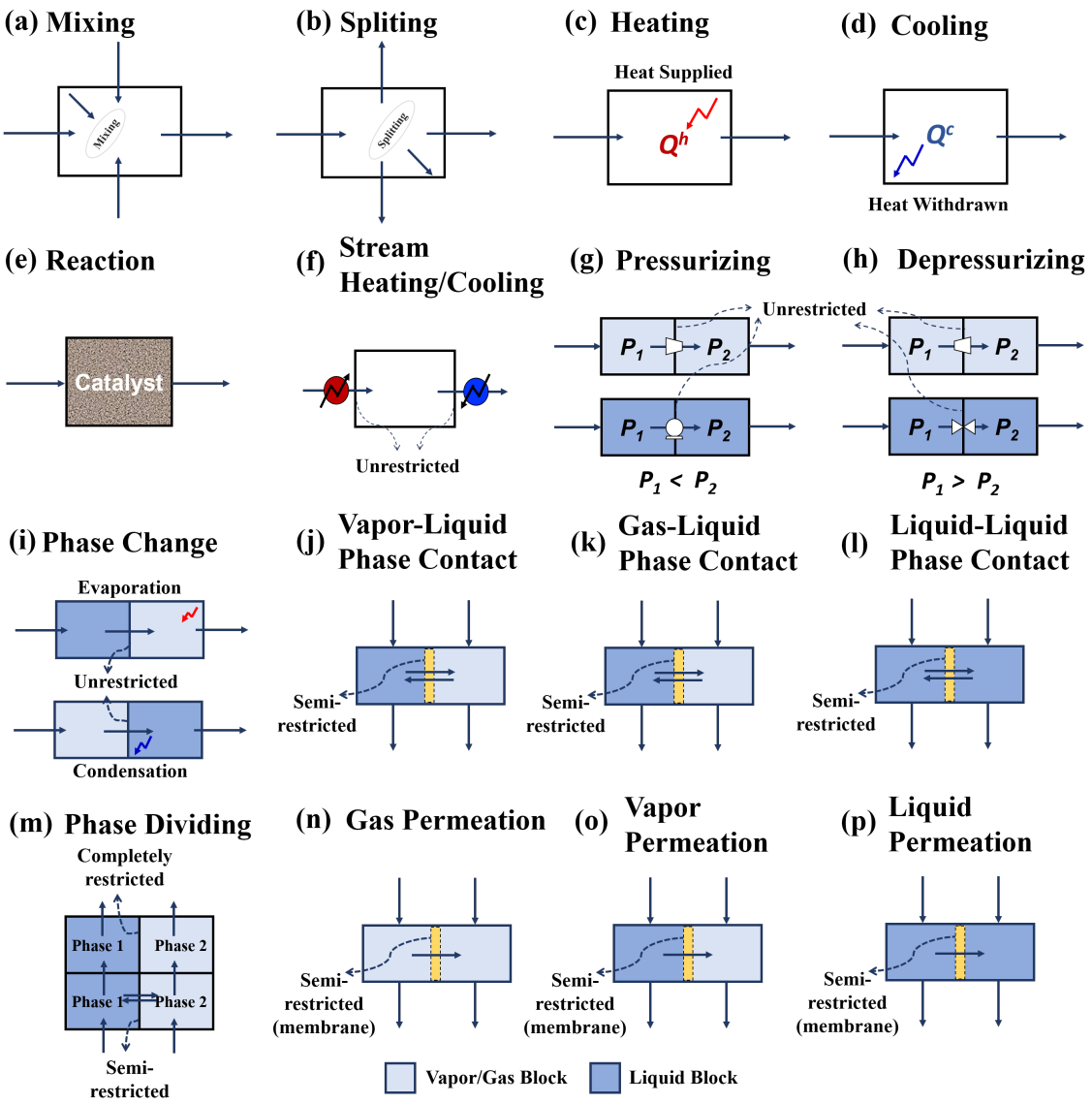

Figure 2.4: Phenomena representations using building blocks. Block Representation for a) mixing, b) splitting, c) heating, d) cooling, e) reaction, f) stream heaters/coolers on the interblock streams, g) pressurizing for gas/vapor and liquid streams, h) depressurizing for gas/vapor and liquid streams, i) phase change from liquid to vapor and vice versa, j) vapor-liquid phase contact, k) gas-liquid phase contact, l) liquid-liquid phase contact, m) phase dividing, n) gas permeation, o) vapor permeation and p) liquid permeation (Adapted with permission from [136]).

other hand, are just for manipulating the standalone connecting streams.

Reaction: Reactions are also considered to occur inside a block. As reactions may require catalyst(s), the existence of a reaction block is also related with the existence of a catalyst in the

Table 2.1: Different physicochemical phenomena and building blocks representations (Adapted with permission from [90]).

Phenomena	No of Blocks	Boundary Type	Enabling Material
Mixing	1	Not required	-
Cooling	1	Not required	-
Heating	1	Not required	-
Reaction	1	Not required	Catalyst
Splitting	2	Unrestricted	Not required
Pressurizing	2	Unrestricted	Not required
Depressurizing	2	Unrestricted	Not required
Phase dividing	2	Completely restricted	Not required
Complete Phase Change	2	Unrestricted	Not required
Vapor-Liquid Phase Contact	2	Semi-restricted	Not required
Liquid-Liquid Phase Contact	2	Semi-restricted	Extractant
Gas-Liquid Phase Contact	2	Semi-restricted	Absorbent
Gas/Vapor Permeation	2	Semi-restricted	Membrane
Liquid Permeation	2	Semi-restricted	Membrane
Pervaporation	2	Semi-restricted	Membrane

block (Figure 2.4e). Multiphase reactions, such as gas-liquid or gas-liquid-solid reactions would require two blocks to exist, one in gas and the other in liquid phase. When a catalyst material is chosen in a block, then corresponding reactions are activated. Note that this does not prevent a homogeneous reaction to occur which does not need any catalyst. These reactions can occur as long as the phase constraints are satisfied.

Component separations, mass transfer between different phases and pressure change require two neighboring blocks. While complete phase change and pressure related phenomena are represented by unrestricted boundary, separation phenomena are represented by semi-restricted boundary.

Pressurizing and Depressurizing: Changes in pressure are only allowed at the unrestricted boundaries. These pressure-related tasks are illustrated in Figures 2.4g-h. Similar to the cooling and heating phenomena, work duties are included to quantify the energy consumed/produced due to change in pressure.

Phase Change: Phase change is the complete shift from one phase to another. Total conden-

sation is an example of phase change, where vapor components condense completely into liquid phase. Phase change needs two blocks separated by an unrestricted boundary, as shown in Figure 2.4i. The composition of material flow remains unchanged after the operation.

Phase Dividing: Phase dividing phenomenon is achieved via completely restricted boundary (Figure 2.4m), which hinders the contact between two phases and prevents any equilibrium relations to be satisfied for those two phases.

Separation Phenomena: We represent any separation phenomena using two building blocks with a common semi-restricted boundary. The building block-based representations of different separation phenomena are illustrated in Figure 2.4. The semi-restricted boundary shared by two neighboring blocks can represent a direct phase contact between two phases, or it can represent a barrier material. Phase contact between two phases can be observed in vapor-liquid phase contact (VL-PC), gas-liquid phase contact (GL-PC) or liquid-liquid phase contact (LL-PC), while barrier materials can be observed in gas permeation (GP), liquid permeation (LP) and vapor permeation (VP) [91, 138]. Gas-liquid phase contact is the underlying phenomenon observed in absorption processes, while liquid-liquid phase contact is the underlying phenomenon observed in extraction processes. While GL-PC and LL-PC require enabling materials (i.e. absorbent and extractant respectively), VL-PC does not require any enabling material. When there is phase contact between different phases, phase transition and phase equilibrium are maintained in a way that a species migrates from one phase to another according to the thermodynamic relations. In the case of presence of a barrier material, the underlying models for mass transfer will differ according to the phase of the material in permeate and retantate sides. Accordingly, we differentiate between different phenomena that require barrier material for separation as GP, LP and VP. For gas (GP) and liquid permeations (LP), phase of the two blocks are the same. While permeating species are in gaseous or in vapor phase in GP, they are in liquid phase for LP, e.g. reverse osmosis. For vapor permeation phenomena (VP), phase of the two blocks are different and the permeating components undergo phase change. Retantate side is in liquid phase and permeate side is in vapor phase. This phenomena is used to represent pervaporation operations. Note that this VP phenomena should

not be confused with the actual vapor permeation membrane operations in which the permeating species are condensable vapor phases. However, the phase of the components are the same at both sides of the membrane material in vapor permeation membranes. Hence, these operations are also considered under GP phenomena.

Material-Enabled Phenomena: Many phenomena depend on the use of functional materials. Examples are membrane separation, heterogeneous reactions, gas adsorption, etc. We consider three types of functional materials: (i) intra-block materials, (ii) inter-block materials, and (iii) barrier materials. Solid catalysts and adsorbents are considered as intra-block materials for which the block is implicitly considered to have a solid phase. However, if the reaction is catalyzed by a liquid catalyst and the reaction medium is in liquid phase, then the catalyst is represented by a separate flow between blocks. Therefore, liquid catalysts, absorbents (solvents) and external reagents are considered as inter-block materials. In this case, a semi-restricted boundary is used between the external reagent and the mixture. For separations that use a barrier material (e.g., membrane), a semi-restricted boundary between the neighboring blocks are assigned along with the barrier material. As there can be different materials with different selectivity toward the same component, there can be multiple alternatives for enabling materials. However, only one barrier material can be assigned to a semi-restricted boundary.

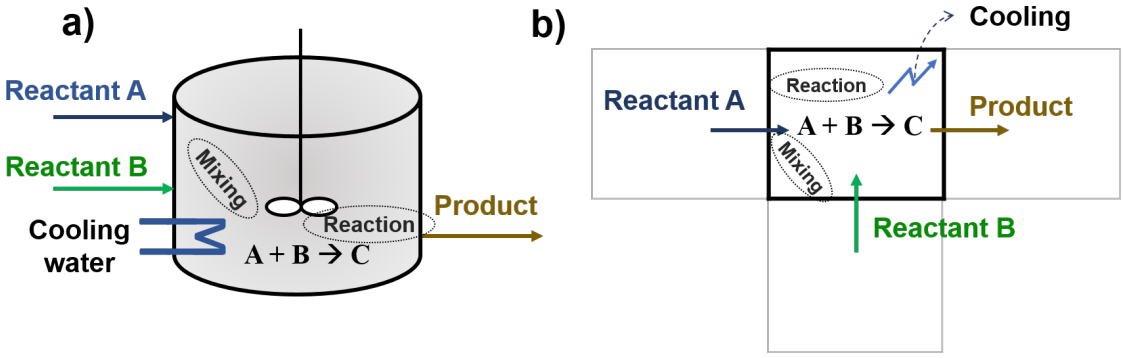

Figure 2.5: Multiple phenomena representation through a single block. a) An isothermal CSTR operation for a liquid-phase exothermic reaction, b) its building block representation.

A single building block can host single or multiple phenomena. To illustrate, let us consider an isothermal operation of an exothermic liquid phase reaction (Figure 2.5a). The operation of this reactor can be described through a combination of mixing, reaction and external cooling phenomena all hosted within a single reaction block (Figure 2.5b). As we assign tasks, phenomena and materials to each block and configure a collection of blocks in a specific fashion, we obtain larger unit operations and process flowsheets (hence the name 'building blocks'). To this end, the building blocks can be not only used to represent different tasks, phenomena or operations, but they can be also used to combine multiple tasks, phenomena and operations to represent process units, flowsheets and superstructures. Next, we describe this in more detail.

2.3 Representing Unit Operations, Process Flowsheets and Superstructures

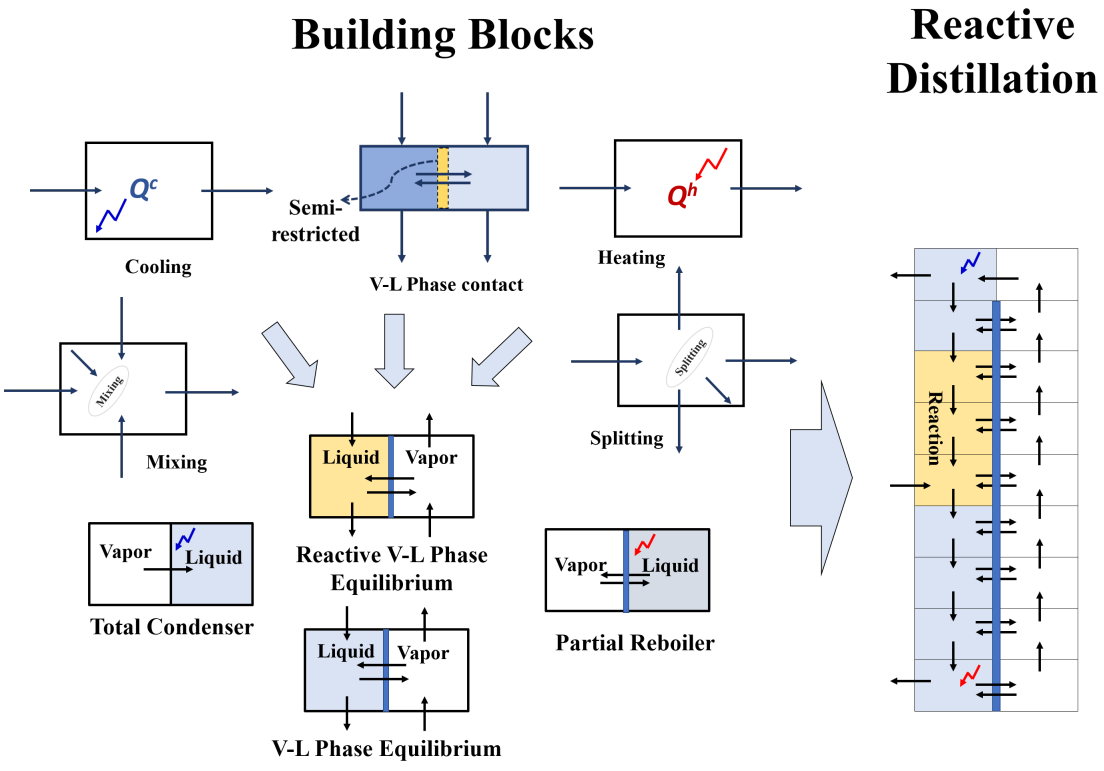

Figure 2.6: Equipment representation by using building blocks with an example on reactive distillation (Adapted with permission from [51]).

Here we describe how we can use building blocks to represent process units or equipment, flowsheets and superstructures. A process unit is obtained by assembling multiple building blocks in an arrangement that captures the phenomena that are sufficient to mimic the unit operation. An assembly of blocks of the same type or blocks with the same material represents a classical unit. For instance, an array of catalyst blocks represents a plug flow reactor (PFR), while an assembly of blocks packed with adsorbents represents a packed adsorption column. An assembly of blocks of different types and/or blocks with different materials results in an intensified unit. For example, if the blocks representing the PFR also have semi-restricted boundaries at the top or at the bottom and if these boundaries are associated with a membrane, then the overall assembly represents a membrane reactor with in situ reaction and separation. An example of this is shown in Figure 2.6. A block holding a liquid mixture in contact of its vapor phase together represent a V-L phase equilibrium. If reaction also takes place in the liquid phase, then these two blocks represent a reactive flash operation or a part of a reactive separation column. A condensation operation with cooling can be represented using a unidirectional phase transition and material flow from one block to another. When all the building blocks are connected to each other, as shown in Figure 2.6, an intensified column with reactive and non-reactive sections can be obtained.

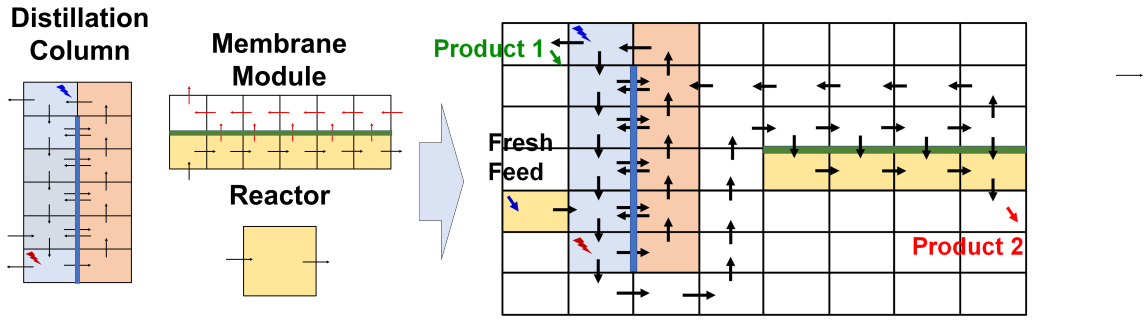

Figure 2.7: Flowsheet representation by using building blocks. By using single or multiple blocks different intensified/traditional unit operations can be represented. When these building blocks are connected through interblock streams, a flowsheet can be constructed.

A block with a single inlet and single outlet but without any assigned task or phenomena is considered as a pipe, which also allows the connectivity between different units. To this end, an assembly of empty and nonempty blocks would represent a process flowsheet with multiple units connected via pipes. An example is shown in Figure 2.7. On the left, a reactor, separation column and a membrane module representations are provided. When these unit operation representations are attached to each other and connected with interblock streams with single inlet and single outlet, we can capture a flowsheet representation with recycle streams. To increase the connectivity within the superstructure, we can also consider "jump streams" which can connect nonadjacent blocks to each other. This also increases the connectivity within the superstructure. The recycle streams shown in Figure 2.7 can be replaced with these jump streams for a more compact representation with less number of blocks (See Li et al. (2018) and Demirel et al. (2019) for a more detailed discussion [139, 51]).

Without loss of generality, we can say that a large enough assembly of building blocks of all types would contain many alternative process flowsheets and can be considered as a process superstructure. To this end, we propose an original superstructure which is an ensemble of building blocks in two dimensions (see Figure 2.8a). Each block is denoted by its coordinate within the superstructure. A block can have entering and outgoing streams in both horizontal and vertical directions. The proposed superstructure captures all plausible process intensification alternatives at the equipment and flowsheet levels. To illustrate, as shown in Figures 2.8b-e, from the same block superstructure, it is possible to obtain membrane reactor configurations (Figures 2.8b-c) with homogeneous reaction or multiple catalysts. The same block superstructure contains absorption, reactive distillation, dividing wall columns for distillation (Figure 2.8d), and task-integrated columns that can transform an entire process flowsheet by stacking multiple unit operations into a single intensified unit (Figure 2.8e).

Different process units can be constructed using the same block superstructure through the appropriate choice of blocks, boundary types, flow directions, and functional materials. Furthermore, with appropriate selection of the size/volume of the building blocks, the proposed method can be

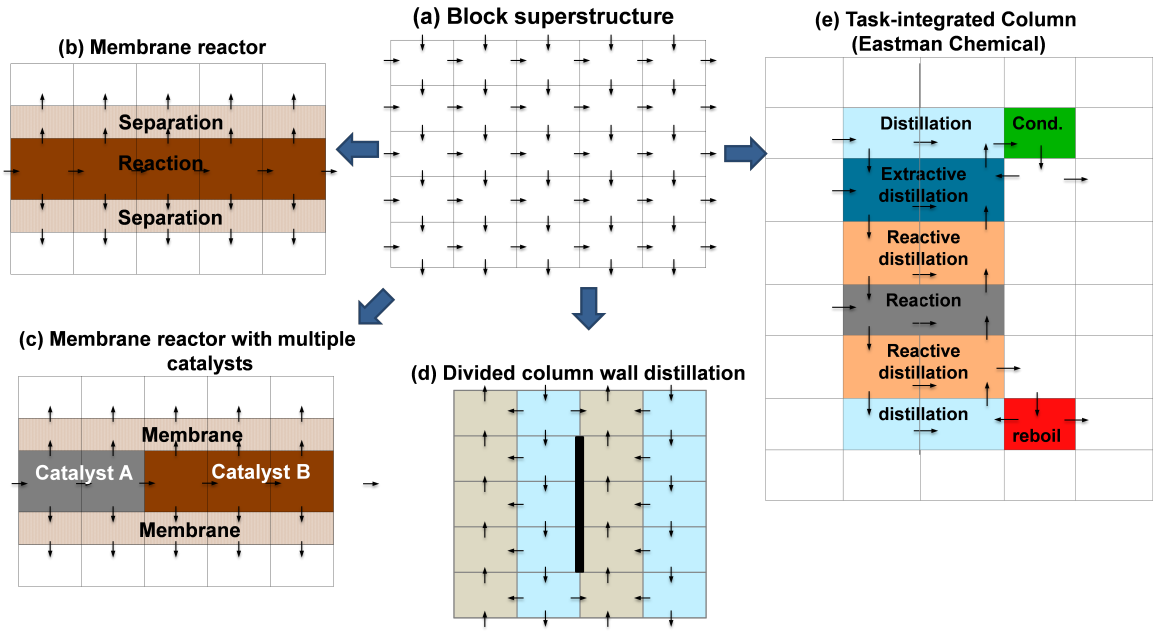

Figure 2.8: Building block superstructure of intensification alternatives. (a) Building block superstructure. From the same block superstructure, it is possible to obtain the configurations for (b) membrane reactor with homogeneous reaction, (c) a packed membrane reactor with two different catalysts, (d) a dividing wall column for distillation where the dividing walls, shown by the dark vertical lines, are obtained by imposing completely restricted boundary between two neighboring blocks, and (e) a task integrated column (Reprinted with permission from [90]).

both scaled-down to construct micro-channel reactors, or can be scaled-up to construct large task-integrated columns. If the blocks representing multiple process units are connected, then we would obtain a classical process flowsheet. Therefore, the block superstructure not only contains intensification alternatives but it also contains alternatives typically considered for process synthesis and integration. To this end, the building block-based approach can lead to a unified approach for process synthesis, integration and intensification using a single optimization-based formulation. To summarize, our building block-based approach

(i) leads to a novel method to represent different phenomena, tasks and unit operations typically encountered in chemical process industry,

(ii) leads to a unified representation approach for process synthesis, integration and intensifica-

tion using a single superstructure, and

(iii) identifies and incorporates many process synthesis and intensification alternatives.

This representation also allows for a systematic mathematical formulation that we can utilize in several ways. Firstly, the phenomena assignments, flow directions, flow rates, temperatures, pressures and other decisions can be can be described with an optimization model. This can allow us to automatically generate different intensified/traditional flowsheet variants. Furthermore, by selecting the position of the active phenomena and materials and designating the connectivity in between by choosing appropriate flow directions, different superstructure-based process synthesis and intensification problems can be addressed. In any case, the solution of the optimization problem dictates the final configuration. In the next section, we will discuss how the solution of the optimization problem can be utilized to infer the final optimal process flow diagram.

2.4 Building Blocks to Process Flow Diagrams

This section describes how the block configuration is transformed into a classical process flowsheet representation. This is performed once the optimal block configuration is obtained. To explain how the transformation is carried out, the block-based configuration given in Figure 2.9a is considered as an illustrative example. In general, the transformation involves the following three steps:

(i) identification of primary unit operations,

(ii) identification of auxiliary unit operations, and

(iii) identification of connections.

These steps are followed based on the solution of the optimization problem and identifying the value of the optimal variables describing the superstructure. For the sake of explanation of this procedure, here we define several variables that describe the superstructure. A more detailed description will be provided in the following chapter. Each block $B_{i,j}$ is denoted with its position

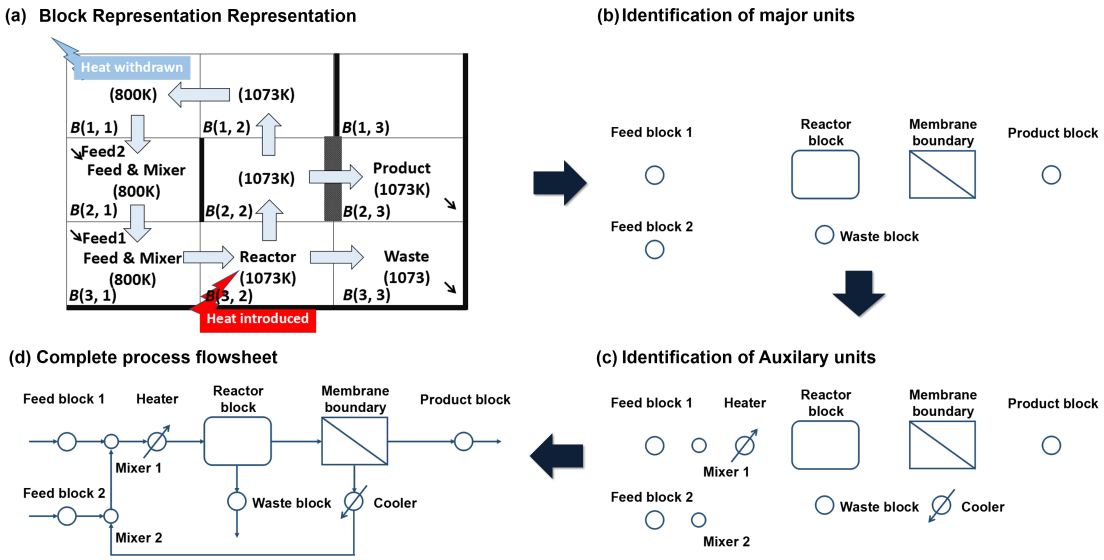

Figure 2.9: Translation of the building block result to process flowsheet. (a) Block superstructure result for the illustrative example, (b) major units that are implied by the binary variables (boundary and block assignments), (c) identification of auxiliary units identified by the change in continuous variables ($Q_{i,j}$ and $W_{i,j}$),and (d) complete process flowsheet equivalent to the block representation (Reprinted with permission from [90]).

in the grid. Where $i = 1, ..., I$ denotes the rows, $j = 1, ..., J$ denotes the columns. Then, the basic block variables shown in Figure 2.2c-d can be indexed according to the position of the blocks. The connectivity within the superstructure is captured through inter-block streams and jump streams. Inter-block streams can go through all four boundaries surrounding the block and flow in either direction to allow reverse flow. These flows are denoted as $F_{i,j,k}$ in the horizontal direction and as $R_{i,j,k}$ in the vertical direction. Component set $k = 1, ..., K$ includes all the chemical species involved in the system. Jump flows are denoted as $J_{i,j,i',j',k}$ to indicate the flow of component k from block $B_{i,j}$ to $B_{i',j'}$. Each block can take materials from outside the system boundaries via the external feed streams and send out product streams. External feed streams are allowed to enter the superstructure with a flow rate $M_{i,j,k,f}$ indicating the amount of component k in feed stream ($f = 1, .., FS$) entering into the block $B_{i,j}$. Similarly, product streams can be taken out from any block as $P_{i,j,k,ps}$ ($ps = 1, .., PS$). $Q^h_{i,j}$ and $Q^c_{i,j}$ represent the external heating and cooling for block $B_{i,j}$, respectively. Let $z^{feed}_{i,j,f}$ binary variable describe the existence of a feed stream

into block $B_{i,j}$ and equal to 1 if feed stream f is introduced into block $B_{i,j}$ and 0 otherwise. Similarly, let $z_{i,j,p}^{product}$ be 1 if product stream p is withdrawn from block $B_{i,j}$ and 0 otherwise. Let $z_{i,j}^{unF}$, $z_{i,j}^{srF}$ and $z_{i,j}^{crF}$ denote the binary variables for unrestricted, semirestricted and completely restricted boundaries, respectively, in the horizontal direction. Similarly, we can define boundary variables in the vertical direction as $z_{i,j}^{unR}$, $z_{i,j}^{srR}$ and $z_{i,j}^{crR}$. If a boundary is semi-restricted, then the corresponding phenomena and enabling material is selected according to the following binary variables in the horizontal and vertical directions: $z_{i,j,s,m}^{F}$ and $z_{i,j,s,m}^{R}$. s represents the indice for the phenomena set and m represents the indice for the corresponding enabling material set. Let $z_{i,j,c}^{rxn}$ denote the existence of a catalyst material c in block $B_{i,j}$. With these definitions, now, we can describe how the building block result shown in Figure 2.9a can be interpreted as a process flow diagram.

***Step* 1: identify primary operations and nodes (e.g., reactions, separation boundaries, feed nodes, product nodes, and waste nodes) which will form the basis of a process flowsheet.**

From Figure 2.9a, through the indication of binary variables, we see that the blocks $B_{2,1}$ and $B_{3,1}$ are feed blocks ($z_{2,1,f2}^{feed} = 1$, $z_{3,1,f1}^{feed} = 1$, $f1$ and $f2$ designate two feed streams respectively), $B_{3,2}$ is a reactor block ($z_{3,2,c1}^{rx} = 1$, $c1$ refers to a catalyst), the block $B_{2,3}$ is the main product block ($z_{2,3,p1}^{product} = 1$, $p1$ is main product stream), and the block $B_{2,3}$ is a waste product block ($z_{2,3,p2}^{product} = 1$, $p2$ represents waste stream). These blocks are interpreted as nodes in the process flowsheet, except for the reactor block. The reactor block is recognized to be a primary unit operation (Figure 2.9b). As for the boundary assignment, the semi-restricted boundary located at the right side of the block $B_{2,2}$ is selected as a membrane boundary ($z_{2,2}^{srf} = 1$ and $z_{2,2,s=GP,m=M1}^{F} = 1$, ***GP*** is the gas permeation phenomena, $M1$ is the membrane material). Therefore, the associated block $B_{2,2}$ is considered as the retentate side and the block $B_{2,3}$ is considered as the permeate side. Besides, the right-side boundaries of the blocks $B_{2,1}$ and $B_{1,2}$ are specified as completely restricted ($z_{2,1}^{crf} = 1$ and $z_{1,2}^{crf} = 1$) which indicate zero flow.

***Step* 2: identify auxiliary operations (e.g., heaters, coolers, expanders, compressors, mixers, and splitters).**

The existence of any utility consumption would indicate heat exchange units and the existence of work-related energy consumption would require expanders or compressors. For this particular case shown in Figure 2.9, since heat utility variables $Q^c_{1,1}$ and $Q^h_{3,2}$ are nonzero, heat is withdrawn from the system through the block $B_{1,1}$ and heat is introduced through the block $B_{3,2}$. These indicate that there should be one cooler on the permeate side of the membrane and one heater for the reactor inlet. Other types of implicit units include the mixer and splitter units. For instance, the inlet flows for the blocks $B_{1,1}$ and $B_{2,1}$ mix with Feed2 and Feed1 respectively, which indicate the existence of Mixer1 and Mixer2. Based on this, we obtain Figure 2.9c. While placing the heaters and coolers based on block duty variables, we assume that the heat is supplied to the inlet stream that has the highest temperature difference between the block and the stream temperature itself as this will result in heat exchangers with less area.

***Step* 3: identify the connectivity between operations to complete the flowsheet.**

Whenever the streams between the nodes are activated, the stream connection can be established between them. For example, Feed1 is mixed with the recycle stream and preheated before being fed into the Reactor, where the stream connection can be built between Feed1 and Heater and between Heater and the Reactor. The outlet flow is split into two streams, one withdrawn as waste from the system and the other entering the retentate side of membrane. Hence, the connection between the Reactor and waste block as well as the one between the Reactor and the membrane can be recognized. By starting from the feed streams and following the flow direction around each unit, we can identify all the nonzero flows and build the explicit connections. For the illustrative example, the classical representation of the given process is shown in Figure 2.9d.

This concludes the discussion on the building block representation. In the next chapter, a generic Mixed Integer Nonlinear Optimization (MINLP) model is provided describing this building block superstructure. This MINLP model can be utilized for automatically generating flowsheet variants with binary variables determining the position of active phenomena within the superstructure. Furthermore, through fixing the position of several phenomena in a specific configuration, as we have shown for reactive distillation and a flowsheet example in Figures 2.6 and 2.7, a fixed

number of alternatives can be considered which results in a generic superstructure-based method for process synthesis and intensification.

3. A MIXED INTEGER NONLINEAR OPTIMIZATION MODEL FOR SYSTEMATIC PROCESS INTENSIFICATION USING BUILDING BLOCK SUPERSTRUCTURE*

In this section, a mathematical foundation is proposed for the building block-based representation of chemical processes. We first start with providing a problem statement for the systematic process intensification problem.

3.1 Problem Statement for Systematic Process Intensification

The systematic process intensification problem is stated as follows. Given a set $FS = \{f|f = 1,,|FS|\}$ of available raw materials or feed streams with maximum availability, F_f^{feed}, a set $K = \{k|k = 1,,|K|\}$ of chemical species, a set $RX = \{r|r = 1,.,|RX|\}$ of plausible chemistry (reactions) and a set of enabling materials for separation, conversion and/or storage, find an optimal intensified process that would produce a set $PS = \{p|p = 1,,|PS|\}$ of products with demands D_p, and wastes that meet certain industrial and/or environmental specifications. The industrial specifications may include minimum product purity and minimum recovery of important materials, while the environmental specifications may include maximum allowable discharge and maximum concentrations of hazardous chemicals. Our goal is to systematically achieve process intensification by optimizing a desired objective or a combination of objectives (e.g., maximum product yield, minimum energy consumption, maximum profit, etc.).

Each feed has a known chemical composition given by $y_{k,f}^{feed}$. The enabling materials, which are considered for systematic process intensification, may include among others a set $CAT = \{c|c = cat1, cat2,,|CAT|\}$ of catalysts, a set $ABS = \{abs|abs = abs1, abs2,,|ABS|\}$ of solvents/absorbents, a set $MEM = \{mem|mem = gasmem, liqmem, pervmem,,|MEM|\}$ of

*Parts of this chapter were adapted with permission from (S. E. Demirel, J. Li, and M. M. F. Hasan, "Systematic process intensification using building blocks," Computers & Chemical Engineering, vol. 105, pp. 2 - 38, 2017.) Elsevier, from (S. E. Demirel, J. Li and M. M. F. Hasan, "A general framework for process synthesis, integration, and intensification," Industrial & Engineering Chemistry Research," vol. 58, no. 15, pp. 5950 - 5967, 2019.) Copyright (2019) American Chemical Society, and from (J. Li, S. E. Demirel, and M. M. F. Hasan, "Process synthesis using a block superstructure with automated flowsheet generation and optimization," AIChE Journal, vol. 64, no. 8, pp. 3082 - 3100, 2018.) Copyright (2018) John Wiley & Sons, Inc.

membrane materials, and a set $EXT = \{ext|ext = ext1, ext2, , |EXT|\}$ of extractant materials. The mass transfer-related parameters such as permeance, mass transfer coefficients, etc., are also provided. Overall, the set for all the separation materials is defined as $m = \{ABS, MEM, EXT\}$. Note that, we can extend this set to include many other material types, such as adsorbents, storage materials, composites, mixed-materials and so on. Lastly, the temperature and pressure at any place within the process are not allowed to exceed T^{max} and P^{max}, and are not allowed to fall behind T^{min} and P^{min}, respectively. These constraints could arise from safety, operational limits and/or available hot/cold utility streams.

3.2 Mixed Integer Nonlinear Optimization Model

Based on the new representation of process superstructure using building blocks, we present a general MINLP model for the systematic intensification of chemical processes. Within the superstructure, a block is denoted by its position in the superstructure as block $B_{i,j}$ where $i = \{i|i = 1, , |I|\}$ and $j = \{j|j = 1, , |J|\}$ represent row and column indices, respectively (See Figure 3.1). Hence, a total of $I \times J$ blocks are considered. The general form of the MINLP model can be written as follows:

$$
\begin{aligned}
\text{max/min} \quad & f(x, z) \\
\textit{s.t.} \quad & h_t(x) = 0 \quad \forall t \in \{1, ..., T\} \\
& g_w(x) = 0 \quad \forall w \in \{1, ..., W\} \\
& g_q(z) = 0 \quad \forall q \in \{1, ..., Q\} \\
& g_l(x, z) = 0 \quad \forall l \in \{1, ..., L\} \\
& x^L \leq x \leq x^U, x \in \mathbb{R}^N, y \in \{0, 1\}^M
\end{aligned}
$$

The model includes formulations at the block, boundary and phenomena levels, where x represents the continuous mass and energy flow variables, and z represents the binary variables used for material, task and phenomena selections. The objective function which is represented by $f(x, z)$

can be any intensification target related to the economics, energy and/or environmental impact of the innovative process solutions. A description of different intensification objectives is provided in the latter sections. $h_t(x) = 0$ represents both linear and nonlinear constraints describing mass and energy balances, thermodynamic and kinetic models and other equalities. The model has three types of inequalities. Firstly, $g_w(x) \leq 0$ represents process specifications (e.g., minimum product purity, recovery, waste, etc.) that must be satisfied. These constraints are formulated based on continuous variables alone. Secondly, $g_q(z) \leq 0$ represents constraints used to assign materials, tasks and phenomena to each block and boundary in the superstructure, which can be formulated using binary variables only. Thirdly, $g_l(x, z) \leq 0$ represents logical constraints which enforce the relationships between continuous and discrete decisions. In what follows, we describe the complete MINLP model formulation.

3.2.1 Block Formulation

Steady state material and energy balances are ensured for each block. Additionally, the directions of the flow streams are considered. Each block allows transfer of component k to and from its neighboring blocks. Each block can have entering and outgoing streams in both horizontal and vertical directions. $F_{i,j,k}$ and $R_{i,j,k}$ represent the mass flow in the horizontal and vertical direction, respectively. A positive $F_{i,j,k}$ denotes the mass flow rate of component k from block $B_{i,j}$ to $B_{i,j+1}$. A negative $F_{i,j,k}$ would indicate that the mass is transferred in the opposite direction, i.e., from block $B_{i,j+1}$ to $B_{i,j}$. Similarly, a positive $R_{i,j,k}$ denotes the mass transfer in the vertical direction between block $B_{i,j}$ and $B_{i+1,j}$. In addition to inter-block mass and heat transfer, we also have mass and heat conversions in each block. We use $G_{i,j,k}$ to denote the amount of component k produced/consumed within block $B_{i,j}$ due to reaction, if any. Positive values indicate generation and negative values indicate consumption. Furthermore, we provide an option to either provide or take away heat from each block through the variable $Q_{i,j}$. When multiple streams enter a block, pressure of these streams should be the same. Therefore, we do not define pressure for every stream, but define it for every block. Pressure of block $B_{i,j}$ is denoted as $P_{i,j}$. Defining pressure for each block rather than for each stream decreases the number of variables. Similarly, we denote

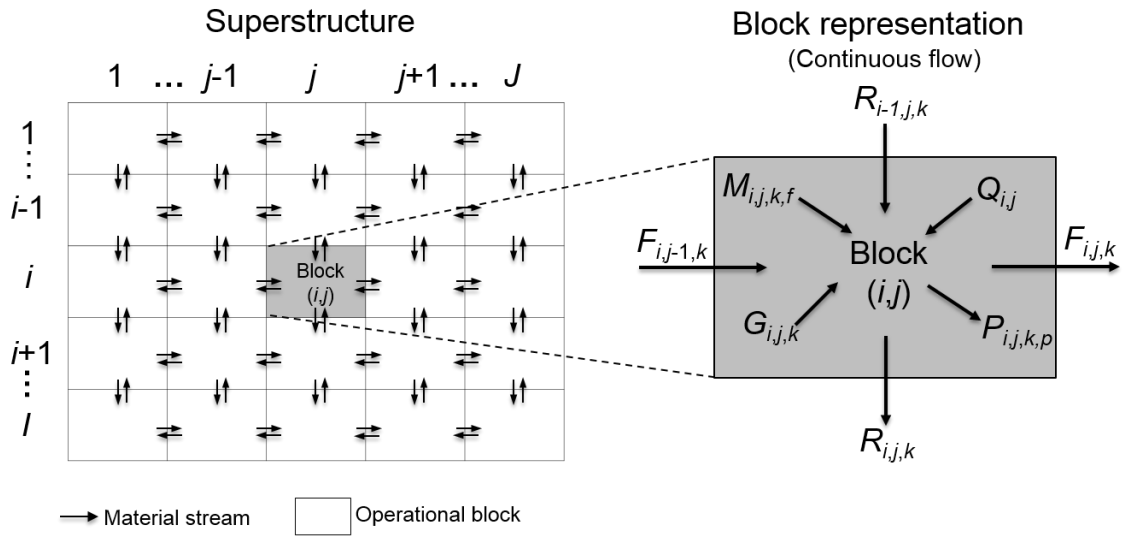

Figure 3.1: Building block superstructure variables. The superstructure is an ensemble of blocks, where each block is associated with inter-block and intra-block transfer of mass and energy (Adapted with permission from [90]).

the temperature of each block as $T_{i,j}$. Temperature and pressure of a stream will be determined by the temperature and pressure of the source block. The temperature and pressure also determine the phase of the block and the phase of the leaving streams.

Each block in our superstructure can act as a feed block to introduce raw materials into the process. It can also act as a product block to withdraw products from the process. The locations of both the feeds and products are allowed to vary. Let f and p denote the indice of feeds and products, respectively. A feed f can enter into the process at any block $B_{i,j}$. This is enabled by $M_{i,j,k,f}$ which represents the flow rate of component k in feed stream f which is to be introduced into block $B_{i,j}$. Similarly, $P_{i,j,k,p}$ represents the flow rate of component k in product stream p withdrawn from block $B_{i,j}$.

3.2.1.1 Block Material Balances

We ensure that the following steady-state molar balance for each component that enters and exits a block $B_{i,j}$ holds:

$$\left\{\begin{array}{c}\text{Amount of}\\ \text{component } k\\ \text{entering}\\ \text{block } B_{i,j}\end{array}\right\} - \left\{\begin{array}{c}\text{Amount of}\\ \text{component } k\\ \text{leaving}\\ \text{block } B_{i,j}\end{array}\right\} + \left\{\begin{array}{c}\text{Amount of}\\ \text{component } k\\ \text{produced or}\\ \text{consumed due}\\ \text{to reaction within}\\ \text{block } B_{i,j}\end{array}\right\} = 0, \qquad \begin{array}{l} i \in I,\\ j \in J,\\ k \in K\end{array}$$

Therefore, we have

$$F_{i,j-1,k} - F_{i,j,k} + R_{i-1,j,k} - R_{i,j,k} + G_{i,j,k} + \sum_{f \in FS} M_{i,j,k,f} - \sum_{p \in PS} P_{i,j,k,p} = 0, \ \forall\, i, j, k \tag{3.1}$$

$$F_{i,j=J,k} = R_{i=I,j,k} = 0. \tag{3.2}$$

The flow variables in Equation 3.2 are fixed to zero because we do not allow any flow at the superstructure boundaries. Similarly, all the variables associated with boundaries can be fixed to be zero. For simplicity, we will not specifically mention all of these fixed variables in the remainder of the discussion but if a variable is defined for the block boundaries, they are not needed at the superstructure borders.

We impose an upper bound on the total supply of feed f, which is F_f^{feed}. This total supply is available to be utilized either in single or multiple blocks. Let $z_{i,j,f}^{feedfrac}$ denote the fraction of the external feed f to be fed to block $B_{i,j}$. Therefore,

$$M_{i,j,k,f} = F_f^{feed} y_{k,f}^{feed} z_{i,j,f}^{feedfrac}, \ \forall\, i, j, k, f \tag{3.3}$$

$$0 \leq \sum_{i \in I} \sum_{j \in J} z_{i,j,f}^{feedfrac} \leq 1, \ \forall \ f \tag{3.4}$$

To satisfy the product specifications, such as the minimum purity and maximum impurity levels, we impose the following constraints on the final component product flow.

$$y_{k,p}^{MIN,prod} \sum_{k' \in K} P_{i,j,k',p} \leq P_{i,j,k,p} \leq y_{k,p}^{MAX,prod} \sum_{k' \in K} P_{i,j,k',p}, \ \forall \ i,j, \ (k,p) \in \ kp \tag{3.5}$$

where, the parameters $y_{k,p}^{MIN,prod}$ and $y_{k,p}^{MAX,prod}$ denote the minimum and maximum concentration (purity) specifications, respectively, for component k in product p.

Similarly, there can be specifications on recovery of a component k from feed f through product stream p. Let KFP be the set which specifies this relationship among components, feeds and products for recovery purposes. In order to realize recovery specifications, we use the following constraint:

$$\sum_{i \in I} \sum_{j \in J} P_{i,j,k,p} \ \geq \ Re_{k,f,p}^{min} \sum_{i \in I} \sum_{j \in J} M_{i,j,k,f}, \ \ (k,f,p) \ \in \ KFP \tag{3.6}$$

where $Re_{k,f,p}^{min}$ is the known minimum fraction of component k which must be recovered from feed f through product stream p. Furthermore, if there is a demand constraint on product p, then we impose

$$\sum_{i \in I} \sum_{j \in J} \sum_{k \in K} P_{i,j,k,p} \ \geq \ D_p, \ \ p \in PS \tag{3.7}$$

Also, there can be some limitations on the relative amounts of the components for particular product $p \in P^* \subseteq PS$ stream, e.g. specific ratio of H_2 and CO in a product stream if the product is syngas. To satisfy this, we include the following constraint.

$$P_{i,j,k,p} \ \geq \ \sum_{k' \in K} \alpha_{k,k',p} P_{i,j,k,p}, \quad \forall i,j, \ p \in P^* \tag{3.8}$$

where, $\alpha_{k,k',p}$ is the parameter which is set as appropriate to ensure the desired flow rate ratio.

To increase connectivity within the superstructure, we also consider jump streams. We denote these streams as $J_{i,j,i'j',k}$ where $i = \{1,..,I\}$, $j = \{1,..,J\}$, $i' = \{1,..,I\}$, $j' = \{1,..,J\}$ and $k \in$

K. This represents flow of component k from block $B_{i,j}$ to $B_{i',j'}$. These streams are mainly used to enable connections between non-adjacent blocks. While these streams can be allowed between all the blocks within the grid, this would increase the model size and symmetry significantly. Hence, they are used only when necessary. With this, Eq. 3.1 can be modified as follows:

$$F_{i,j-1,k} + R_{i-1,j,k} - F_{i,j,k} - R_{i,j,k} + G_{i,j,k} + \sum_{f \in FS} M_{i,j,k,f} - \sum_{p \in PS} P_{i,j,k,p} + \sum_{(i',j') \in LN} J_{i',j',i,j,k} - \sum_{(i',j') \in LN} J_{i,j,i',j',k} = 0, \quad \forall\, i, j, k \tag{3.9}$$

LN describes the active jump stream connections. To restrict the number of connections, this set can be modified to ensure only a limited number of elements. This is also highly useful in representing intensified or traditional flowsheets and superstructures with pre-specified connections. Connectivity can be built via these streams without using interblock streams for material transfer. This provides an additional flexibility in using the building block-based approach as a generic superstructure-based framework for process synthesis and intensification.

3.2.1.2 Flow Directions

We use the following convention for flow directions. $F_{i,j,k}$ is positive when the flow direction is from left to right, *i.e.* from $B_{i,j}$ to $B_{i,j+1}$, and it is negative when the flow direction is from right to left, *i.e.* from $B_{i,j+1}$ to $B_{i,j}$. Similarly, $R_{i,j,k}$ is positive when the flow direction is from top to bottom, *i.e.* from $B_{i,j}$ to $B_{i,j+1}$, and it is negative when the flow direction is from bottom to top, *i.e.* from $B_{i+1,j}$ to $B_{i,j}$. To determine the flow direction, we define and use the following two binary variables:

$$z^{Fplus}_{i,j,k} = \begin{cases} 1 & \text{if } F_{i,j,k} \text{ is from left to right} \\ 0 & \text{otherwise} \end{cases}$$

$$z^{Rplus}_{i,j,k} = \begin{cases} 1 & \text{if } R_{i,j,k} \text{ is from left to right} \\ 0 & \text{otherwise} \end{cases}$$

While we allow both forward and reverse flows, a stream can have only one direction. To this end, let $FP_{i,j,k} \geq 0$ (vs. $FN_{i,j,k} \geq 0$) be the variable which explicitly accounts for the flow in the direction from left to right (vs. right to left). Then, we can model the overall horizontal flow as follows:

$$F_{i,j,k} = FP_{i,j,k} - FN_{i,j,k}, \quad \forall i, j, k \tag{3.10}$$

$$FP_{i,j,k} \leq FU_{i,j,k}\, z_{i,j,k}^{Fplus}, \quad \forall i, j, k \tag{3.11}$$

$$FN_{i,j,k} \leq FU_{i,j,k} \left(1 - z_{i,j,k}^{Fplus}\right), \quad \forall i, j, k \tag{3.12}$$

This unidirectional flow requirement can be relaxed for certain cases in which different components can move in separate directions, such as in a phase equilibrium where components with different equilibrium coefficients can move in opposite directions at the same time.

Similarly, we define $RP_{i,j,k} \geq 0$ and $RN_{i,j,k} \geq 0$ such that unidirectional flow is confirmed in the vertical direction by the following:

$$R_{i,j,k} = RP_{i,j,k} - RN_{i,j,k}, \quad \forall i, j, k \tag{3.13}$$

$$RP_{i,j,k} \leq RU_{i,j,k}\, z_{i,j,k}^{Rplus}, \quad \forall i, j, k \tag{3.14}$$

$$RN_{i,j,k} \leq RU_{i,j,k} \left(1 - z_{i,j,k}^{Rplus}\right), \quad \forall i, j, k \tag{3.15}$$

We also keep track of the total incoming flows for block $B_{i,j}$. Let $\phi_{i,j,k}$ be the total amount of component k entering into block $B_{i,j}$. This implies

$$\phi_{i,j,k} = FP_{i,j-1,k} + FN_{i,j,k} + RP_{i-1,j,k} + RN_{i,j,k} + \sum_{f} M_{i,j,k,f} + \sum_{(i',j') \in LN} J_{i',j',i,j,k}, \ \forall i, j, k \tag{3.16}$$

3.2.1.3 Energy Balances

The following steady-state energy balances are ensured for each block:

$$\left\{\begin{array}{c}\text{Energy into}\\ \text{block } B_{i,j}\\ \text{with entering}\\ \text{streams}\end{array}\right\} - \left\{\begin{array}{c}\text{Energy}\\ \text{leaving}\\ \text{block } B_{i,j}\\ \text{via outgoing}\\ \text{streams}\end{array}\right\} + \left\{\begin{array}{c}\text{Energy}\\ \text{into or out}\\ \text{from block}\\ B_{i,j} \text{ as heat}\\ \text{by utility}\\ \text{streams}\end{array}\right\} + \left\{\begin{array}{c}\text{Energy}\\ \text{into or out}\\ \text{from block}\\ B_{i,j} \text{ as work}\end{array}\right\} = 0 \quad \begin{array}{l} i \in I,\\ j \in J\end{array}$$

In addition to stream enthalpies, other forms of energy, such as the work consumed or produced by compression or expansion and the heat introduced by heating or cooling, are incorporated as separate variables. The energy balance for block $B_{i,j}$ is formulated as follows (without jump streams):

$$EF_{i,j-1} - EF_{i,j} + ER_{i-1,j} - ER_{i,j} + EM_{i,j} - EP_{i,j} + Q_{i,j} + W_{i,j} + EG_{i,j} + \Delta H_{i,j}^{lat} = 0, \quad \forall i, j \tag{3.17}$$

where, $EF_{i,j}$ is the enthalpy carried by the overall horizontal flow, $ER_{i,j}$ is the enthalpy carried by the overall vertical flow for block $B_{i,j}$, $EM_{i,j}$ denotes the total enthalpy introduced by the feed streams, $EP_{i,j}$ represents the total enthalpy taken away by the product streams from block $B_{i,j}$, $Q_{i,j}$ is the amount of heat introduced or withdrawn from block $B_{i,j}$ by the utility streams, $W_{i,j}$ is the work related corresponding to a compression or expansion operation, $EG_{i,j}$ is the heat of reaction if reactions occur within the block, and $\Delta H_{i,j}^{lat}$ is the contribution from latent heat if there is any change in phase. Graphically, these variables used in the energy balance are shown in Figure 3.2 for block $B_{i,j}$. Following Eq. 3.2, we can fix $EF_{i,j=J} = 0$ and $ER_{i=I,j} = 0$.

The enthalpy carried by a material stream is dependent on the flow rate, temperature, pressure and the composition of the stream. Different thermodynamic properties can be used to calculate these enthalpy terms. Here, the most simplistic approach is provided by assuming ideal thermo-

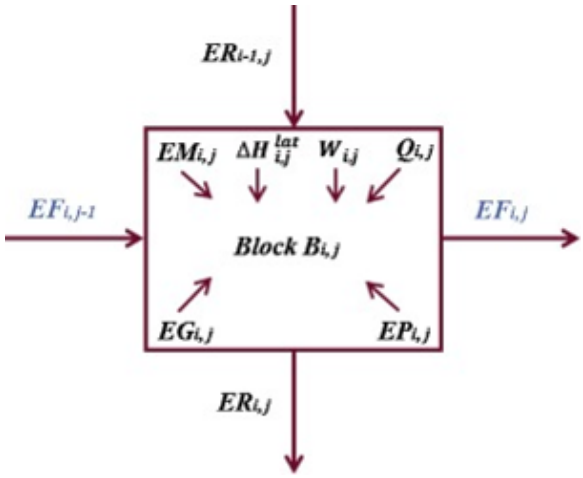

Figure 3.2: Energy balance variables for each block. For each block, enthalpy of the streams in horizontal direction are designated by $EF_{i,j}$ and in vertical direction as $ER_{i,j}$ (Jumps stream enthalpies are not shown). Enthalpy coming in by feed streams is defined as $EM_{i,j}$ and enthalpy going out by product streams is designated as $EP_{i,j}$. Heat supplied or removed by reaction and utilities are designated with $EG_{i,j}$ and $Q_{i,j}$, respectively (Reprinted with permission from [90]).

dynamics with constant heat capacities. More detailed alternatives can be found in the Appendix A.2. The flow rate of component k is represented by $FP_{i,j,k}$, $FN_{i,j,k}$, $RP_{i,j,k}$ or $RN_{i,j,k}$ depending on the direction of the flow. The temperature of a stream is equal to the temperature of the block from which the flow is leaving. For $FP_{i,j,k}$, which is the flow rate of component k from block $B_{i,j}$ to $B_{i,j+1}$, temperature is equal to temperature of block $B_{i,j}$, *i.e.*, $T_{i,j}$. For $FN_{i,j,k}$, however, this temperature is $T_{i,j+1}$. Accordingly, enthalpies are calculated as follows:

$$EF_{i,j} = \sum_k \Big(FP_{i,j,k} \left[Cp_k(T_{i,j} - T_k^{ref}) \right] - FN_{i,j,k} \left[Cp_k(T_{i,j+1} - T_k^{ref}) \right] \Big), \quad \forall i,j \tag{3.18}$$

$$ER_{i,j} = \sum_k \Big(RP_{i,j,k} \left[Cp_k(T_{i,j} - T_k^{ref}) \right] - RN_{i,j,k} \left[Cp_k(T_{i+1,j} - T_k^{ref}) \right] \Big), \quad \forall i,j \tag{3.19}$$

$$EM_{i,j} = \sum_k \sum_f M_{i,j,k,f} \Big(Cp_k \left(T_{i,j} - T_k^{ref} \right) \Big), \quad \forall i,j \tag{3.20}$$

$$EP_{i,j} = \sum_k \sum_p P_{i,j,k,p} \Big(Cp_k \left(T_{i,j} - T_k^{ref} \right) \Big), \quad \forall i,j \tag{3.21}$$

where, Cp_k is the heat capacity of component k, and T_k^{ref} is the reference state temperature for

component k. Heat withdrawn or heat supplied by utility streams is represented as follows:

$$Q_{i,j} = \quad Q^h_{i,j} - Q^c_{i,j}, \quad \forall i,j \tag{3.22}$$

where, $Q^h_{i,j} \geq 0$ is the variable for the heat introduced into block $B_{i,j}$ through hot utility streams, and $Q^c_{i,j} \geq 0$ is the variable for the heat withdrawn form block $B_{i,j}$ via the cold utility streams.

When the pressure of two neighboring blocks are not the same and there is a stream connection between those two blocks, work related with the transfer of this stream into a different pressure should be accounted for. For instance, if the stream is leaving a low pressure block and entering into a higher pressure block, then the energy required for compressing this stream should be calculated. However, the only case when the work calculations should be performed is in the case of an unrestricted boundary separating two blocks with different pressures. There is no need to account energy related phenomena (*i.e.* expansion or compression) across a semi-restricted boundary. Similar to the heat calculations, work added/extracted from a block $B_{i,j}$ is dissected into $W^{com}_{i,j}$ and $W^{exp}_{i,j}$:

$$W_{i,j} = \quad W^{com}_{i,j} - W^{exp}_{i,j}, \quad \forall i,j \tag{3.23}$$

where $W^{com}_{i,j}$ is the work energy added into block $B_{i,j}$, and $W^{exp}_{i,j}$ is the work energy removed from block $B_{i,j}$. Both are defined as positive variables. Further details of the work calculations are provided in Appendix. Moreover, the calculations for $EG_{i,j}$ involve reaction phenomena and are discussed in Section 3.2.3.1. If there is phase change in the superstructure, then $\Delta H^{lat}_{i,j}$ needs to be considered and its formulation is provided in Section 3.2.1.5. More details on the energy balances can be found in the Appendix A.

3.2.1.4 Task Assignments and Logical Relationships

Assigning tasks to each block in the superstructure is accomplished by the use of logical constraints. A block can be a feed block, product block and/or a reaction block. To this end, we define

the following binary variables:

$$z_{i,j,f}^{feed} = \begin{cases} 1 & \text{if feed stream } f \text{ is introduced into block } B_{i,j} \\ 0 & \text{otherwise} \end{cases}$$

$$z_{i,j,p}^{product} = \begin{cases} 1 & \text{if product stream } p \text{ is withdrawn from block } B_{i,j} \\ 0 & \text{otherwise} \end{cases}$$

$$z_{i,j,c}^{rxn} = \begin{cases} 1 & \text{if catalyst } c \text{ is positioned in block } B_{i,j} \\ 0 & \text{otherwise} \end{cases}$$

If a feed is introduced into block block $B_{i,j}$, then that block should be a feed block. Hence,

$$z_{i,j,f}^{feedfrac} \leq z_{i,j,f}^{feed}, \quad \forall i, j, f \tag{3.24}$$

Similarly, the following logical relationship is used to define the product binary variable:

$$\sum_{k} P_{i,j,k,p} \leq M^{out}\, z_{i,j,p}^{product}, \quad \forall i, j, p \tag{3.25}$$

where, M^{out} is the maximum product flow rate that can be withdrawn from a block.

Relations for reaction binary variable are given in the reaction section. Yet, as there can be only one catalyst material for one block, we need to restrict the number of catalysts that can be present in block $B_{i,j}$. Therefore, we have

$$\sum_{c \in CAT \setminus \{null\}} z_{i,j,c}^{rxn} \leq 1, \quad \forall i, j \tag{3.26}$$

Note that the above relation excludes the homogeneous reactions which are depicted within the $null$ set.

3.2.1.5 Phase Assignments

Each block has only one phase which is determined based on thermodynamics. Following binary variable is used to determine the phase of a block.

$$z_{i,j}^{phase} = \begin{cases} 1 & \text{if } B_{i,j} \text{ is in vapor/gas phase} \\ 0 & \text{otherwise} \end{cases}$$

When $z_{i,j}^{phease}$ is 1, block is in gas/vapor phase. Separate binary variables can be also defined for different phases. For instance, if heterogeneous liquid mixtures are present, then separate binary variables can be defined for different liquid phases. When only liquid and gas mixtures are present within the process conditions, then no other binary variable is needed and $z_{i,j}^{phease}$ is 0 for the liquid phase block.

For each block, phase can be assigned in accordance with the pressure, temperature and composition of the block. We present an equation-oriented approach to model phase rigorously for each block based on bubble and dew points. This, along with the necessary considerations for phase assignment, is presented in Appendix A.1.

If a block is a product block, then the block phase should be in accordance with the product phase requirements. Therefore,

$$z_{i,j}^{phase} \geq z_{p}^{phaseprod} - (1 - z_{i,j,p}^{product}), \quad \forall i, j, p \tag{3.27}$$

$$z_{i,j}^{phase} \leq z_{p}^{phaseprod} + (1 - z_{i,j,p}^{product}), \quad \forall i, j, p \tag{3.28}$$

where $z_{p}^{phaseprod}$ is a 0-1 parameter defining the known phase of product stream p. Furthermore, if there is phase change in the process, latent heats should be also considered. We consider that the phase of a stream is determined by the phase of the source block. Accordingly, $\Delta H_{i,j}^{lat}$ in equation

3.17 is calculated as follows:

$$\Delta H_{i,j}^{lat} = \sum_{k \in K} \Delta H_k^{vap} \times \Big\{ FP_{i,j-1,k} \left(z_{i,j-1}^{phase} - z_{i,j}^{phase} \right) + FN_{i,j,k} \left(z_{i,j+1}^{phase} - z_{i,j}^{phase} \right) + RP_{i-1,j,k} \left(z_{i-1,j}^{phase} - z_{i,j}^{phase} \right) + RN_{i,j,k} \left(z_{i+1,j}^{phase} - z_{i,j}^{phase} \right) + \sum_{f} M_{i,j,k,f} \left(z_f^{phasefeed} - z_{i,j}^{phase} \right) \Big\}, \quad \forall i, j \tag{3.29}$$

where ΔH_k^{vap} is the enthalpy of vaporization of component *k* at the reference temperature. If a stream leaves a liquid block and enters into a gas block, then its latent heat term becomes negative indicating that the latent heat should be added to the destination block in order to compensate for the change in latent heat of the stream. Similarly, if a stream leaves a gas block and enters into a liquid block, then its latent heat term becomes positive indicating that the latent heat should be removed from the destination block in order to compensate for the change in latent heat of the stream. If the phase of the both destination and source blocks are the same, then the associated change in latent heat becomes zero. The bilinear terms within this formulation can be exactly reformulated using McCormick relaxations. This formulation combined with the one given in Section 3.2.1.3 assumes that the heat capacity remains constant with change in phase. More rigorous energy balances are provided in Appendix A.2.

3.2.1.6 Multi-block Material and Energy Balances

In phenomena-based description of building blocks, when two neighboring blocks in the superstructure are set to be in interaction through equilibrium-based models, e.g. vapor liquid equilibrium, then the amount of flow through semirestricted boundary is determined through the equilibrium conditions and overall material balance around each neighboring building block. However, if no rate-based mass transfer model is considered, simulating the operation of such phenomena might not require to know the exact flow rate through the semi-restricted boundary, and satisfaction of the equilibrium conditions on the outlet streams from the two blocks is sufficient. In such cases, elimination of the semi-restricted streams and related enthalpy terms reduces the model size. Furthermore, if the mass and energy transfer at the phase interphase is not rigorously accounted for

with a non-equilibrium model and energy transfer from conduction at the interphase is not considered, then $Q^h_{i,j}$ or $Q^c_{i,j}$ might be non-zero for both phases even if the overall operation is adiabatic [140, 141]. As a remedy, on top of material and energy balances around each block, a second set of material and energy balances can be written around each horizontal and vertical pair of blocks. Material balance around a horizontal building block pair can be written as below:

$$\begin{aligned} & F_{i,j-1,k} + R_{i-1,j,k} - R_{i,j,k} - F_{i,j+1,k} + R_{i-1,j+1,k} - R_{i,j+1,k} + G_{i,j,k} + \sum_{f \in FS} M_{i,j,k,f} \\ & - \sum_{p \in PS} P_{i,j,k,p} + G_{i,j+1,k} + \sum_{f \in FS} M_{i,j+1,k,f} - \sum_{p \in PS} P_{i,j+1,k,p} \\ & + \sum_{(i',j') \in LN} J_{i',j',i,j,k} - \sum_{(i',j') \in LN} J_{i,j,i',j',k} \\ & + \sum_{(i',j') \in LN} J_{i',j',i,j+1,k} - \sum_{(i',j') \in LN} J_{i,j+1,i',j',k} = 0, \quad \forall\, i,j,k \end{aligned} \tag{3.30}$$

A similar constraint can be also written in the vertical direction. A more detailed discussion on these constraints along with multiblock energy balances is provided in Appendix A.4.

3.2.2 Block Boundary Assignments

Each boundary between two neighboring blocks can be unrestricted, semi-restricted or completely restricted. We define the following binary variables to select the type of the boundary:

$$z^{unF}_{i,j} = \begin{cases} 1 & \text{if boundary between } B_{i,j} \text{ and } B_{i,j+1} \text{ is unrestricted} \\ 0 & \text{otherwise} \end{cases}$$

$$z^{unR}_{i,j} = \begin{cases} 1 & \text{if boundary between } B_{i,j} \text{ and } B_{i+1,j} \text{ is unrestricted} \\ 0 & \text{otherwise} \end{cases}$$

$$z^{srF}_{i,j} = \begin{cases} 1 & \text{if boundary between } B_{i,j} \text{ and } B_{i,j+1} \text{ is semi-restricted} \\ 0 & \text{otherwise} \end{cases}$$

$$z_{i,j}^{srR} = \begin{cases} 1 & \text{if boundary between } B_{i,j} \text{ and } B_{i+1,j} \text{ is semi-restricted} \\ 0 & \text{otherwise} \end{cases}$$

$$z_{i,j}^{crF} = \begin{cases} 1 & \text{if boundary between } B_{i,j} \text{ and } B_{i,j+1} \text{ is completely restricted} \\ 0 & \text{otherwise} \end{cases}$$

$$z_{i,j}^{crR} = \begin{cases} 1 & \text{if boundary between } B_{i,j} \text{ and } B_{i+1,j} \text{ is completely restricted} \\ 0 & \text{otherwise} \end{cases}$$

As blocks share boundaries with the neighboring blocks in both horizontal and vertical direction, two different binary variables are defined for each type. For the boundary between block $B_{i,j}$ and $B_{i,j+1}$, we define $z_{i,j}^{unF}$, $z_{i,j}^{srF}$ and $z_{i,j}^{crF}$ to select whether the boundary is unrestricted, semi-restricted and completely restricted, respectively. Similarly, for the boundary between block $B_{i,j}$ and $B_{i+1,j}$, we define $z_{i,j}^{unR}$, $z_{i,j}^{srR}$ and $z_{i,j}^{crR}$ to select whether the boundary is unrestricted, semi-restricted and completely restricted, respectively. Only one of these boundary types can be active for each boundary. Therefore,

$$z_{i,j}^{unF} + \ z_{i,j}^{srF} + \ z_{i,j}^{crF} = 1, \quad \forall i, j \tag{3.31}$$

$$z_{i,j}^{unR} + \ z_{i,j}^{srR} + \ z_{i,j}^{crR} = 1, \quad \forall i, j \tag{3.32}$$

An unrestricted flow would be observed in the case of a splitter where the outlet composition of each leaving stream should be the same. We define $y_{i,j,k}$ to indicate the composition of component k in block $B_{i,j}$. Therefore, $y_{i,j,k}$ also refers to the composition of all leaving streams (*i.e.*, $FP_{i,j,k}$, $RP_{i,j,k}$, $FN_{i,j-1,k}$, $RN_{i-1,j,k}$) from a block through unrestricted boundaries. This strict relation holds only if the stream is unrestricted, which can be ensured for each interblock stream using big-M constraints as follows:

$$FP_{i,j,k} \leq y_{i,j,k} \sum_{k' \in K} FP_{i,j,k'} + \ FU_{i,j,k} \left(1 - z_{i,j}^{unF}\right), \quad \forall i, j, k \tag{3.33}$$

$$FP_{i,j,k} \geq y_{i,j,k} \sum_{k' \in K} FP_{i,j,k'} - \ FU_{i,j,k} \left(1 - z_{i,j}^{unF}\right), \quad \forall i,j,k \tag{3.34}$$

$$FN_{i,j,k} \leq y_{i,j+1,k} \sum_{k' \in K} FN_{i,j,k'} + \ FU_{i,j,k} \left(1 - z_{i,j}^{unF}\right), \quad \forall i,j,k \tag{3.35}$$

$$FN_{i,j,k} \geq y_{i,j+1,k} \sum_{k' \in K} FN_{i,j,k'} - \ FU_{i,j,k} \left(1 - z_{i,j}^{unF}\right), \quad \forall i,j,k \tag{3.36}$$

$$RP_{i,j,k} \leq y_{i,j,k} \sum_{k' \in K} RP_{i,j,k'} + \ RU_{i,j,k} \left(1 - z_{i,j}^{unR}\right), \quad \forall i,j,k \tag{3.37}$$

$$RP_{i,j,k} \geq y_{i,j,k} \sum_{k' \in K} RP_{i,j,k'} - \ RU_{i,j,k} \left(1 - z_{i,j}^{unR}\right), \quad \forall i,j,k \tag{3.38}$$

$$RN_{i,j,k} \leq y_{i+1,j,k} \sum_{k' \in K} RP_{i,j,k'} + \ RU_{i,j,k} \left(1 - z_{i,j}^{unR}\right), \quad \forall i,j,k \tag{3.39}$$

$$RN_{i,j,k} \geq y_{i+1,j,k} \sum_{k' \in K} RP_{i,j,k'} - \ RU_{i,j,k} \left(1 - z_{i,j}^{unR}\right), \quad \forall i,j,k \tag{3.40}$$

Furthermore, product streams should also have the same composition with the other unrestricted outlet streams. Hence,

$$P_{i,j,k,p} = \ y_{i,j,k} \sum_{k' \in K} P_{i,j,k',p}, \quad \forall i,j,k,p \tag{3.41}$$

The above equation also allows multiple product streams with different flow rates but the same compositions. Similar constraints are also valid for jump outlet streams which have the same composition with their source blocks.

When the block boundary is completely restricted, the flow rate associated with this boundary should be zero. This requirement is satisfied by the following constraints:

$$FL_{i,j,k}(1 - z_{i,j}^{crF}) \leq F_{\ i,j,k} \leq FU_{i,j,k} \left(1 - z_{i,j}^{crF}\right), \quad \forall i,j,k \tag{3.42}$$

$$RL_{i,j,k}(1 - z_{i,j}^{crR}) \leq R_{\ i,j,k} \leq RU_{i,j,k} \left(1 - z_{i,j}^{crR}\right), \quad \forall i,j,k \tag{3.43}$$

A semi-restricted boundary is considered between two neighboring blocks if they represent a separation phenomenon. We discuss the assignment of semi-restricted boundaries in detail in the following section.

3.2.2.1 Stream Energy Balances

In addition to general block energy balances, we can also consider stream energy balances around each stream heater and cooler (Shown in Figure 2.4f). Each stream can be either assigned with a heater or a cooler. For each positive horizontal flow $FP_{i,j,k}$ of block $B_{i,j}$, the inlet and outlet temperature for these units can be denoted as $T_{i,j}$ and $T_{i,j}^{sF}$ respectively. Similarly, in the positive vertical direction, the inlet and outlet temperatures can be denoted as $T_{i,j}$ and $T_{i,j}^{sR}$. Accordingly, heat duties can be determined as follows:

$$Q_{i,j}^{FP,h} - Q_{i,j}^{FP,c} = \sum_{k \in K} FP_{i,j,k} Cp_k (T_{i,j}^{sF} - T_{i,j}) \quad i \in I, j \in J \tag{3.44}$$

$$Q_{i,j}^{RP,h} - Q_{i,j}^{RP,c} = \sum_{k \in K} RP_{i,j,k} Cp_k (T_{i,j}^{sR} - T_{i,j}) \quad i \in I, j \in J \tag{3.45}$$

Similarly, we can denote the following constraints for the streams flowing in the negative direction:

$$Q_{i,j}^{FN,h} - Q_{i,j}^{FN,c} = \sum_{k \in K} FN_{i,j,k} Cp_k (T_{i,j}^{sF} - T_{i,j+1}) \quad i \in I, j \in J \tag{3.46}$$

$$Q_{i,j}^{RN,h} - Q_{i,j}^{RN,c} = \sum_{k \in K} RN_{i,j,k} Cp_k (T_{i,j}^{sR} - T_{i+1,j}) \quad i \in I, j \in J \tag{3.47}$$

Here, the inlet temperature of the stream heaters and coolers are denoted by the source blocks similar to the positive direction streams. Note that, when these stream heaters/coolers are utilized, then stream enthalpy terms also need to be modified to reflect the true temperature. For instance, for block $B_{i,j}$ horizontal inlet streams include $FP_{i,j-1,k}$ and $FN_{i,j,k}$. In the absence of stream heaters and coolers, the enthalpy of these inlet streams are based on $T_{i,j-1}$ (for $FP_{i,j-1,k}$) and $T_{i,j+1}$ (for $FN_{i,j,k}$). However, when the stream heaters and coolers are utilized, then the temperature of these streams become $T_{i,j-1}^{sF}$ (for $FP_{i,j-1,k}$) and $T_{i,j}^{sF}$ (for $FN_{i,j,k}$). The energy balances need to be modified according to these new temperature values. Energy balances when both stream heaters/coolers and compressors are utilized are provided in Li et al. (2018) [139] and Demirel et al. (2019) [51]. In the rest of the discussion, we will not consider any stream heaters or coolers.

3.2.3 Phenomena Formulations

Mixing, heating, cooling and reaction phenomena are represented by a single block. Phenomena that require two blocks are splitting, pressure change, phase dividing and separation. Material and energy balances are sufficient to describe the mixing phenomenon. We assume that the materials coming into a block mix immediately and then participate into the proceding phenomenon. Heating and cooling phenomena are described by the positive values of the continuous variables assigned for determining the cooling and heating requirement (*i.e.* $Q^h_{i,j}$ and $Q^c_{i,j}$).

3.2.3.1 Reaction Phenomena

In this section, how to determine the amount of material generation or consumption through reaction phenomena, *i.e.* $G_{i,j,k}$, is demonstrated. This term is active when there is a reaction within the block and it is equal to zero when there is none. This is determined through the reaction binary variable $z^{rxn}_{i,j,c}$ which is 1 when catalyst material c is positioned within block $B_{i,j}$. For homogeneous reaction systems, we define a dummy or 'null' catalyst and update the catalyst material set as follows: $CAT = \{c|c = null, cat1, cat2, \ldots, |CAT|\}$. $React_{i,j,k,r,c}$ is the amount of component k consumed/or produced by reaction r on catalyst c in block $B_{i,j}$. This is related to the generation term as follows:

$$G_{i,j,k} = \sum_{r,c \in rxc} React_{i,j,k,r,c}, \quad \forall i, j, k \tag{3.48}$$

$G_{i,j,k}$ and $React_{i,j,k,r,c}$ terms can be positive or negative according to the stoichiometric coefficient $\gamma_{r,k}$ of component k. Depending on the reaction system and data availability, stoichiometric, kinetic or equilibrium models can be used to describe the reaction phenomenon. We define subsets $Stoic(r)$, $Kinet(r)$ and $EqRxn(r)$ of set r for stoichiometric, kinetic and equilibrium models, respectively. Regardless of the model type, an extent of reaction term is needed. Let $Cons_{i,j,r}$ denote the extent of reaction. For the kinetic reaction model, this term denotes the rate of the potential reaction r in block $B_{i,j}$ per unit reaction volume or per unit amount of catalyst.

$$Cons_{i,j,r} = ki_r exp\left(-\frac{Ea_r}{RT_{i,j}}\right) \prod_{k' \in kin} f^{rxn}(y_{i,j,k'}, \gamma_{r,k'}, T_{i,j}, P_{i,j}) \quad \forall i, j, r \in Kinet \tag{3.49}$$

Here, ki_r refers to the pre-exponential factor for reaction r, Ea_r indicates activation energy for reaction r and R is the gas constant. $f^{rxn}(y_{i,j,k'}, \gamma_{r,k'}, T_{i,j}, P_{i,j})$ is a function determining the concentration dependence of the rate expression based on the components involved in the reaction $\{k1, .., k\}$ in set $kin(k, r)$. These expressions can be based on power law, LHHW (Langmuir–Hinshelwood–Hougen–Watson) or any other type of kinetics. If reactions depend on molar concentrations, then molar density of the components might be needed and calculated as a function of block composition, temperature and pressure.

For the stoichiometric modeling of the reaction phenomenon, a key reactant is chosen to calculate the reactant and product flow rates. We denote the key reactant using k^*. The total inlet flow rate of this key reactant is divided by its stoichiometric coefficient to calculate the unit amount of reactant fed into a reaction block. In this case, $Cons_{i,j,r}$ is the normalized amount of the key reactant k^* entering block $B_{i,j}$. Then,

$$Cons_{i,j,r} = -\frac{\phi_{i,j,k^*}}{\gamma_{r,k^*}}, \quad \forall i, j, \ (k^*, r) \in kr, \ r \in Stoic \tag{3.50}$$

These extent of reaction terms can be related to the actual amount of consumed/generated based on the activation of the reaction in block $B_{i,j}$ as follows:

$$React_{i,j,k,r,c} = V_{i,j} Conv_{r,c} \gamma_{r,k} ConsR_{i,j,r,c}, \quad \forall i, j, k, \ (r, c) \in rxc \tag{3.51}$$

$$ConsR_{i,j,r,c} = z_{i,j,c}^{rxn} Cons_{i,j,r}, \quad \forall i, j, k, \ (r, c) \in rxc \tag{3.52}$$

where, $V_{i,j}$ refers to the volume or liquid holdup or catalyst weight in block $B_{i,j}$. For the reaction models that are not based on kinetics, these terms can be fixed to one, i.e. $V_{i,j} = 1$. The conversion fraction, $Conv_{r,c}$, of a reaction r for catalyst c is needed for stoichiometric models. For the reaction models that are not based on fixed conversion, this term is taken as one, i.e. $Conv_{r,c} = 1$. $ConsR_{i,j,r,c}$ is the actual amount of component k generated or consumed if the reaction phenomena is activated within the block $B_{i,j}$. The expression shown in equation 3.52

for $ConsR_{i,j,r,c}$ relates the extent of reaction terms to the actual reaction rates if the reaction is activated, i.e. $z^{rxn}_{i,j,c} = 1$. This constraint contains bilinear terms with multiplication of continuous and binary variables. These can be exactly reformulated using a set of linear inequalities based on McCormick relaxations as follows:

$$ConsR_{i,j,r,c} \leq Cons_{i,j,r}\ , \quad \forall i,j,\ (r,c) \in rxc,\ r \in Kinet \cup Stoic \tag{3.53}$$

$$ConsR_{i,j,r,c} \geq Cons_{i,j,r} - Cons^{Up}_{i,j,r,c}\,(1 - z^{rxn}_{i,j,c}), \quad \forall i,j,\ (r,c) \in rxc,\ r \in Kinet \cup Stoic \tag{3.54}$$

$$ConsR_{i,j,r,c} \leq Cons^{Up}_{i,j,r,c}\, z^{rxn}_{i,j,c}, \quad \forall i,j,\ (r,c) \in rxc \tag{3.55}$$

where, the upper bound $Cons^{Up}_{i,j,r,c}$ can be determined as follows for kinetic and stoichiometric reaction models:

$$Cons^{Up}_{r} = ki_r exp\left(-\frac{Ea_r}{T^{max}}\right) \prod_{k' \in kin} f\left(y_{i,j,k'} = 1, \gamma_{r,k'}\right), \quad \forall r \in Kinet \tag{3.56}$$

$$Cons^{Up}_{r} = \sum_{k\ \in kr} \left[\phi^{up}_{i,j,k} / - \gamma_{r,k}\right], \quad \forall r \in Stoic \tag{3.57}$$

Equation 3.56 is the upper bound on kinetic rate expressions based on maximum possible temperature and concentrations. Note that, instead of taking concentration terms equal to 1, bound tightening problems can be solved to determine tighter maximum reaction rates. Equation 3.57 is the upper bound when stoichiometric reactions are considered. Here, $\phi^{up}_{i,j,k}$ denotes the maximum possible flow rate that can enter into block $B_{i,j}$. This term is based on the upper bound on the interblock and external feed streams. As each block has at most four boundaries with two vertical and two horizontal inlets, $\phi^{up}_{i,j,k}$ can be determined based on position of the block within the superstructure. For the inner blocks for which there are a maximum of 4 interblock stream inlets (if no

jump streams are used), this is written as follows:

$$\phi^{up}_{i,j,k} = 2 \times (FU_{i,j,k} + RU_{i,j,k}) + \sum_{f} F^{feed}_{f} y^{feed}_{k,f},\ i \in \{2, ..., I-1\}, j \in \{2, ..., J-1\}, k \in K \tag{3.58}$$

Although this bound can be used for all the blocks, it can be made tighter for the ones near the superstructure boundaries. For instance, for the block positioned on the fist row and column, i.e. $B_{i=1,j=1}$, there can be only two inlet streams apart from the external feed: one from horizontal and one from vertical direction. Accordingly, upper bound for this block can be written as follows:

$$\phi^{up}_{i,j,k} = \ FU_{i,j,k} + RU_{i,j,k} + \ \sum_{f} F^{feed}_{f} y^{feed}_{k,f}, \quad i = 1, j = 1, k \in K$$

Similar constraints can be written for the blocks that are positioned near the boundaries of the superstructure.

In describing the reaction via equilibrium model, extent of reaction is determined through thermodynamic reaction equilibrium and material balance constraints around the block. As the material balance constraints are already covered through equation 3.1, the following constraints are sufficient for describing the equilibrium reaction model:

$$K^{eq}_{i,j,r,c}(T_{i,j}) = \frac{\prod\limits_{k \in Prod_{k,r}} (f(P_{i,j}, y_{i,j,k}, T_{i,j}))^{\gamma_{r,k}}}{\prod\limits_{k \in React_{k,r}} (f(P_{i,j}, y_{i,j,k}, T_{i,j}))^{\gamma_{r,k}}} \quad i \in I, j \in J, (r,c) \in rxc, r \in EqRxn \tag{3.59}$$

where $Prod_{k,r}$ and $React_{k,r}$ relate the reaction products and reactants k with reaction r. $K^{eq}_{i,j,r,c}$ denotes the equilibrium constant for reaction r catalyzed by c in block $B_{i,j}$. While the reaction equilibrium is independent of catalyst and this term does not depend on the catalyst type, it still includes the catalyst indice c. This might be needed if a given set of fixed temperatures are considered for the same equilibrium reaction and each temperature level is described with a different element of set CAT.

With equation 3.59, the component concentrations satisfying the reaction equilibrium is deter-

mined. $ConsR_{i,j,r,c}$ is activated if the reaction is active in block $B_{i,j}$ and it denotes the extent of reaction through Eq. 3.55. With this, amount of generated/consumed for each equilibrium reaction, $React_{i,j,k,r,c}$, can be obtained via equation 3.51 with $V_{i,j} = 1$ and $\gamma_{r,k} = 1$. Note that upper bound on the extent of reaction $ConsR^{up}_{i,j,r,c}$ in Eq. 3.55 can be taken as the maximum amount of material that can enter or leave the block. Another important point is that, if the reverse reaction can be dominant within the given process bounds, then to prevent infeasibility, $ConsR_{i,j,r,c}$ should be defined as a free variable for the equilibrium reaction model and a constraint similar to Eq. 3.55 should be also added to the formulation for the lower bound. Note that variable $Cons_{i,j,r}$ and Eqs. 3.53-3.54 are not needed for the equilibrium reaction model.

If the stream enthalpy terms do not include enthalpy of formation, then enthalpy change due to reaction, $EG_{i,j}$ in equation 3.17, can be described via the following:

$$EG_{i,j} = \sum_{(r,c)\in rxc} \sum_{k\in kr} React_{i,j,k,r,c}\, Q^{rxn}_{r} \quad \forall\, i,j \tag{3.60}$$

where, Q^{rxn}_{r} is the heat of reaction for reaction r based on per unit consumption of key reactant at the reference temperature and set $kr(k,r)$ denotes the key reactant for reaction r. If reaction is exothermic (endothermic), then $EG_{i,j}$ term is positive (negative) indicating that heat is released into (withdrawn from) the block.

As some reactions only occur in liquid or gas phase, phase of the block and the existense of reaction should be described as follows:

$$z^{phase}_{i,j} + z^{rxn}_{i,j,\hat{c}} \leq 1, \quad \forall i,j,\ c = \hat{c} \tag{3.61}$$

$$z^{rxn}_{i,j,\hat{c}} \leq z^{phase}_{i,j}, \quad \forall i,j,\ c = \hat{c} \tag{3.62}$$

while $\hat{c}$ is the catalyst material that has phase restrictions. While the former equation describes phase and catalyst relationships for liquid phase heterogeneous catalysts, latter describes the same relationship for gas phase heterogeneous catalysts. For homogeneous liquid phase reactions, *null*

catalyst set, these constraints become strict equalities meaning that reaction will be active as long as the phase requirement holds:

$$z_{i,j}^{phase} + z_{i,j,c=null}^{rxn} = 1, \quad \forall i, j \tag{3.63}$$

$$z_{i,j,c=null}^{rxn} = z_{i,j}^{phase}, \quad \forall i, j \tag{3.64}$$

There can be also constraints on the operating conditions of the reactions. For instance, adiabatic conditions can be enforced through the following:

$$Q_{i,j}^{h} \leq EU(1 - z_{i,j,c}^{rxn}) \quad \forall i, j, \ c \in AdR \tag{3.65}$$

$$Q_{i,j}^{c} \leq EU(1 - z_{i,j,c}^{rxn}) \quad \forall i, j, \ c \in AdR \tag{3.66}$$

where $AdR(c)$ denotes the catalysts with adiabatic reaction requirements. EU is the upper bound on the amount of energy provided through external utilities.

3.2.3.2 Separation Phenomena

Let $s = \{VL-PC, GL-PC, LL-PC, GP, LP, VP\}$ be the set of all separation phenomena. These separation phenomena are represented by two blocks partitioned by a semi-restricted boundary with or without barrier materials. If no barrier material is assigned to a semi-restricted boundary, then the boundary represents a mass transfer interphase. VL-PC is an example of material-free phenomenon. Membranes on the other hand can be used as barrier materials. In general, any semi-restricted boundary can be characterized based on an associated material. Even when there is no material assigned, we can consider a hypothetical 'null material'. Hence the superset m of materials includes the sets of materials of different types. Therefore, $m = \{null, ABS, EXT, MEM\}$.

Accordingly, the separation phenomena could be modeled with equilibrium-based relations (VL-PC, GL-PC, LL-PC) or rate-based relations (GP, LP, VP). The following subset relating different separation-phenomena s with separation material m are defined: the subset for equilibrium-

based separation phenomena $Equil(s,m) = \{(VL-PC, null), (GL-PC, abs), (LL-PC, ext)\}$ and the subset for rate-based separation phenomena $Rate(s,m) = \{(GP, gasmem), (LP, liqmem), (VP, pervmem)\}$. These are summarized in Table 3.1.

Table 3.1: Modeling, enabling material and boundary types for separation phenomena (Reprinted with permission from [90]).

Separation Phenomena	Semi-restricted Boundary	Modeling Relations	Material
VL-PC	Interphase	Equilibrium-based	Null
GL-PC	Interphase	Equilibrium-based	Absorbent
LL-PC	Interphase	Equilibrium-based	Extractant
GP	Barrier materials	Rate-based	Membrane
LP	Barrier materials	Rate-based	Membrane
VP	Barrier materials	Rate-based	Membrane

We define $z^F_{i,j,s,m}$ as the variable to indicate which separation phenomenon and enabling material is activated for horizontal semi-restricted boundary. When $z^F_{i,j,s,m}$ is one, there exists a semi-restricted boundary between block $B_{i,j}$ and $B_{i,j+1}$ with separation phenomenon s and enabling material m.

$$z^F_{i,j,s,m} = \begin{cases} 1 & \text{if the boundary between } B_{i,j} \text{ and } B_{i,j+1} \text{ is occupied by} \\ & \text{phenomena } s \text{ with material } m \\ 0 & \text{otherwise} \end{cases}$$

A similar binary variable is also defined for the vertical direction:

$$z^R_{i,j,s,m} = \begin{cases} 1 & \text{if the boundary between } B_{i,j} \text{ and } B_{i+1,j} \text{ is occupied by} \\ & \text{phenomena } s \text{ with material } m \\ 0 & \text{otherwise} \end{cases}$$

Either an equilibrium-based or a rate-based separation might take place at the semi-restricted boundary. However, only one separation phenomenon is allowed for a semi-restricted boundary and only one corresponding material would be activated. Therefore,

$$z^{srF}_{i,j} = \sum_{(s,m)\in Equil\cup\ Rate} z^F_{i,j,s,m}, \quad \forall i,j \tag{3.67}$$

$$z^{srR}_{i,j} = \sum_{(s,m)\in Equil\cup\ Rate} z^R_{i,j,s,m}, \quad \forall i,j \tag{3.68}$$

The above equations also confirm that only one phenomenon and one material are selected for each boundary. For instance, we do not allow membrane and absorbent to be selected at the same time.

Equilibrium-based Modeling of Separation Phenomena

VL-PC, GL-PC, LL-PC separation phenomena are described using equilibrium-based models. For example, the vapor-liquid phase contact (VL-PC) phenomena observed in distillation, flash, partial boiling and partial condensing can all be modeled with equilibrium models. Since the equilibrium between two phases require a phase contact, two blocks with different phases separated by a semi-restricted boundary is used to represent an equilibrium-based separation phenomenon. In the following discussion, we present the model for VL-PC and GL-PC under the subset of $Equil(s,m)$. Note that, for LL-PC, similar constraints are written by defining a separate phase binary variable for different liquid phases.

It is assumed that the phases leaving from two adjacent blocks separated by a semi-restricted boundary, which describes a phase contact, are in equilibrium. At equilibrium, some components may transfer from gas phase to liquid phase, while some others can transfer from liquid phase to

gas phase. However, in the absence of equilibrium, we need to satisfy unidirectional flow for all the components of a stream. To satisfy unidirectional flow, if there is no phase contact prevalent between blocks $B_{i,j}$ and $B_{i,j+1}$ in the horizontal direction, we write

$$z_{i,j,k}^{Fplus} \leq z_{i,j,k^*}^{Fplus} + z_{i,j,s,m}^{F}, \quad \forall i,j,k,k^*, k \neq k^*, \ (s,m) \in Equil \tag{3.69}$$

$$z_{i,j,k}^{Fplus} \geq z_{i,j,k^*}^{Fplus} - z_{i,j,s,m}^{F}, \quad \forall i,j,k,k^*, k \neq k^*, \ (s,m) \in Equil \tag{3.70}$$

Similar relations are also written for the vertical direction:

$$z_{i,j,k}^{Rplus} \leq z_{i,j,k^*}^{Rplus} + z_{i,j,s,m}^{R}, \quad \forall i,j,k,k^*, k \neq k^*, \ (s,m) \in Equil \tag{3.71}$$

$$z_{i,j,k}^{Rplus} \geq z_{i,j,k^*}^{Rplus} - z_{i,j,s,m}^{R}, \quad \forall i,j,k,k^*, k \neq k^*, \ (s,m) \in Equil \tag{3.72}$$

The equilibrium distribution of component k between the block $B_{i,j}$ and $B_{i,j+1}$ for separation phenomena s through material m is represented by the phase equilibrium constant $K_{i,j,s,m,k}^{eq,F}$. This variable requires several thermodynamic relations, for instance, Henry's Law or Antoine equation. The general expression for the phase equilibrium constant in horizontal direction is:

$$K_{i,j,s,m,k}^{eq,F} = f^{eq}\{P_{i,j}T_{i,j}, y_{i,j,k}, y_{i,j+1,k}\}, \quad \forall i,j, \ k \in K \backslash inert, (s,m) \in Equil \tag{3.73}$$

Note that when non-ideal phase equilibrium considerations are needed, then $K_{i,j,s,m,k}^{eq,F}$ is a function of the block compositions at either side of the semi-restricted boundary, i.e. $y_{i,j,k}$ and $y_{i,j+1,k}$. Similarly, in the vertical direction, following equilibrium relations hold:

$$K_{i,j,s,m,k}^{eq,R} = f^{eq}\{P_{i,j}T_{i,j}, y_{i,j,k}, y_{i+1,j,k}\}, \quad \forall i,j, \ k \in K \backslash inert, (s,m) \in Equil \tag{3.74}$$

If phase equilibrium is assumed to be ideal, then the equilibrium relations can be written based on a single phase equilibrium constant that does not depend on the block compositions. Then, the

phase equilibrium constant variable is independent of the alignment of the blocks:

$$K^{eq}_{i,j,s,m,k} = \frac{P^{sat}_{i,j,k}}{P_{i,j}}, \quad \forall i,j,\ k \in K \backslash inert, (s,m) \in Equil \tag{3.75}$$

while $inert$ is the set for inert, i.e. non-volatile, components, $P^{sat}_{i,j,k}$ is the saturation pressure or solubility of the component k in block $B_{i,j}$ for which detailed explanation is given in Appendix A. For simplicity, we will continue with ideal phase equilibrium assumption. If non-ideal phase equilibrium relations are needed, constraints below can be modified according to the Eqs. 3.73-3.74.

The set of two blocks representing a separation phenomenon can have different phases. Therefore, it is important to identify the phases of the adjacent blocks. Depending on the block position and its phase, we use the following conditional relationships to account for the equilibrium-based phase assignments.

$$y_{i,j,k} \leq K^{eq}_{i,j,s,m,k} y_{i,j+1,k} + \left(2 - z^{F}_{i,j,s,m} - z^{phase}_{i,j}\right), \quad \forall i,j,\ k \in K \backslash inert, (s,m) \in Equil \tag{3.76}$$

$$y_{i,j,k} \geq K^{eq}_{i,j,s,m,k} y_{i,j+1,k} - K^{eq,U}_{k} \left(2 - z^{F}_{i,j,s,m} - z^{phase}_{i,j}\right), \quad \forall i,j,\ k \in K \backslash inert, (s,m) \in Equil \tag{3.77}$$

Equations 3.76-3.77 provide a valid equilibrium relationship when block $B_{i,j}$ is in gas phase and block $B_{i,j+1}$ is in liquid phase. In this case, $y_{i,j,k}$ is the vapor phase composition leaving the gaseous part of the phase contact unit, and $y_{i,j+1,k}$ is the liquid phase composition leaving the liquid part of the phase contact unit. A safe value of Keq^{Upper}_{k} could be the equilibrium constant at the highest temperature allowed in the process, *i.e.*, T^{max} for the species obeying Antoine's Equation. In order to make the formulation tighter, we take the Big-M parameter in Equation 3.76 equal to one as it satisfies the upper bound for concentration variable $y_{i,j,k}$. For the case when block $B_{i,j}$ is in liquid phase and block $B_{i,j+1}$ is in gas phase, the phase equilibrium relation is ensured as follows.

$$y_{i,j+1,k} \leq K^{eq}_{i,j,s,m,k} y_{i,j,k} + \left(2 - z^{F}_{i,j,s,m} - z^{phase}_{i,j+1}\right), \quad \forall i,j,\ k \in K \backslash inert, (s,m) \in Equil \tag{3.78}$$

$$y_{i,j+1,k} \geq K^{eq}_{i,j,s,m,k} y_{i,j,k} - K^{eq,U}_{k} \left(2 - z^{F}_{i,j,s,m} - z^{phase}_{i,j+1}\right), \quad \forall i,j,\ k \in K \backslash inert, (s,m) \in Equil \tag{3.79}$$

Similarly, the phase equilibrium between blocks $B_{i,j}$ and $B_{i+1,j}$ in the vertical direction is attained as the following equations are satisfied.

$$y_{i,j,k} \leq K^{eq}_{i,j,s,m,k} y_{i+1,j,k} + \left(2 - z^{R}_{i,j,s,m} - z^{phase}_{i,j}\right), \quad \forall i,j,\ k \in K \backslash inert, (s,m) \in Equil \tag{3.80}$$

$$y_{i,j,k} \geq K^{eq}_{i,j,s,m,k} y_{i+1,j,k} - K^{eq,U}_{k} \left(2 - z^{R}_{i,j,s,m} - z^{phase}_{i,j}\right), \quad \forall i,j,\ k \in K \backslash inert, (s,m) \in Equil \tag{3.81}$$

$$y_{i+1,j,k} \leq K^{eq}_{i,j,s,m,k} y_{i,j,k} + \left(2 - z^{R}_{i,j,s,m} - z^{phase}_{i+1,j}\right), \quad \forall i,j,\ k \in K \backslash inert, (s,m) \in Equil \tag{3.82}$$

$$y_{i+1,j,k} \geq K^{eq}_{i,j,s,m,k} y_{i,j,k} - K^{eq,U}_{k} \left(2 - z^{R}_{i,j,s,m} - z^{phase}_{i+1,j}\right), \quad \forall i,j,\ k \in K \backslash inert, (s,m) \in Equil \tag{3.83}$$

For all direct phase contact phenomena modeled with equilibrium model, the temperature and pressure of the two phases need to be equal. Hence, in addition to the bounds $T^{\min} \leq T_{i,j} \leq T^{\max}$ we impose the following constraints for temperature for of the blocks participating in an equilibrium-based separation in the horizontal direction:

$$T_{i,j} \geq T_{i,j+1} - \left(T^{max} - T^{min}\right)\left(1 - z^{F}_{i,j,s,m}\right), \quad \forall i,j,\ (s,m) \in Equil \tag{3.84}$$

$$T_{i,j} \leq T_{i,j+1} + \left(T^{max} - T^{min}\right)\left(1 - z^{F}_{i,j,s,m}\right), \quad \forall i,j,\ (s,m) \in Equil \tag{3.85}$$

Similarly, in the vertical direction:

$$T_{i,j} \geq T_{i+1,j} - \left(T^{max} - T^{min}\right)\left(1 - z^{R}_{i,j,s,m}\right), \quad \forall i,j,\ (s,m) \in Equil \tag{3.86}$$

$$T_{i,j} \leq T_{i+1,j} + \left(T^{max} - T^{min}\right)\left(1 - z^{R}_{i,j,s,m}\right), \quad \forall i,j,\ (s,m) \in Equil \tag{3.87}$$

Similarly, in addition to the bounds $P^{\min} \leq P_{i,j} \leq P^{\max}$ on pressure, we have

$$P_{i,j} \geq P_{i,j+1} - \left(P^{max} - P^{min}\right)\left(1 - z^{F}_{i,j,s,m}\right), \quad \forall i,j,\ (s,m) \in Equil \tag{3.88}$$

$$P_{i,j} \leq P_{i,j+1} + \left(P^{max} - P^{min}\right)\left(1 - z^{F}_{i,j,s,m}\right), \quad \forall i,j,\ (s,m) \in Equil \tag{3.89}$$

Similarly, in the vertical direction:

$$P_{i,j} \geq P_{i+1,j} - \left(P^{max} - P^{min}\right)\left(1 - z^{R}_{i,j,s,m}\right), \quad \forall i,j,\ (s,m) \in Equil \tag{3.90}$$

$$P_{i,j} \leq P_{i+1,j} + \left(P^{max} - P^{min}\right)\left(1 - z^{R}_{i,j,s,m}\right), \quad \forall i,j,\ (s,m) \in Equil \tag{3.91}$$

Any equilibrium phenomenon should be associated with two blocks with different phases. This is confirmed when the following two equations are active together for $B_{i,j}$ and $B_{i,j+1}$. For the equilibrium phenomena involving vapor and liquid phases, this can be ensured by the following:

$$z^{phase}_{i,j} + z^{phase}_{i,j+1} + z^{F}_{i,j,s,m} \leq 2, \quad \forall i,j,\ (s,m) \in Equil \tag{3.92}$$

$$z^{phase}_{i,j} + z^{phase}_{i,j+1} \geq z^{F}_{i,j,s,m}, \quad \forall i,j,\ (s,m) \in Equil \tag{3.93}$$

For instance, when both $B_{i,j}$ and $B_{i,j+1}$ are in vapor phases, first equation ensures that $z^{F}_{i,j,s,m} = 0$. On the other hand, when both $B_{i,j}$ and $B_{i,j+1}$ are in liquid phases, then second equation ensures that $z^{F}_{i,j,s,m}$ = 0. Similarly, in the vertical direction:

$$z^{phase}_{i,j} + z^{phase}_{i+1,j} + z^{R}_{i,j,s,m} \leq 2, \quad \forall i,j,\ (s,m) \in Equil \tag{3.94}$$

$$z^{phase}_{i,j} + z^{phase}_{i+1,j} \geq z^{R}_{i,j,s,m}, \quad \forall i,j,\ (s,m) \in Equil \tag{3.95}$$

Rate-based Modeling of Separation Phenomena

For rate-based models, mass transfer rate is calculated by using the driving force for separation, mass transfer coefficient of individual species and the size of the mass transfer surface. Depending on the type of the separation, the driving force can be concentration difference, partial pressure difference, *etc*. Let the driving force for a separation phenomenon s for component k between blocks $B_{i,j}$ and $B_{i,j+1}$ can be defined as $(DR_{i,j,k,s} - DR_{i,j+1,k,s})$. If this difference is positive, then the flow rate of component k is in positive direction, *i.e.* from block $B_{i,j}$ to $B_{i,j+1}$. If it is negative, then the flow rate is in the reverse direction. As an example to rate-based modeling, for the gas separation phenomena, $DR_{i,j,k,s=GP} - DR_{i,j+1,k,s=GP} = P_{i,j}\, y_{i,j,k} - P_{i,j+1}\, y_{i,j+1,k}$.

Similarly, we define mass transfer coefficient of a component k in phenomenon s realized by material m as $MTC_{i,j,k,s,m}$. As an example, the mass transfer coefficient for membranes are the permeance of component k through the membrane material m. The mass transfer area for phenomenon s realized by material m is denoted by either $CA^F_{i,j,s,m}$ or $CA^R_{i,j,s,m}$ depending on the direction of the mass transfer boundary. Furthermore, $M^{rateF}_{i,j,k,s,m}$ and $M^{rateR}_{i,j,k,s,m}$ designate the upper bound for horizontal and vertical flux respectively. Accordingly, the following constraints realize a rate-based separation model in the horizontal direction of the block superstructure:

$$\begin{aligned} F_{i,j,k} \geq\ & MTC_{i,j,k,s,m} \times (DR_{i,j,k,s} - DR_{i,j+1,k,s}) \times CA^F_{i,j,s,m} \\ & - M^{rateF}_{i,j,k,s,m}(1 - z^F_{i,j,s,m}), \quad \forall i,j,k,\ (s,m) \in Rate \end{aligned} \tag{3.96}$$

$$\begin{aligned} F_{i,j,k} \leq\ & MTC_{i,j,k,s,m} \times (DR_{i,j,k,s} - DR_{i,j+1,k,s}) \times CA^F_{i,j,s,m} \\ & + M^{rateF}_{i,j,k,s,m}(1 - z^F_{i,j,s,m}), \quad \forall i,j,k,\ (s,m) \in Rate \end{aligned} \tag{3.97}$$

A similar relation is written for the vertical direction:

$$\begin{aligned} R_{i,j,k} \geq\ & MTC_{i,j,k,s,m} \times (DR_{i,j,k,s} - DR_{i+1,j,k,s}) \times CA^R_{i,j,s,m} \\ & - M^{rateR}_{i,j,k,s,m}(1 - z^R_{i,j,s,m}), \quad \forall i,j,k,\ (s,m) \in Rate \end{aligned} \tag{3.98}$$

$$R_{i,j,k} \leq MTC_{i,j,k,s,m} \times (DR_{i,j,k,s} - DR_{i+1,j,k,s}) \times CA^{R}_{i,j,s,m} + M^{rateR}_{i,j,k,s,m}(1 - z^{F}_{i,j,s,m}), \quad \forall i,j,k,\ (s,m) \in Rate \tag{3.99}$$

The Big-M parameters, $M^{rateF}_{i,j,k,s,m}$ and $M^{rateR}_{i,j,k,s,m}$, in the above equations can be obtained by considering the maximum driving force that can be achieved in the given process conditions:

$$M^{rateF}_{i,j,k,s,m} = MTC^{max}_{i,j,k,s,m} \times DR^{max}_{i,j,k,s} \times CA^{max,R}_{i,j,s,m} + FU_{i,j,k}, \quad \forall i,j,k,\ (s,m) \in Rate$$

The same bound can be also used in the vertical direction.

Similar to the equilibrium-based separation models, phase relations can be also written for the rate-based separation models and the corresponding phenomena. If the separation is performed by a gas membrane, then the two blocks separated by the membrane should have the same phase. This leads to the following constraints:

$$z^{phase}_{i,j} - z^{phase}_{i,j+1} + z^{F}_{i,j,s,m} \leq 1\ , \quad \forall i,j,\ s = GP,\ m = gasmem \tag{3.100}$$

$$-z^{phase}_{i,j} + z^{phase}_{i,j+1} + z^{F}_{i,j,s,m} \leq 1 \quad \forall i,j,\ s = GP,\ m = gasmem \tag{3.101}$$

$$z^{phase}_{i,j} - z^{phase}_{i+1,j} + z^{R}_{i,j,s,m} \leq 1\ , \quad \forall i,j,\ s = GP,\ m = gasmem \tag{3.102}$$

$$-z^{phase}_{i,j} + z^{phase}_{i+1,j} + z^{R}_{i,j,s,m} \leq 1 \quad \forall i,j,\ s = GP,\ m = gasmem \tag{3.103}$$

Similar constraints can be also written for the other membrane types. Finally, note that these rate-based relations can be extended to consider mass transfer rates at the interphase with multicomponent mass transfer models, e.g. Maxwell Stefan diffusion model. Furthermore, interphase balances can be included for energy transfer and the model accuracy can be increased as discussed in Section 3.2.1.6 at the expense of increasing the model complexity.

Short-cut Models

Semi-restricted boundary can be also described through short-cut models if it corresponds to a pre-specified separation equipment. As each separation equipment requires at least one rich

and one lean outlet stream with different compositions in terms of a key component, a single block with at least two outlet streams can be used to represent the equipment. A semirestricted boundary indicates the position of one of these streams. Flow through the semi-restricted boundary is described through a split fraction variable: $\tau_{i,j,k,s,m}$. This indicates the fraction of the component k entering into block $B_{i,j}$ that is separated through the semi-restricted boundary with phenomena s and enabling material m. The phenomena set definition can be updated to include the pre-specified equipment type and we also define a set SM to denote the separation operation s and enabling material m described through short-cut model. Accordingly, split fraction model for modeling the flow rate through a horizontal semi-restricted boundary can be written as follows:

$$FP_{i,j,k} \leq \tau_{i,j,k,s,m}\phi_{i,j,k} + FU_{i,j,k}\left(2 - z^{F}_{i,j,s,m} - z^{Fplus}_{i,j,k}\right),\ \forall i,j,k,(s,m) \in SM \tag{3.104}$$

$$FP_{i,j,k} \geq \tau_{i,j,k,s,m}\phi_{i,j,k} - \phi^{up}_{i,j,k}\left(2 - z^{F}_{i,j,s,m} - z^{Fplus}_{i,j,k}\right),\ \forall i,j,k,(s,m) \in SM \tag{3.105}$$

$$FN_{i,j,k} \leq \tau_{i,j+1,k,s,m}\phi_{i,j+1,k} + FU_{i,j,k}\left(1 - z^{F}_{i,j,s,m} + z^{Fplus}_{i,j,k}\right),\ \forall i,j,k,(s,m) \in SM \tag{3.106}$$

$$FN_{i,j,k} \geq \tau_{i,j+1,k,s,m}\phi_{i,j+1,k} - \phi^{up}_{i,j,k}\left(1 - z^{F}_{i,j,s,m} + z^{Fplus}_{i,j,k}\right),\ \forall i,j,k,(s,m) \in SM \tag{3.107}$$

While the first two set of equations are for the positive horizontal direction, the latter two are for the negative horizontal direction. Equations 3.104-3.105 dictate that when the semi-restricted boundary is assigned with a separation operation and the flow is in positive direction, then the flow rate through this boundary is dictated by the total inlet flow rate into the block and the split fraction. Similar equations can be also written in the vertical direction.

Note that this split fraction variable can be either a parameter with a fixed value or it can be kept as a variable. Short-cut design calculations, e.g. Fenske-Underwood-Gilliland, can be performed to determine the design and operating variables and the corresponding split fractions. We show an example on distillation column modeling in the Appendix. A more detailed discussion on the use of short-cut models for semi-restricted boundaries with other equipment types can be found elsewhere [51, 139].

Also note that while these short-cut models provide flexibility in the modeling and representation and can be used for obtaining base-case solutions with traditional equipment types, identification of the benefits that can be accrued from process intensification requires rate-based or equilibrium models.

The MINLP model described in this section can be used to determine which reactions should be active and the position of the corresponding blocks, boundary types and the corresponding phenomena and materials, block temperatures, pressures, compositions and flow rates according to an objective function to automatically generate different flowsheet variants. Now, we will continue with describing how this formulation can be also utilized for considering a fixed number of alternatives for superstructure-based process synthesis and intensification.

3.3 Tailoring Model for Superstructure-based Synthesis of Intensified Systems

The original MINLP model provided in the previous section includes many disjunctive terms to decide on the position of the active phenomena, flow directions, etc. But this formulation can be considered as a generic superstructure-based framework for process synthesis, integration and intensification. Here, we will present a reduced form of that formulation for vapor-liquid phase contact and reaction phenomena. These phenomena can be addressed to optimize either the reactor-separator-recycle or intensified reactive separation column configurations. With a similar logic, many different superstructure formulations are possible. Disjunctions are replaced by subsets which determine the position of the allowed phenomena within the superstructure. By changing the blocks belonging to these subsets and objective functions, different synthesis problems can be formulated:

$$\begin{aligned} &F_{i,j-1,k} + R_{i-1,j,k} - F_{i,j,k} - R_{i,j,k} + G_{i,j,k} + \sum_{fs \in FS} M_{i,j,k,fs} - \sum_{ps \in PS} P_{i,j,k,ps} \\ &+ \sum_{(i',j') \in LN} J_{i',j',i,j,k} - \sum_{(i',j') \in LN} J_{i,j,i',j',k} = 0, \quad i,j \in SB, k \in K \end{aligned} \tag{3.108}$$

$$F_{i,j-1,k} - F_{i,j+1,k} + R_{i-1,j,k} - R_{i,j,k} + R_{i-1,j+1,k} - R_{i,j+1,k} + G_{i,j,k} + \sum_{fs \in FS} M_{i,j,k,fs} - \sum_{ps \in PS} P_{i,j,k,ps} + G_{i,j+1,k} + \sum_{fs \in FS} M_{i,j+1,k,fs} - \sum_{ps \in PS} P_{i,j+1,k,ps} + \sum_{(i',j') \in LN} J_{i',j',i,j+1,k} - \sum_{(i',j') \in LN} J_{i,j+1,i',j',k} = 0, \quad i,j \in TB, k \in K \tag{3.109}$$

$$G_{i,j,k} = f^{rxn}(T_{i,j}, P_{i,j}, y_{i,j,k}, k_r^0, E_r^A, V_{i,j}) \;\; i,j \in RxnB, k \in K \tag{3.110}$$

$$F_{i,j,k} = FP_{i,j,k} - FN_{i,j,k}, \;\; i,j \in ActF; \quad R_{i,j,k} = RP_{i,j,k} - RN_{i,j,k}, \;\; i,j \in ActR \tag{3.111}$$

$$y_{k,ps}^{MIN,prod} \sum_{k' \in K} P_{i,j,k',ps} \leq P_{i,j,k,ps}, \;\; i,j,ps \in ProdB, k, ps \in kp \tag{3.112}$$

$$P_{i,j,k,ps} \leq y_{k,ps}^{MAX,prod} \sum_{k' \in K} P_{i,j,k',ps}, \;\; i,j,ps \in ProdB, k, ps \in kp \tag{3.113}$$

$$\sum_{i \in I} \sum_{j \in J} P_{i,j,k,ps} \geq D_{k,ps} \quad k, ps \in kp \tag{3.114}$$

$$FP_{i,j,k} = y_{i,j,k} FP_{i,j}^T \;\; i,j \in HP, k \in K; \quad FN_{i,j,k} = y_{i,j+1,k} FN_{i,j}^T \;\; i,j \in HN, k \in K \tag{3.115}$$

$$RP_{i,j,k} = y_{i,j,k} RP_{i,j}^T \;\; i,j \in VP, k \in K; \quad RN_{i,j,k} = y_{i-1,j,k} RN_{i,j}^T \;\; i,j \in VN, k \in K \tag{3.116}$$

$$y_{i,j,k} P_{i,j,ps}^{p,total} = P_{i,j,k,p} \; i,j,ps \in ProdB, k \in K, \; i,j,i',j' \in LN, k \in K \tag{3.117}$$

$$y_{i,j,k} J_{i,j,i',j'}^T = J_{i,j,i',j',k}, \;\; i,j,i',j' \in LN, k \in K \tag{3.118}$$

$$y_{i,j+1,k} = K_{i,j,k,s,m}^{eq}(T_{i,j}, P_{i,j}, y_{i,j,k}, y_{i,j+1,k}) y_{i,j,k} \quad i,j \in VLPC, k \in K, s, m \in Equil \tag{3.119}$$

$$P_{i,j} \geq P_{i,j}^{bub} \; i,j \in LB^{check}; P_{i,j} \leq P_{i,j}^{dew} \; i,j \in VB^{check} \tag{3.120}$$

$$J_{i,j,i',j'}^{pump} = \sum_{k \in K} J_{i,j,i',j',k} MW_k (P_{i',j'} - P_{i,j}) / \rho_{i,j}^{mix} \;\; i,j,i',j' \in LN^{pump} \tag{3.121}$$

$$EF_{i,j-1} + ER_{i-1,j} - EF_{i,j} - ER_{i,j} + EM_{i,j} - EP_{i,j} + EJ_{i,j}^f - EJ_{i,j}^p + Q_{i,j}^h - Q_{i,j}^c = 0, \;\; i,j \in SB \tag{3.122}$$

$$EF_{i,j-1} + ER_{i-1,j} - EF_{i,j+1} + ER_{i-1,j+1} - ER_{i,j+1} - ER_{i+1,j+1} + EM_{i,j} - EP_{i,j} + EJ_{i,j}^f - EJ_{i,j}^p + EJ_{i,j+1}^f - EJ_{i,j+1}^p + EM_{i,j+1} - EP_{i,j+1} + Q_{i,j}^{hF} - Q_{i,j}^{cF} = 0, \; i,j \in TB \tag{3.123}$$

Equation 3.108 is for material balance around a single block. Equation 3.109 designates the material balance for a horizontal block pair. This helps to reduce the model size when the boundary between two building blocks is semi-restricted and it is described by an equilibrium model. Here, SB and TB designate the subsets for the blocks within which these equations are activated. Equation 3.110 describes the reaction within a block for which the exact description is system dependent. Equation 3.111 describes the horizontal and vertical flow rates with respect to their directions. Equations 3.112-3.114 describe the purity requirement and demand constraints for the product streams, respectively. Equations 3.115-3.118 are used to calculate the purity of the outlet streams from a block. Sets HP and HN correspond to the active flow directions for the horizontal positive (to the right) and negative (to the left) streams, respectively. VP and VN are for the vertical positive (downwards) and negative (upwards) streams, respectively. Equation 3.119 is to calculate the equilibrium composition of each block when there is a semirestricted phase contact boundary between two horizontal block pairs and $VLPC$ set describes the block pairs for which these equilibrium conditions hold. Equations 3.120 are used to ensure a block is in liquid or in vapor phase based on bubble and dew pressures, respectively. LB^{check} and VB^{check} sets determine the position of these liquid and vapor blocks. Equations 3.121 is to determine the work required for liquid pressure change through the jump streams. Similar equations can be written for other interblock streams as well as for compression of vapor streams. Equations 3.122-3.123 are block energy balances for single block and two horizontal block pairs, respectively. By changing the set definitions for which these constraints active, different optimization formulations can be formulated. For instance, one can designate the reaction set $RxnB = \{(1,1),(1,2)\}$ just to allow reactions to be assigned to blocks $B_{1,1}$ and $B_{1,2}$. Similarly, all the constraints written in the previous sections can be manipulated to designate the position within the superstructure where they are valid.

3.4 Objective Functions

There can be many different objectives for process intensification. Here, a few examples of these objectives are provided. Also, an extension on considering multi-objective optimization

problems is discussed.

3.4.1 Maximization of Product Yield

The overall yield of a product can be maximized using the following simple objective function:

$$\max \sum_{i\in I}\sum_{j\in J}\sum_{k=\tilde{k}}\sum_{p=\tilde{p}} P_{i,j,k,p} \tag{3.124}$$

in which $\tilde{k}$ refers to the main component in the desired product $\tilde{p}$ which is to be maximized.

3.4.2 Maximization or Minimization of Resource Utilization

The overall utilization of a material can be maximized or minimized using the following simple objective function:

$$\max/\min \quad \left(\sum_{i\in I}\sum_{j\in J}\sum_{k=\overline{k}}\sum_{f\in FS} M_{i,j,k,f} - \sum_{i\in I}\sum_{j\in J}\sum_{k=\overline{k}}\sum_{p\in PS} P_{i,j,k,p} \right) \tag{3.125}$$

in which $\overline{k}$ refers to the component to be utilized. One example is the maximization of CO_2 utilization or conversion from flue gas.

3.4.3 Minimization of Energy Consumption

The objective related to minimizing the overall energy consumption of the process is formulated as:

$$min \omega_1 \sum_{i\in I}\sum_{j\in J} \left(Q^h_{i,j} + Q^c_{i,j}\right) \; + \; \omega_2 \sum_{i\in I}\sum_{j\in J} \frac{1}{\eta_c}(W^{com}_{i,j}) \tag{3.126}$$

Here $Q^c_{i,j}$ and $Q^h_{i,j}$ are the amount of heat that is used in cooling and heating in block $B_{i,j}$, respectively. $W^{com}_{i,j}$ is the total amount of work consumed as a result of compression in block $B_{i,j}$. η_c is the compressor efficiency. Furthermore, ω_1 and ω_2 are parameters used either to provide different weights on heat and work. They both can be selected as one. If we are only interested in one form of energy (either heat or work) minimization, then one of the two parameters is fixed to be zero.

3.4.4 Minimization of the Operating Cost

The operating cost includes the costs of hot utility, cold utility, raw materials, and compression.

$$\begin{aligned}\min \quad & UC_{hu}\sum_{i\in I}\sum_{j\in J}Q^{h}_{i,j} + UC_{cu}\sum_{i\in I}\sum_{j\in J}Q^{c}_{i,j} + \sum_{i\in I}\sum_{j\in J}\sum_{k\in K}\sum_{f\in FS}UC_{f}M_{i,j,k,f} \\ & + \frac{UC_{elect}}{\eta_c}\sum_{i\in I}\sum_{j\in J}W^{com}_{i,j} \end{aligned} \tag{3.127}$$

where, UC_{hu}, UC_{cu}, UC_f and UC_{elect} represent the unit cost of hot utility, cold utility, feed and electricity, respectively.

3.4.5 Emission Minimization

Emission minimization can include direct and indirect GHG (Green House Gas) emissions. Here, we provide an objective function for minimizing CO_2-eq emissions from the process:

$$\begin{aligned}\min \quad & f^{CO_2} = \frac{\omega^{El}}{\eta_c}\sum_{i\in I}\sum_{j\in J}W^{com}_{i,j} + \omega^{Fuel}\sum_{i,j\in Hot}Q^{h}_{i,j} + \sum_{i,j,k,f\in FeedB}\omega^{feed}_{k,f}M_{i,j,k,f} \\ & + \sum_{i,j,k,ps\in ProdB}\omega^{prod}_{k}H_{i,j,k,p} \end{aligned} \tag{3.128}$$

Here, the first term is the CO_2-eq GHG emissions due to the electricity consumption with ω^{El} designating the emissions per unit amount of electricity consumption. The second term is the CO_2-eq GHG emissions due to the fuel consumption for the hot utilities and ω^{Fuel} describes the equivalent emissions per unit amount of the fuel consumed. The third term accounts for well-to-gate emissions released until the raw material is delivered, e.g. natural gas extraction and transport. $\omega^{feed}_{k,f}$ is the CO_2-eq GHG emissions per unit amount of component k fed into the process through feed stream f. The fourth term describes the emissions from production of hazardous chemicals, waste streams, etc. ω^{prod}_{k} is the conversion factor for calculating the CO_2-eq emissions per unit amount of emitted chemical k.

3.4.6 Objectives including Capital Costs and Multi-Objective Optimization

When rigorous phenomena models are used, it is not trivial and sometimes impossible to know the resulting unit operations before the optimization problem is solved. Furthermore, most of the intenified equipment do not have well-established cost functions. These points make it rather challenging incorporating the capital cost considerations into the building block superstructure model. However, there are at least two cases where it is possible to use capital costs within the objective: (i) when certain regions within the superstructure are specified beforehand as an equipment with known capital cost function, and (ii) when operations that require only single blocks are used in the problem definition. We present below two different objective functions for these cases. While doing that, we also discuss how we can perform multi-objective optimization with a set of economic and sustainability objectives.

Firstly, we can designate some regions in the building block superstructure as an equipment with known capital cost function formulation. Examples of these equipment were demonstrated in Figure 2.3. In terms of mathematical representation, we designate a set of building blocks as an equipment when they are connected to each other in a continuous manner and physical conditions do not differ drastically in between. For instance, if there is a major change in pressure from one block to another, this will require an additional pressure change operation that will prevent the building blocks from being translated as part of the same equipment. We denote these regions with set $EqR(i, j, e)$ to define blocks $B_{i,j}$ that belong to an equipment e where $e \in E = 1, ..., |E|$ correspond to a set of equipment for which capital cost functions are readily available. Accordingly, costs of these equipment can be embedded into the formulation. Considering capital costs allows us to perform multi-objective optimization while considering economics along with several other objectives as discussed within the previous sections. In this work, we use the ε-constraint method where one of the design targets is selected as the main objective, while keeping the other targets as constraints with successive changes on bounds. We consider the economic objective as the primary objective and incorporate other objectives as constraints to obtain the pareto fronts. An example of this is shown below for a reactive separation column comprised of an array of building pairs

separated by an vapor-liquid phase contact boundary positioned vertically (See Figure 2.6 and 2.8 for reactive separation column representation examples). Here, the objective is to maximize the return on investment while minimizing a set of sustainability objectives:

$$\max \quad ROI = \frac{[(Income - (AOC + Depreciation)) \times (1-\theta) + Depreciation]}{TCI} \tag{3.129}$$

$$s.t. \quad f_l \leq \varepsilon_l \quad \forall l \in \{1, ..., L\} \tag{3.130}$$

$$Income = \sum_{i,j,k,ps \in ProdB} SP_{k,p} P_{i,j,k,p} \tag{3.131}$$

$$AOC = \sum_{i,j,k,f \in FB} UC_f M_{i,j,k,f} + UC_{cold} \sum_{i,j \in Cond} Q^c_{i,j} + UC_{hot} \sum_{i,j \in Reb} Q^h_{i,j}$$
$$+ \quad UC_{elec} \sum_{i,j,i',j' \in LN^{pump}} J^{pump}_{i,j,i',j'} + Maintenance \tag{3.132}$$

$$Depreciation = \alpha^{dep} \times \alpha^{FCI} \times ICC; \quad TCI = \alpha^{TCI} \times ICC \tag{3.133}$$

$$ICC = \sum_{e \in E^{Dist}} a_0 (HE_e)^{b_0} (D_e)^{c_0} + \sum_{e \in E^{Dist}} a_1 (HE_e)^{b_1} (D_e)^{c_1} +$$
$$+ \quad a^{pump} \sum_{i,j,i',j' \in LN} (J^{pump}_{i,j,i',j'})^{b_{pump}}$$
$$+ \quad a^{Reb} \sum_{i,j \in Reb} \left[\frac{Q^h_{i,j}}{U^{reb} LMTD_{i,j}} \right]^{b_{reb}} + a^{Cond} \sum_{i,j \in Cond} \left[\frac{Q^c_{i,j}}{U^{cond} LMTD_{i,j}} \right]^{b_{cond}} \tag{3.134}$$

$$HT_{i,j,e} = HT^0_e + 1.27 V_{i,j} / D^2_e, \quad i,j,e \in EqR, \; e \in E^{Dist} \tag{3.135}$$

$$HE_e = HT^{0,total}_e + \sum_{i,j \in EqR} HT_{i,j,e}, \quad e \in E^{Dist} \tag{3.136}$$

$$D^2_e \geq D^0 \sum_{k \in K} RN^{vapor}_{i,j,k} \sqrt{T_{i,j} \sum_{k' \in K} y_{i,j,k} MW_k / P_{i,j}} \quad i,j,e \in EqR, \; e \in E^{Dist} \tag{3.137}$$

$$P_{i+1,j} = P_{i,j} + \Delta P_{i,j}, \quad i,j \in EqR, \; e \in E^{Dist} \tag{3.138}$$

Equation 3.129 is to calculate the return on investment (ROI). Equation 3.130 denotes a set of sustainability objectives pertaining to emissions, waste, etc. Equation 3.131 is to calculate the revenue from the selling product streams and Equation 3.132 denotes the operating costs. Equation 3.133 is to calculate the total capital investment and depreciation costs. Equation 3.134 is to determine the installed capital cost of the equipment. While Eq. 3.135 is to determine the individual height of

the block pairs, Eq. 3.136 is to calculate the total height of the reactive separation region. Equation 3.137 is to calculate the diameter of the corresponding column based on vapor flow rate. Equation 3.138 is to denote that all the building blocks in this region operate within a certain pressure. $\Delta P_{i,j}$ denotes the pressure drop variable across block $P_{i,j}$ which can be bounded from above and below limiting the maximum pressure drop. When pressure drop is assumed negligible, all the blocks belonging to the same region have the same pressure. If this problem is solved for a range of ε_l values, pareto fronts can be obtained. Note that here we only wrote this function for a reactive separation column with a fixed number of stages, yet this model can be extended to cover optimization of number of stages along with many other equipment types and objective functions.

A second case in which capital cost considerations can be included in the model formulation is when operations that require only single blocks are used in the problem definition. In these cases, an objective function for maximizing the total annual profit (TAP) can be written as follows [139]:

$$
\begin{aligned}
\max \quad TAP = & \sum_{i\in I}\sum_{j\in J}\sum_{k\in K}\sum_{p\in PS} SP_{k,p}P_{i,j,k,p} - \sum_{i\in I}\sum_{j\in J}\sum_{k\in K}\sum_{f\in FS} UC_f M_{i,j,k,f} \\
& - \sum_{i\in I}\sum_{j\in J}\sum_{(s,m)\in SM} \kappa(z^{sep}_{i,j,s,m}\mu_s + \omega_s(\sum_{k\in K} F^{in,s}_{s,k}/\theta_s)^{\beta_s} + TP_s N^{sep}_s) \\
& - \sum_{i\in I}\sum_{j\in J}\sum_{c\in CAT} \kappa(z^{rxn}_{i,j,c}\mu_c + \omega_c(\sum_{k\in K}\phi_{i,j,k}/\theta_c)^{\beta_c} + TP_c V_{i,j}) \\
& - \sum_{i\in I}\sum_{j\in J} \kappa CC_h(Q^h_{i,j}) - \sum_{i\in I}\sum_{j\in J}\kappa CC_c(Q^c_{i,j})^{\upsilon^h} \\
& - \sum_{i\in I}\sum_{j\in J} \kappa CC_h((Q^{FP,h}_{i,j})^{\upsilon^h} + (Q^{FN,h}_{i,j})^{\upsilon^h} + (Q^{RP,h}_{i,j})^{\upsilon^h} + (Q^{RN,h}_{i,j})^{\upsilon^h}) \qquad (3.139) \\
& - \sum_{i\in I}\sum_{j\in J} \kappa CC_c((Q^{FP,c}_{i,j})^{\upsilon^c} + (Q^{FN,c}_{i,j})^{\upsilon^c} + (Q^{RP,c}_{i,j})^{\upsilon^c} + (Q^{RN,c}_{i,j})^{\upsilon^c}) \\
& - \sum_{i\in I}\sum_{j\in J} \kappa CC_{com}(W^{com}_{i,j})^{\omega^{com}} - \sum_{i\in I}\sum_{j\in J} OC_{com} W^{com}_{i,j} \\
& - \sum_{i\in I}\sum_{j\in J} \big(UC_{hu}(Q^h_{i,j} + Q^{FP,h}_{i,j} + Q^{FN,h}_{i,j}) + Q^{RP,h}_{i,j} + Q^{RN,h}_{i,j})\big) \\
& - \sum_{i\in I}\sum_{j\in J} \big(UC_{cu}(Q^c_{i,j} + Q^{FP,c}_{i,j} + Q^{FN,c}_{i,j} + Q^{RP,c}_{i,j} + Q^{RN,c}_{i,j})\big)
\end{aligned}
$$

This can be used while using equilibrium or stoichiometric models for reactions, when the variables for a single block can be used to determine the cost function for the reactors. Similarly, when sharp split models are used, one block corresponds to one whole separation equipment and block variables are sufficient to determine the cost of the whole equipment. Here, the first term corresponds to the revenue. The second term is raw material cost. The third term is the capital cost for separation operations. It includes fixed costs and variables investment cost based on either inlet flow rates, with cost parameter ω_s, or design variables, with cost parameter TP_s. These design variables, N_s^{sep}, can include membrane area, number of trays, etc. Here, $z_{i,j,s,m}^{sep}$ is a 0-1 continuous variable describing whether any of the four boundaries of block $B_{i,j}$ assigned with a separation operation or not (See Appendix for definition and use in short-cut models). κ denotes the capital recovery factor. The fourth term is the capital cost for reaction operations. It includes fixed costs and variables investment cost based on either inlet flow rates, with cost parameter ω_c, or design variables, i.e. reaction volume $V_{i,j}$, with cost parameter TP_c. The fifth and sixth terms are the capital costs for block heaters and coolers, respectively. Seventh and eighth terms are for the capital costs of the stream heaters and coolers. The ninth term is the capital cost for the compressors as a function of the work duty (For simplicity, here $W_{i,j}^{com}$ is shown as a single term but it is in practice dissected into several parts as discussed in Appendix A.3). The last three terms are the operating costs for compressors, heaters and coolers, respectively.

3.5 Simultaneous Heat Integration

By building connections between different heat duty variables at different locations of the superstructure, simultaneous heat integration opportunities can be also captured. We can perform simultaneous heat exchanger network synthesis (HENS) to consider the automated generation of the flowsheet along with the corresponding heat exchanger network. In this case, stream identities (hot/cold) are not known beforehand. We can also consider a utility targeting problem with pinch location method while including these unclassified streams. Both approaches have been applied to building block superstructure model. Li et al. (2018) presented a HENS model for unclassified streams with building block superstructure. This formulation can be applied to address HENS

problems and superstructures similar to the ones proposed by Yee and Grossman (1990) [61]. One example of this can be found in Demirel et al. (2018) [142]. We can also consider utility targeting with unclassified streams and perform simultaneous HENS and process synthesis. An application of this type of model can be found in our previous work [143]. Here, we will only provide a brief discussion on implementation of heat integration that we used in the case studies. More information can be obtained from the previous works.

The idea behind the simultaneous HENS model is to allow the heat duty variables at different locations within the superstructure to be matched with each other. There are three different types of heat duty variables: (i) block heat duty variables, i.e. $Q^{h}_{i,j}$ and $Q^{c}_{i,j}$, (ii) heat duty variables for the horizontal and vertical building block pairs, i.e. $Q^{hF}_{i,j}$, $Q^{cF}_{i,j}$, $Q^{hR}_{i,j}$ and $Q^{cR}_{i,j}$ (See Appendix A for definitions), and (iii) stream heat duties, i.e. $Q^{FP,h}_{i,j}$, $Q^{FN,h}_{i,j}$, $Q^{RP,h}_{i,j}$, $Q^{RN,h}_{i,j}$, $Q^{FP,c}_{i,j}$, $Q^{FN,c}_{i,j}$, $Q^{RP,c}_{i,j}$, $Q^{RN,c}_{i,j}$ In Chapter 4, we considered simultaneous heat integration between the condenser and reboiler blocks for which the positions within the superstructure are known. While total condenser blocks include only cooling heat duty terms, i.e. $Q^{c}_{i,j}$, reboiler blocks, which are taken as partial reboilers, include only heating duty for horizontal block pairs, i.e. $Q^{hF}_{i,j}$. Hence, we present here the formulation for a possible match between only these two utility terms. But similar logic applies to all other possible matches.

A binary variable $z^{hx}_{i,j,i',j'}$ is defined to designate the match between the streams associated with these two streams:

$$z^{hx}_{i,j,i',j'} = \begin{cases} 1 & \text{if the hot stream from } B_{i,j} \text{ supplies heat to the cold stream at } B_{i',j'} \\ 0 & \text{Otherwise} \end{cases}$$

We define sets $Cond$ and Reb to denote the position of condenser and reboiler blocks within the superstructure. Also, $Cond^{hex} \subseteq Cond$ and $Reb^{hex} \subseteq Reb$ sets designate the condenser and reboiler blocks that are allowed to be included in the heat exchanger network. We define $hex = \{i, j, i', j' | (i, j) \in Cond^{hex}\ AND\ (i', j') \in Reb^{hex}\}$ to denote the building block pairs that are allowed to exchange heat. We define $q^{hex}_{i,j,i'j'}$ to denote the amount of heat that is exchanged between

condenser block $B_{i,j}$ and reboiler block $B_{i',j'}$. Then, we write the following energy balances for a possible integration between the two blocks:

$$Q^{hF}_{i,j} = Q^{h3}_{i,j} + \sum_{(i',j',i,j)\in hex} q^{hex}_{i'j',i,j} \quad i,j \in Reb^{hex} \tag{3.140}$$

$$Q^{c}_{i,j} = Q^{c3}_{i,j} + \sum_{(i,j,i',j')\in hex} q^{hex}_{i,j,i',j'} \quad i,j \in Cond^{hex} \tag{3.141}$$

In the above constraints, if there is no heat integration between the two blocks, or there is partial heat integration, then the heat duty terms $Q^{h3}_{i,j}$ and $Q^{c3}_{i,j}$ terms are used to quantify these residual heat terms.

For a feasible heat exchange operation, we need to also satisfy the following approach temperature constraint assuming isothermal condenser and reboiler operation:

$$dt^{hex}_{i,j,i',j'} \leq T_{i,j} - T_{i',j'} + (\Delta T^{max})(1 - z^{hx}_{i,j,i',j'}) \quad i,j,i',j' \in hex \tag{3.142}$$

Heat duty of a stream match is zero if the two streams do not exchange heat:

$$q^{hex}_{i,j,i',j'} \leq q^{max}(1 - z^{hx}_{i,j,i',j'}) \quad i,j,i',j' \in hex \tag{3.143}$$

3.6 Model Complexity and Solution Strategies

The proposed MINLP model for systematic process intensification can be used to automatically generate flowsheet variants without specifying the equipment types beforehand. Also, it provides a generic superstructure-based methodology for addressing process synthesis, integration and intensification problems. Here, we discuss several solution strategies when it is utilized for automated flowsheet generation. First, we provide some discussion over the MINLP model and present some integer cuts that we found useful in solving the optimization model. Then, in Section 3.6.2, we present several reformulations on the original MINLP that can help to reduce model complexity. In Section 3.6.3, we present a divide-and-conquer strategy that can be used to obtain good quality

initial solutions. In Section 3.6.4, we present a reduced superstructure model based on the one introduced in Section 3.3. for reactive separation systems that can be used to automatically identify different intensified/traditional structures based on an iterative refinement of the solutions with a reduced number of building blocks. In Section 3.6.5, we conclude our discussion on the modeling with some remarks over the number of building blocks required to solve a synthesis/intensification problem when building block-based approach is adapted.

3.6.1 Model Discussion and Integer Cuts

The quality of the solutions obtained from the superstructure is directly related with the size of the block-superstructure used in solving the model. As larger block superstructure with more number of blocks is used, more process alternatives are embedded in the solution space. However, problem size also increases with the increase in the number of blocks included in the superstructure and the effect of nonlinearity becomes more apparent. There are several different type of nonlinear terms in the model. There are bilinear terms in splitting and energy balance equations due to the multiplication of flow rate and composition, and temperature and flow rate terms, respectively. Signomial terms appear in phase equilibrium and work calculations. An indicative list of different types of nonlinear terms and their use in the model are summarized in Table 3.2 with reference to the equation numbers given in Demirel et al. [90].

Table 3.2: Nonlinear terms in the MINLP model.

Nonlinear terms	Type of nonlinearity	Use in the model	Equation*
$FP_{i,j,k} \times T_{i,j}$	Bilinear	Flow enthalpy	8a-d, A2b-s
$FP_{i,j,k} \times y_{i,j,k}$	Bilinear	Unrestricted boundary	18a-20
$K^{eq}_{i,j,k,s,m} \times y_{i,j,k}$	Bilinear	Phase equilibrium	31a-33b
$P^{sat}_{i,j,k}/P_{i,j}$	Fractional	Phase equilibrium	29
$P_{i,j} \times y_{i,j,k} \times CA_{i,j,s,m}$	Trilinear	Driving force	38a-39b
$P^{sat}_{i,j,k} \times y_{i,j,k}$	Bilinear	Bubble point	A1a
$P^{dew}_{i,j} \times \sum_k \frac{y_{i,j,k}}{P^{sat}_{i,j,k}}$	Signomial	Dew point	A1b
$P_{i,j+1}/P_{i,j}$	Fractional	Pressure ratio	B3, B6
$FP_{i,j,k} \times T_{i,j} \times (PR^F_{i,j})^{\frac{\gamma-1}{\gamma}}$	Signomial	Compression/expander work	B11-15

* Equation numbers refer to Demirel et al. (2017)[90].

Due to the model size, nonlinearity and nonconvexity, solving the MINLP model for large superstructure (5×5 or more) may be challenging. To this end, we have observed that providing redundant constraints, specially in the form of integer cuts, significantly help reducing the time and iterations needed for finding local solutions using commercial solvers in GAMS. For instance, we can impose that the only one boundary among the four surrounding boundaries of a block, can be assigned as semi-restricted. This constraint is written as

$$z^{srf}_{i,j} + z^{srr}_{i,j} + z^{srf}_{i,j-1} + z^{srr}_{i-1,j} \leq 1, \quad \forall i,j \tag{3.144}$$

Also, taking the phase of the feed block equal to the phase of the feed stream that enters into this block helps to reduce the time for finding feasible solutions:

$$z^{phase}_{i,j} \geq z^{phasefeed}_{f} - (1 - z^{feed}_{i,j,f}), \quad \forall i,j,f \tag{3.145}$$

$$z^{phase}_{i,j} \leq z^{phasefeed}_{f} + (1 - z^{feed}_{i,j,f}), \quad \forall i,j,f \tag{3.146}$$

$$z^{feed}_{i,j,f} \leq (1 - z^{feed}_{i,j,f'}), \quad \forall i,j,\ f \in GFS,\ f' \in LFS \tag{3.147}$$

where *GFS* is the set for gas feed streams and *LFS* is for liquid feed streams, and $z^{phasefeed}_{f}$ is a 0-1 parameter indicating the known phase of the feed stream. $z^{phasefeed}_{f}$ is one if the stream is in gas phase and is zero otherwise. The first two equations states that phase of the feed stream is equal to the phase of the block that it enters and the third equation ensures that if two feed streams are in different phases, then they cannot be fed into the same block.

Another issue of the current model is that, if $P_{i,j,k,p}$ = 0 and there is no unrestricted flow leaving block $B_{i,j}$, then the composition variables become arbitrary. As the semi-restricted flow is associated with a separation phenomenon and composition relations are essential for modeling separation phenomenon, there should exist at least one non-zero unrestricted outlet stream from block $B_{i,j}$ to prevent the concentration variables to become arbitrary. To address this issue, we need to ensure that there is a net non-zero flow across the boundaries apart from the semi-restricted

boundary. For instance, when Eq. 3.144 is utilized, if the boundary between block $B_{i,j}$ and $B_{i,j+1}$ is semi-restricted ($z_{i,j}^{srF} = 1$), then there should be at least ε amount of material flow from both block $B_{i,j}$ and $B_{i,j+1}$. To impose this we write the following constraints:

$$\sum_k \left(RP_{i,j,k} + RN_{i-1,j,k} + FN_{i,j-1,k} + \sum_p P_{i,j,k,p} \right) \geq \varepsilon \, z_{i,j}^{sF}, \quad \forall i,j \tag{3.148}$$

$$\sum_k \left(RP_{i,j+1,k} + RN_{i-1,j+1,k} + FP_{i,j+1,k} + \sum_p P_{i,j,k,p} \right) \geq \varepsilon \, z_{i,j}^{sF}, \quad \forall i,j \tag{3.149}$$

As these constraints are required for each boundary in the superstructure, similar equations are also written for vertical boundary.

$$\sum_k \left(FP_{i,j,k} + RN_{i-1,j,k} + FN_{i,j-1,k} + \sum_p P_{i,j,k,p} \right) \geq \varepsilon \, z_{i,j}^{sR}, \quad \forall i,j \tag{3.150}$$

$$\sum_k \left(FP_{i+1,j,k} + RP_{i+1,j,k} + FN_{i+1,j-1,k} + \sum_p P_{i,j,k,p} \right) \geq \varepsilon \, z_{i,j}^{sR}, \quad \forall i,j \tag{3.151}$$

We denote this minimum flow rate parameter as ε. The exact value of this parameter depends on the flow rates used in the system (For example, this value was taken as 10^{-5} for case study 1).

One method to find a feasible starting point is to divide the overall problem into one subproblem with the objective of minimizing the summation of slack variables added in the material balance and one master problem with the original objective. If the value for each slack variable returns to zero, then this solution could be regarded as a feasible solution of the original problem. However, there are several other approaches that we can use by utilizing the unique features of building block superstructure. These are explained in the next sections.

3.6.2 Reformulations

One reformulation is related with the superstructure boundaries. As we do not allow flow through the boundaries, we can eliminate the constraints that are written for the superstructure borders. For instance, Eqs. 3.10-3.12 are not required when $j = J$ as we do not allow flows

through the boundaries. Similarly, Eqs. 3.13-3.15 are not required when $i = I$. Hence, these constraints can be eliminated for the boundaries by ensuring that they are valid when $i < I$ in the vertical direction and $j < J$ in the horizontal direction. This is valid for all the remaining constraints written for the block boundaries and similar reductions can be performed.

Furthermore, in the original model described above, there are $K \times (I \times (J-1) + J \times (I-1))$ direction binary variables, i.e. $z^{Fplus}_{i,j,k}$ and $z^{Rplus}_{i,j,k}$, which scales with the number of number of chemical components included in the problem. Apart from the flow direction relationships, these binary variables appear in Eqs. 3.69-3.72 to satisfy unidirectional flow if there is no phase contact between the adjacent blocks. If we do not consider any phase contact in a problem, then we can remove the component indice from these variables as we would not need Eqs. 3.69-3.72. However, it is also possible to completely replace these direction relations along with Eqs. 3.11-3.15 for all cases if we apply the following constraints:

$$FP_{i,j,k} \leq FU_{i,j,k} \left(z^{srF}_{i,j} + z^{Fplus}_{i,j} \right), \quad \forall i,j,k \tag{3.152}$$

$$FP_{i,j,k} \leq FU_{i,j,k} \left(z^{srF}_{i,j} + 1 - z^{Fplus}_{i,j} \right), \quad \forall i,j,k \tag{3.153}$$

Similarly, in the vertical direction:

$$RP_{i,j,k} \leq RU_{i,j,k} \left(z^{srR}_{i,j} + z^{Rplus}_{i,j} \right), \quad \forall i,j,k \tag{3.154}$$

$$RP_{i,j,k} \leq RU_{i,j,k} \left(z^{srR}_{i,j} + 1 - z^{Rplus}_{i,j} \right), \quad \forall i,j,k \tag{3.155}$$

Another reformulation is related with the equilibrium reaction and sharp split models for the semi-restricted boundaries. Only one block is sufficient to represent the whole operation when these models are utilized. Hence, one does not need to define the underlying constraints for all the blocks within the superstructure. For instance, short-cut models for semi-restricted boundaries use $\tau_{i,j,k,s,m}$ to denote the split fraction (See Eqs. 3.104-3.107). If these models are used for incorporating design correlations for distillation columns to determine number of stages, minimum

reflux ratio, etc., then the design correlations are needed for each block. However, these models include nonlinear and nonconvex terms and including these variable with block superstructure indices, i.e. i, j, result in highly nonlinear models. Accordingly, when using sharp split models with design correlations, instead of defining each design variable to each block, we perform a reformulation and denote each of these design variables with their equipment indices only. For instance, $\tau_{i,j,k,s,m}$ is written as $\tau_{k,s}$ without the block indices. We use the following additional constraints to simplify the semi-restricted flow constraints (block inlet flow rate $\phi_{i,j,k}$ is assigned to the inlet flow rate of the boundary operation s, $F^{in}_{s,k}$, and semi-restricted flow, e.g. $FP_{i,j,k}$, is assigned with the separator flux, e.g. $F^{bot}_{s,k}$). See Appendix A for the details) :

$$F^{bot}_{s,k} = \tau_{s,k} F^{in}_{s,k} \quad k \in K, s \in S \tag{3.156}$$

Similar reformulations are performed for the reaction equilibrium constraints as well. An example on design of distillation columns is provided in Appendix A.5 with all the required constraints for this reformulation. A more detailed discussion can be found in Li et al., (2018) [139].

3.6.3 Frame Movement

Good initial guess on both binary variables and continuous variables can ease the search for feasible solutions [53]. Without a good initial guess, a feasible MINLP model can be diagnosed as infeasible by a convexity-based local solver. In obtaining good initial points, we can start from block representation of a known feasible flowsheet if it is available. Fixing binary variables based on such information helps to simplify the model formulation. Alternatively, if there is no initial flowsheet, we follow a 2-stage strategy to generate one: We first fix all the direction binary variables as 1 to only allow positive flows in both horizontal and vertical directions (as shown in Figure 3.3a). With this, we first investigate the alternative structures without recycle streams. To increase the number of utilized blocks within the block superstructure, we also fix the position of feed stream and main product stream at two corners of the superstructure (as indicated by the red and blue arrows). In the second iteration, we fix all the binary variables except the ones related with

the stream directions to the values obtained in the initial structure and relax the direction binary variables. Accordingly, recycle alternatives, if exist, can be identified in the second iteration. Note that if no feasible solution obtained within the current block superstructure after implementing 2-stage strategy, then larger block superstructures can be used to increase the number of alternatives. As mentioned above, the search for the feasible solution is exacerbated by the non-convexity of proposed MINLP model. Because of this, after initialization for the full model, the solution may get stuck at the initial feasible solution without further improvement. However, a subset of the superstructure (we refer it as a frame) is easier to conquer due to the smaller scale of MINLP problem. As long as there exists a feasible solution in the frame, this feasible solution is also valid for the original superstructure. While investigating the smaller domain, we exploit the possibility of integration and recycle within that region to refine the feasible solution. Based on the concept of frame, we develop an iterative solution strategy to improve the solution quality.

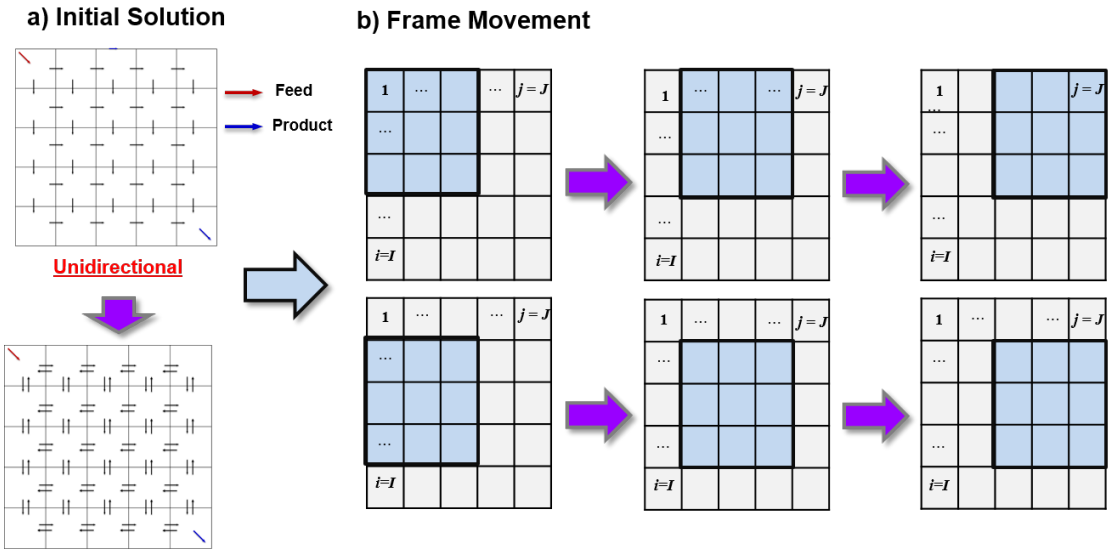

Figure 3.3: Frame movement strategy. a) If no initial solution is available, one can be generated through fixing the position of the feed and product blocks along with the stream directions. This significantly decreases the model size. b) Frame movement strategy is used to iteratively refine the initial solutions by exploring different solutions while focusing on a subset of building blocks (Modified with permission from [139]).

As is shown in Figure 3.3b, a frame is a collection of adjacent blocks in the block superstructure (blue blocks in Figure 3.3a). For given superstructure (here $I = 5$ and $J = 5$), we select a frame which is a subset of superstructure. Outside of this frame, all the binary variables are fixed to the solution available from the previous iteration. For the first iteration, this solution is the initial solution that is readily available or obtained through the strategy demonstrated in Figure 3.3a. All the binary variables within the frame are free to be optimized. After the first iteration (frame in the upper left corner), this solution is further utilized as an initial guess for a new frame (first move in the horizontal direction and then move in the vertical direction), as shown in the Figure 3.3b. The algorithm for frame movement ends until all the blocks in block superstructure are explored (see Figure 3.3b). It is important to mention that the frame movement strategy is not guaranteed to converge to a global solution, rather it is aimed at providing good initial solutions. Given the model complexity, we also found this to be a practical approach to obtain very good initial guesses when attempting to solve the MINLP problem using a global solver such as BARON[144] or ANTIGONE [145].

3.6.4 Iterative Refinement with Local Solvers

Here, we provide a method to automatically determine different equipment regions based on the reactive separation model introduced in Section 3.3. This methodology is found to be very useful for generating extractive, reactive or azeotropic systems. We consider a superstructure size of $I \times J = 2$ in which each building block pair in the horizontal direction share a VL-phase contact semirestricted boundary. We designate the blocks on the first column as liquid and in the second column as vapor blocks. We define completely restricted binary variables for each boundary between the vertical adjacent vapor blocks: $z_{i,j}^{crR}$. When it is 1, there is no mass transfer between the adjacent blocks and the pressures of the blocks are free. If it is zero, then the blocks belonging to the same equipment and their pressures are within the same range. This can be ensured through the following constraints:

$$RN_{i,j,k} \leq RU_{i,j,k}(1 - z_{i,j}^{crR}) \;\; i, j \in VN, k \in K \tag{3.157}$$

$$P_{i,j} \leq P_{i+1,j} - \Delta P_{i,j} + U z_{i,j}^{crR}; \quad P_{i,j} \geq P_{i+1,j} - \Delta P_{i,j} - U z_{i,j}^{crR} \;\; i,j \in VN, \;\; k \in K \quad (3.158)$$

where $\Delta P_{i,j}$ is a positive variable indicating the pressure drop between $B_{i,j}$ and $B_{i+1,j}$. Eqs. 3.157 ensure there is no flow when the boundary is completely restricted and Eq. 3.158 states that pressures of the neighboring blocks in the vertical direction do not necessarily stay within the same range if they are separated by a completely restricted boundary. Otherwise, this pressure relation holds and change in pressure within the same region is limited by the pressure drop. Note that if pressure drop is neglected, pressures within the same region becomes equal. We also allow jump stream connections between non-adjacent liquid blocks to allow for additional connectivity. This results in a generic formulation through which many different alternatives can be generated. This is demonstrated in Figure 3.4a-b. From this representation and optimization model, it is possible to generate a separation column with a side reactor configuration (Figure 3.4a) and a sequence of distillation columns including a reactive separation and stripper columns, among many other solutions (Figure 3.4b).

3.6.4.1 Symmetry Breaking Constraints

When equipment regions are not specified beforehand and jump streams activated, proposed MINLP model becomes highly nonlinear. Also, the superstructure becomes symmetric as the same solutions can be obtained with different block structures. To reduce this, we include the following symmetry breaking constraint which states that pressures of the blocks should decrease in the vertical direction after accounting for the pressure drop:

$$P_{i,j} \geq P_{i+1,j} - \Delta P_{i,j} \;\; i,j \in VN, \;\; k \in K \quad (3.159)$$

We also utilize the initialization strategy described in Figure 3.4c to obtain good initial solutions. Here, boundary assignments and jump stream connections are activated in an iterative manner. This can be visualized as a frame movement which moves one row at a time until all completely restricted boundaries and jumps streams are activated. In solving the problem, we use DICOPT with an initial solution from a known structure, e.g. base-case design. Then this initial

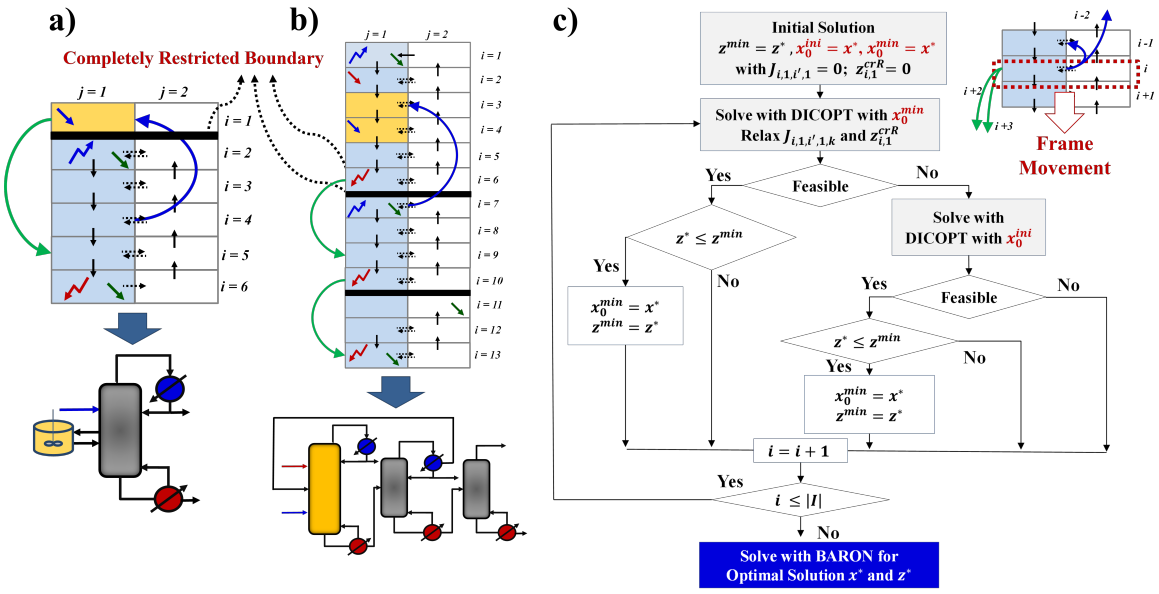

Figure 3.4: Iterative refinement algorithm for generation of novel reactive separation processes. Different solutions can generated from the same superstructure through the proposed optimization formulation. From the same superstructure, a) a separation column with a side-reactor configuration, b) a reactive distillation column followed by a distillation and stripper columns can be generated. c) Solution algorithm with an iterative activation of completely restricted boundary and jump stream variables.

solution is updated if a better solution can be located within the loop. After all connections and binary variables are activated, solution is used for initializing a final iteration with global MINLP solver BARON[146]. Furthermore, although this formulation can be directly used with the objectives that do not require any capital cost calculation, using economic objective requires additional variables to designate all possible equipment alternatives. While this is possible, it will result in large number of binary variables. Instead, we consider the whole superstructure as a single reactive separation column and use Eqs. 3.135-3.137 to penalize the high vapor flow rates and reaction volumes while using economic objectives. This assumption generally underestimates the solution as it will be shown in the case study.

3.6.5 Discussion on Number of Blocks

As aforementioned, the quality of the solutions obtained from the superstructure is directly related with the size of the block-superstructure used in solving the model. As larger block superstructures are used, more process alternatives are embedded in the solution space. Number of blocks used in a problem depends on several factors.

The number of blocks within the superstructure should ensure that there are enough blocks to allow for sufficient number of phenomena combinations for a feasible operation. Also, connectivity between phenomena need to be ensured through either direct connections or jump streams. In other words, a fully connected block superstructure with all possible phenomena combinations is the one that includes all the solutions. But, ensuring this is not a trivial task. Though this depends on several other factors as discussed below, one remedy for determining the building block superstructure size is to start with a small superstructure size which can be solved easily and increase the size until no better solution can be located. Here, the solutions obtained from smaller superstructures can be directly embedded as an initial solution for the larger ones.

Secondly, number of blocks might affect the model accuracy when representing traditional and/or intensified equipment types. For the operations that require distributed models, building blocks operates on discretized spaces, e.g. CSTRs-in-series model. For a packed-bed reactor (PBR), if one chooses an equilibrium reaction model in which the equilibrium conditions are reached instantaneously, then one building block would be sufficient to describe the operation of the whole PBR. If, on the other hand, kinetic models (e.g., power law kinetics) are used to describe the reactions, then each building block with reaction would represent a single continuous stirred-tank reactor (CSTR) and the operation of the entire PBR could be approximated with an array of equal-volume reaction building blocks. This corresponds to a CSTRs-in-series model, and the number of building blocks determines the accuracy of the reactor model. Similarly, with an equilibrium-stage model of a distillation column, each building block pair (i.e., adjacent vapor and liquid blocks separated by a semi-restriced boundary) represents an equilibrium stage, and the total number of building blocks required to represent a distillation column is equal to the total

number of equilibrium stages required for separation. With a more-rigorous rate-based model of multicomponent mass transfer between vapor and liquid phases (e.g., the Maxwell-Stefan diffusion model), each building block pair represents an actual stage, and the total number of building blocks required to represent a distillation column is equal to the total number of real stages required for separation [136].

Thirdly, according to the objective function, there can be an optimal number of building blocks that can deliver the process requirements. For instance, for a distillation column comprised of multiple vapor-liquid phase contact building blocks, number of block pairs determine the number of stages required for separation. If we use an objective function with economic considerations, there will be an optimal number of building blocks which yield the minimum cost for separation based on the trade-off between operating and capital costs. However, if we use an objective function which requires to minimize the energy required for the process, then each additional building block pair will contribute to less energy consumption due to higher number of stages. In this case, we can utilize different sizes of building block sizes and denote the optimal structure when the improvement with respect to previous solution decreases below a certain value.

4. CASE STUDIES*

In this chapter, several different examples are used to demonstrate the use of building block superstructure as a generic method for systematic process intensification. Problems are chosen from a variety of chemical process design problems.

The purpose of the case study in Section 4.1 is to demonstrate the utility of our proposed method for systematic process design and intensifcation using building blocks through a problem on waste reduction via conversion of hazardous chemicals. Specifically, we use the block superstructure to demonstrate how we can (i) eliminate the need for a process superstructure with fixed connections and prespecified units, (ii) optimize integrated and intensified process alternatives using building blocks, and (iii) obtain nonintuitive and better alternatives than those typically considered for process intensification.

In Section 4.2., we specifically demonstrate that many attractive process alternatives can be obtained using the same block superstructure based on an example on CO_2 utilization from power plant flue gas. We will demonstrate that both intensified and non-intensified flowsheet alternatives can be automatically generated.

In Section 4.3., we again use an example on the processing of power plant flue gas streams, yet, this time we will introduce phase considerations and aim to generate a process for CO_2 capture from a flue gas stream. This problem demonstrates how phases can be automatically identified based on the proposed MINLP model.

In Section 4.4., we demonstrate the benefit of the frame movement solution strategy on a problem for the synthesis of methanol from biogas stream. We will use a larger superstructure than the previous three problems and incorporate an objective function considering capital costs. Fur-

*Parts of this chapter were adapted with permission from (S. E. Demirel, J. Li, and M. M. F. Hasan, "Systematic process intensification using building blocks," Computers & Chemical Engineering, vol. 105, pp. 2 - 38, 2017.) Elsevier, from (S. E. Demirel, J. Li and M. M. F. Hasan, "A general framework for process synthesis, integration, and intensification," Industrial & Engineering Chemistry Research," vol. 58, no. 15, pp. 5950 - 5967, 2019.) Copyright (2019) American Chemical Society, from (J. Li, S. E. Demirel, and M. M. F. Hasan, "Process synthesis using a block superstructure with automated flowsheet generation and optimization," AIChE Journal, vol. 64, no. 8, pp. 3082 - 3100, 2018.) Copyright (2018) John Wiley & Sons, Inc., and from

thermore, we will show how short-cut models for the separation phenomena can be utilized. As a result of the solution, we demonstrate that not all intensified alternatives are desirable.

In Section 4.5, we show the use of the proposed framework as a generic superstructure-based method for the synthesis of reactive distillation systems. Specifically, two simple example problems based on an ideal and non-ideal system are considered. Resulting design for the non-ideal system is also verified based on rigorous simulations.

In Section 4.6, we show the use of the building blocks for the synthesis of membrane-based separation systems. Specifically, we use two different examples. First, we use a literature example on the separation of a syngas mixture into pure H_2 through a gas separation membrane network. We first use building block superstructure to replicate the same alternatives as were considered in the literature example. Solution of the problem through this superstructure provides a more economically viable alternative than the best known literature solution. Furthermore, by using the full potential of building block superstructure, we could identify an even better solution highlighting the benefit of the proposed methodology

As a second example in Section 4.6., we use the building block superstructure for the synthesis of hybrid separation systems along with material optimization. We demonstrate this with a separation problem ubiquitous in chemical systems, i.e. methanol/water separation. Specifically, we investigate whether a zeolite-based membrane module can be used to retrofit a distillation column for high purity separation of this binary mixture. We show that while standalone membrane process is not an attractive alternative to distillation, using distillation and membrane together provides a slightly better alternative compared to standalone distillation column. But using simultaneous heat integration, we come up with a hybrid scheme that promises much more potential. We also perform a sensitivity analysis on the membrane properties and identify several targets for further improvement.

In Section 4.7, we demonstrate how short-cut and more rigorous phenomena models can be sequentially utilized to perform systematic process intensification with an example on high purity ethylene glycol production. We first use the building block superstructure to screen between

the traditional equipment types and generate a base-case. We also demonstrate the benefit of simultaneous heat integration considerations on the synthesis of chemical systems. The resulting heat integrated process is used as a base-case for process intensification with rigorous phenomena-based models. As a result of intensification, several different alternatives are generated. The most promising design suggests a much more compact process than the base case with 40% reduction in number of equipment requiring less capital investment.

In Section 4.8., we use ethylene glycol production problem as an example to demonstrate the use of the proposed model and representation for sustainable process intensification with multi-objective optimization. We first compare two base-case designs and show that intensification do not yield an attractive alternative compared to non-intensified counterpart. Then, we use the building blocks to automatically generate multiple alternatives suggesting substantial improvement in both economics and sustainability fronts.

Unless otherwise stated, all example problems were solved in GAMS on a Dell Optiplex 9020 computer (Intel 8 Core i7-4770 CPU 3.4GHz, 15.5 GB memory) running Springdale Linux.

4.1 Waste Reduction through Conversion of Hazardous Chemicals

This case study addresses a waste reduction problem from a gaseous stream containing two components A and B, where A is a hazardous chemical that we want to convert to B as much as possible before discharging the gaseous stream to the environment. Similar problems are often encountered in the reduction of greenhouse gas emissions from industrial processes. Examples include the catalytic decomposition of NO into N_2 and O_2, the reduction of CO_2 from combustion exhausts, the conversion of H_2S into elemental sulfur, etc. In these processes, the reactions at hand are equilibrium limited but obtaining high conversion is a challenge [147]. Here, we consider an equimolar mixture of A and B (50% A and 50% B) at a flow rate of 0.5 kmol/s. A catalyst material ($catAB$) is available to convert A to B according to the following heterogeneous reversible and isothermal gas phase reaction:

$$A \leftrightarrow B \quad -r_A = k_f P_A \left(1 - \frac{P_B}{K P_A}\right)$$

where k_f is 0.3 kmol/bar.kg-cat and K is 4. If needed, we can also use a membrane (*M1*) which is highly selective to B with a maximum available area of 1000 m^2, a permeance of 3.125×10^{-7} mol/m^2-s-bar for A and a permeance of 4.689×10^{-5} mol/m^2-s-bar for B. The objective here is to maximize the yield of B in the treated stream. We do not impose any purity specification for the product stream as the goal is to remove the hazardous material as much as possible.

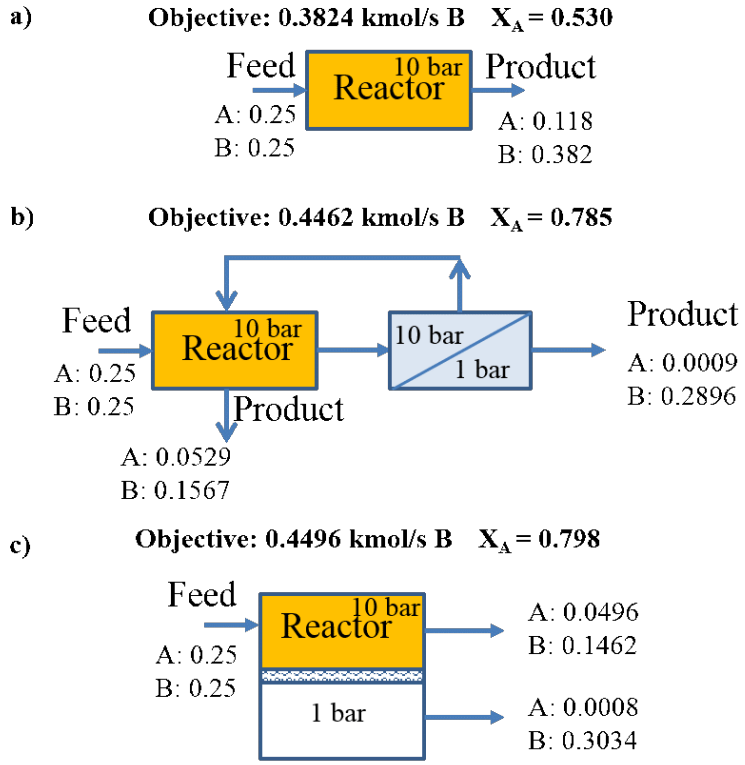

Figure 4.1: Base case designs for the conceptual waste reduction problem. Traditional design utilizing a reactor only, (b) integrated design utilizing isolated membrane and reactor units which are integrated via recycle, and (c) intensified design using a membrane reactor. Above each flowsheet, the optimum flow rate of product B is shown with the corresponding overall conversion of reactant A. Numbers near each feed and product stream indicate the amount of flow in kmol/s (Reprinted with permission from [90]).

Before applying the proposed approach, three intuitive process alternatives are investigated as base designs (Figure 4.1a-c). For comparision, the amount of catalyst is taken to be 1 kg for all cases. The first base design (Figure 4.1a) is the simplest and includes only a reactor. Overall conversion of A is 53% while equilibrium conversion of *A* at these inlet conditions is 60.0%. To increase the overall conversion per kg of catalyst, we may consider a second alternative (Figure 4.1b) which is an 'integrated' process where the unreacted *A* from the reactor effluent is separated using membrane and is recycled back to the reactor. In this way, the overall conversion of *A* is increased to 78.5%, when the recycle stream has a flow rate of 2 kmol/s (a recycle-to-feed ratio of 4). Lastly, we can have a third alternative (Figure 4.1c) which is a classical 'intensified' process - a membrane reactor. As the product removal and reaction proceeds simultaneously within the membrane reactor, it also achieves increased conversion of *A* of 79.8%. Integrated process (Figure 4.1b) has a slightly lower overall conversion than that of the intensified process (Figure 4.1c). It should be noted that the conversion achieved by the integrated process can be further improved by increasing the recycle-to-feed ratio. In fact, the integrated process will converge to the intensified process alternative as the recycle-to-feed ratio approaches to very large values. This observation is in line with that of Baldea (2015) [96] who showed that process intensification corresponds to tight process integration with large recycles and material hold ups. However, there are physical and practical limitations on the amount of flow rates that can be utilized in a process. This underpins the importance of process intensification which allows enhanced process performance, such as increased conversion, without large recycles and material hold ups. (Note that the three base designs shown in Figures 4.1a-c are optimized using our block superstrcuture by fixing the process topologies while considering the reactors as CSTR and assuming complete mixing for the membrane separator. An upper bound of 2 kmol/s is used for the flow rate of each component in each stream. This upper bound on stream flow rate also acts as an upper bound on the amount of material recycled for the integrated process alternative. Upper and lower bound on the pressure is taken as 10 and 1 bar, respectively. Global solutions are obtained using ANTIGONE within few seconds with 10^{-8} absolute tolerance).

Now, we solve the same problem through proposed building block superstructure-based approach and demonstrate that it is possible to systematically obtain nonintiutive process alternatives achieving even higher conversions than that of the already intensified membrane reactor. For this case study, we use a 3 $\times$ 3 block superstructure $I = 3$ and $J = 3$. This means that all the process alternatives are considered to be embedded within and represented using at most 9 building blocks. A smaller superstructure may not contain all plausible process alternatives. On the other hand, a larger superstructure will increase the model size. Furthermore, we consider the following: $s = \{GP\}$, $m = \{M1\}$, $c = \{catAB\}$, $k = \{A, B\}$, $f = \{Feed1\}$, $p = \{Prod1\}$, $r = \{forward, reverse\}$. Since only gas phase operations are plausible, the model equations which are related to other phases (e.g., liquid, two-phase) are excluded. Since we do not have two-phase mixtures and the relevant equilibrium conditions, only unidirectional flows are present. Therefore, for Equations 3.11, 3.12, 3.14, 3.15, we redefine the direction binary variables, $z_{i,j}^{Rplus}$ and $z_{i,j}^{Fplus}$, without the component index *k*. This further reduces the model size. We select the kinetic reaction model to describe the reaction. In Equation 3.49, we define $f^{rxn} = P_{i,j}\ y_{i,j,k'}$ and kin set as $\{A, forward\}$ and $\{B, reverse\}$. Temperature dependency terms are removed and $ki_{forward} = 0.3$ and $ki_{reverse} = 0.075$. In Equation 3.51, $V_{i,j} = 1$ kg for fixed amount of catalyst and $Conv_{r,c} = 1$ as the reaction model is based on kinetics. To be able to compare with the three base case results, we further (i) restrict the selection of reactor blocks to one ($\sum_{i,j} z_{i,j,c=catAB}^{rxn} = 1$), (ii) restrict a reactor block to have 1 kg of the catalyst ($V_{i,j} = 1$ kg), and (iii) allow only one boundary to be semi-restricted. With this, the MINLP model includes 111 binary variables, 270 continuous variables, and 604 contraints with 2063 nonzero elements. (Specifically, Eqs. 1-2, 4-6, 11-13, 17-21, 22b, 23a, 23c, C1-C3, C5, 38-39, 46, 51 and 53 given in Demirel et al. (2017) [90] are included to solve this particular problem.)

We obtain a solution to this model using the global solver ANTIGONE with 24 hours as the maximum CPU time (Note that the feasible solution is obtained in a couple of minutes). A product yield of 0.451 kmol/s for *B* is obtained with 10.9% optimality gap. This corresponds to a conversion of 80.3% for *A*, which is higher than the conversion obtained by a mebrane reactor (Figure

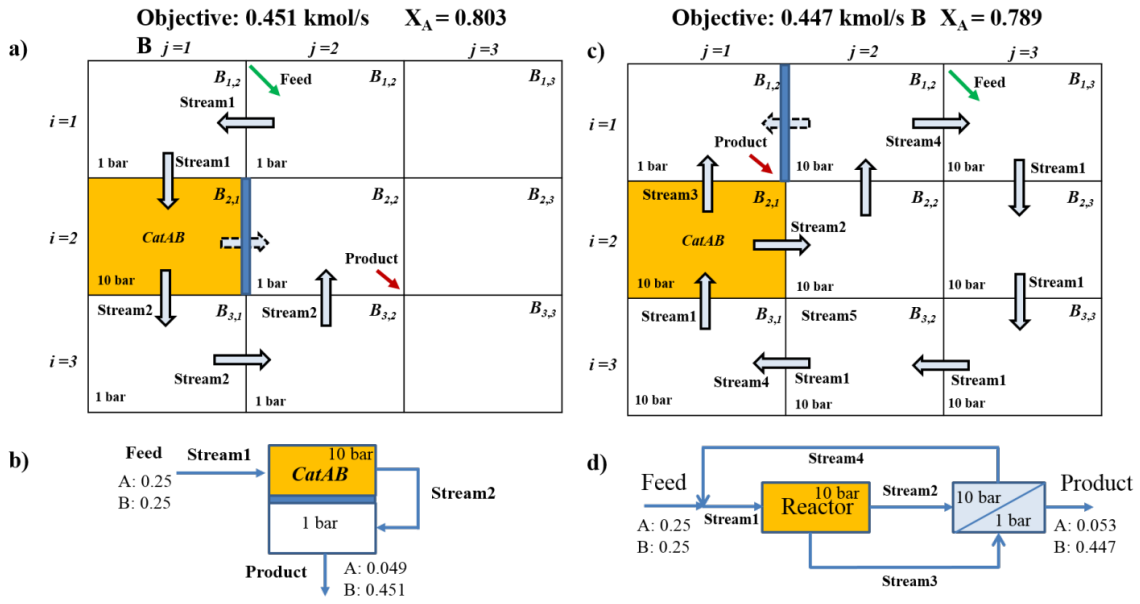

Figure 4.2: Building block results for the conceptual waste reduction problem. While (a) and (b) show the block and flowsheet representations of the optimal intensified process, (c) and (d) show the block and flowsheet representations of the optimal integrated process, respectively (Reprinted with permission from [90]).

4.1c) using the same amount of catalyst and membrane materials. The resulting block structure and its equivalent process flowsheet are shown in Figures 4.2a and 4.2b, respectively. There is one feed and one product stream assigned to blocks $B_{1,2}$ and $B_{2,2}$, respectively. The catalyst material is assigned to block $B_{2,1}$ and boundary between blocks $B_{2,1}$ and $B_{2,2}$ is assigned to the membrane. As the reaction block and semi-restricted boundary are adjacent to each other, we identify a membrane reactor that is the combination of blocks $B_{2,1}$ and $B_{2,2}$ in which $B_{2,1}$ acts as the retantate and $B_{2,2}$ acts as the permeate side of the membrane reactor (Figure 4.2b). We also observe that the retantate stream, which is also the effluent of the reactor, is sent to the permeate side of the membrane which acts as a sweep gas and dilutes the permeate side in terms of the product *B*. The use of reactor outlet as sweep gas fascilitates a lower concentration of *B* in the membrane permeate side, which increases the separation driving force. Hence, a higher concentration of reactant *A* can be achieved in the reactor block to increase the overall conversion to 80.3%.

From the above results, we observe that the block superstructure can identify both typical and

enhanced intensification alternatives. Furthermeore, we have increased the conversion from 53% to 80.3% for the given problem. This corresponds to more than 51% improvement in conversion through our proposed method, compared to the base case. We will now show that the same block superstrucure also contains different process integration alternatives. To this end, we can impose the following special constraint to discard any membrane reactors from the solution of this case study:

$$z^{srf}_{i,j} + z^{srr}_{i,j} + z^{srf}_{i,j-1} + z^{srr}_{i-1,j} + \sum_{c} z^{rxn}_{i,j,c} \leq 1, \quad \forall i, j \tag{4.1}$$

The above integer cut imposes that if a block is assigned with a catalyst, then none of boundaries can be semi-restricted. Furthermore, if one of the boundaries surrounding the block is assigned as semi-restricted, then that block cannot be assigned with a catalyst material. When we include the above constraint in the model and solve again with ANTIGONE for 24 hours, we obtain an objective value of 0.4473 kmol/s with 11.8% optimality gap. This result corresponds to 78.9% overall conversion of *A*. The resulting block structure and the corresponding flowsheet representation are shown in Figures 4.2c and 4.2d, respectively. We observe from Figure 4.2c that there is one feed and one product stream assigned to blocks $B_{1,3}$ and $B_{1,1}$, respectively. The catalyst is assigned to block $B_{2,1}$ and the boundary between blocks $B_{1,1}$ and $B_{1,2}$ is assigned a membrane. For this membrane, the block $B_{1,1}$ acts as the permeate side and the block $B_{1,2}$ acts as the retantate side. The outlet from the retantate side is mixed with the feed stream in block $B_{1,3}$. The mixed stream (as Stream1) is then fed to the reactor block $B_{2,1}$. The reactor effluent is split into two sub-streams (Stream2 and Stream3). Stream2 is sent to the retantate side of the membrane, while Stream 3 enters the permeate side and acts as a sweep stream. Overall, this process is well-integrated in a sense that it separetes a portion of the unreacted feed and sends back to the reactor for increased conversion. This newly integrated process alternative achieves 0.6% higher conversion of reactant *A* than that of the alternative shown in Figure 4.1b. This improvement is again attributed to the use of a fraction of the reactor effluent in the permeate side of the membrane.

4.2 CO_2 Utilization from Power Plant Flue Gas

In this case study, we investigate on the synthesis of a process for the utilization of CO_2 from an oxy-combustion flue gas stream. Specifically, we want to convert the CO_2 from the flue gas stream by using natural gas and steam to produce syngas (CO and H_2) suitable for the production of value-added chemicals (e.g., methanol). We consider the reactions that can be used for the direct conversion of CO_2 for syngas production. These are dry reforming (DR) and bi-reforming (BR) reactions. Furthermore, we allow separate high temperature water-gas shift (HT-WGS) and partial oxidation of methane (POM) reactions to adjust the product syngas ratio. If needed, a hydrogen selective membrane material can be used. Four feeds are considered: oxy-combustion Flue Gas[148] (60% CO_2, 19% H_2O, 17% N_2, 4% O_2) at 1 bar and 400 K, methane (NG) at 20 bar and 298 K, Steam at 1 bar and 800 K, and Air (21% O_2, 79% N_2) at 1 bar and 298 K. The available fow rates of the Flue Gas, NG, air and stream are 1 kmol/s, 1 kmol/s, 5 kmol/s and 5 kmol/s, respectively. These feeds can be split and provided at multiple places within the process.

Table 4.1: Reaction data for flue gas utilization problem (Adapted with permission from [90]).

Reaction	Stoichiometry	Reaction Conditions
Water-Gas Shift[149]	$CO + H_2O \rightarrow CO_2 + H_2$	X_{CO}=0.90, 773 K, 1 bar
Dry Reforming[150]	$CH_4 + CO_2 \rightarrow 2CO + 2H_2$	X_{CO_2}=0.98, 873 K, 1 bar
Bi-Reforming[151]	$3CH_4 + 2H_2O + CO_2 \rightarrow 8H_2 + 4CO$	X_{CO_2}=0.71, 1103 K, 1 bar
Partial Oxidation[152]	$CH_4 + 0.5\ O_2 \rightarrow 2H_2 + CO$	X_{CH_4}=0.96, 1173 K, 1 bar

The objective is to maximize the net utilization of CO_2 as follows:

$$\max \sum_{i,j,f} M_{i,j,CO_2,f} - \sum_{i,j,p} P_{i,j,CO_2,p} - GWP_{CH_4} \sum_{i,j,p} P_{i,j,CH_4,p} - Eq_{NG} \sum_{i,j,k} M_{i,j,k,NG} - Eq_{el} \sum_{i \in I} \sum_{j \in J} W_{i,j}^{com} \tag{4.2}$$

The first term in the objective function indicates the total amount of CO_2 entering into the system, the second term is the total amount of CO_2 leaving the system through product streams. In CO_2 utilization problems, one considers both the direct and indirect CO_2 emissions [153]. Accordingly, the third term in the objective function is the CO_2 equivalent of the total amount of CH_4 leaving the system. GWP_{CH_4} has a value of 25 [154]. The fourth term indicates the indirect CO_2 emission related with the natural gas usage. Eq_{NG} is the amount of CO_2 emission caused by the unit amount of natural gas use in the process and it is taken as 0.131 kmol CO_2/kmol natural gas. The fifth term indicates the indirect CO_2 emission caused by the electric consumption of the process and Eq_{el} is the amount of CO_2 emission caused by the unit amount of energy used by the compressors. Eq_{el} is taken as 0.00233 kmol CO_2/MW [155].

Table 4.2: Membrane data for flue gas utilization problem (Adapted with permission from [90]).

Membrane Data	CH_4	H_2O	H_2	CO	CO_2	N_2	O_2
Permeance[156] ($\times 10^{-7}$ kmol/bar m^2 s)	3.03	2.54	13.6	2.08	2.54	2.08	2.08

The overall problem is set as follows. We use a 3×3 block superstructure $I = 3$ and $J = 3$. which means that the process is to be represented using at most 9 building blocks. Problem includes following sets: $f = \{FG, NG, Steam, Air\}$, $p = \{Prod, Waste\}$, $s = \{GP\}$, $m = \{M1\}$, $r = \{DR, BR, POM, HT - WGS\}$, $k = \{CH_4, H_2O, H_2, CO, CO_2, N_2, O_2\}$, $c = \{DRcat, BRcat, POMcat, HTWGScat\}$. *Prod* is the main product stream by which we want to obtain the syngas stream with the specified requirements. The product is required to be

at least 0.8 kmol/s with 50% H_2 while satisfying the ratio: $H_2 \geq 2CO + 3CO_2$ in order to be suitable for methanol production [153]. Product flow rate and composition requirements are satisfied by taking: $y^{MIN,prod}_{k=H2,p=Prod} = 0.5$, $D_{p=Prod} = 0.8$ kmol/s, $Ra^{min}_{\bar{k}=CO2\ ,\bar{\bar{k}}=H2,\ p=Prod} = 2$ and $Ra^{\min}_{\bar{k}=CO\ ,\bar{\bar{k}}=H2,\ p=Prod} = 3$. For *Waste* stream, we do not have any purity or flow rate requirements. Since we consider only gas phase operations, the model equations which are related to other phases (e.g., liquid, two-phase) are excluded. Similar to the previous problem, we redefine the direction binary variables, $z^{Rplus}_{i,j}$ and $z^{Fplus}_{i,j}$, without the component index *k* which further reduces the problem size. We select the stoichiometric reaction model to describe the reactions. Conversion values and at which reactor conditions that those conversion values obtained are listed in Table 4.1 along with their references. For HT-WGS and POM reactions, it is assumed that the conversion values are independent of the reactor pressure. For all the reactions, given reactor conditions are enforced by using Eq. 41 in Demirel et al. (2017) [90]. For the BR and DR reactions, the presence of oxygen in the reactor inlet may result in a different reaction stoichiometry than the given by Table 4.1. Hence, for these two reactions, Eq. 42 from Demirel et al. (2017) [90] is used with k^* as O_2 and c^* as *BRcat* and *DRcat*. Also, in order to realize the inlet flow requirements for HT-WGS and DR reactions, Eq. 44 from Demirel et al. (2017) [90] is enforced with $Ratio_{c^*=HTWGScat,k'=H2O,k''=CO} = 4$ and $Ratio_{c^*=DRcat,k'=CO2,k''=CH4} = 1.1$. Membrane material permeance values are given in Table 4.2. For the species that the data were not supplied in the reference study, permeance values for the similar membrane structures are compared and, accordingly, CO, N_2, O_2 permeances and CO_2 and H_2O permeances are assumed to be the same. Furthermore, in membrane diffusion calculations, permeance values are assumed to be independent of temperature, pressure and concentration. Maximum allowed membrane area is 1×10^6 m^2. *FU* and *RU* are taken as 5 kmol/s. We assign P^{min} = 1 bar, P^{max} = 20 bar, T^{min} = 298 K, and T^{max} = 1500 K. The compressor and expander efficiency is considered to be 80%. The resulting model has 174 binary variables, 1140 continuous variables, 2338 constraints with 9099 nonzero elements. (Specifically, Eqs. 1-3a,3c-d, 4-13, 17-21, 22a, 23a-b, C1-C4, 24, 27, 38-39, 41-42, 44, 51, 53 and B1-15 given in Demirel et al. (2017) [90] are included to solve this particular problem.)

We specifically investigate on three process alternatives that we obtain from the solutions of this model. The first alternative is obtained by solving the model using ANTIGONE for 10800 CPU seconds with an objective value of 0.4385 kmol CO_2 with 18.9% optimality gap (Upper bound is 0.5214 kmol/s). As the objective value is positive, a net CO_2 utilization is achieved. Obtained block structure and its equivalent process flowsheet is given in Figure 4.3. We name this alternative as Process Alternative 1. In this alternative, only 4 blocks are utilized and the rest of the blocks are empty. All of these four blocks are assigned with a catalyst material and there is a membrane material between blocks $B_{1,2}$ and $B_{2,2}$. As the membrane material is sandwiched between two catalyst materials, we can identify a highly intensified membrane reactor from the blocks $B_{1,2}$ and $B_{2,2}$. In this membrane reactor, both retantate and permeate sides of the membrane are filled with catalyst *POXcat* and there is 3.5 bar total pressure difference between the two sides. POX reaction is chosen as the feed flue gas stream contains oxygen and this oxygen needs to be utilized before entering into the dry reforming reactors. Outlet streams from both permeate and retantate sides of the membrane reactor are sent to dry reforming reactors. These dry reformers are used to utilize the CO_2 left in the membrane outlet streams. Product stream with 0.4 kmol/s H_2 flow rate and with hydrogen content of (H_2 = 2CO + 3CO_2) is obtained from the dry reformer that utilizes the outlet of the retantate side of the membrane reactor. Although dry reforming reaction produces syngas with 1:1 ratio, as the retantate side of the membrane reactor is richer in hydrogen due to the use of a hydrogen selective membrane, dry reforming reaction becomes a feasible alternative for the utilization of CO_2. The other dry reformer, with the permeate side of the membrane reactor as the inlet stream (reactor positioned at block $B_{1,3}$), is simply chosen to utilize left-over CO_2 and CH_4 which results in decrease in the amount of CO_2 emitted from the waste stream.

If we solve the same model with ANTIGONE for 24 hours, we obtain another process flowsheet with an objective value of 0.4894 kmol CO_2 with 6.5% optimality gap (upper bound is 0.5214 kmol/s). The resultant block structure and its equivalent process flowsheet are shown in Figures 4.4a-b (Process Alternative 2). When we analyze this result, we observe that a POX reactor (block $B_{3,1}$) is seleted followed by a Dry Reformer (block $B_{3,2}$). The effluents from the dry reformer

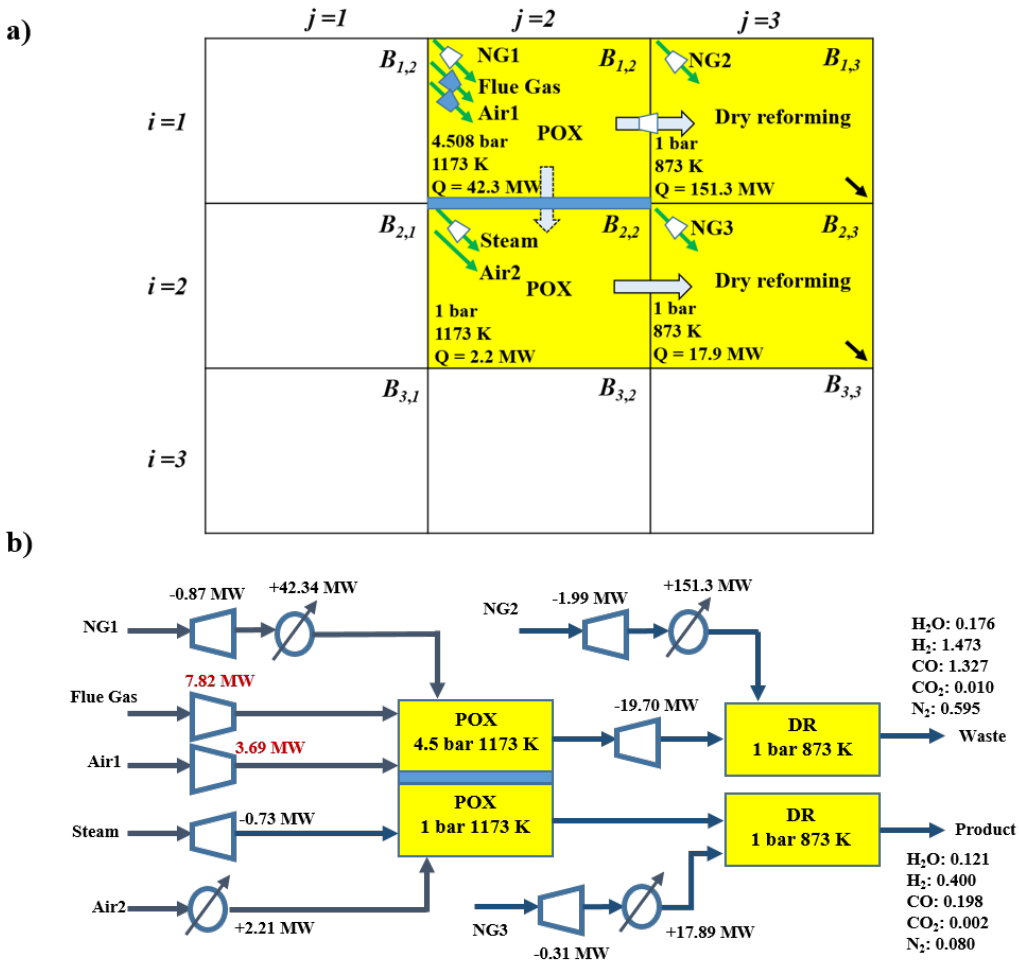

Figure 4.3: Process alternative 1 for the CO_2 utilization from flue gas process. (a) optimal block results, and (b) its equivalent process flowsheet. In block configuration, there are seven feed streams shown in green, and two product streams shown in black color. There are four reaction blocks shown in yellow and one membrane material positioned on semi-restricted boundary between blocks $B_{1,2}$ and $B_{2,2}$ shown in blue. In the bottom flowsheet, compressor works are shown in red and expander works are indicated with a negative sign. The numbers near the product and waste streams indicate the component flow rates in kmol/s. As it can be seen from the classical process flowsheet representation, process is composed of one membrane reactor with catalyst materials placed on both sides of the membrane material, and 2 reactors which are used in further CO_2 abatement (Reprinted with permission from [90]).

are first cooled (block $B_{2,2}$) and then compressed to 2.397 bar. The cooling step is included to decrease the stream temperature which in turn decreases the required work for compression. The compressed mixture enters into block $B_{2,3}$ which is separated from block $B_{1,3}$ by a semi-restricted boundary. This boundary is also assigned a membrane material. For the membrane, block $B_{2,3}$ acts

as the retantate side and block $B_{1,3}$ acts as the permeate side. Steam is taken as feed to dilute the permeate side and to increase the driving force accross the membrane. Therefore, steam acts as a sweep gas for the membrane separation. The product is taken out from the block $B_{1,3}$, which is the permeate side of the membrane.

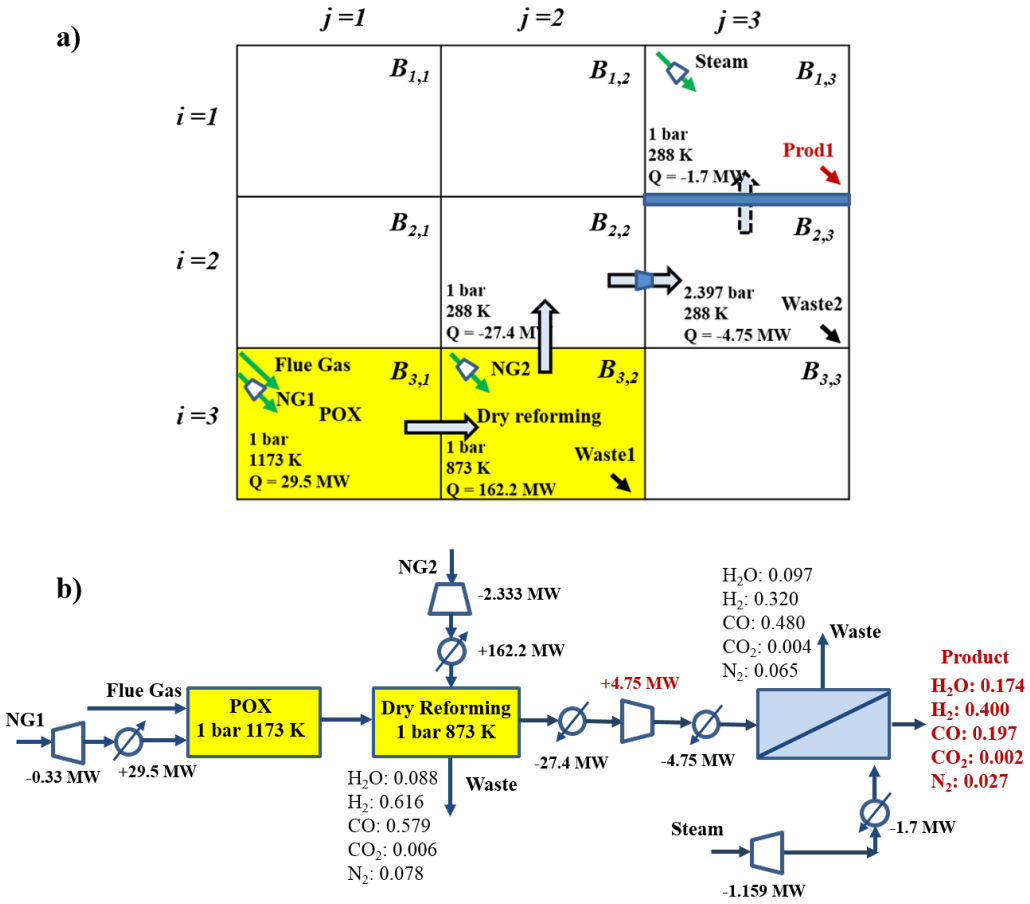

Figure 4.4: Process alternative 2 for the the CO_2 utilization from flue gas process (Reprinted with permission from [90]).

The third process alternative is obtained by solving the same model with ANTIGONE for 24 hours while changing the default solver option for the maximum RLT cuts (max_rlt_cuts) to 10. In this case, the objective value is further improved to 0.4918 kmol/s while the upper bound still remains to be 0.5214 kmol/s (optimality gap is decreased to 6.0%). The resultant block structure

and its equivalent process flowsheet are shown in Figures 4.5a-b. When we analyze this result, we again observe a POX reactor (block $B_{3,3}$) followed by a Dry Reformer (block $B_{2,3}$). The effluents from the dry reformer are first cooled (using block $B_{1,3}$) and are then compressed to 2.386 bar. The compressed mixture enters into block $B_{1,2}$ which is separated from block $B_{1,1}$ by a membrane. The area of this membrane is also reported as 1×10^6 m^2. Until this point, except for the differences in the amount of reformer effluent, we have the same process configuration as before. However, this time we observe that the permeate block $B_{1,1}$ is assigned as a reactor block for the Dry Reforming reaction. This indicates that the blocks $B_{1,1}$ and $B_{1,2}$, which are separated by a membrane material in between, form a membrane reactor with the catalyst filling the permeate side of the intensified equipment.

It is important to note that not all intensification alternatives are optimal. For instance, in Process Alternative 1, we have a highly intensified membrane reactor with both retantate and permeate sides are packed with catalysts. However, this alternative is not the most optimal and better results are obtained when we increase the solution time. In Process Alternative 2, we do not have any intensified equipment. Process Alternative 3, which is the best result we could obtain within 24 hours of CPU time, uses a membrane reactor with the catalyst positioned in the permeate side.

4.3 Separation of CO_2 from Power Plant Flue Gas

In this case study, we use the block-based approach to design and intensify a process for the post-combustion capture of CO_2 from a coal-fired power plant flue gas mixture containing 77% N_2, 9% H_2O and 14% CO_2 and with a total flow rate of 0.1 kmol/s. The goal is to capture at least 90% of the CO_2 from the flue gas stream with at least 90% purity of captured CO_2 while minimizing the process operating cost.

The overall problem is set as follows. We use a 3×3 block superstructure (I = 3 and J = 3), and define the following sets: f = {*FG, Steam, Absnt, Water*}, p = {*Prod, Waste1, Waste2*}, s = {*GP, GL-PC* }, m = {*Memb, null*}, k = {CO_2, N_2, H_2O, *MEA*, MEA_2CO_2}, r = {*Forward, Reverse*}, c = {*Forcat, Revcat*}. Here, *FG* is the flue gas feed stream and enters into the system at 1 bar 328 K. *Steam* is saturated steam that is available at 5 bar with a maximum flow rate of 1 kmol/s. *Water*

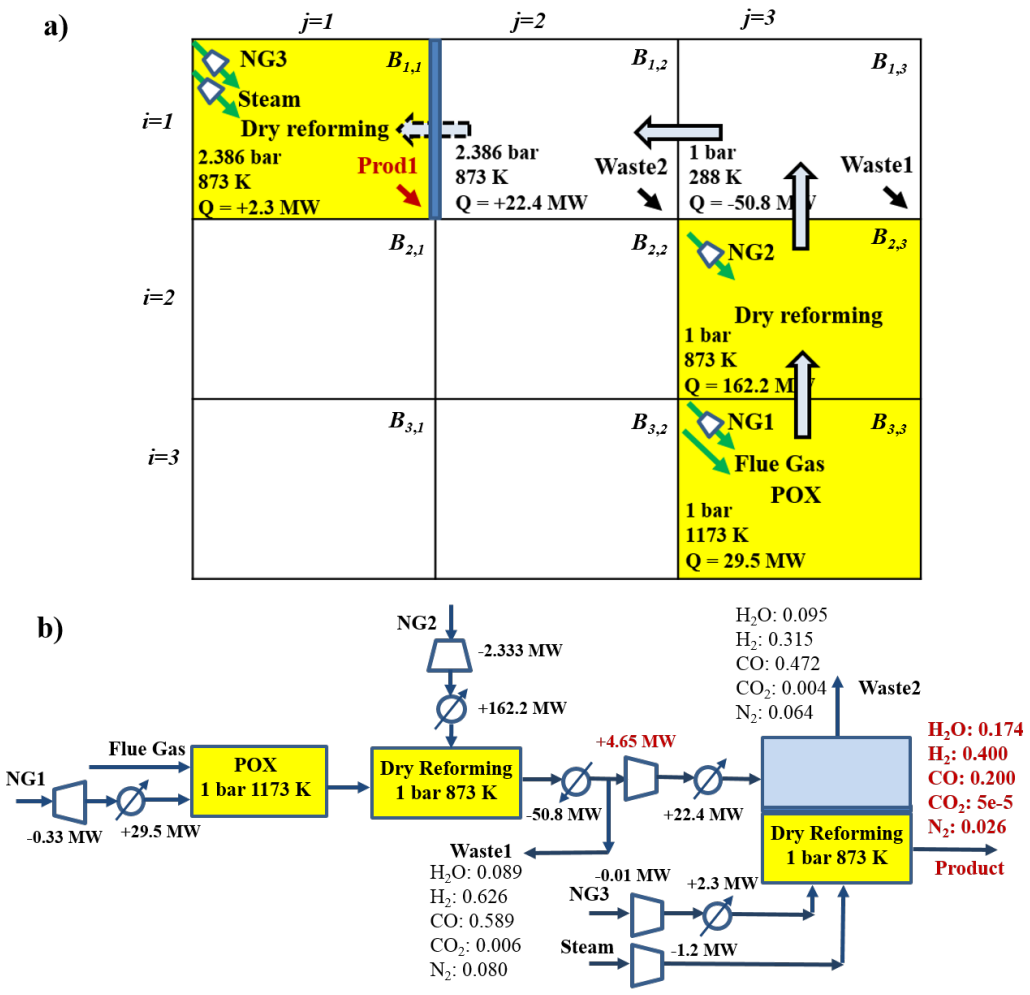

Figure 4.5: Process alternative 3 for the the CO_2 utilization from flue gas process (Reprinted with permission from [90]).

is the liquid water at 298 K which is available with 1 kmol/s. *Prod* is the main product stream by which we want to obtain at least 90% pure CO_2 with a minimum recovery of 90%. Hence, $y^{MIN,prod}_{k=CO2,p=prod} = 0.90$ and $Re^{min}_{k=CO2,f=FG,p=prod} = 0.90$. *Waste1* and *Waste2* are gas and liquid waste streams for which no purity requirements are considered. The feed and product phases are set as follows: $z^{phasefeed}_{f=FG} = 1$, $z^{phasefeed}_{f=Steam} = 1$, $z^{phasefeed}_{f=Absnt} = 0$, $z^{phasefeed}_{f=Water} = 0$, $z^{phaseprod}_{p=prod} = 1$, $z^{phaseprod}_{p=Waste1} = 1$, $z^{phaseprod}_{p=Waste2} = 0$. The pressure and temperature are allowed to vary between 1–5 bar and 298–393 K, respectively. An upper bound of 1 kmol/s is set for any flow rate. *Memb* is the membrane material and *null* is a dummy material to allow for Gas-Liquid phase contact which does

not require any material in reality. The membrane permeance data is taken from the literature [148]. For CO_2, N_2 and H_2O, permeance values are 2.7×10^{-5}, 6.7×10^{-7} and 1.323×10^{-5} kmol/m^2-s bar, respectively. The maximum available area for the membrane is taken to be 1×10^5 m^2. *Absnt* is the MEA-water solution (30 wt% MEA which is equivalent to 11.2 mol% MEA) that is available at 1 bar and 298 K for use. We consider a liquid phase reaction for the chemisorption of CO_2 using MEA. In particular, we choose MEA-CO_2-H_2O reaction according to the Zwitterion Mechanism as shown below[157]:

$$CO_2 + RNH_2 \leftrightarrow RNH_2^+CO_2^-$$

$$RNH_2^+CO_2^- + RNH_2 \rightarrow RNHCO_2^- + RNH_3^+$$

The forward reaction (absorption) is favored at lower temperatures, while the reverse reaction (desorption) takes place at higher temperatures. Both forward and reverse reactions are assumed to be taking place with 100% conversion. Two MEA molecules are required to capture one CO_2 molecule resulting in a CO_2 loading of 0.5 kmol CO_2/ kmol MEA [158]. Reaction enthalpies are assumed to be independent of temperature and are taken as the overall reaction enthalpy of the real MEA-CO_2-H_2O reacting system. All data related to the reaction system are given in Table 4.3. Key reactants for the two reactions are defined as follows: *kr* = $\{$*(Forward, CO_2), (Reverse, MEA_2CO_2)*$\}$. MEA ions are assumed to be nonvolatile components. Although these reactions do not require a catalyst material, we define two arbitrary catalyst materials for each reaction so as to relate the existense of each reaction. Finally, as we use equilibrium data for water, *GL-PC* phenomenon does not require any other specific data and it does not require a separate material set. Hence, we define the following subsets: *Equil* = $\{$*GL-PC, null*$\}$ and *Rate* = $\{$*GP, Memb*$\}$.

Table 4.3: Reaction data for the hypothetical CO_2 chemisorption reaction for separation of CO_2 from Power Plant Flue Gas (Adapted with permission from [90]).

Hypothetical Reaction: 2 MEA + $CO_2 \leftrightarrow MEACO_2^- + MEA^+$	
Forward reaction:	T $\leq$ 353 K, X_{CO_2}=1, $\Delta H^{forward}$ = -79.08 kj/mol (25 °C)[158]
Reverse reaction:	T $\geq$ 373 K, X_{MEACO2}=1, $\Delta H^{reverse}$ = 98.7 kj/mol (120 °C)[158]

As the system might include phase change, the problem is solved by including the phase considerations. The enthalpy of vaporization are taken into account in energy balance equations. Furthermore, we consider *KA* = $\{Water, MEA\}$ and *KH* = $\{CO_2, N_2\}$ while deciding on the appropriate thermodynamic relations. The coefficients used in the equilibrium relations are given in Table 4.4. As MEA_2CO_2 is assumed to be nonvolatile, *inert* = $\{MEA_2CO_2\}$. Furthermore, we set UC_{hu} = 0.00465 \$/MW, UC_{cu} = 4.8×10^{-5} \$/MW, UC_{elect} = 0.019 \$/MWs, $Cost_{f=Absnt}$ = 36.07 \$/kmol MEA solution, $Cost_{f=Water}$=1.8×10^{-5} \$/kmol, $Cost_{f=Steam}$=0.0108 \$/kmol [82, 148, 159, 160]. We restrict the maximum composition of MEA to 11.2% ($y^{up}_{k=MEA}$=0.112) as higher MEA concentrations may result in corrosion problems. The compressor and expander efficiency is taken to be 75%. We assume 8000 hours of annual operation. As the system might include phase change, the problem is solved while considering the following constraints: Eqs. 1-2, 3a-b, 4-6, 9-15, 17-21, 22a, 23a-b, 24, 25a, 27-41, 43, 45, 49, 51-53, A1a-f, A2a-s, B1-B15 and C1-C4. The enthalpy of vaporization are taken into account in energy balance equations (Equation numbers correspond to the ones given in Demirel et al. (2017) [90]).

Table 4.4: Phase equilibrium parameters for CO_2 separation from flue gas process (Adapted with permission from [90]).

Species	A_k^{ant}	B_k^{ant}	C_k^{ant}	$\tilde{H}_k$	$\tilde{T}_k$
H_2O	16.54	3985	-39	-	-
MEA	9.88	3244	-116	-	-
CO_2	-	-	-	6.144×10^{-4}	2400
N_2	-	-	-	1.175×10^{-5}	1300

The resultant model contains 1155 continuous variables, 270 binary variables, 3487 constraints with 13447 nonzero elements. We solve the MINLP model using ANTIGONE with a feasible solution with an objective value of \$792,000 per year (\$0.0275 per second) as the starting point. After 24 hours of CPU time, an objective value of \$495,360 per year (\$0.0172 per second) is obtained. While the solution is improved by 37.5% compared to the starting point, ANTIGONE

could not find a better lower bound than zero in 24 hours. In the final solution, the major cost components are heating utility cost of \$313,920 per year (63.4%), MEA reagent cost of \$144,000 per year (29.1%), steam cost of \$34,560 per year (7.0%), and cooling utility cost of \$2,880 per year (0.5%). For existing processes, yearly operating costs are given in the range of \$500,000-600,000 per year depending on the degree of heat integration [148]. Even without any heat integration, our cost is comparable with the costs of existing processes, which highlights the benefit of the MINLP approach.

The resulting block structure and its classical flowsheet representation are given in Figures 4.6a and 4.6b, respectively. First, we observe that blocks $B_{1,2}$, $B_{1,3}$ $B_{2,2}$ and $B_{2,3}$ are in liquid phase and blocks $B_{1,1}$, $B_{3,2}$ and $B_{3,3}$ are in gas phase. In total, there are 3 semi-restricted boundaries which are assigned to be Gas-Liquid Phase Contact phenomenon. Blocks $B_{1,1}$ and $B_{1,2}$ separated by *GL-PC* boundary acts as absorption stage. Flue gas enters into block $B_{1,1}$ and CO_2 and trace amount of N_2 is absorbed into block $B_{1,2}$. Some water in the liquid side, in block $B_{1,2}$, simultaneously vaporizes into block $B_{1,2}$. Left-over N_2 from the flue gas and H_2O vaporized into the gas block leaves block $B_{1,1}$ as the waste stream (Waste 1). Block $B_{1,2}$ is assigned to the forward reaction and all the CO_2 absorbed into this block is captured by MEA. We observe that very few amount of Absorbant feed is taken into the process from block $B_{1,2}$ which compensates for the loss of the MEA by evaporation at the later stages. The reacted MEA and CO_2 (MEA_2CO_2) and water leaves block $B_{1,2}$ and heated before entering into block $B_{2,3}$. Block $B_{2,3}$ and $B_{3,3}$ are separated by semi-restricted boundary and together they act as a desorber stage which operates at 5 bar and 373 K. Block $B_{2,3}$ is assigned to the reverse reaction by which CO_2 is released. Most of the CO_2 released by the reverse reaction and trace amounts of N_2 and MEA go into the vapor phase, while some water vapor, which is taken into the system as steam from block $B_{3,3}$, condenses into the block $B_{2,3}$. Liquid phase from block $B_{2,3}$ leaves the equilibrium stage and it is recycled back to the absorber stage so as to recover the MEA solution. The operating pressure for the desorber stage is high as the increased pressure helps into reduce the amount of MEA lost. Also, increasing pressure at the liquid side does not result in any cost as we neglected pump costs. Hence, desorder stage

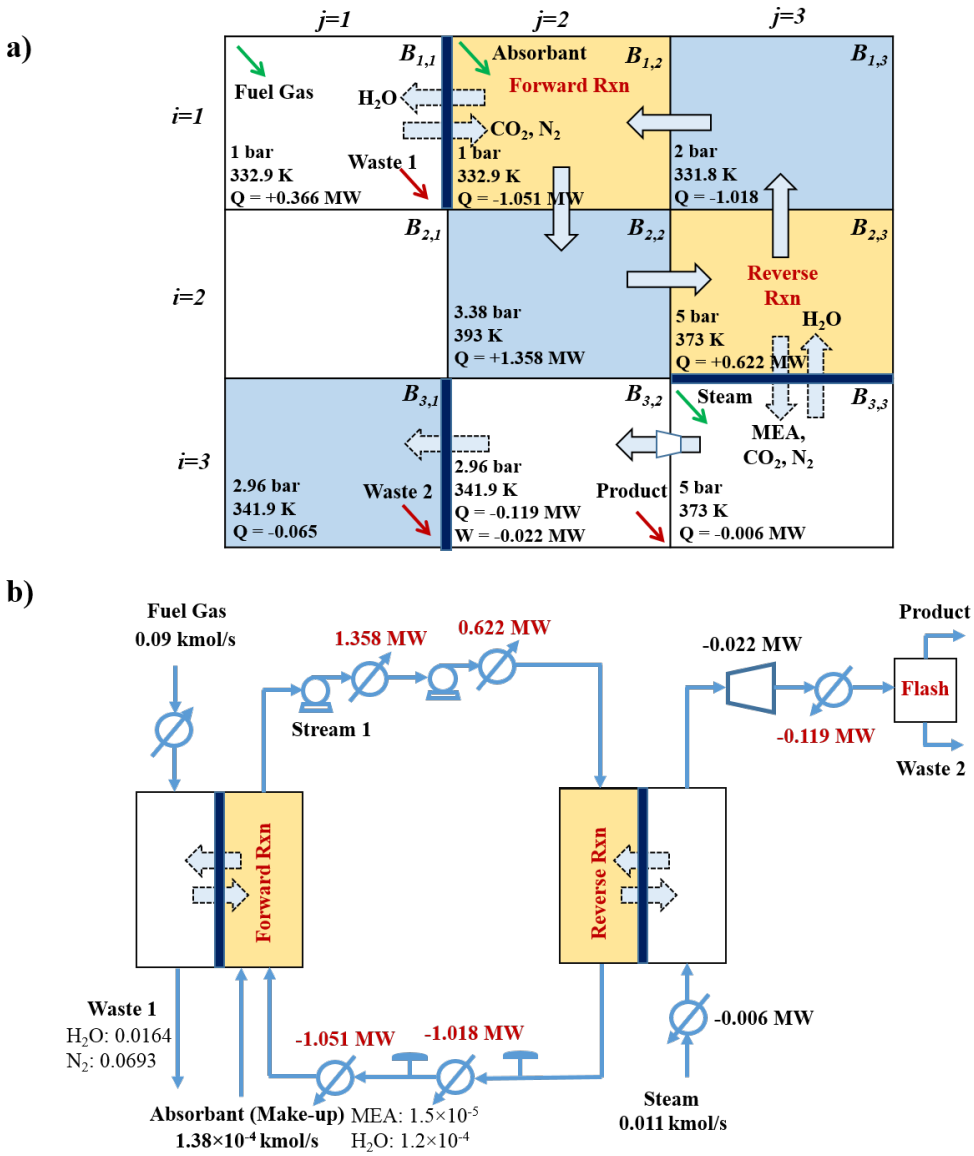

Figure 4.6: Building block result the CO_2 separation from flue gas process. Resulting CO_2 separation process a) with block superstructure and, b) its equivalent process flowsheet. In block configuration, feed streams shown in green, and product streams are shown in red color. Blocks $B_{1,2}$, $B_{1,3}$, $B_{2,2}$, $B_{2,3}$, $B_{3,1}$ are in liquid phase, blocks $B_{1,1}$, $B_{3,2}$, and $B_{3,3}$ are in gas phase (Reprinted with permission from [90]).

could operate at a such high pressure. Gas phase leaving the block $B_{3,3}$ is decreased in pressure and then flashed to decrease the amount of water vapor in the gaseous product. Then, the gaseous stream leaves the process as the product and the liquid stream is taken out of the system as waste stream.

We note that the membrane separation is not selected in the final solution, which agrees with the fact that current membrane separations are economically viable only at higher CO_2 compositions in the feed flue gas [148]. Furthermore, as the reverse reaction for MEA-based capture is endothermic, high amount of the of the heating utility is used for the desorption stage. Indeed, it is reported in the literature that 90% of the overall energy requirement of a CO_2-MEA absorption system is for the desorber reboiler [161].

4.4 Methanol Production from Biogas

Biogas can be produced via various organic waste streams and current utilization practices mainly focus on heat and electricity generation [162]. However, as it is mainly composed of methane and CO_2, it can be also considered for production of value-added products, such as methanol [163]. Here, we investigate the conversion of biogas to methanol via block superstructure with automated flowsheet generation for maximization of the total annualized profit. A fixed amount of biogas feed is used, namely, 0.2 kmol/s (60% CH_4 and 40% CO_2), to synthesize a biogas utilization process. Four different reactor alternatives are considered: (i) a Dry reformer (DR) and (ii) a bi-reformer (BR) for conversion of biogas to syngas, which is used for methanol production or purified to obtain hydrogen product, (iii) a CO hydrogenation reactor for conversion of syngas to methanol (MR) and (iv) a Water Gas Shift (WGSR) reactor for adjustment of syngas composition. Separation alternatives include two flash tanks (FS1 and FS2) for separation of methanol and water from other gases at low and high pressures, respectively, a distillation column (D) for methanol-water separation and a H_2 selective membrane (M). Apart from the biogas feed (available at 1 bar and 400 K), a saturated steam (available at 5 bar with 5 kmol/s) and pure hydrogen (available at 300 K with 5 kmol/s) are considered as additional feed streams. Hydrogen feed is assumed to be available at the required pressure of the process. Both methanol (with minimum 98% purity) and hydrogen are considered as viable end-products from the process while hydrogen in the product stream is only allowed to contain water as the impurity which can be easily separated from hydrogen via a flash operation. While DR, BR and WGSR are modeled as equilibrium reactors operating at fixed temperatures, MR is modeled as a stoichiometric reactor with CO hydrogenation being the

only reaction. Operating pressures for DR, BR and WGSR are considered as variables while the MR pressure is fixed to be 50 bar. The flash and distillation units are modeled as non-sharp splitters with fixed temperatures and pressures. Membrane is modeled via rate-based model and H_2 is assumed to be the only permeating component as the considered membrane material has very high selectivity toward H_2. Permeance towards H_2 is taken as 1.75 $\times$ 10^{-5} kmol/m^2 s bar [164]. Bounds on the temperature and pressure of the operation are taken as 300-1173 K and 1-50 bar, respectively. The upper bound on the flow rate of any component, FU, is taken as 5 kmol/s. The module ratio for MR inlet, (H_2-CO_2)/(CO+CO_2), is enforced to be greater than 2 [153]. In cost calculations, a capital recovery factor of 0.154 is assumed, the annual maintenance cost is taken as 5% of the total product cost (TPC), which is assumed to be 1.52 TIC (total installed cost) [165]. Accordingly, κ is taken as 0.31. Hydrogen feed cost and selling prices is taken as \$1.898/kmol [165]. Methanol price is taken as \$11.73/kmol [153]. Steam feed cost is taken as 0.133 \$/kmol. Hot and cold utility costs are taken as 0.0028 \$/MW and 2.4×10^{-5} \$/MW [165]. The capital costs for heaters/coolers and compressors/expanders are not considered. For this case study, annual operation of 8000 h is considered. Information on separation equipment performance and cost functions, and reaction equipment are given in Table 4.5, 4.6 and 4.7, respectively.

Table 4.5: Separation alternatives for methanol production from biogas problem [166, 167] (Adapted with permission from [139]).

Separator s	Splitting fraction $\tau_{s,k}$	P (bar)	T (K)
FS1	H_2O=1, CO_2=0.01, CH_3OH=1	50	311
FS2	H_2O=1, CH_3OH=1	1 - 20	473
Dist	CH_4=1, H_2O=0.01, H_2=1, CO=1, CO_2=1, CH_3OH=0.99	1	311

The frame movement strategy is used to solve this problem. In the first iteration, Biogas feed is fixed at block $B_{1,1}$ and methanol product stream is fixed at $B_{4,3}$. All the direction binary variables are fixed to be in the positive direction and a separation boundary is only allowed to be positioned in the horizontal direction. In the second iteration, all the binary variables related with the unit

Table 4.6: Cost parameters for the separation alternatives in methanol production from biogas problem [166, 167] (Adapted with permission from [139]).

Separator s	ω_s (MM$)	θ_s (kg/s)	β_s
FS1-FS2	1.115	39.29	0.6
Dist	4.202	36.6	0.6

Table 4.7: Reactor data for the methanol production from biogas problem [167, 168, 169] (Adapted with permission from [139]).

Reaction c	T(K)	P(bar)	Conversion	ω_c (MM$)	θ_c (kg/s)	β_c
BR, DR	1123	1 - 50		23.286	12.20	0.67
WGS	473	1 - 50		3.576	150	0.67
MR	523	50	0.39	7.969	44.1	0.6

assignments are fixed to the results obtained in the first iteration and the direction binary variables are relaxed. Results from the second iteration are used for refinement of the solution via frame movement with 3×2 frame and, in total 4 iterations are used for frame movements. Finally, the resulting structure from these initial iterations are used as an initial guess to solve the overall problem. In total, 7 iterations are utilized. While the first 6 subproblems are solved for 2 h of CPU time each, the last problem is solved for 10 h of CPU time. At the end of this procedure, an objective value of 42.49 MM$/yr is obtained. Objective function values obtained at the end of each iteration is summarized in Table 4.8. The solution found in the first iteration is improved in the fifth iteration and it is further updated to its final value at the end of the sixth iteration. This solution is used as an initial solution to the problem in which no fixing is applied (7th iteration) and no improvement has been achieved. Repeating the final iteration with jump flows also did not yield any improvement. The block superstructure and flowsheet representation of these results are depicted in Figure 4.7.

The first solution to the problem suggests a process with both methanol and hydrogen as end-products. This process starts with a BR operating at 1.58 bar. Effluents from the reformer are directed toward the methanol reactor after being cooled and compressed to the MR reactor condi-

Table 4.8: Model statistics for the methanol production from biogas problem (Reprinted with permission from [139]).

Iteration	1	2	3	4	5	6	7
Binary variables	132	65	90	86	90	86	213
Continuous variables	1092	1186	1105	1090	1085	1100	1418
Bilinear terms	1016	1758	1366	1482	1370	1418	1916
Signomial terms	102	124	107	110	107	116	148
CPU time (h)	2	2	2	2	2	2	10
Solution (MM$/yr)	19.23	19.23	19.23	19.23	33.20	42.49	42.49
Upper Bound (MM$/yr)	36.24	55.78	60.17	60.17	60.05	57.27	60.17
Optimality gap (%)	88	190	212	212	81	35	41

tions. Additional hydrogen is also fed into the MR in order to satisfy the module ratio. MR outlet is then sent to WGSR where additional hydrogen is produced and simultaneously removed via the membrane M. It should be noted that the WGSR unit assigned to $B_{3,2}$ together with the membrane boundary assigned to the right side of $B_{3,2}$ suggests a membrane reactor. The block superstructure can identify the existence of this intensified unit without $a\ priori$ postaulation of its existence and utilize it for increasing the conversion obtained from WGS reactor (96% CO conversion is achieved while the equilibrium conversion at the same conditions is only 86%). It should be noted that, the cost for membrane reactor is assumed to be the summation of the WGSR and membrane capital costs. This may lead to an underestimation of the real cost for a membrane reactor. The permeated H_2 stream through the membrane is taken out as product from block $B_{3,3}$. Effluents from the WGS membrane reactor are sent to FS2 for separation of methanol and water from other gases and sent out as the second end-product from $B_{4,3}$.

The solution obtained at the end of fifth iteration has much higher annual profit than the one obtained from the first subproblem due to the increased methanol yield from the process. WGS membrane reactor is eliminated and only BR and MR are used with two recycle streams: one from MR outlet to BR inlet and one from FS2 outlet to the MR inlet. With the introduction of these two recycle streams, all the carbon introduced by Biogas feed can be converted to methanol. However, better solution can be obtained at the end of sixth iteration which is the best flowsheet alternative.

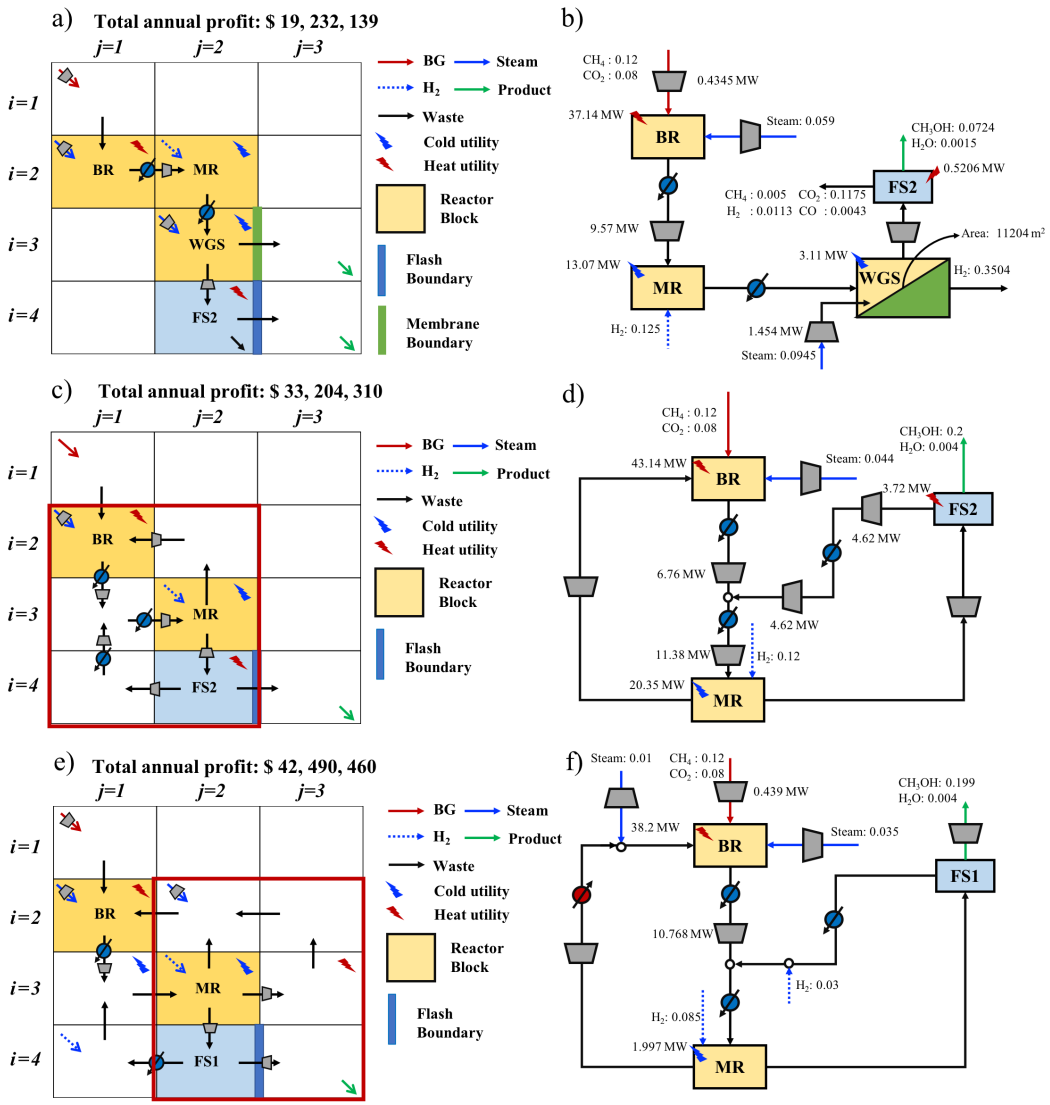

Figure 4.7: Structural refinement for the biogas to methanol process. a) Initial block representation b) initial process flowsheet, c) block representation at the first change, d) process flowsheet at the first change, e) block representation at the final change and f) process flowsheet at the final change (Reprinted with permission from [139]).

In this flowsheet, instead of FS2, FS1 is used for the separation of methanol and water from other gases. Accordingly, the MR outlet does not have any pressure drop and compression work required for the recycle stream from FS2 outlet to MR is eliminated.

4.5 Synthesis of Reactive Separation Systems

The proposed model and representation is generic in that it can be also used as a generic modeling and optimization framework for the intensified systems. Here, two examples on the synthesis of reactive separation systems are provided.

4.5.1 2-pentene Metathesis Reaction

Olefin metathesis reactions provide an efficient method for C-C double bond formation [170]. Through the metathesis reactions, olefins can be converted into lower and higher molecular weight counterparts. Owing to relatively moderate reaction conditions, i.e. liquid phase at ambient to moderate conditions, they are ideal for reactive distillation applications [171]. For instance, Dow Chemical Company patented a reactive distillation process for 1- butene metathesis reaction [172]. In this case study, 2-pentene metathesis to 2-butene and 3-hexene will be investigated. The objective is to synthesize a reactive distillation column with minimum total annualized cost for 50 kmol/h of distillate with 99% (mole percent) 2-butene and bottoms with 99% 3-hexene. While reactive distillation columns can have variable reaction volumes at each reactive stage, this might make it harder to construct the equipment. Accordingly, two different designs will be investigated: i) a column with variable molar holdup at each stage, and ii) a column with reactive stages having the same molar holdup. The locations of the reaction blocks is among the optimization variables.

While modeling, ideal phase equilibrium is assumed. Reaction rate is considered with the following kinetics[173]: Building block superstructure of size 25 $\times$ 2 is used to optimize this

$$C_5H_{10} \text{ (2-pentene)} \leftrightarrow C_4H_8 \text{ (2-butene)} + C_6H_{12} \text{ (3-hexene)}$$

$$r_{C6} \;=\; k_f \;(x_{C5}^2 - (x_{C4} \times x_{C6}/K^{eq}))$$

$$k_f \;=\; 3553.6 exp\left(\frac{-6.6(kcal/gmol)}{R \times T}\right) \;\; [min^{-1}]$$

$$K^{eq} \;=\; 0.25$$

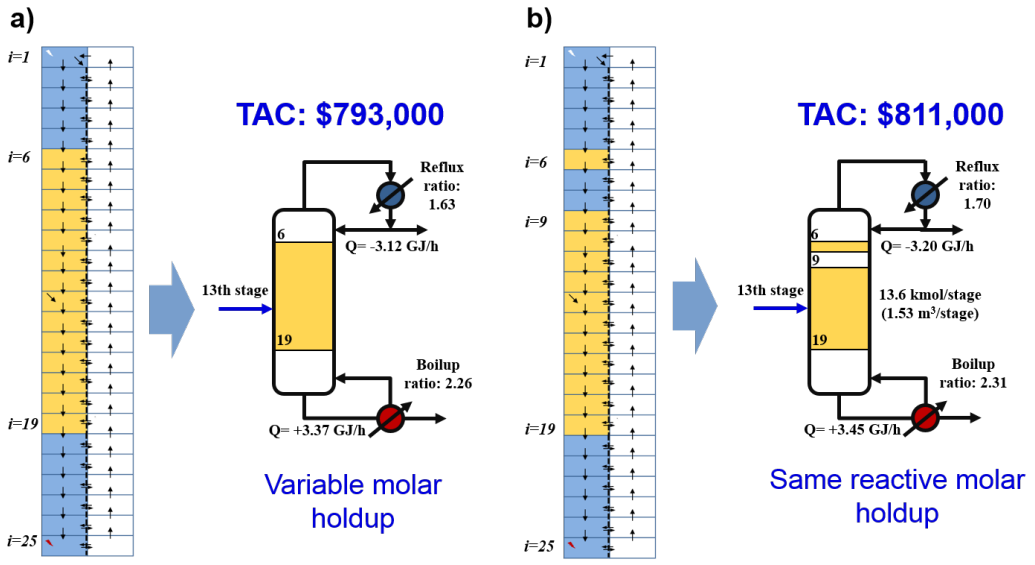

Figure 4.8: Optimal 2-pentene methatesis processes. a) Optimal building block result (left) and the corresponding reactive separation column (right) for the variable molar holdup case, and b) optimal result for the same molar holdup case.

process. The column size is fixed to 25 stages including a partial reboiler and total condenser. While the blocks in the first column of the superstructure are assigned as liquid phase, the ones in the second column are designated as vapor blocks. The block pairs at the top are designated as the total condenser blocks and the blocks at the bottom are designated as partial reboiler blocks. The blocks in between are separated by semi-restricted boundary with vapor-liquid phase contact phenomena to account for the mass transfer in between the two phases. Reaction is allowed only in the liquid phase blocks. Reaction within the reboiler and condensers are not allowed. Two problem are solved with ANTIGONE and the resulting building block superstructures are given in Figure 4.8 along with their flowsheet representation. Yellow blocks represent the optimal location of the catalysts. These blocks in which reaction and vapor-liquid phase contact take place simultaneously, correspond to the reactive separation regions of the reactive separation column.

The optimal design with variable molar holdup has a TAC of $\$793,000$/year with 14 reactive stages. The second case in which the reactive stages are restricted to have the same molar holdup, on the other hand, results in a design with a TAC of $\$811,000$/year with 2% higher TAC. This

Table 4.9: Optimal results for the metathesis reaction problem.

Molar Holdup	Variable	Same
Height (ft)	107.4	108.6
Diameter (ft)	3.6	3.6
Height/Diameter	30	30
# of stages	23	23
# of reactive stages	14	12
Total Holdup	155.8 kmol (17.5 m^3)	162.7 kmol (18.3 m^3)
Annualized Cost (k$/year)		
Shell	131	132
Tray	16.8	17.1
Fixed cost	24.5	24.5
Reboiler	31	32
Condenser	116	118
Steam	210	215
Cooling (Refrigerant)	264	271
Operating Costs	474	486
Capital Costs	319	325
Total Annualized Cost	793	811

design also requires 4.4% higher reactive molar holdup in total, yet it has 12 reactive stages. Interestingly, reactive stages for both designs are located within the same stage locations, i.e. from 6th to 19th stages from top (including the condenser). However, design with the same molar holdup at each reactive stage demonstrates a disjoint behavior. In this design, 7th and 8th stages are not assigned with reaction. Based on these optimal designs, it can be observed that allowing for variable molar holdup do not result in a drastic increase in the TAC, 2% increase. Hence, the simpler design can be adopted.

4.5.2 Methyl Acetate Production

Methyl acetate production is one of the biggest success stories for the reactive distillation technology [39, 174]. It is produced through an esterification reaction between acetic acid (HOAC) and methanol (MeOH) which yields water (W) along with the methyl acetate (MeAC) product. Reaction is equilibrium limited and there are two binary minimum boiling azeotropes methyl acetate/methanol (x_{MeAC} = 0.66) and methyl acetate/water (x_{MeAC} = 0.92) that hinder high purity

MeAC production. Yet, by performing reaction and separation simultaneously, these azeotropes and equilibrium limitations can be avoided. This case study addresses the optimization of a heterogeneous reactive separation column for achieving high purity methyl acetate production. Proposed building block representation and optimization model will be used to synthesize a process for the production of 280 kmol/h methyl acetate with 95% purity. The objective is to minimize the annual cost of production. Reaction is performed in the presence of an acid catalyst (e.g., sulfuric acid, or a sulfonic acid ion exchange resin) at atmospheric pressure. Assuming chemical equilibrium is reported to be accurate for a wide range of operating conditions for this heterogeneous reaction system [175]. Reaction stoichiometry and equilibrium are provided below [174]: Building block

$$HOAC + Methanol \leftrightarrow MethylAcetate + Water$$

$$K^{eq} = \frac{\alpha_{MeAC} \ \alpha_{W}}{\alpha_{HOAC} \ \alpha_{MeOH}} = 2.32 \ exp\left(\frac{782.98}{T}\right)$$

superstructure of size 27 $\times$ 2 is used to optimize this process. The building block superstructure has the same structure as the previous case study. However, reaction system here is heterogeneous. Accordingly, optimization model now determines the optimal location for the solid catalyst material. Reaction is not considered within the reboiler and condensers, hence the catalyst material is not allowed to be positioned within these blocks. Activity coefficients for phase equilibrium and reaction equilibrium are calculated based on Wilson activity coefficient model. With these, problem includes 3196 continuous and 25 binary variables, 3490 bilinear, 816 signomial, 473 exponential and 224 logarithmic terms. Problem is solved with ANTIGONE and the resulting building block superstructure is given in Figure 4.9 along with its flowsheet representation. Yellow blocks represent the optimal location of the catalysts. These blocks in which reaction and vapor-liquid phase contact take place simultaneously, correspond to the reactive separation regions of the reactive separation column. The resulting structure provides a process with \$671.8/ton production cost and it corresponds to a column with 15 reactive, 6 enriching and 4 stripping sections. Optimal reflux and

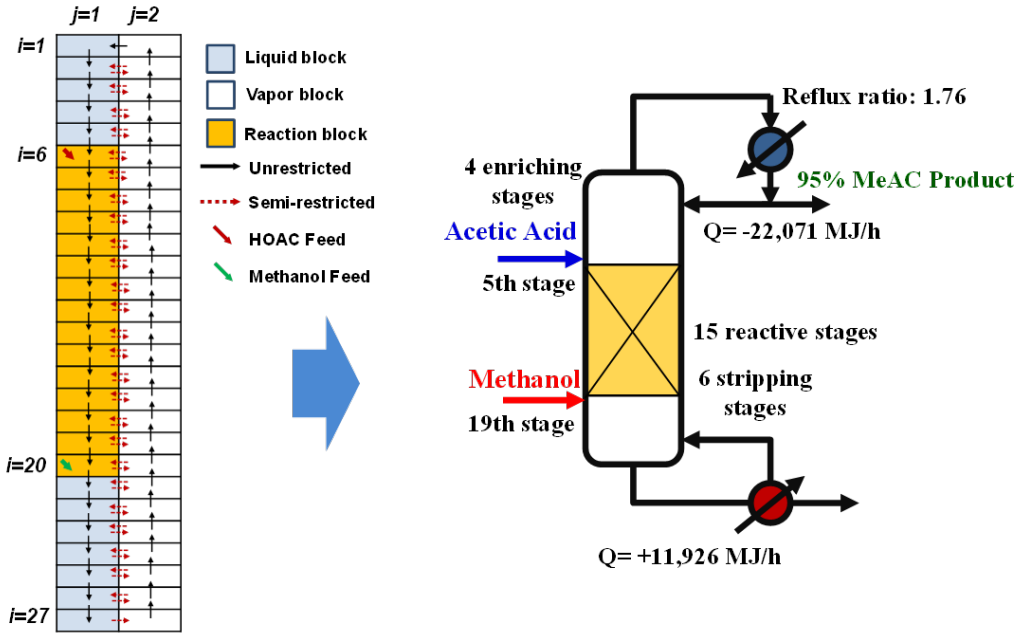

Figure 4.9: Optimal methyl acetate production process. Optimal building block result (left) and the corresponding reactive separation column (right) for the methyl acetate production process.

boil-up ratios are 1.76 and 1.10, respectively. The optimal feed locations from the top and bottom of the reactive region. As the more volatile component, methanol is fed from the bottom of the reactive region and the heavier acetic acid is fed from the top of the reactive region. This reactive separation column is then simulated by using ASPEN Plus with RADFRAC column and building block profiles for liquid mole fractions, temperature and vapor flow rates are shown along with the simulation results in Figure 4.10. All the resultant block profiles are in close agreement with the simulation results indicating the accuracy of the proposed building block superstructure model.

4.6 Design of Membrane-based Separation Systems

Membrane separations play an indispensable role in many areas of chemical industry via facilitating (i) molecular separations (e.g., reverse osmosis), (ii) chemical transformations (e.g., membrane reactors), and (iii) enhanced mass and energy transfer between different phases through integration of hybrid separation techniques in a single unit (e.g., membrane contactors) [49, 176, 13]. With these benefits, membrane-based separations can facilitate significant benefits in terms of pro-

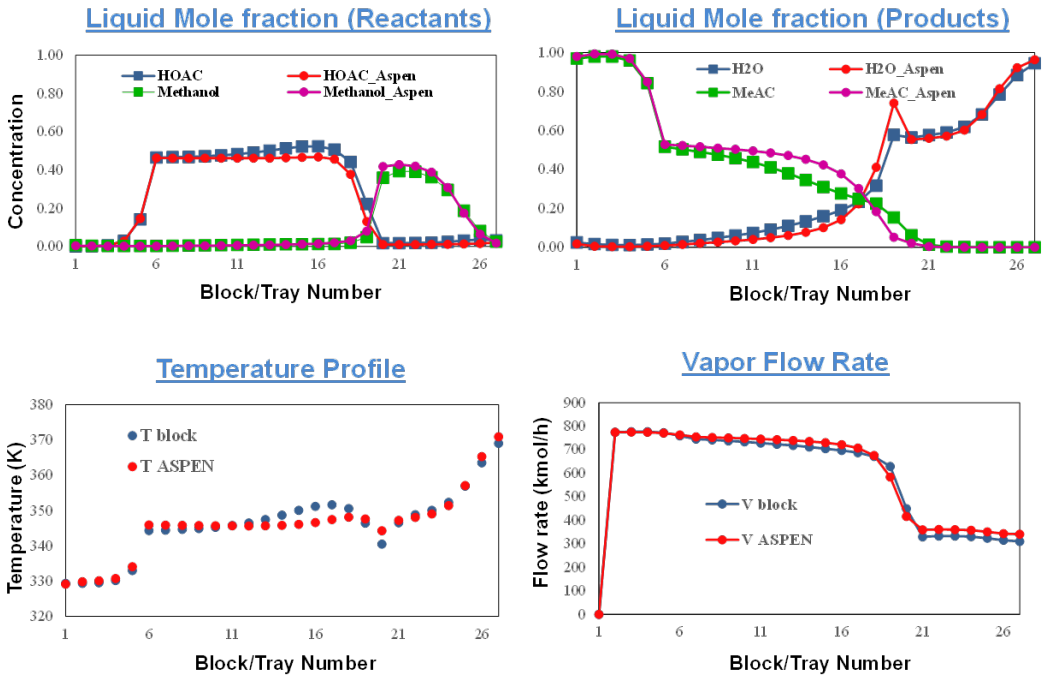

Figure 4.10: ASPEN Plus validation for the methyl acetate production process.

cess intensification. In the previous examples, we showed that building block-based intensification methodology can capture the advantages of membrane-based separations within the reactive separation applications. Here, we will show further examples on the use of building block superstructure for the synthesis of membrane-based separation systems.

4.6.1 Gas Separation Membrane Networks

Different separation network problems can be also represented via the proposed superstructure representation and can be solved via the proposed superstructure model. Here, an example on a gas membrane network problem is presented. Building block representation of a membrane unit consists of two blocks separated by a semi-restricted boundary. The function of the block, i.e. retantate or permeate side, is determined according to the direction of the permeating stream. Different flow patterns can be captured via this representation by including multiple compartments for each membrane unit. For instance, a membrane unit represented via 10 compartments will require a 2x10 superstructure while the boundary between the two rows is assigned to the membrane material.

Via changing the flow direction in the permeate side of the membrane units, counter-current, co-current and cross-current flow patterns can be captured with the proposed superstructure as shown in Figure 4.11.

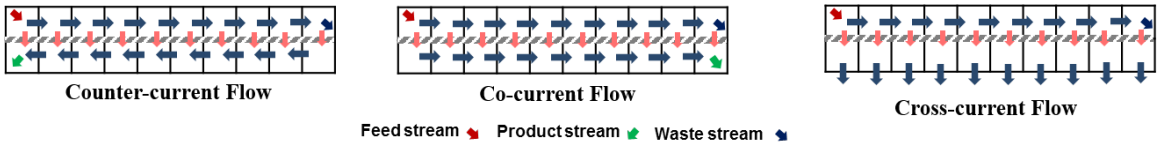

Figure 4.11: Representation of different flow patterns in a membrane module via building block superstructure. Representation of different flow patterns in a membrane unit in which 10 compartments are used to model one single membrane module. With the same superstructure cross-current, co-current and cross-current flow patterns can be obtained via altering the direction of the permeate side streams.

The benefits of using building block superstructure for different process network problems can be shown via an example problem on gas permeation networks taken from Uppaluri et al. (2004) [177]. They presented a modeling and optimization framework for gas separation membrane networks in which they consider different membrane flow patterns with different recycle and compression options. An example gas membrane separation process obtained from their superstructure (Figure 4.12a) and its equivalent block superstructure representation (Figure 4.12b) are shown in Figure 4.12. The process in the example problem is used to recover 90% of the H_2 with 99% purity from a syngas mixture (75% H_2, 25% CO) and contains 3 counter-current membrane modules each modeled with 10 compartments. Hence, 10 building blocks are used for each. Feed stream is splitted into two and fed into the retantate sides of the 1st and 3rd modules. And there is a recycle stream from the 3rd membrane module to the 1st membrane module which is compressed to the feed pressure before being fed into the first membrane module.

In total, a superstructure of a size of 3×31 can be utilized to represent this process. While the blocks within the first row, starting with the blocks on the second column, are used to represent the retantate side, i.e. $B_{i=1,2\leq j\leq 31}$, blocks within the second column are used to represent the

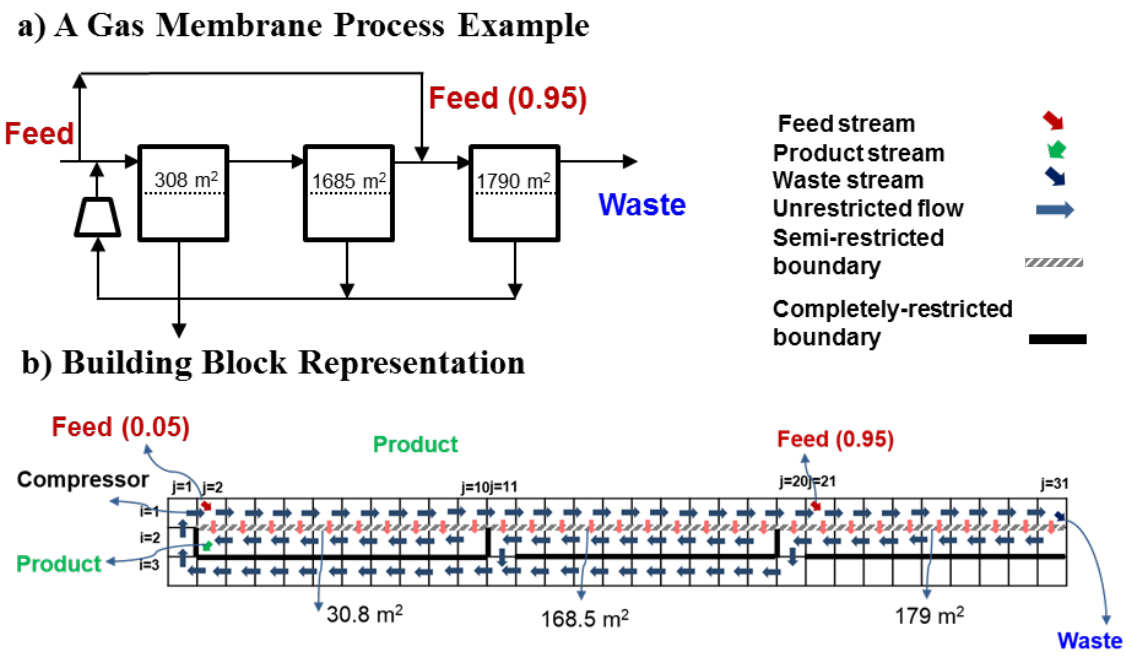

Figure 4.12: Representation of a membrane network with three counter-current units. Representation includes three counter-current units each containing 10 compartments: a) with classical flowsheet representation, b) its building block representation.

permeate side of the membrane units, i.e. $B_{i=2,2\leq j\leq 31}$. Recycle stream from membrane permeate to retantate side is facilitated by considering an additional row of blocks. Retantate outlet from the 3rd membrane module is directed to the block $B_{1,1}$ which serves as the permeate inlet for the 1st membrane module and it is compressed before being fed into the membrane. This example is shown to explain how different membrane networks can be represented by using building block representation. The corresponding mathematical formulation can be also used to address the solution of the problem. Next, we will demonstrate how this can be achieved through a more generic superstructure representation.

While the recycle streams between membrane permeates and retantates can be considered through using additional row of blocks, this increases the number of blocks and the model size. Furthermore, not all recycle structures can be captured by only considering additional blocks. This limitation can be addressed via jump streams between non-adjacent block. This is also highly beneficial in terms of simplifying the mathematical formulation. This is shown in Figure 4.13. Here,

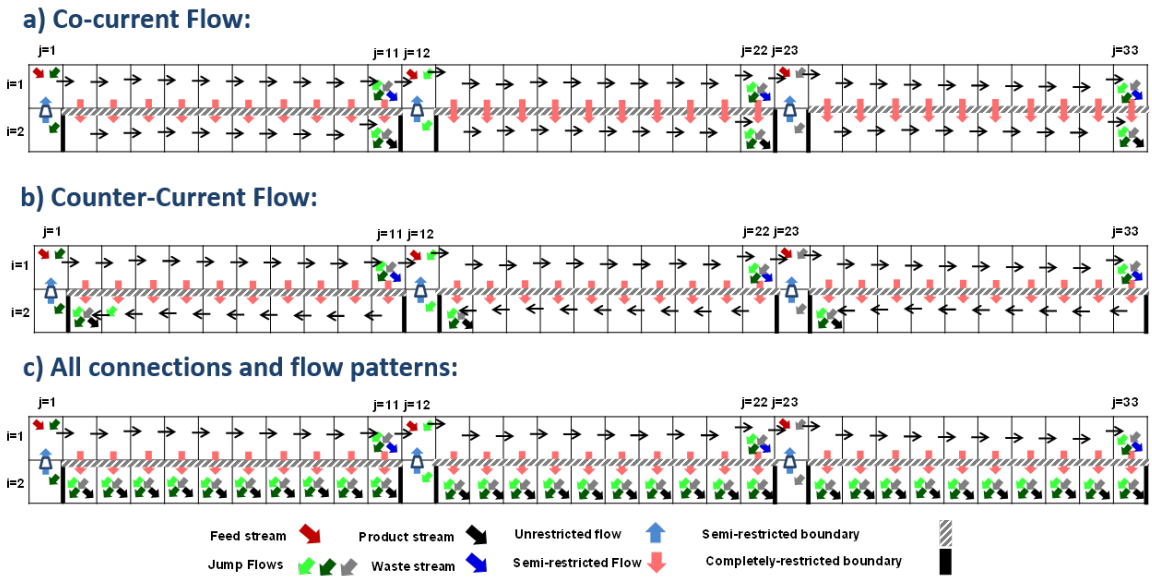

Figure 4.13: Representation of a membrane network superstructure with 3 modules and different recycle considerations. Superstructure with all permeate-retantate and retantate-retantate recycle streams for a) co-current flow, b) counter-current flow and c) all flow patterns including cross flow pattern. Note that when all flow patterns are considered simultaneously, stream directions in the permeate sides becomes variable. Stream arrows at the bottom of the blocks stand for the jump outlet and product streams. Stream arrows at the top of the blocks represent the possible external feed and jump inlet streams. Different colors represent the inlet and outlet destinations for the jump streams.

all the recycle connections between permeate-retantate and retantate-retantate are incorporated via jump streams. Instead of using three rows in the superstructure, now two rows are sufficient to capture many additional recycle connections. While this superstructure network can be used for specific flow patterns separately, as shown in Figure 4.13a for co-current and Figure 4.13b for counter-current flow pattern, it can be also used to address the simultaneous determination of the flow patterns as shown in Figure 4.13c. Here, all the jump stream connections are active at each block to consider cross-flow. Unlike the superstructures for the cocurrent and counter-current flow patterns, the stream directions in the permeate sides becomes variable (Hence, not shown in the figure). If the solution yields a counter-current pattern, flows will be aligned in the reverse direction to the retantate side streams. If it results in co-current pattern, flows will be aligned in the same direction with the retantate side streams. And, if the solution yields cross-flow pattern, all

the interblock streams in the retantate side will have zero flows.

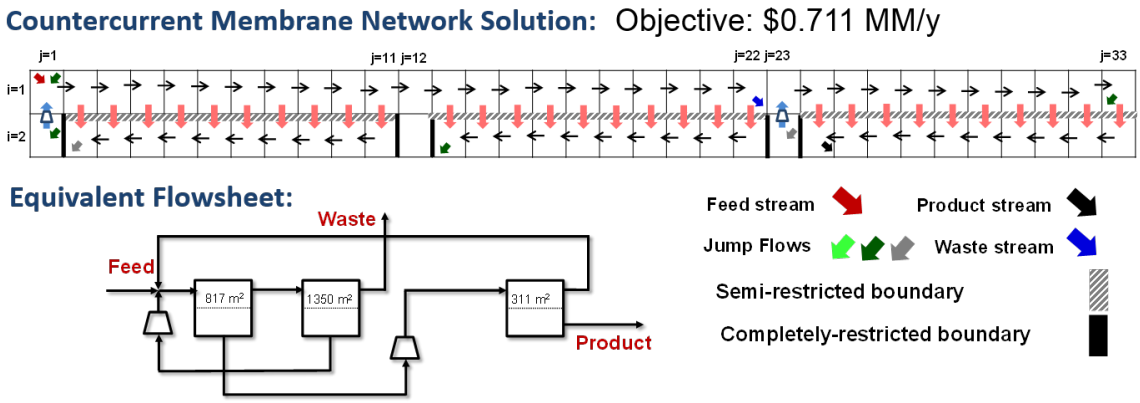

Figure 4.14: Solution of the membrane network synthesis problem with counter-current flow pattern.

Now, we address the solution of the membrane network synthesis problem taken form Uppaluri et al. (2004) [177]. The aim is to synthesize a membrane network with minimum total annualized cost to recover 90% of the H_2 with 99% purity from a a syngas feed mixture with 75% H_2 and 25% CO. Objective function includes the investment cost for the membrane modules, recycle compressors and the operating cost associated with the electricity required for compression. All the economic and membrane property data are taken from the literature work [177] and provided in Table 4.10. In that work, the solution for different flow patterns are obtained separately and the best solution corresponds to a counter-current membrane network with $1.624 MM/year total annual cost as shown in Figure 4.12. We also first solve the problem with counter-current flow pattern while considering all the recycle connections as given in Figure 4.13b. The solution of the problem with BARON yields a membrane network with $0.711 MM/year as given in Figure 4.14. This network has 56% less cost than the reference case. Instead of one as in the reference solution, it has two permeate to retantate recycle streams. One of the major reasons that we obtain much better solution is related with the solution method. While the reference study utilized genetic algorithm with simulated annealing [177], we used a state-of-the-art MINLP solver BARON.

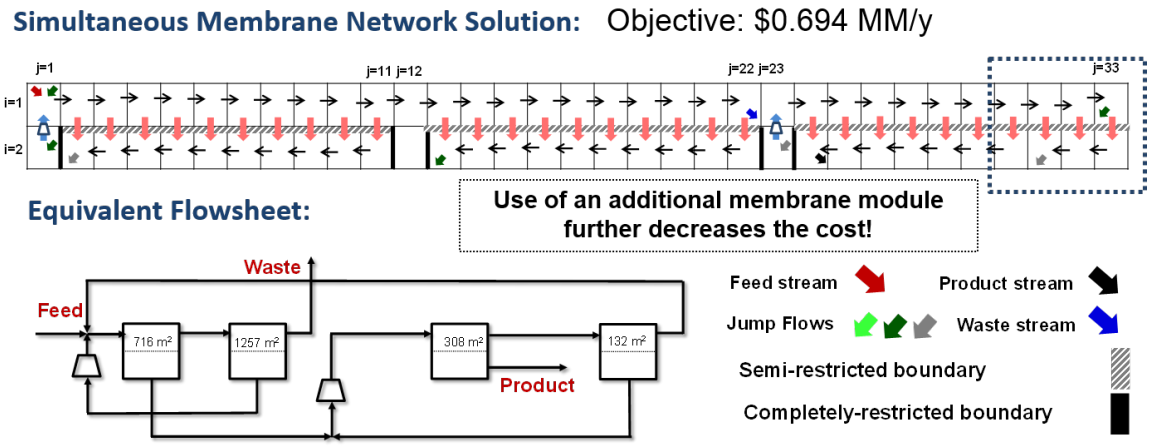

Figure 4.15: Solution of the membrane network synthesis problem with simultaneous consideration of all flow patterns.

Next, we address the same problem by using the superstructure representation as shown in Figure 4.13c while considering different flow patterns simultaneously. Although the problem size increases drastically due to the increase in the number of active jump streams, we use the previous countercurrent solution as an initial solution for the problem. The solution of the problem yields the block superstructure and a corresponding membrane network result as shown in Figure 4.15. This network has a TAC of $0.694 MM/year with 57% improvement in TAC compared to the reference solution and 2% improvement compared to the countercurrent network solution. Interestingly, this network also utilizes counter-current flow pattern, yet we observe from the building block superstructure that the there is a discontinuity in the interblock streams within the permeate region of the third membrane module. Specifically, flow through the right boundary of the block $B_{2,30}$ has a zero flow. This discontinuity results in two separate membrane regions and indicate an additional membrane module. With this additional module a network with lower TAC can be obtained. Although we did not specify the existence of such structure beforehand, considering all flow patterns simultaneously enabled us to come up with such an improved solution. This highlights the use of building block approach as a powerful tool for superstructure-based process synthesis problems.

Next, we will show an example on how to utilize building block-based approach for hybrid

Table 4.10: Membrane network synthesis problem data [177].

Permeate pressure (bar)	10
Retantate Pressure (bar)	22
H_2 Permeance (kmol/m^2.s.bar)	4.689×10^{-6}
CO Permeance (kmol/m^2.s.bar)	3.125×10^{-7}
Feed Flow rate (kmol/s)	0.0225 (75% H_2)

separation systems.

4.6.2 Synthesis of Hybrid Separation Systems

While distillation operations are the primary vehicles for separation within the chemical industry, they incur high utility costs due to their low thermal efficiencies. Distillation technologies account for half of the energy demand for the chemical separation operations [178]. And over 50% of energy required for distillation is used for purifying the last 5 - 10% of the distillate product [179]. This results in significant burden on the economics as well as on the environmental footprint of the overall operation when high-purity end products are targeted. Alternative tech-

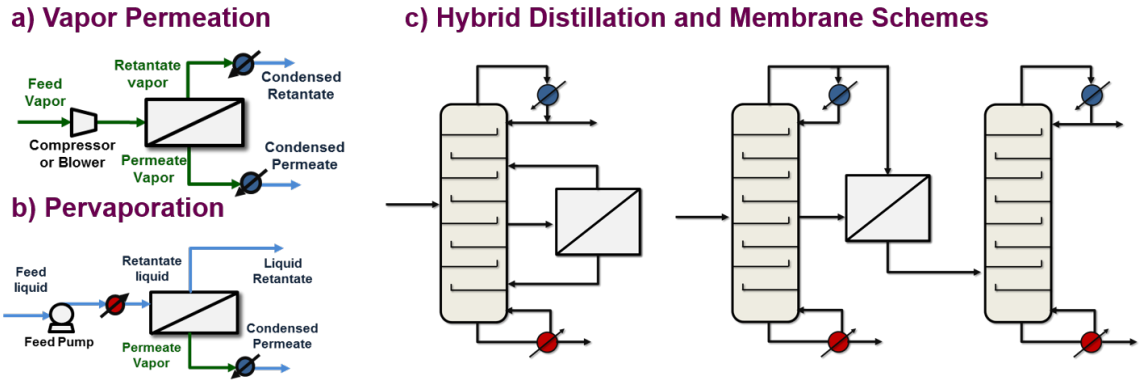

Figure 4.16: Different membrane separation operations and examples of hybrid membrane and distillation schemes. a) Vapor permeation membrane, b) Pervaporation membrane module, c) examples of hybrid membrane and distillation processes.

niques with membrane-based separation technologies can help to alleviate this energy burden.

Vapor permeation and pervaporation membrane modules can be utilized to separate azeotropic mixtures, e.g. water/ethanol, and/or separation of close-boiling point mixtures e.g. acetone/water, propane/propylene. However, membranes suffer from several disadvantages. They cannot handle large volumes and they require substantial capital investment [179]. Accordingly, standalone widespread utilization of these membrane technologies require the development of highly selective materials amenable to cost-effective scale up to compete with conventional standalone distillation equipment. However, hybrid separation systems combining aspects of both distillation and membrane technologies can be optimally designed to reduce energy input and costs while retaining advantages of conventional distillation units (Figure 4.16). Here, we will utilize building block representation to identify the optimal topology of the separation sequence along with the operational conditions where the synergy is maximum.

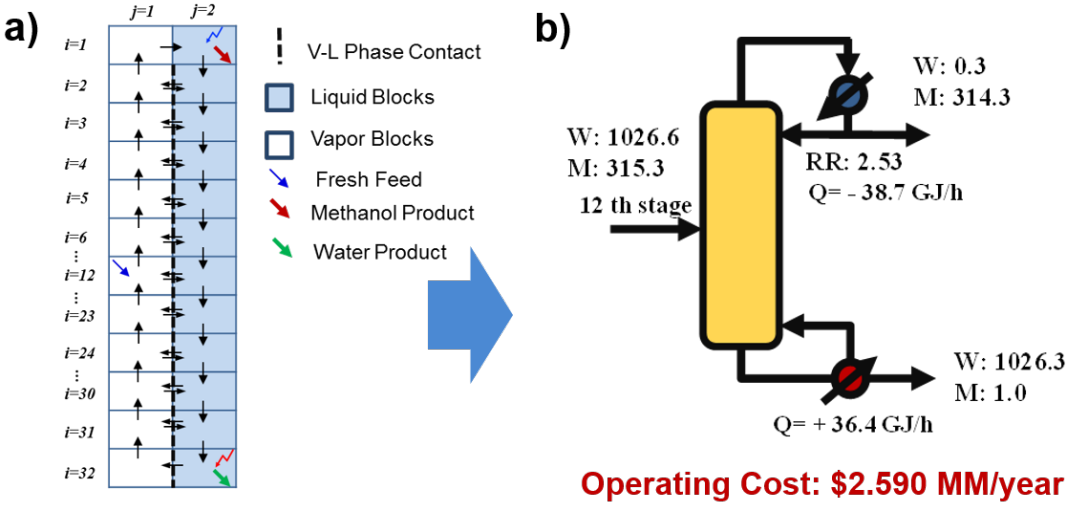

Figure 4.17: Base case distillation column for the hybrid separation process. Figure on the left is the building block representation for the base case methanol/water separation column and the figure on the right is the corresponding optimal distillation column design.

In this case study, a literature example on methanol/water separation system will be used to demonstrate the optimal synthesis of hybrid separation schemes via building block superstructure.

Luyben (2005) investigated the pressure-swing and extractive distillation processes for methanol recovery in TAME production process and found that extractive distillation is more favorable [180]. In that work, a distillation column is utilized to separate methanol/water mixture for methanol recovery. Here, this design will be considered as a base-case and the potential savings from deployment of a vapor permeation membrane will be investigated. Following assumptions are made for the modeling. Membrane permeance and selectivity data are assumed to be independent of concentration, temperature and pressure. Isothermal membrane operation with counter-current flow pattern is assumed for the vapor permeation module. Pressure drop through the distillation column and membrane modules are assumed negligible. Concentration polarization is neglected. Wilson activity coefficient model is used to describe the VLE behaviour. Note that the feed location for the distillation column is kept as the same with the reference case for all optimization problems.

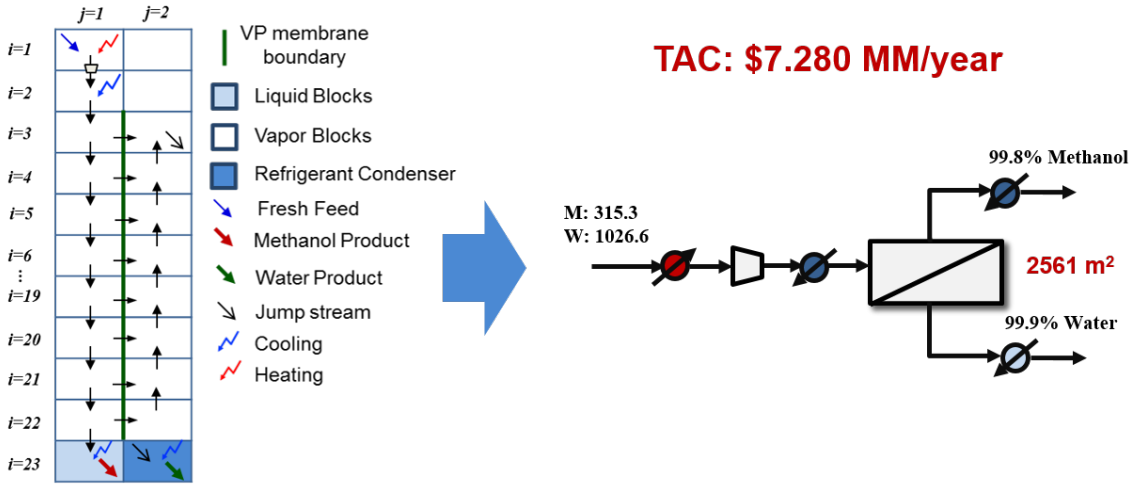

Figure 4.18: Standalone vapor permeation membrane solution for methanol/water separation. Figure on the left is the building block representation for the membrane module and the figure on the right is the corresponding optimal membrane process.

First, the distillation column design proposed by the reference is optimized as a benchmark for the membrane-based schemes. Column has a liquid feed mixture of 1342 kmol/h methanol/water mixture (23.5% methanol) and has 32 stages (including condenser and reboiler). It produces a

methanol top product with 99.75% methanol and a bottoms stream with 99.9% water. This distillation column process can be represented by the building block superstructure as shown in Figure 4.17a. Here, the feed location is fixed to the same stage as in the reference case and the process is optimized for minimum yearly operating costs. The resulting design is given in Figure 4.17b. The operating cost is \$2.590 MM/year with \$2.490 MM/year hot and \$0.110 MM/year cold utility costs. This cost will serve as a target for the membrane-based process. If we can achieve any savings compared to this annual cost, then the retrofitting with membrane unit can be considered as a viable alternative.

Before investigating a hybrid scheme, a standalone vapor permeation unit is optimized to check whether the whole distillation column can be retrofitted with the vapor permeation process. This is performed through the building block superstructure given in Figure 4.18. NaA zeolite is chosen as the membrane material with the permeance data obtained from the literature [181]. This zeolite material is highly selective towards water. A block superstructure of size 23×2 is used. Membrane representation is similar to the one given in Figure 4.11, yet, here 20 blocks are used to represent the membrane module. As the feed mixture is in liquid state, a feed heater is considered to vaporize the feed in block $B_{1,1}$. This vapor mixture then can be compressed to higher pressures to increase the driving force within the membrane module. Note that use of this compressor is optional. After this compressor, a cooler option is also provided to cool down the feed if the compressor outlet temperature is above the membrane operating temperature. Furthermore, although mostly neglected in the literature, vapor permeation operations yield permeate and retantate products in vapor state which need to be condensed before they can be sent to the other parts of the process or storage units. As the permeate side is mostly operated under vacuum conditions, condensation of the permeate outlet generally requires refrigerants or brine solutions. Here, we consider a refrigerant at 263 K for the permeate condenser. High purity methanol mixture can be taken out as the retantate outlet from block $B_{23,1}$ and high purity water mixture can be taken out from $B_{23,2}$. We optimize this membrane process while minimizing the TAC by considering capital investment costs for the membranes, heaters/coolers and compressors. Annualization factor of 0.2

is used for TAC calculation. Optimal membrane result is shown in Figure 4.18b. This standalone membrane unit incurs a TAC of $7.280 MM/year. While the annualized investment cost accounts for $1.260 MM/year, total operating costs are $6.020 MM/year. Comparison with the operating cost of the standalone distillation unit shows that standalone membrane module is not favorable for the retrofitting. Next, we will consider a hybrid distillation-membrane scheme.

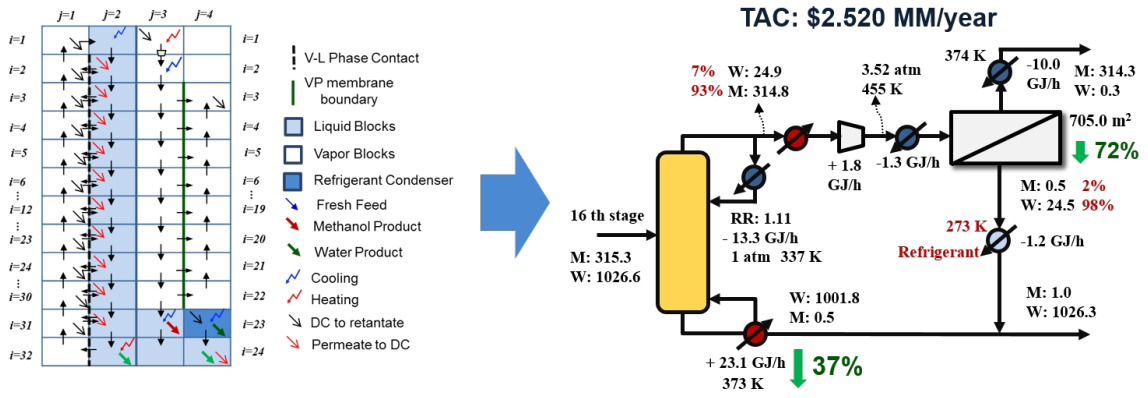

Figure 4.19: Optimal hybrid separation scheme for methanol/water separation. Figure on the left is the building block representation used for obtaining the optimal hybrid separation scheme. Figure on the right is the corresponding optimal hybrid separation design.

For the hybrid scheme, we use the building block superstructure shown in Figure 4.19. This block configuration is obtained by appending the distillation column representation with the membrane module representation. While the overall size is 32×4, blocks under the membrane module (not shown in the Figure), i.e. $B_{24\leq i\leq 32,j=3}$ and $B_{25\leq i\leq 32,j=4}$, are not utilized. In addition to the membrane module representation as shown in 4.18, an additional block at the permeate side outlet is considered for the water product. This is to account for a possible mixing between the distillation bottoms and permeate outlet before the high purity water can be withdrawn from the process. Furthermore jump streams are activated from the vapor blocks within the distillation column region ($B_{1\leq i\leq 31,j=1}$) to the retantate inlet ($B_{i=1,j=3}$) and from the permeate outlet ($B_{i=32,j=4}$) to the liquid blocks ($B_{2\leq i\leq 31,j=2}$) within the distillation column region. These jump streams can be utilized

if needed for possible connections from the intermediate stages of the distillation column to the membrane unit and also the recycle from the permeate outlet back to the distillation column. We solve this superstructure for minimizing the TAC while considering the capital investment costs for the membranes, heaters/coolers and compressors, and operating costs due to steam, electricity, cooling water and refrigerant. Resulting flowsheet is shown in Figure 4.19. The top vapor stream from the distillation column is split into two while one is sent back to the column as reflux the other stream is sent to the membrane module. This top vapor product has a methanol purity of 93% which is much lower than the required purity. However, the following membrane module performs the rest of the separation. Before being fed to the membrane, this vapor stream is first heated to prevent any condensation in the compressor and then compressed to 3.5 atm to increase the driving force within the membrane module. As a result of the compression, vapor gets heated to 455 K which is highly above the membrane working conditions. Hence, the cooler is used to bring down the retantate inlet stream temperature. After separation, methanol outlet is taken from the retantate and condensed with cooling water. Permeate outlet on the other hand, is condensed through the refrigerant. We observe that the water purity in the permeate stream is 98% which is below the purity limit of 99.9%. Hence, this stream is mixed with distillation bottoms stream which has a slightly higher purity than the standalone distillation bottoms stream before it is sent out as a product. The recycle connections from the intermediate stages are not utilized and there is no permeate to distillation recycle.

In overall, this process has a TAC of \$2.520 MM/year which implies 3% savings compared to the standalone distillation column process. Operating costs account for \$1.970 MM/year and annualized capital costs account for \$0.550 MM/year. As the distillation column operates with a much lower load and performs a sloppier separation, the reboiler duty decreases 37%. Also, the membrane area required for separation is 72% lower than the standalone membrane process. While there is a 24% savings in the operating costs compared to the standalone distillation column, additional capital investment costs decrease the impact of these savings. However, this process can be made more attractive by utilizing heat integration strategies. We can allow several streams within

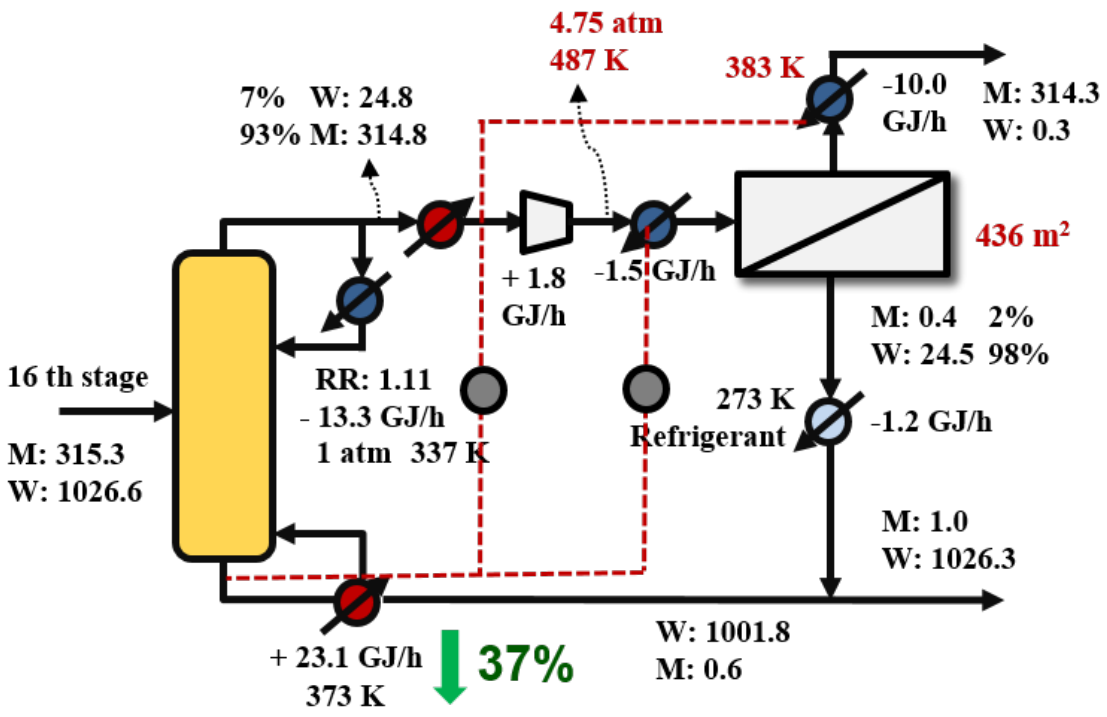

Figure 4.20: Optimal heat integrated hybrid separation process.

the superstructure to be matched with each other for energy integration. Specifically, we observe that the reboiler of the distillation column operates at a lower temperature than the retantate inlet cooler. Furthermore, if the pressure of this stream is increased, it can also exchange heat with the retantate outlet condenser. But this option will not be enforced, it will be provided as an alternative. We address this simultaneous synthesis and heat exchanger network synthesis problem through the same superstructure representation and by allowing two possible heat integration matches between the reboiler and retantate inlet and outlet streams. The resulting flowsheet is shown in Figure 4.20. Both allowed heat integration alternatives are utilized in the optimal structure. Vapor retantate inlet compressed to a higher pressure, 4.75 atm, which increases the temperature for both retantate inlet and outlet streams, decreasing the cost of the heat exchangers. This increase in pressure also decreases the membrane area required by 38%. Distillation top stream has the same purity with 93% methanol and reboiler duty is the same with the non-heat integrated alternative. In overall, this heat integrated hybrid scheme has a TAC of $1.810 MM/year with 30% savings compared

to the standalone distillation column process. It has $1.220 MM/year operating costs and $0.590 MM/year investment costs. This translates into 53% savings in the operating costs which covers the additional investment cost required for the membrane module providing a very attractive retrofitting option. The membrane material used within the process might have a high impact on

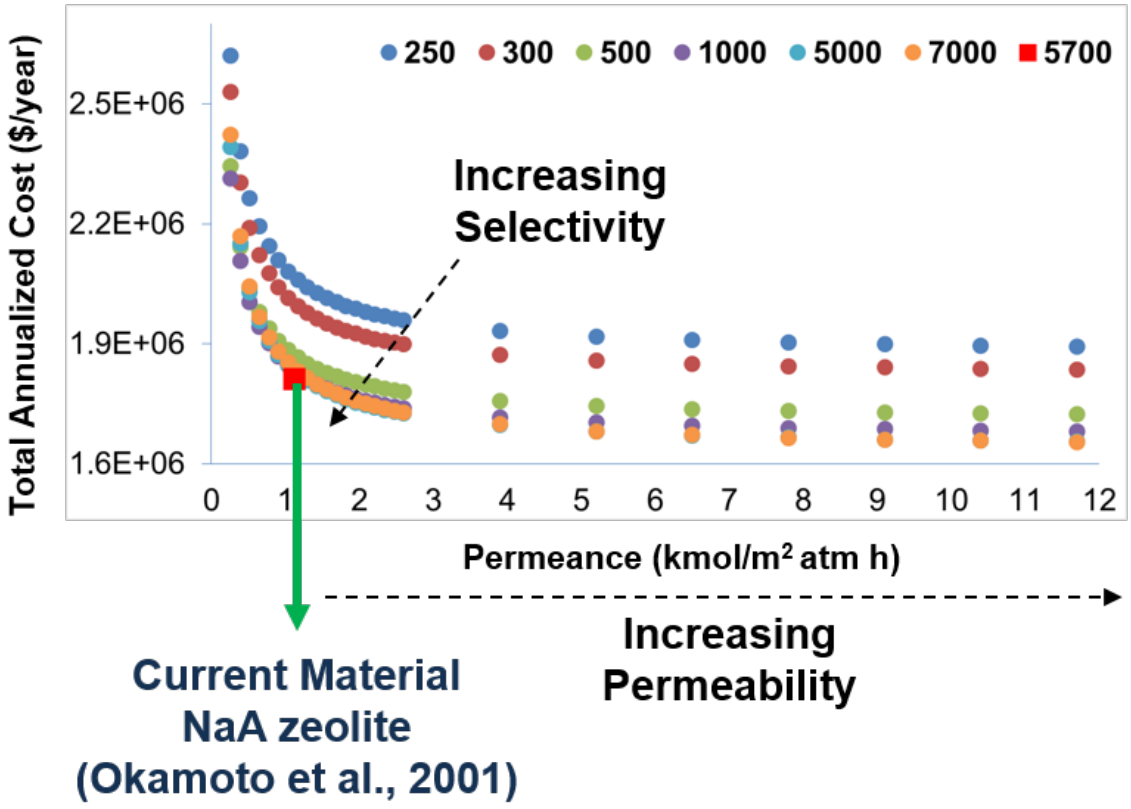

Figure 4.21: Analysis of the effect of membrane properties on the optimal heat interated hybrid separation process.

the performance of the proposed hybrid scheme. To investigate the effect of membrane permeance and selectivity on the economics, we perform an optimization-based sensitivity analysis on the heat integrated hybrid scheme. We use a range of permeance and selectivity values and optimize the process by using the same building block superstructure. Results are shown in Figure 4.21. Based on this plot, we observe that as the selectivity toward water increases, the cost of the hybrid scheme decreases. Similarly, enhancement in water permeance also decreases the cost of the module. For

the selectivity, we observe that the enhancement in process performance gets less pronounced for the selectivity values beyond 500. The NaA membrane material used in the case study has a much higher selectivity than this threshold value, i.e. 5700. As for the permeance towards water, we observe a similar trend. The permeance values above 2 kmol / m^2 atm h shows rather incremental improvement in the economics. The NaA membrane, on the other hand, has a lower permeance than this, i.e. 0.9 kmol / m^2 atm h. This shows that the new materials or enhanced zeolite structures with higher permeance while keeping the selectivity above 500, might be beneficial and material synthesis activities should be guided through these performance targets. The lowest TAC of $1.650 MM/year is possible if the selectivity can be improved to 7000 and the permeance can be improved beyond 11 kmol / m^2 atm h. This corresponds to 36% savings with the hybrid retrofit compared to the standalone distillation column.

4.7 A Hybrid Solution Approach: Process Synthesis and Intensification

In this section, an example problem on production of ethylene glycol is solved via building block superstructure approach. Ethylene glycol (EG) is an important chemical used as an antifreeze in automobiles, desiccant for natural gas production, and a raw material for the production of polyester fibers and resins [182]. Its industrial production is mainly based on the reaction of ethylene oxide (EO) with water (W). Further reaction between the reactant EO and product EG results in diethylene glycol (DEG) production: Heavier glycols, e.g. tri-ethylene glycol, are also

$$\begin{aligned} &\text{Main Reaction:} && C_2H_4O + H_2O \rightarrow C_2H_6O_2 \\ &\text{Side Reaction:} && C_2H_4O + C_2H_6O_2 \rightarrow C_4H_{10}O_3 \end{aligned}$$

possible via side reactions between glycol products. The side reaction between EO and EG and the other side reactions producing heavier glycols can be avoided if high water content is introduced into the reactor [183]. This, however, results in high separation costs as the excess amount of water needs to be removed before high purity EG can be obtained. To show different aspects of the devel-

oped framework, this problem is first solved as a traditional process synthesis problem in which an equipment-based representation is used. Then, on the same problem, sequential and simultaneous heat exchanger network synthesis is demonstrated. Finally, a transition to the phenomena-based representation is made for obtaining intensified process flowsheets for the same problem.

4.7.1 Base-Case Generation

In this section, how building block superstructure can be used to address superstructure-based synthesis problems is demonstrated. Equipment-based representation and short-cut models are used to solve the problem. For reaction, kinetic reaction model with data from Altiokka and Akyalcin [184] is used. This implies that each building block with reaction operations correspond to a CSTR unit. Several different reactor configurations including CSTRs-in-series and PFR reactors are considered as different reactor alternatives. For the product purification, distillation columns are utilized [185, 186]. Here, each distillation column is represented as a single block with a semi-restricted boundary which designates the position of the bottoms stream. Flows through semi-restricted boundary are described based on split-fraction models which are kept as variable to optimize the recovery and purity of the top and bottom streams. The objective is to generate a flowsheet featuring minimum total annual cost of production for 25 kmol/h EG production with 99.8% (mol) purity. Reactor type and volume, total number of distillation columns, their reflux ratio, reboiler duty and area, condensor duty and area, column dimensions, product recovery and purity are among the decision variables. Fenske-Underwood-Gilliland correlations [57] are used while optimizing the distillation columns. Note that, total annual cost includes raw material costs, i.e. EO and water, utility costs, i.e. cooling water, steam and electricity, annualized capital costs for reactors, separation columns, recycle pumps and heat exchangers. Capital cost functions, design formulations and utility costs are taken from literature [57, 187, 188, 189, 64, 190, 191] and provided in Appendix B. Temperature and pressure bounds of the process are taken as 340–520 K and 1–36 bar, respectively[186].

In addressing this problem through block superstructure, a grid size of 2×9 is considered as shown in Figure 4.22a. Reaction and separation operations are assigned to the separate positions

on this grid. While reaction is allowed to be positioned within the first five columns (yellow blocks), separation blocks are allowed to be positioned on the last four columns (green blocks). These separators are only allowed to be positioned at the second row. Total number of separation columns are restricted to 4. This is achieved through allowing the semirestricted boundary at only the designated positions (shown in green color in Figure 4.22a). These streams, if activated, denote the bottoms streams of the distillation columns and flow rates through these boundaries are determined according to the short-cut design correlations. If they are not chosen as semirestricted, then the unrestricted boundary relations (i.e. splitting constraints) are activated and the corresponding distillation column is bypassed. In this way, number of distillation columns required for product separation is determined. Connectivity within the flowsheet is increased by activating recycle streams from the potential separator blocks. These streams are all connected to the inlet block of the reaction region, i.e. $B_{1,6}$. While the recycle from the first potential separator block is achieved through a vertical interblock stream from block $B_{1,6}$, recycle streams from the other potential separator blocks are represented through jump streams. Furthermore, fresh raw materials are allowed to enter at any block excluding the separator blocks and final product withdrawal with 99.8% EG is only activated from the block $B_{2,9}$. Note that pressure of the selected units are also considered as decision variables. Hence, pumping units are activated for all these recycle streams to account for possible difference in pressures. Distillation column reboiler and condenser pressures are determined based on bubble point calculations. As the reactions are in liquid phase, a phase check is performed at the block $B_{2,5}$ based on bubble point calculations. This liquid phase constraint is only considered at the exit block from the reaction region as the reactions are exothermic and the reacting mixture will be at its highest temperature at the outlet of the reaction zone where its likelihood for phase change is the highest. In solution of the problems, the separator located on $B_{2,9}$ was always active. First no capital cost for stream heaters/coolers are considered and all the separators except the one on $B_{2,8}$ are activated. Then binary variables related with the other separators are freed one by one in the subsequent two iterations. Finally, with this as initial solution, full problem with the stream heater/cooler capital costs are solved. Following this solution strategy

yields global optimal solution for the presented case studies in this section.

First, a base-case with a single CSTR [188] is considered. Reaction is allowed in block $B_{2,5}$ only. Problem includes 341 continuous and 3 binary variables, 620 nonlinear terms and 977 constraints. The overall problem is solved with ANTIGONE [145] to optimality and the resulting block superstructure and its equivalent flowsheet representations are shown in Figure 4.22b-c (Alternative 1). In the resultant flowsheet, CSTR is followed by three distillation columns: First two columns are used to separate water from the reactor effluents and the top products are recycled back to the reactor. Third distillation column takes in mainly EG and DEG and yields EG as the top product with 99.8% purity. Process has an total annual cost of $13.68 MM/year (Table 4.11). Single-pass conversion of EO in the CSTR is 39.9% and the selectivity of EG/DEG is 11.5 kmol EG/ kmol DEG. The recycle flow rate is very high which increases the water concentration in the reactor inlet. This results in higher selectivity towards EG. High recycle flow rate between separators and reactor also provides clue for a potential intensification opportunity. As indicated by Baldea [96], process intensification can be observed as tight material integration and, in this case, reaction and separation operations can be combined in a single unit to obtain a reactive distillation system. This was also suggested by others for the EG production [81, 112, 82, 186]. This intensified alternative will be investigated further with phenomena-based representation in Section 4.7.3.

Next, different CSTR unit configurations are investigated. Number of blocks that can be assigned

Table 4.11: Cost summary for the flowsheets generated through unit operation based process synthesis for ethylene glycol production (Reprinted with permission from [51]).

Flow. Alt.	Feed (MM$/year)	Hot Utility (MM$/year)	Cold Utility (MM$/year)	TOC (MM$/year)	Capital (MM$/year)	TAC (MM$/year)
1	11.252	1.674	0.080	13.007	0.666	13.672
2	10.849	1.357	0.066	12.272	0.878	13.150
3	10.867	1.372	0.067	12.306	0.655	12.960
4	10.863	1.375	0.067	12.305	0.661	12.966
5	10.682	0.949	0.047	11.678	0.742	12.420

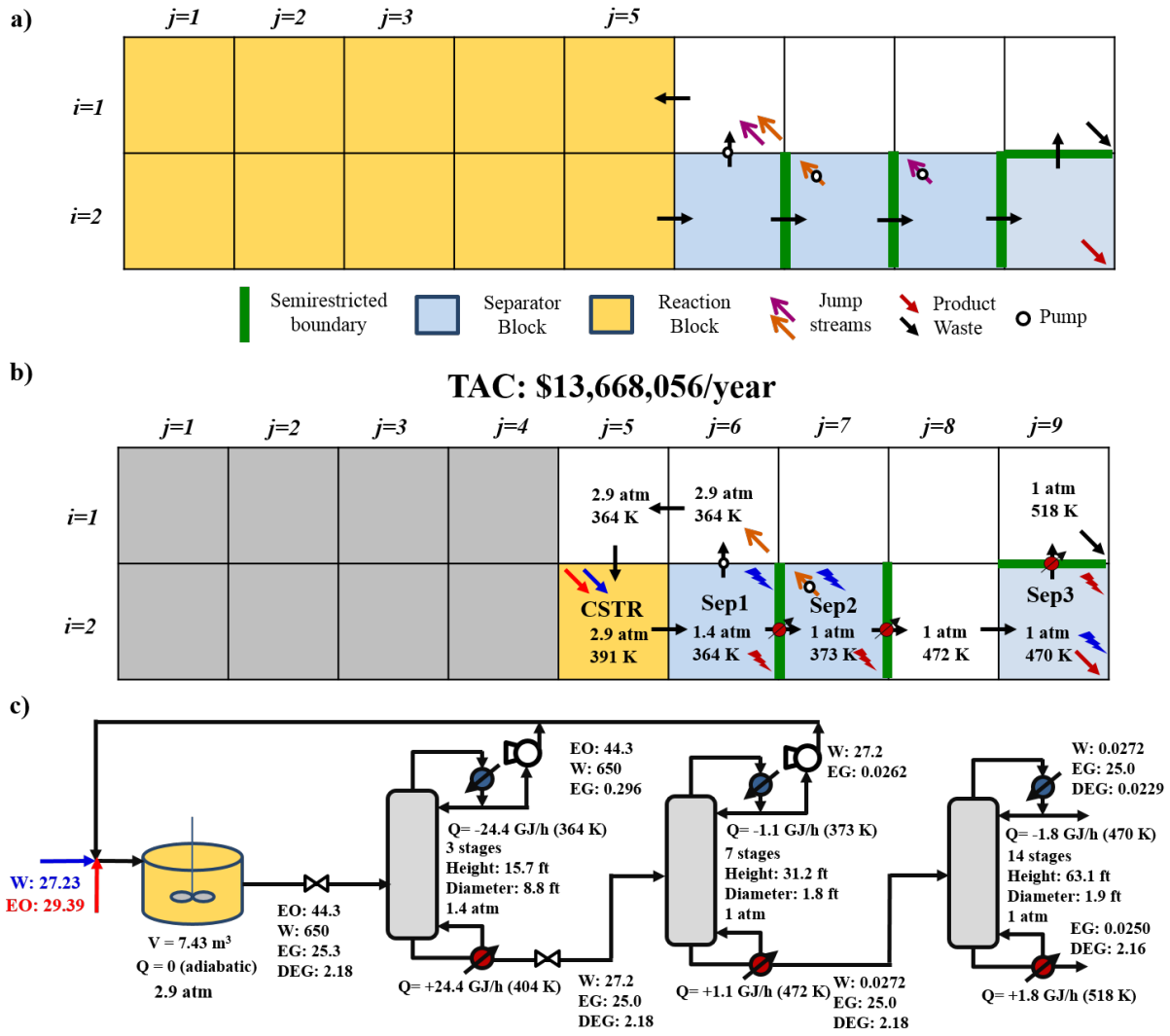

Figure 4.22: Process synthesis superstructure and solution with single CSTR for ethylene glycol production. a) Process synthesis superstructure for ethylene glycol production, b) building block result for the flowsheet with single CSTR (Alternative 1), and c) equivalent flowsheet representation (Reprinted with permission from [51]).

with reactors is increased to 6 ($B_{1,3}$ to $B_{2,5}$). In the solution, only 4 out of 6 blocks alowed to be assigned with reaction is active which suggests 4 CSTRs-in-series. Problem includes 485 continuous and 9 binary variables, 770 nonlinear terms and 1379 constraints. Resultant process flowsheet is shown in Figure 4.23a (Alternative 2). Number of active searator units are the same with flowsheet Alternative 1. Volume of these CSTRs hit to the lower bound specified for the CSTRs. Capital

cost is increased compared to single CSTR case, but TAC decreases to $13.15 MM/year (3.8% reduction) as shown in Table 4.11. Main contribution to this much decrease in cost is due to the reduction in the amount of fresh EO fed into the system. This is made possible by increased EO conversion, 50.4%, and EG/DEG selectivity, 15.1 kmol EG/kmol DEG. As is observed from this case, multiple CSTR system performs better than the single CSTR case with better control over the reactant concentrations and less degree of mixing. It is also known that plug-flow reactors (PFRs) are preferable to maintain a high concentration of reactants [192]. Next, this alternative is investigated.

For PFR representation, 10 blocks (at equal volume and pressure) are considered. This corresponds to a 10 CSTRs-in-series model. Problem includes 580 continuous and 3 binary variables, 897 nonlinear terms and 1661 constraints. Solution of this problem yields an optimal flowsheet with $12.96 MM/year TAC (Alternative 3). Resulting block superstructure and its equivalent flowsheet representations are shown in Figure 4.23b-c. 5.2% decrease in the TAC is obtained compared to Alternative 1 (Table 4.11). Block supertructure result features a distributed feed to the reactor suggesting a differential side stream reactor (DSR). To understand the effect of distributed feed, problem is also solved with no feed allowed into the reaction blocks. In this case, a process alternative with slightly higher TAC is obtained ($12.97 MM/year) (Alternative 4). It should be noted that DSR and PFR cost functions are assumed to be the same in this problem. Although PFR results in $4,900 more cost, this might not justify the construction of a DSR with additional inlet ports. The objective of this case study is, however, to show that developed block superstructure representation and corresponding model can identify such complex reactor structures. Also, the same problem can be addressed simultaneously with PFR and multiple CSTR alternatives by considering a larger block superstructure. Solution of this simultaneous problem does not yield any better solution.

4.7.2 Simultaneous Heat Exchanger Network Synthesis

Material integration is already considered through recycle streams in the previous problem. Here, heat integration alternatives are investigated with building block superstructure representation. Only the integration between the distillation columns is considered. As PFR configuration

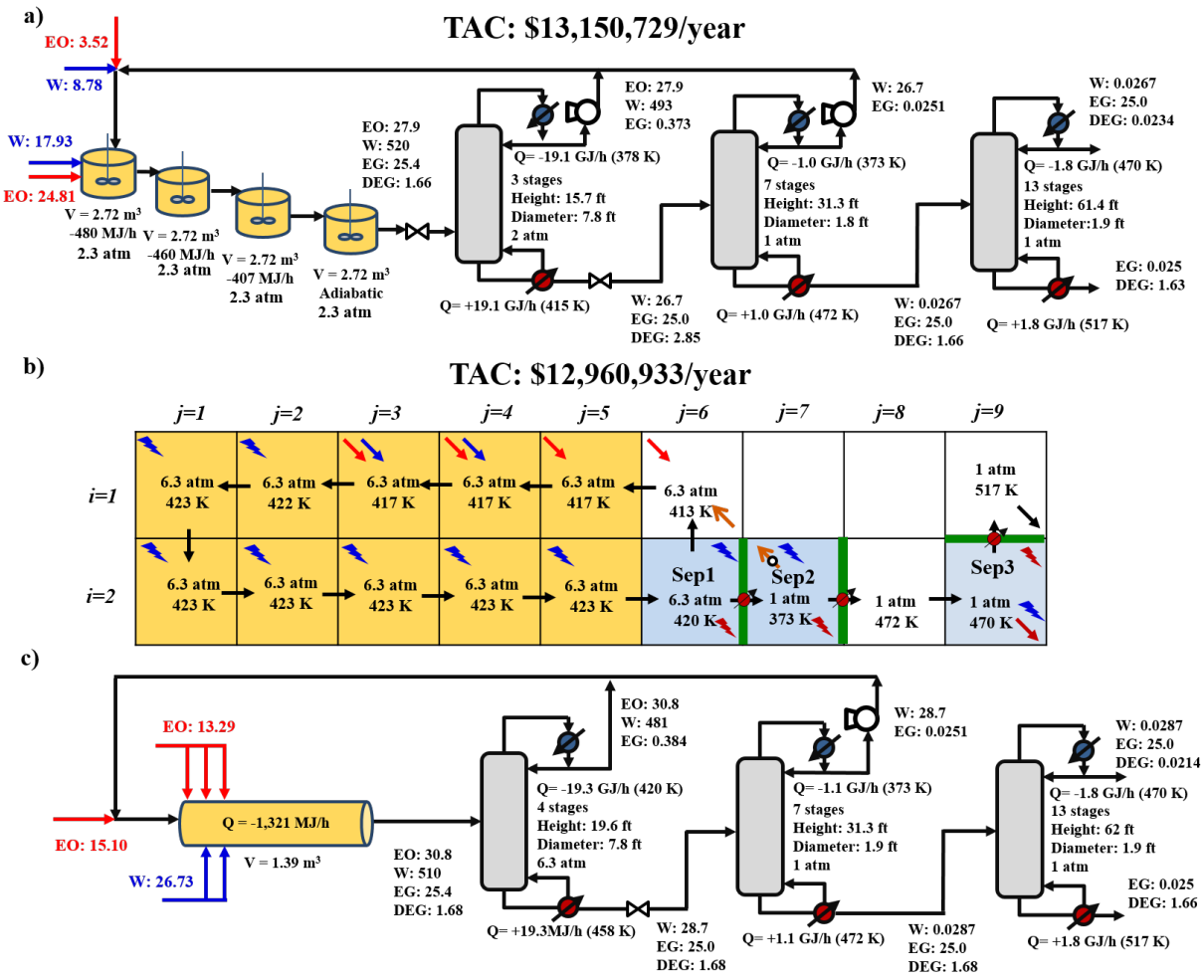

Figure 4.23: Process synthesis results with multiple CSTRs and PFR reactor for ethylene glycol production. a) Flowsheet representation for the optimal result with multiple CSTRs (Alternative 2), b) building block result for the solution with PFR featuring a DSR (distributed side-stream reactor - Alternative 3), c) flowsheet representation of the optimal result with DSR (Reprinted with permission from [51]).

resulted in lower TAC than the CSTRs, we will consider PFR as the reactor and we will not consider DSR configuration. In flowsheet Alternative 4, isothermal streams from distillation column reboilers and condensors can be integrated. A superstructure for the resulting Heat exchanger network synthesis (HENS) problem can be constructed through the building block-based approach with the heat integration representation as described in detail in Li et al. (2018) [193]. However, there are only two streams that can be matched in this flowsheet: Bottoms of Sep1 and distillate

of Sep3. Hence, there is no need to address this problem through a superstructure-based approach. Instead, we will address the HENS and process synthesis problem simultaneously. Here, representation stays the same and heat duties of the reboilers and condensers are allowed to be integrated with each other. Problem includes 544 continuous and 9 binary variables, 933 nonlinear terms and 1590 constraints. Solution of this problem yields an optimal flowsheet with \$12.42 MM/year TAC (Figure 4.24b - Alternative 5). Unlike the not integrated one, this flowsheet contains four distillation columns. Operating pressure of the Sep1 is increased to 12 bar. Hence, it can operate at a higher temperature while performing a much sloppier water separation. This is compensated by the use of an additional column for EG/water separation. With these changes, annualized capital cost increases, but hot utility consumption decreases by 31% and cold utility consumption decrease by 29%. In overall, 4.2% decrease in the TAC is obtained compared to the non heat-integrated PFR alternative (Table 4.11). With this heat integration scheme, Alternative 5 resembles the industrial EG production process which also includes three columns for water/EG separation as described by Dye [185].

4.7.3 Process Synthesis, Integration and Intensification

In this section, intensification of the EG production problem is addressed through phenomena-based representation. Here, we will explore several different flowsheet alternatives that cannot be identified with pre-specified unit operations as it was the case in the previous case studies. To enable this, we adopt phenomena-based representation. Accordingly, semi-restricted boundaries will be used to represent V-L phase contact phenomena rather than a whole pre-specified unit. First, we address the optimal heat integrated flowsheet obtained in the previous section and consider it as a base-case structure for the further analysis of the problem. Phenomena-based representation of this flowsheet (Figure 4.24b) can be obtained within a 14×9 grid size as shown in Figure 4.25. Here, the first column ($j = 1$) contains the PFR which is represented as 10 CSTRs-in-series. Each pair of the remaining grid columns are used to represent a distillation unit. Required number of rows is given by the number of theoretical stages. For instance, the first distillation column (Sep1 in Figure 4.24) requires 3 theoretical stages including a partial reboiler. Hence, 2 rows of vapor-liquid

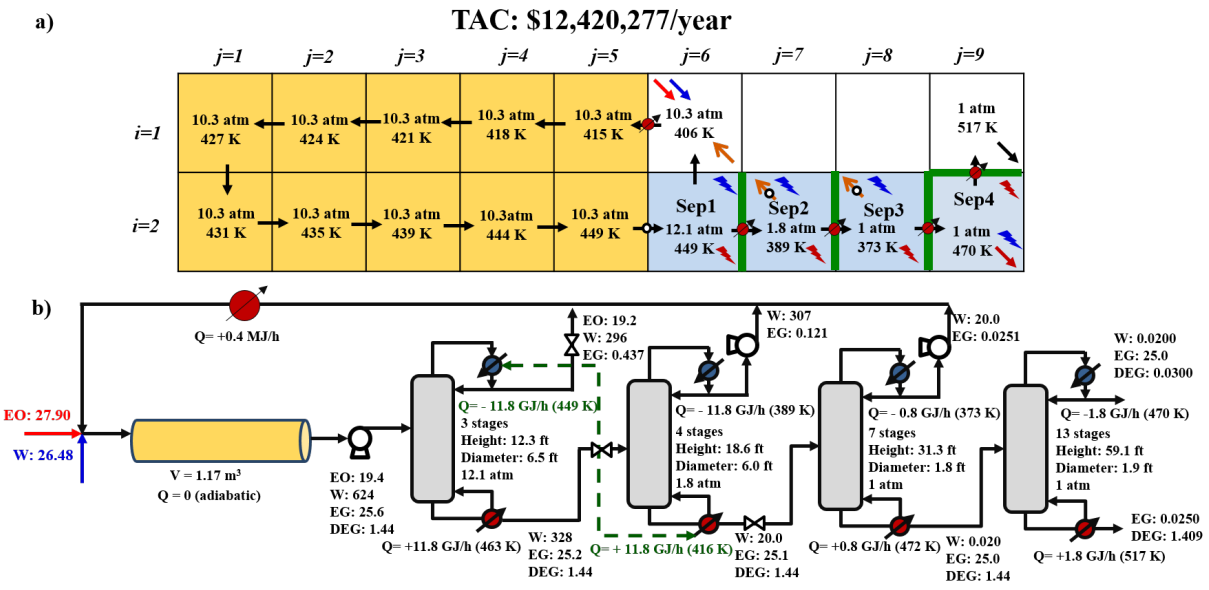

Figure 4.24: Simultaneous process synthesis and heat exchanger network synthesis result for ethylene glycol production process. a) Building block superstructure result for the simultaneous process synthesis and HENS problem (Alternative 5), and b) corresponding flowsheet representation (Reprinted with permission from [51]).

block pairs, i.e. (blocks $B_{2,2}$ to $B_{3,4}$), can be used to represent these trays with equilibrium model. Then, blocks $B_{1,2}$ and $B_{1,3}$ are assigned as total condenser and blocks $B_{4,2}$ and $B_{4,3}$ are assigned as partial reboiler. The remaining distillation columns are also represented in a similar manner. To compare the solutions obtained from equipment-based and phenomena-based representations, we fix the reactor volume, reactor and distillation column pressures to the values obtained from equipment-based representation. Similarly, we provide lower bounds for the reflux ratios from the equipment-based solution. Problem includes 1137 continuous variables, 2248 constraints and 2971 nonlinear terms and solution with BARON for 6 hours of CPU time yields TAC of $12.35 MM/year (18.1% optimality gap) which is lower than the one obtained with equipment-based representation, i.e. $12.42 MM/year. And the difference between the two results mainly due to the hot utility consumption. Hot utility cost is 9.4% lower with the phenomena-based rigorous model. Now, we will explore several different flowsheet alternatives while using this result as the base-

case. For simplicity, we will first solve several different flowsheet alternatives for minimization of the total annual operating cost (TOC) and only consider capital cost of the in the objective if a promising flowsheet candidate is identified.

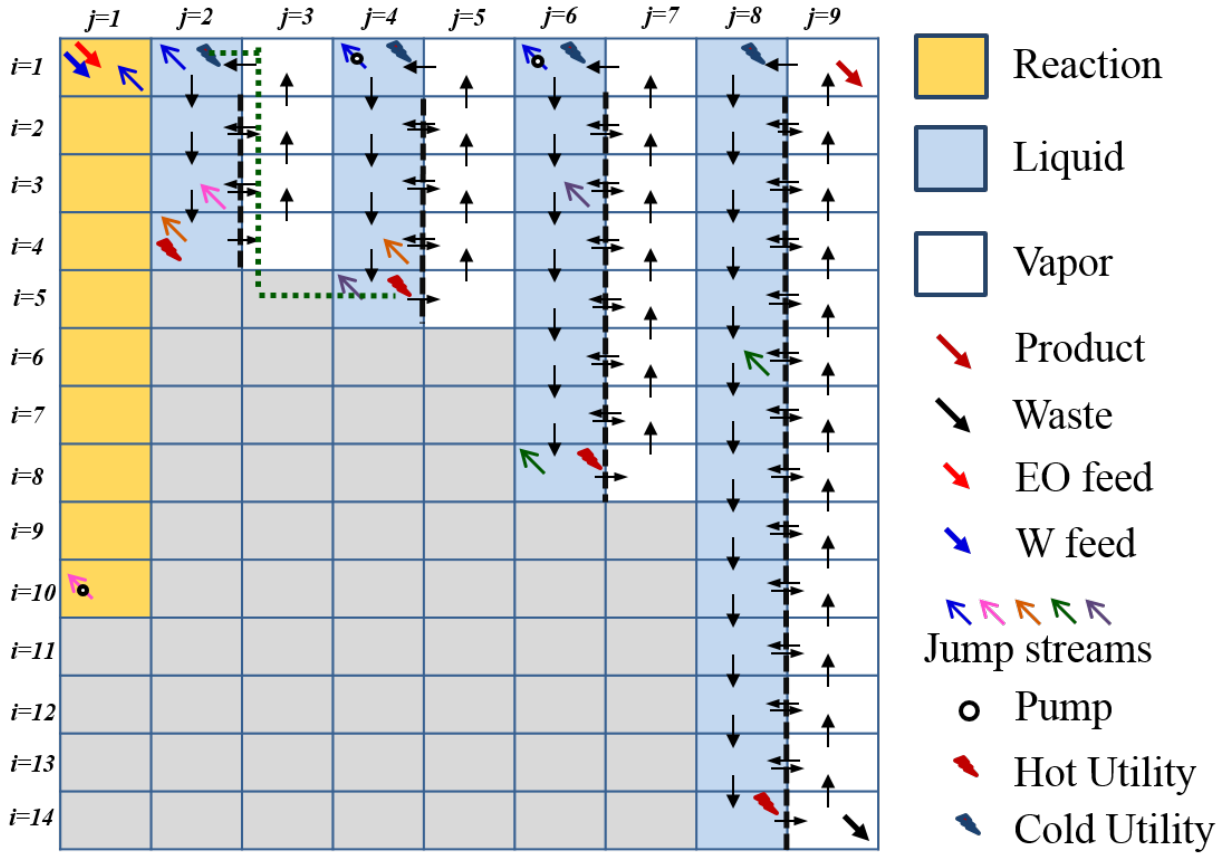

Figure 4.25: Phenomena-based representation of the optimal heat integrated flowsheet (Reprinted with permission from [51]).

With phenomena-based representation and model, numerous eccentric flowsheets can be generated. For a smaller grid size, this was demonstrated in Demirel et al. (2017)[90]. However, if this model is utilized with 14×9, model P4 becomes a large-scale MINLP with many nonlinear terms which cannot be addressed with current commerical solvers. Hence, here, we adopt a guided approach through fixing several structural decisions beforehand and generate and screen different

intensified alternatives with reduced model sizes.

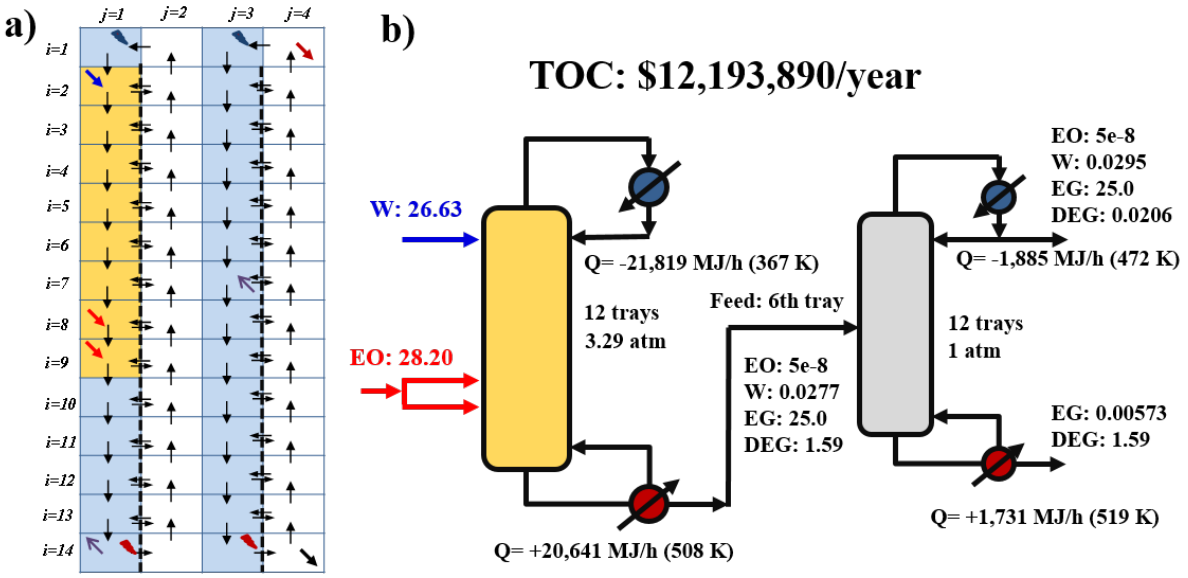

Figure 4.26: Flowsheet with reactive distillation followed by a distillation column for ethylene glycol production. a) Building block superstructure result, b) corresponding flowsheet (Alternative 2) (Reprinted with permission from [51]).

We observed from the previous results that recycle flow rates from the separation columns to the reactors are very high. This indicates that reaction and distillation operations can be combined in a single reactive distillation unit as is also indicated in Section 4.7.1. We first investigate a single reactive distillation column to perform the given conversion and separation simultaneously. However, using 14 building block pairs (a grid size of 14×2) to represent and solve this problem do not provide a feasible solution. To investigate further, we increased the grid size to 100×2 and solved the problem for maximizing EG purity in the product. This corresponds to a reactive distillation column with 98 equilibrium trays. Solution of this problem yields 96.3% of purity, significantly less than 99.8% EG purity target. Hence, a second separation stage needs to follow this reactive distillation unit for feasible operation. To investigate this alternative, first four columns of the building block superstructure given in Figure 4.25 is utilized. This gives rise to a grid size of

14×4 (Figure 4.26). In this structure, liquid (to the first and third columns of the grid) and vapor phase (to the second and forth columns of the grid) are fixed and the boundary between two phases are designated as vapor-liquid equilibrium boundary. Reaction is only allowed to be assigned to the first column of the grid (Blocks $B_{1,1}$ to $B_{14,1}$). Accordingly, blocks $B_{1,1}$ to $B_{14,2}$ represent a reactive distillation column and blocks $B_{1,3}$ to $B_{14,4}$ represent a distillation column. We solve this problem with BARON for 6 CPU hours for minimizing total annual operating cost (Alternative 2). Problem includes 1052 continuous variables, 1778 constraints and 2204 nonlinear terms. Solution of this block superstructure yields a flowsheet with \$12.19 MM/year (21.3% optimality gap). This is significantly higher than the annual operating cost of the base case flowsheet, i.e. 5.3%.

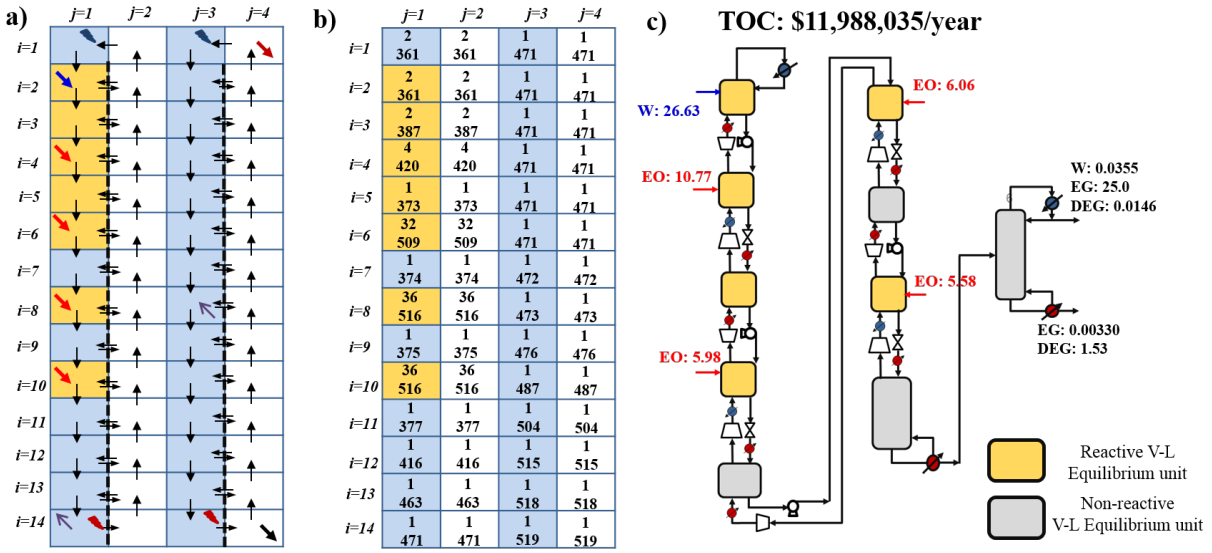

Figure 4.27: Flowsheet alternative when equipment constraints are removed. a) Block superstructure result, b) temperature and pressure of the building blocks, c) a flowsheet representation for this result containing several reactive and non-reactive V-L equipment with pressure manipulations in between (Alternative 3). This result shows that while reaction is favored at high pressure and temperature, separation of EG from the reaction products is favored at low pressure and temperature (Reprinted with permission from [51]).

Can the reactive distillation operation be made more favorable? To investigate different design alternatives, we remove several constraints that are used to assign the building block aggrega-

Table 4.12: Cost summary for the flowsheets generated through phenomena-based process synthesis for the ethylene glycol production (The first five lines are reprinted with permission from [51]).

Flow. Alt.	Feed (MM$/year)	Hot Utility (MM$/year)	Cold Utility (MM$/year)	TOC (MM$/year)	Capital (MM$/year)	TAC (MM$/year)
1	10.704	0.860	0.043	11.612	0.736	12.347
2	10.795	1.335	0.065	12.194	-	-
3	10.755	1.176	0.057	11.989*	-	-
4	10.660	1.219	0.059	11.939	-	-
5	10.600	0.882	0.044	11.526	-	-
6	10.683	0.861	0.043	11.587	0.674	12.26

*Does not include all hot/cold utility and operating costs from compressors/pumps.

tions as pre-specified equipment. One such constraint dictates that pressure of the building blocks around the vapor-liquid boundaries should be the same which ensures that the resulting structure can be translated as a single distillation column. Furthermore, we do not include any cost for pressure change operations. When we solve this problem for minimizng total annual operating cost, a building block result with $11.99 MM/year is obtained (Figure 4.27a-c) (Alternative 3). As there is no cost associated with pressure change, there exists multiple pressure changes throughout the block superstructure. There are several separate reactive vapor-liquid equilibrium regions followed by non-reactive phase equilibrium regions. The reactive separation blocks operate at higher temperature and pressure than the non-reactive separation blocks which operate at the lowest allowed pressure, i.e. 1 atm. A flowsheet alternative that can realize this block superstructure result is given in Figure 4.27c. It includes 10 different equipment with pumps, compressors, expanders and valves in between. With this number of equipment and multiple pressure and temperature change operations, this flowsheet is not favorable. However, by judging from this building block result, we can propose a new flowsheet. As reactive V-L sections require high pressure and non-reactive V-L sections require low pressure, reactive distillation column can be separated into two separate units that can operate at different pressures. Accordingly, we introduce a third distillation column between the two distillation columns used before as shown in Figure 4.28a. We solve this problem with BARON for 6 hours with minimizing the TOC as objective. Problem includes 1916 continuous

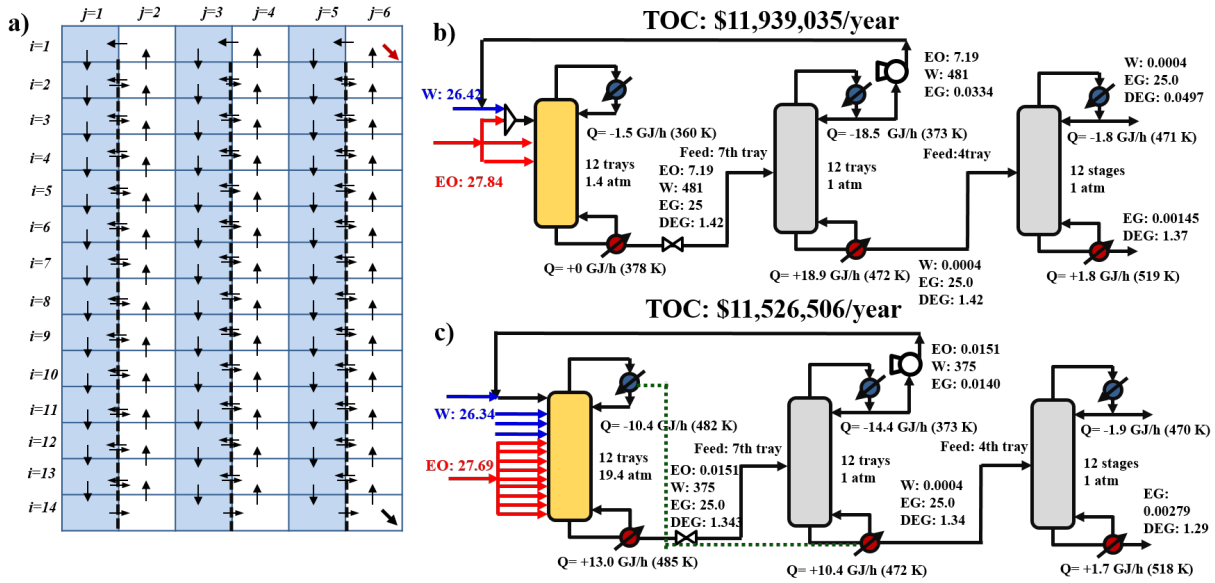

Figure 4.28: Flowsheet alternatives with three columns. a) Block superstructure representation used in obtaining these flowsheets, b) flowsheet Alternative 4 with RD followed by two non-reactive separation column operating at lower pressure, c) flowsheet alternative 5 with heat integration between the RD and the low-pressure column (Reprinted with permission from [51]).

variables, 3009 constraints and 3903 nonlinear terms. This yields a solution with $11.94 MM/year (19.6% optimality gap) (Alternative 4). The resultant flowsheet is shown in Figure 4.28b. As expected, result improved compared to the two-column reactive distillation system, yet TOC is still higher than the flowsheet Alternative 1. However, we can further enhance the energy utilization and observe the benefits that can be accrued from heat integration. Accordingly, we investigate a possible integration between the condenser of the reactive distillation column and the second distillation column (Alternative 5). We solve this problem with BARON for 6 hours with minimizing the TOC as objective. Problem includes 1918 continuous variables, 3012 constraints and 3903 nonlinear terms. This yields a solution with $11.53 MM/year (16.9% optimality gap) The resultant flowsheet is shown in Figure 4.28c. This result is slightly better than the TOC of the flowsheet alternative 1. Hence, we investigate this flowsheet further with TAC minimization. While doing so, we also investigate several different block superstructure sizes and change the number of rows for the superstructure shown in Figure 4.28a between 8 and 16. The best solution is obtained with

a block superstructure size of 16 rows (Alternative 6). This flowsheet alternative is shown in Figure 4.29. The TAC of the optimized flowsheet is $12.26 MM/year which is slightly better than the Flowsheet Alternative 1. Yet, this flowsheet includes only 3 units instead of 5 as in flowsheet alternative 1.

Although cost savings from this final flowsheet featuring a heat-integrated reactive distillation system is not drastic, 40% reduction in the number equipment provides a novel intensification pathway. Note that, this alternative could not be identified with an equipment-based representation as is demonstrated in Section 4.7.1. and 4.7.2 even the problems could be solved to optimality. These higher level representations can be utilized to enhance the process performance for a given number of alternatives. However, identification of novel structures requires a lower level representation as is shown here. This also highlights the benefit of phenomena-based building block representation in systematic process intensification.

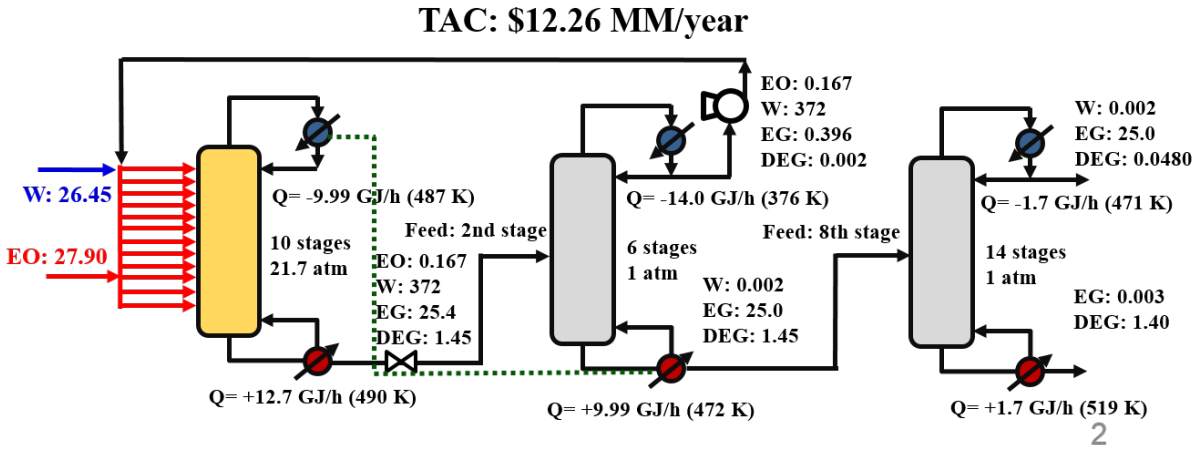

Figure 4.29: Flowsheet alternative 6 from phenomena-based process synthesis and intensification.

4.8 Sustainable Process Intensification with Multi-objective Optimization

In this problem, we again consider EG production and perform multi-objective optimization while accounting for both economic and environmental objectives and search for designs that are simultaneously more economic and environmentally sustainable. The aim of the process is to produce 25 kmol/h EG with 95% purity. Although EG production was investigated before [81, 112, 82, 186, 194, 195], there exists no rigorous optimization-based work focusing on the environmental impact of this process along with the process economics.

We will focus on the intensification of the non-catalytic homogeneous production route with the kinetics provided by Altıokka and Karayalçın (2009)[184]. We consider two different objectives. Economics is evaluated by return on investment (ROI) which includes operating costs, i.e. hot utility, cold utility and electricity costs, and capital investment costs. Price of EO and EG are taken as \$665/ton[196] and \$904.8/ton [197], respectively. Although there is no direct CO_2 emission from the process, three different sources of indirect emissions are identified and used in evaluating the environmental footprint of the process: CO_2 emissions from the steam production[198], 0.0967 kg CO_2/MJ for HP steam at 527 K, CO_2-eq emissions related with the electricity production[198], 0.1541 kg CO_2-eq/MJ, and CO_2-eq of the raw material use for EO[199], 163 kg CO_2-eq/kmol EO. CO_2-eq emissions from the production of EO includes emissions related to ethylene production. We implemented all the optimization models in General Algebraic Modeling Software (GAMS) and used Ada supercomputing cluster at Texas A&M University.

4.8.1 Base Case Designs

First, we investigate two base-case designs: a non-intensified reactor-separator-recycle system (F1) which includes a plug-flow reactor (PFR) followed by a distillation column (DC), and (ii) an intensified reactive separation system (F2) which includes a single reactive distillation column (RD). A single RD column for EG production has been investigated in the context of modeling, simulation and/or optimization of reactive separation processes [81, 112, 82, 195]. These works do not consider the non-intensified counterpart of this RD process although industrial production

of EG utilizes plug flow reactors [185]. Hence, to make a fair comparison between the intensified RD process and the proceeding results obtained by building block-based approach, this reactor-separator-recycle system is also considered.

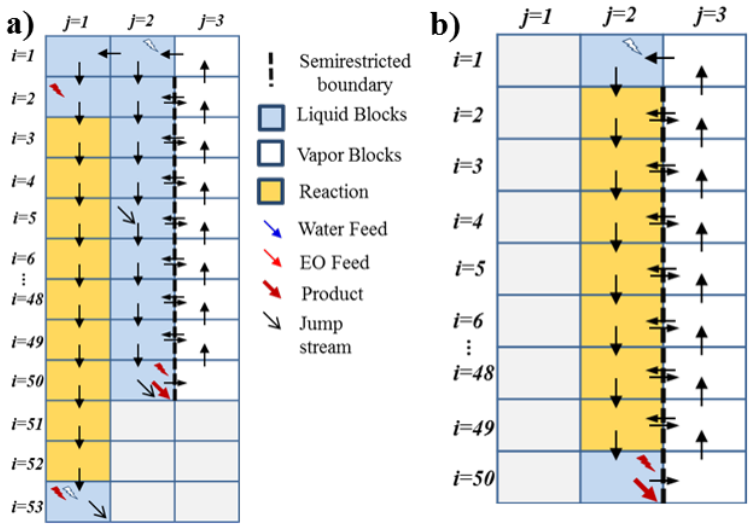

Figure 4.30: Building superstructure representation for the base case designs for sustainable process intensification. Building superstructure representation for a) reactor-separator-recycle system (F1), and b) intensified reactive distillation process (F2).

In optimizing the base-case flowsheets, block representations shown in Figure 4.30 are used. In Figure 4.30a, non-intensified flowsheet alternative is shown. The first column is used to represent the plug flow reactor. 50 building blocks (shown in yellow) in series is used to obtain a 50-CSTRs-in-series model. Here, block $B_{1,1}$ acts as a reactor inlet mixer and fresh feed and recycle streams from the separator are mixed here. Block $B_{2,1}$ is used as a reactor inlet heater or cooler. Similarly, block $B_{53,1}$ is used for reactor outlet heating/cooling. This block also serves a splitter block from which jump streams are used to transport the reactor outlet to the distillation region of the block superstructure. Distillation region is comprised of blocks between blocks $B_{1,2}$ to $B_{50,3}$. Here the blocks in the second column ($j = 2$) are in liquid phase and blocks in the third column ($j = 3$) are in vapor phase. Blocks $B_{1,2}$ and $B_{1,3}$ represents the phase change from vapor to liquid in the total

condenser. Similarly, blocks $B_{50,2}$ and $B_{50,3}$ are used to represent the partial reboiler. Boundaries between second and third columns except the one in the first row are designated as semi-restricted vapor-liquid phase contact boundaries to represent the phase equilibrium. The boundary in the first row is unrestricted as there is no composition change during the total condensation of the top vapor stream. Condensed vapor at $B_{1,2}$ can be either recycled to the reactor inlet mixer block $B_{1,1}$, sent to block $B_{2,2}$ as reflux stream and/or taken out as the distillate product. The bottom product from the distillation region is taken out from block $B_{50,2}$. Note that jump streams from reactor outlet block ($B_{53,1}$) can be connected to each of the liquid phase blocks within the distillation region. the flow rate of each of these jump streams are variables by which the feed location is determined. The number of active building block pairs within the distillation region is a decision variable which stands for the optimal number of stages. An upper bound of 50 is set for the number of building block pairs that can be used in separation including condenser and reboiler stages.

Building block representation for the intensified reactive distillation is shown in Figure 4.30b. Here, representation is similar to the non-intensified flowsheet representation except that reaction is allowed to occur in the liquid phase blocks within the distillation region. Also, external feed streams can enter into the process from any of the liquid blocks.

As the pressures of the equipment are among the optimization variables, phase of the several blocks need to be checked to fascilitate a physically realizable operation. For F1, this is done for the PFR inlet and outlet heater/cooler blocks. Also, to fascilitate liquid phase reaction, phase of the last block representing the PFR reactor is also ensured to stay in liquid phase. This is done only for the last block as the reaction is exothermic and the temperature of the reactor will always tend to increase and it will be the highest at this block where the likelihood of phase transition be the highest.

In optimizing base-case design alternatives, following assumptions are made. Temperature and pressure bounds of the process are taken as 326–524 K and 0.1–36 bar[186]. Ideal vapor-liquid phase equilibrium is assumed. Enthalpy and liquid densities are assumed to be a function of temperature. Cost of PFR is approximated as a HEX with 1-in diameter tubes. Maximum

volume of the PFR is 30 m^3. Both reactive and non-reactive tray efficiencies are taken as 1. Cost of realizing vacuum conditions is assumed to be negligible. A tray spacing of 0.61 m is assumed for all stages. Downcomer cross-sectional area is assumed to be 12% of the overall column cross-sectional area to prevent donwcomer flooding. F-value which is related to the flooding velocity within the column is assumed as 1.84 [57]. We assumed a maximum holdup of 3 m^3 on each reactive tray. Pressure drop through the V-L building block pairs and in PFR is neglected. External liquid feed streams are assumed to be available at the required process pressure. Capital cost functions of all units include the pressure correction factors according to the maximum pressure allowed within the process (i.e. 36 atm). No reaction is assumed to occur in the reboiler and condensers. Reactive tray heights are determined based on the diameter of the column, tray spacing and the additional holdup required for reaction. Maximum holdup is limited by the weir height which can be larger than the normal distillation columns. Weir heights of even 1 m is reported for reactive distillation systems [200]. We assumed a maximum weir height of 0.5 m. Height of the columns are restricted to 175 ft and a maximum of L/D (Height/Diameter) ratio of 30 is assumed to prevent very tall and skinny columns[56].

Capital investment costs include the PFR, column shell and tray, reboiler, condenser and recycle pump costs for flowsheet alternative F1 and reactive column shell and trays, reboiler and condenser costs for alternative F2. Capital cost functions, design formulations and utility costs are taken from literature [57, 187, 190, 191, 201]. Physical parameters used in the case study are taken from ASPEN Plus and provided in the Appendix B.

4.8.1.1 Single-objective Optimization Results

We optimize these base case designs with economic and environmental objectives separately. For flowsheet F1, optimization variables include reactor volume, pressure and cooling duty, heat duty and areas for the reactor inlet and outler heaters/coolers, number of stages, feed location and pressure of the distillation column, reboiler and condenser duty and areas and reflux and recycle ratios. For flowsheet F2, on top of the distillation column variables in F1, reactive volume at each stage is also considered as variable.

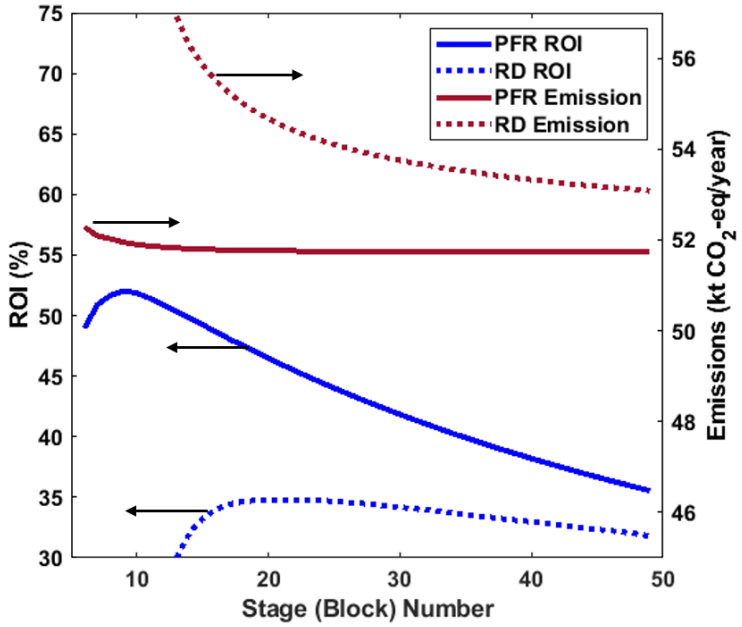

Figure 4.31: Effect of number of stages on the sustainability and economic objectives. Left axis designates ROI and right axis shows indirect CO_2 emission levels.Two red lines on top correspond to the optimization with emission objective and two blue lines at the bottom correspond to the optimization results with economic objective.

We solve these problems for increasing building block superstructure sizes as NLPs with BARON[146]. Results are shown in Figure 4.31. For F1, max ROI of 52%/year occurs when the number of stages for the distillation column is 9 (including reboiler and condenser). For F2, max ROI of 35%/year occurs with 21 stages. For CO_2-eq minimization results, as discussed in Section 3.6.5, we observe a monotonic decrease in emissions with the increase in number of blocks. As the reaction and separation operations are combined, the effect of number of stages is more dominant for the intensified flowsheet F2. F1 shows a rather flat profile after 12 stages. For both flowsheets we designate the flowsheet with the minimum emissions by observing the relative decrease in the emissions. We say the emissions are minimum when the relative change is less than or equal to 0.05%. This corresponds to a flowsheet with 12 stages for F1 and 46 stages for F2.

All the optimal designs are shown in Figure 4.32. Cost breakdowns are provided in Table 4.13 (See Appendix B for more details). Economically most favorable non-intensified flowsheet

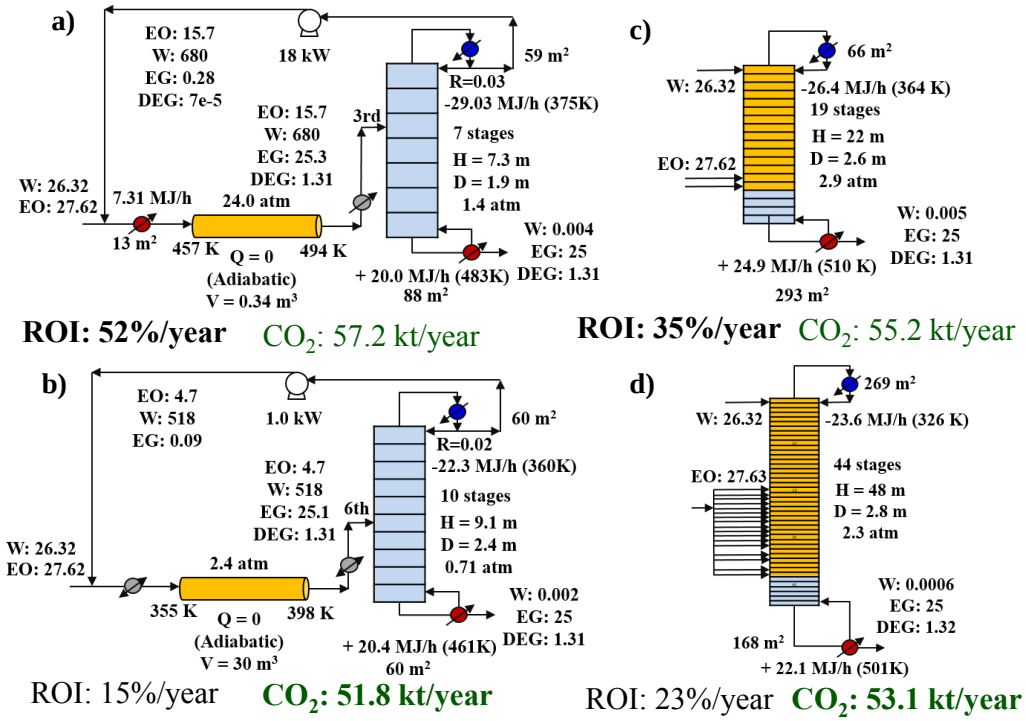

Figure 4.32: Cost optimal base case designs. Non-intensified flowsheet (F1) a) with maximum ROI, b) CO_2 minimization. Intensified flowsheet alternative (F2) with c) maximum ROI, and d) CO_2 minimization.

features an adiabatic PFR operating at high pressure with an inlet heater (Figure 4.32a). Reactor effluents contain high amount of water and EG/water separation is performed in the following distillation column. EG product is separated from the bottom and EO and water are recycled back to the PFR from the top. Column has a very low reflux ratio due to the large relative volatility difference between the products. Although waste withdrawal from the top is allowed, all of the top stream is recycled back to the PFR. Single pass EO conversion is 63.7% and W/EO ratio in the reactor inlet is high, i.e. 16.3. This facilitates a higher selectivity towards EG production by favoring the main reaction as is the case in the industrial production [185]. Although separation column is allowed to operate at vacuum conditions, this is not the case in the optimal result. There are several trade-offs between the recycle temperature and the column pressure. If the column were to operate at vacuum conditions, relative volatility differences could be increased and sepa-

ration would become easier. Yet, this would lower down the condenser temperature necessitating a larger condenser as well as a larger reactor inlet heater. Higher reactor temperatures are also more favorable to improve the reaction rate and reduce the PFR volume. These trade-offs prevent the column to operate at vacuum conditions. In overall, process has an ROI of %52/year and has 57.2 kt CO_2/year. Figure 4.32b shows the design with minimum CO_2 emissions. It features a very large PFR which increases the single-pass conversion of EO significantly (85.5%) and decreases the recycle rate. Accordingly, separation becomes easier and cheaper in terms of hot utility, i.e. fuel, consumption. Inlet W/EO ratio is similar to ROI maximization result with 16.8. Furthermore, as the capital cost is not included in the objective, trade-off between the distillation pressure and recycle cost is alleviated and distillation column operates below atmospheric pressure which also contributes to the decrease in hot utility consumption. Optimal result do not feature any reactor inlet heater although it is available in the superstructure and there is no temperature change between the condenser and reactor inlet. In overall, this process results in 51.8 kt CO_2/year with 9.4% reduction in emissions compared to the economically optimal design in the expense of much lower ROI, i.e. 15%/year.

The intensified counterpart of this process is comprised of only one equipment, yet it results in a lower ROI, i.e. 35%/year. RD features a total reflux column without any top product withdrawal (Figure 4.32c). This keeps the water concentration high throughout the reactive region. RD has no enriching section. This type of structure was also reported by others [81, 82]. Column operates at above atmospheric pressure at 2.9 atm. Operating at high pressure increases the temperature at the reactive stages and results in lower reactive holdup requirement. Yet, this makes the separation harder and increases the reboiler temperature and cost. Intensified design featuring minimum CO_2 also has a similar column structure with total reflux and without any enriching section (Figure 4.32d). It operates at a lower pressure than the ROI optimal design and it has 44 stages: 38 reactive and 6 stripping stages. With higher number of stages and no economics considerations, it utilizes a much higher reaction holdup than the most economic design: 110.9 vs 37.7 m^3. This allows to decrease the pressure and favors the separation with reduced steam consumption at the expense

Table 4.13: Cost breakdown for the base case designs.

Flowsheet	F1	F1	F2	F2
Objective	max ROI	min CO_2	max ROI	min CO_2
Stage	7	10	19	44
Rxn/PFR Volume (m^3)	0.3	30	37.7	110.9
Emissions				
Steam (kt CO_2/year)	21.14	15.81	19.24	17.13
EO (kt CO_2/year)	36.02	36.02	36.01	36.03
Electricity (kt CO_2/year)	0.08	0.004	-	-
Total (kt CO_2/year)	57.23	51.84	55.25	53.15
Economics				
Total Installed Capital ($1000)	1267	5400	2046	3347
Hot Utility ($1000/year)	2165	1620	1971	1755
Cold Utility ($1000/year)	75	58	69	62
Fresh EO ($1000/year)	6473	6474	6472	6474
Fresh W ($1000/year)	0.42	0.42	0.42	0.42
Electricity ($1000/year)	10	0.6	-	-
Op. Cost ($1000/year)	8724	8153	8512	8291
ROI (%/year)	52	14.7	34.8	22.9

of larger capital cost. In overall, this design results in 4% reduction is the indirect CO_2 emissions compared to the most economic intensified design.

An interesting observation is that although most economical intensified flowsheet F2 has a lower ROI, it results in nearly 2 kt/year less indirect CO_2 emissions than the most economical non-intensified design. This is facilitated by the lower hot utility requirement of the intensified process which is 9% less than the ROI optimal non-intensified design. As this reaction system is slightly exothermic, reaction heat is utilized in the combined reaction-separation process to supply heat for the latent heat of vaporization. This results in less hot utility requirement which, in turn, results in less indirect emissions. However, intensified system requires a much higher reaction holdup and this increases the column dimensions along with the capital investment. In overall, while intensification yields a more environmentally friendly cost optimal design, it results in a more expensive alternative. This shows that there is significant trade-off between economics and environmental objectives for intensification for the EG production. To investigate these trade-offs

further, we performed multi-objective optimization and obtained pareto fronts for both flowsheets.

4.8.1.2 Pareto-optimal Solutions

While performing multi-objective optimization, we use 19 different ε values. Pareto fronts are given in Figure 4.33a. x-axis shows the CO_2-eq emissions and y-axis shows ROI. Better designs are located towards upper left corner of the Pareto space. None of the points on pareto curve for the intensified flowsheet F2 yield more economic design than the F1 for the same emission levels. This also indicates that with the same ROI, we can indeed obtain a more environmental-friendly design without considering intensification. While the gradient gets steeper as we move towards lower emissions, this is more pronounced for the intensified design. A similar trend can be also observed in the capital investment costs as shown in Figure 4.33c. Also, there is a linear dependence between the operating costs and emission levels for both flowsheets (Figure 4.33b). As the raw material costs do not change significantly among different designs and electricity costs are negligibly small, the most distinctive operating cost component is the utility consumption. This also translates into emission levels. Figure 4.34 shows the change in several variables in F1 as a function of the emissions. We observe a sharp change in the operating variables around 53.2 kton/year CO_2 emission levels. This corresponds to 75% decrease in emissions with respect to the total range of emission levels for F1. The aforementioned trade-off between the reactor inlet temperature and distillation operating conditions reveals itself at this point. Up until this point, distillation pressure increases as the emission level decreases (Figure 4.34a). This also increases the condenser and recycle temperatures (Figure 4.34b). While increase in pressure results in higher hot utility requirement for the reboiler, overall hot utility consumption decreases (Figure 4.34c). Until 75% decrease, reduction in emissions is facilitated by the decrease in the hot utility requirement for the PFR inlet heater. However, further reduction in emission requires a decrease in the emissions from reboiler as well. To enable this, reactor volume starts to increase rapidly which also increases the conversion (Figure 4.34d-e). Increased conversion relieves the burden on separation by decreasing the amount of PFR product that needs to be separated. This also enables the PFR to operate at lower temperatures. Hence, PFR inlet heater can be eliminated. However,

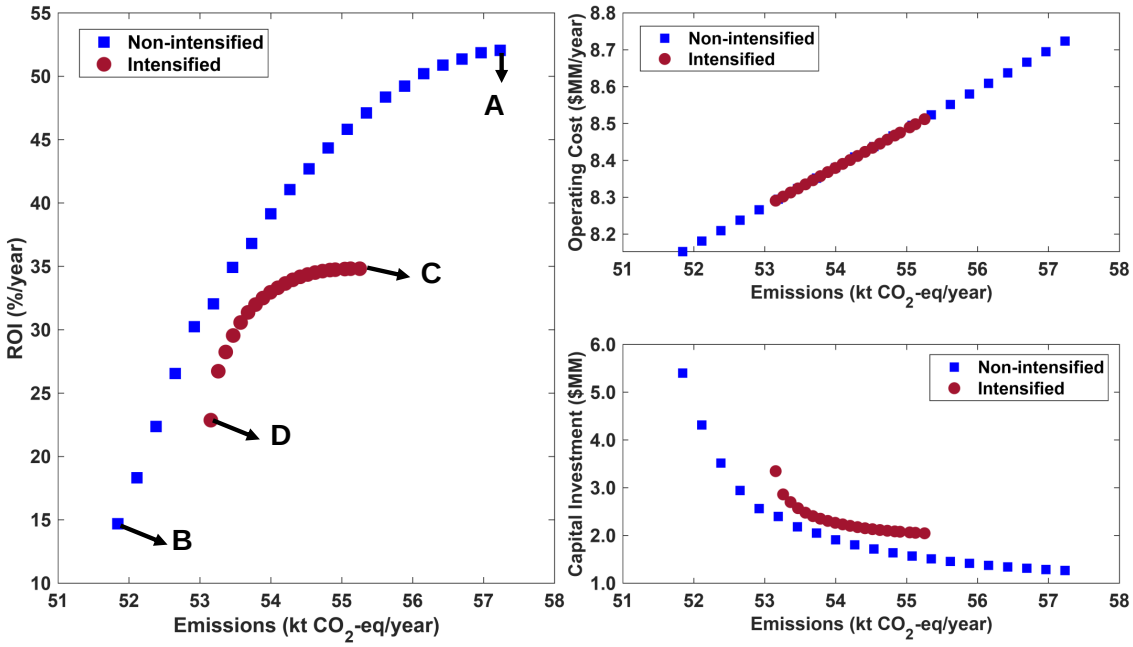

Figure 4.33: Pareto fronts base case designs. a) Pareto fronts for the objectives. Points A (Figure 4.32a) and B (Figure 4.32b) corresponds to the emission and cost optimal designs for flowsheet F1, respectively, points C (Figure 4.32c) and D (Figure 4.32d) correspond to the emission and cost optimal designs for the intensified flowsheet F2. b) operating costs, and e) capital investment for the pareto points.

these changes in the flowsheet structure results in much higher capital cost requirements. Capital cost contribution from the reaction task (PFR and inlet heater) starts to exceed the cost required for the separation task (Separation column with condensers and reboilers) (Figure 4.34f).

For the intensified design F2, there is also an inflection point where there is a stark change in the operating conditions. While column operates at nearly same pressure levels in the higher emission levels, it starts to decrease when the emissions fall below 53.7 kton/year CO_2 (Figure 4.35a). This also corresponds to 75% decrease in emissions with respect to the total range of emission levels. We also observe a change in the slope of increase in reaction volume after this point (Figure 4.35b). Boilup ratio of the RD also starts to decrease with a higher rate (Figure 4.35c). This decrease in column pressure results in lower temperatures along the reactive region and column as a whole (Figure 4.35e). Liquid molar holdup increases sharply to compensate

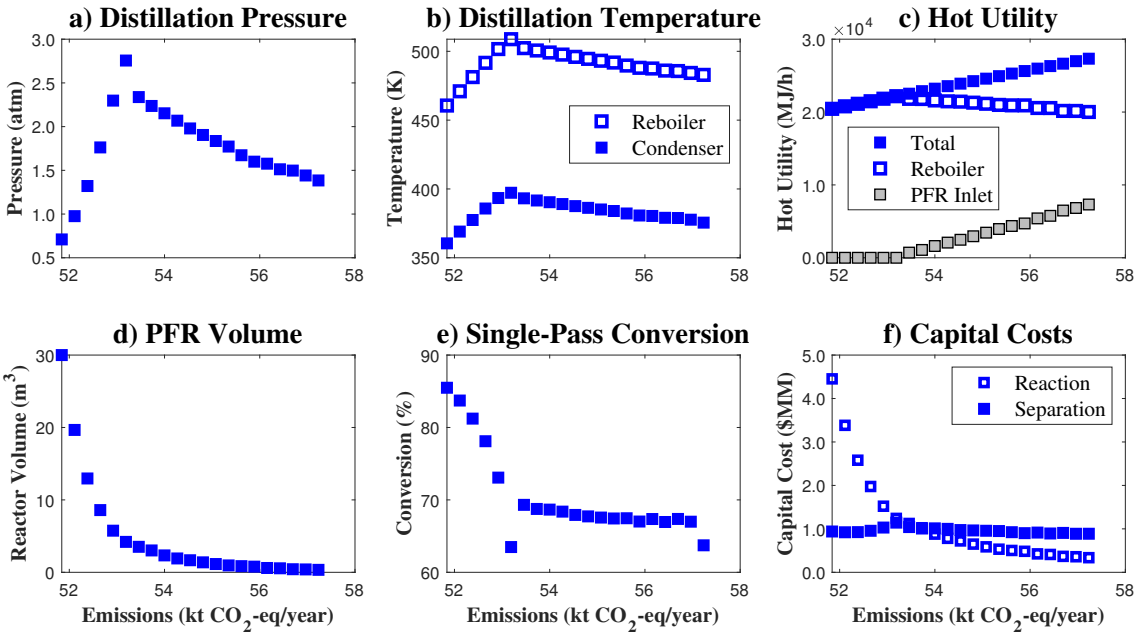

Figure 4.34: Analysis of the pareto results for the reactor-separator-recycle system.

for the decreasing temperatures along the reactive region. We also observe the effect of these changes on the capital cost. Column cost (summation of tray and shell costs) starts to increase sharply after this point while reboiler cost decreases due to the decreased pressure. This is similar in nature to the flowsheet F1 in which going towards lower emissions requires to increase the reactor cost for decreasing the separation cost. Yet, unlike the non-intensified case, RD cannot manipulate the conditions to that extent to increase the relative volatility and ease the separation as they are coupled in the intensified design. From this analysis, it is evident that both non-intensified and intensified designs feature a trade-off between separation and reaction operations in terms of economics and environmental impact. Now, we will search for better designs through the building block-based design methodology with the tools introduced in Section 3.6.4.

4.8.2 Building Block-based Generation of Sustainable Solutions

In generating new solutions, we use the ROI optimal intensified design as the building block superstructure size, i.e. 21×2 and use the solution strategy given in Section 3.6.4. We first perform

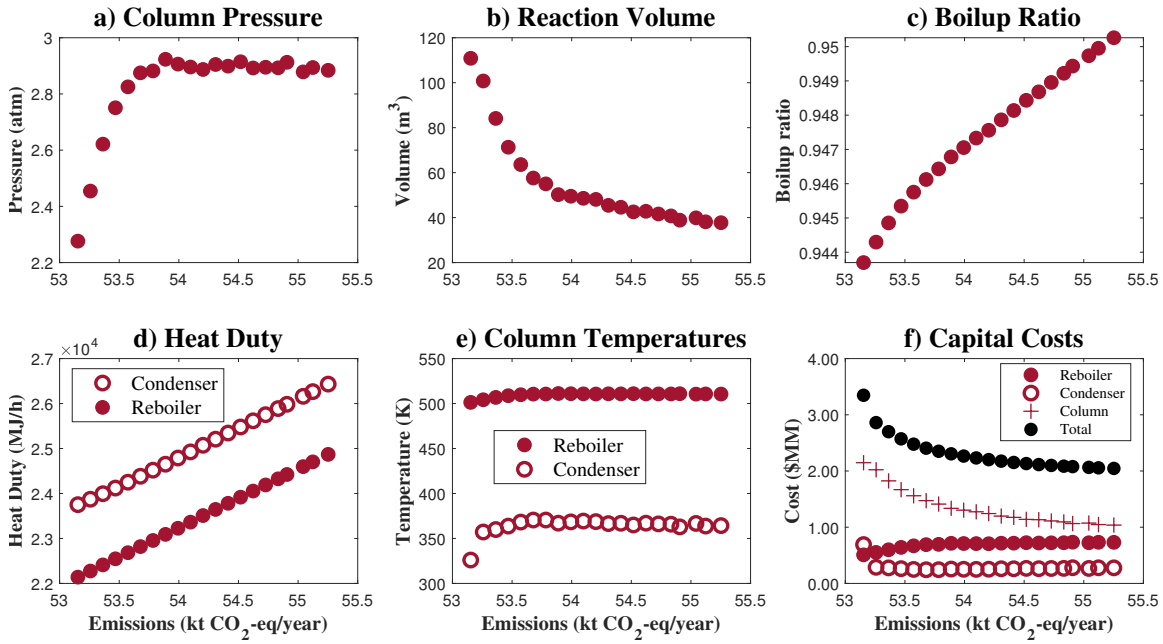

Figure 4.35: Analysis of the pareto results for the intensified system.

the search with economic objective and give two solutions obtained with different solution times in Figure 4.36. Figure 4.36a features a block superstructure result in which all the building blocks are active and none of the jump connectivities are utilized. At row 15 ($i = 15$), we observe a second hot utility stream in addition to the reboiler positioned at row 21. This second hot utility stream indicates an intermediate reboiler and the equivalent flowsheet is shown in Figure 4.36a (Flowsheet F3). A comparison with the ROI optimal design (F2 in Figure 4.32c) shows that the introduction of intermediate reboiler provides significant improvement in ROI.

Temperature and liquid flow rate profiles of the original ROI optimal flowsheet F2 and this new design are provided in Figure 4.37. Liquid flow rate profiles indicate that the reboiler at the bottom of F3 operates with a much lower liquid flow rate. As the temperature driving force at the bottom is the lowest, operating the bottom reboiler at a lower capacity reduces the cost of the reboiler and enables an increase in the column pressure, from 2.9 atm in F2 to to 3.7 atm in F3. This facilitates a higher temperature at the reactive stages. At each point of the column, F3 has a higher temperature than F2. This increase in temperature enhances the reaction rates and decrease

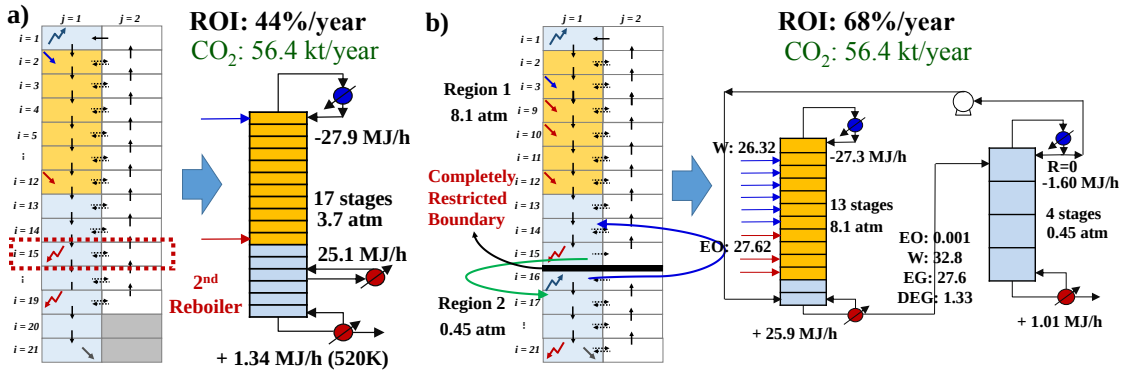

Figure 4.36: Search for new designs with economic objective. a) Building block result with economic objective featuring an intermediate reboiler and its equivalent flowsheet representation. b) The best building block result with economic objective suggesting two separate regions of V-L regions operating at different pressures and its equivalent flowsheet representation.

the required molar holdup for reaction which also translates into a reduction in column capital cost. All these factors contribute to an increase in ROI from 35%/year to 44%/year. It should be noted that although using an intermediate reboiler could be automatically identified by the building block-based approach, it is also reported in the literature as a viable alternative for EG production with reactive distillation[202].

Second solution generated by building block superstructure with the economic objective (Figure 4.36b) provides a much higher ROI with 68%/year and suggests a partially intensified structure. This is even higher than the most economic base case design F1. In this flowsheet we observe that completely restricted boundary below the row 15 ($i = 15$) is activated restricting the flow between the blocks above and blocks below. While blocks above this boundary are operated at a much higher pressure, i.e. at 8.1 atm, the blocks below are operated at vacuum conditions at 0.45 atm. This difference in pressure indicates two separate equipment operating at different conditions. While the higher pressure region contains reactive V-L phase contact blocks, lower pressure region is comprised of blocks with non-reactive V-L phase contact blocks only. There are two cooling (at the first and 16th rows) and heating blocks (at the rows 15 and 21) and two jump streams connecting high and low pressure regions of the superstructure. This block result is translated into an

equivalent flowsheet representation as shown in Figure 4.36d (Flowsheet Alternative F4). Here, two separate regions of different pressures are translated as separate distillation columns. While the higher pressure column performs the reaction and provides a bottom stream with 45% EG purity, second column performs the separation between EG and water. Water separated from the second column is fed back to the first column. The advantage of this structure can be observed by the liquid flow rate and temperature profiles (Figure 4.37). While the region above row 15 (Region 1 in Figure 4.37) operates at higher temperatures than the both F2 and F3, blocks below this row (Region 2 in Figure 4.37) operates at lower temperatures. Similar to F3, operating the reactive region at higher pressure improves the reaction rate and decreases the column size. Operating the separation region at lower temperature on the other hand, helps to increase the relative volatility difference and making the separation easier. These result in much favorable economics. Furthermore, this two-column process also enables the consideration of heat integration between the high and low pressure columns between the condenser of RD and reboiler of the DC (Flowsheet F5). This improved flowsheet F4 and its heat-integrated version was also investigated in the previous section [51]. Here, the proposed methodology in Section 3.6.4 allows us to identify this structure automatically.

These new designs addresses the trade-offs identified for the base-case designs where the reaction and separation tasks featured significant difference between their optimal conditions. However, both flowsheets F3 and F4 result in higher emissions than the intensified F2 while providing less emissions than the most economic design F1. As discussed in Section 3.6.5, number of building blocks is a factor to consider here to realize the full potential of these designs. Hence, these new flowsheets F3, F4 and F5 are all optimized with both economic and environmental objectives by considering larger block superstructure sizes. Cost breakdown of these results are given in Table 4.14 and optimal designs are shown in Figure 4.38 (See Appendix B for more details).

ROI optimal intensified column with intermediate reboilers is shown in Figure 4.38a. Note that emission minimization for this flowsheet features no intermediate reboilers and result in the same optimal design with the reactive distillation process. Hence, this process is not shown. Here, the

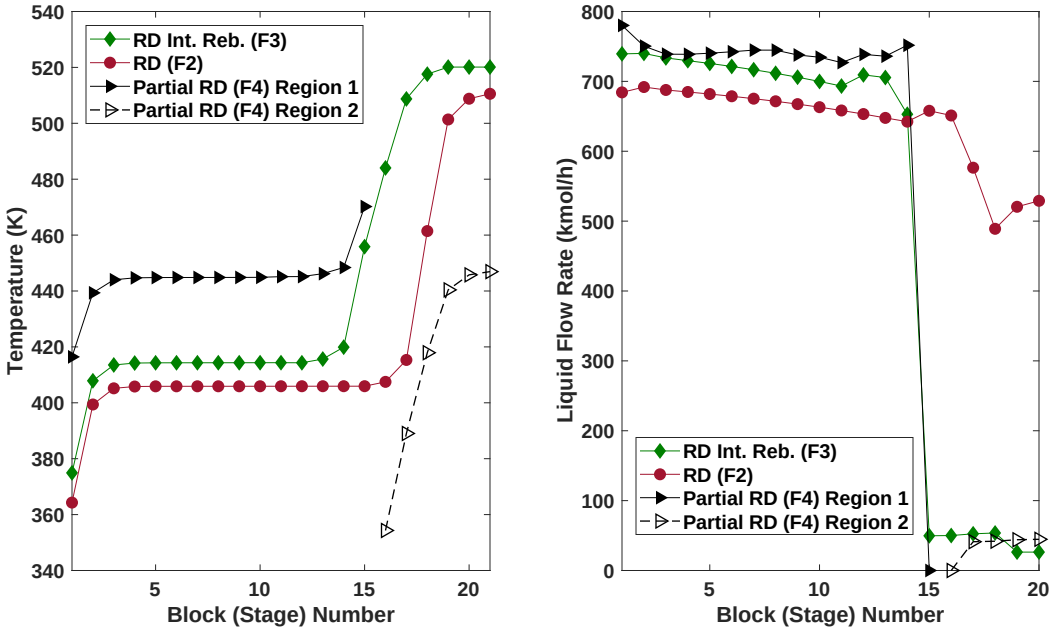

Figure 4.37: Block temperature and liquid flow rates for the generated results. Block temperature (left) and liquid flow rate (right) profiles. x-axis indicates the position of the blocks starting from the top.

optimal design features an RD column with 23 stages of which 16 are reactive. Economics are significantly improved when compared to single RD (F2). ROI of this new design is 47%/year. It includes not one but two intermediate reboilers positioned along the stripping section. These help into decrease the reboiler duty at the bottom and also allows to increase the column pressure significantly, i.e. 4.1 atm vs 2.9 atm. This results in nearly 50% reduction in the reaction volume. In overall, this flowsheet structure enables 29% decrease in capital costs compared to F2. However, its utility consumption is slightly higher than F2 and this results in 1.5% higher emissions. Still, this design results in less emissions than the ROI optimal non-intensified flowsheet F1.

Optimal designs for the partially intensified flowsheets F4 and F5 are shown in Figure 4.38b-e. These new designs result in improvement in both economics and environmental impact. Most economical designs for both F4 and its heat-integrated counterpart F5 enable significant improvement in economics with 75%/year and 82% ROI/year, respectively (Figure 4.38 b and d). These designs

Table 4.14: Cost breakdown for the generated designs.

Flowsheet	F3	F4	F4	F5	F5
Objective	max ROI	max ROI	min CO_2	max ROI	min CO_2
Stage RD	25	18	30	23	30
Stage DC	-	6	12	7	12
Reaction Volume (m^3)	19.8	0.9	27.3	2.0	84.0
Emissions					
Steam (kt CO_2/year)	20.13	17.47	14.99	10.20	8.46
EO (kt CO_2/year)	35.95	35.98	36.03	35.99	36.03
Electricity (kt CO_2/year)	0	0.03	0.07	0.03	0.01
Total (kt CO_2/year)	56.09	53.47	51.08	46.22	44.50
Economics					
Total Ins. Capital ($1000)	1459	1027	2823	1183	4478
Hot Utility ($1000/year)	2063	1789	1536	1045	867
Cold Utility ($1000/year)	71	63	56	39	34
Fresh EO ($1000/year)	6461	6465	6475	6467	6475
Fresh W ($1000/year)	0.42	0.42	0.42	0.67	0.42
Electricity ($1000/year)	-	4.0	8.3	3.5	0.7
Operating Cost ($1000/year)	8595	8322	8074	7556	7377
ROI (%/year)	47.5	74.7	29.2	81.9	22.4

also perform much better in terms of environmental impact. Compared to the ROI optimal non-intensified flowsheet F1, F4 and F5 result in 6.5% and 19.2% less indirect emissions, respectively. Although there is also a slight decrease in the emissions from the raw material EO consumption, a major portion of this decrease is due to hot utility consumption. F4 results in 17.4% and F5 results in 51.7 % decrease in hot utility consumption and related emissions from the process compared to F1. Designs featuring minimum CO_2 (Figure 4.38c and 4.38e) also have much less emissions than the both base-case designs with minimum CO_2 emissions.

Both cost and emission optimal designs of flowsheet F4 (Figure 4.38b and 4.38c) have a reactive distillation column operating at high pressure with all stages being reactive stages. The outlet from this reactive distillation column has nearly 95% water which indicates that it is solely used for reaction task. Purification of the EG from this stream takes place in the separation column operating at vacuum conditions. The optimal feed locations to this column are from the first stage below the condenser. This also shows that these separation columns act as stripping columns. An inter-

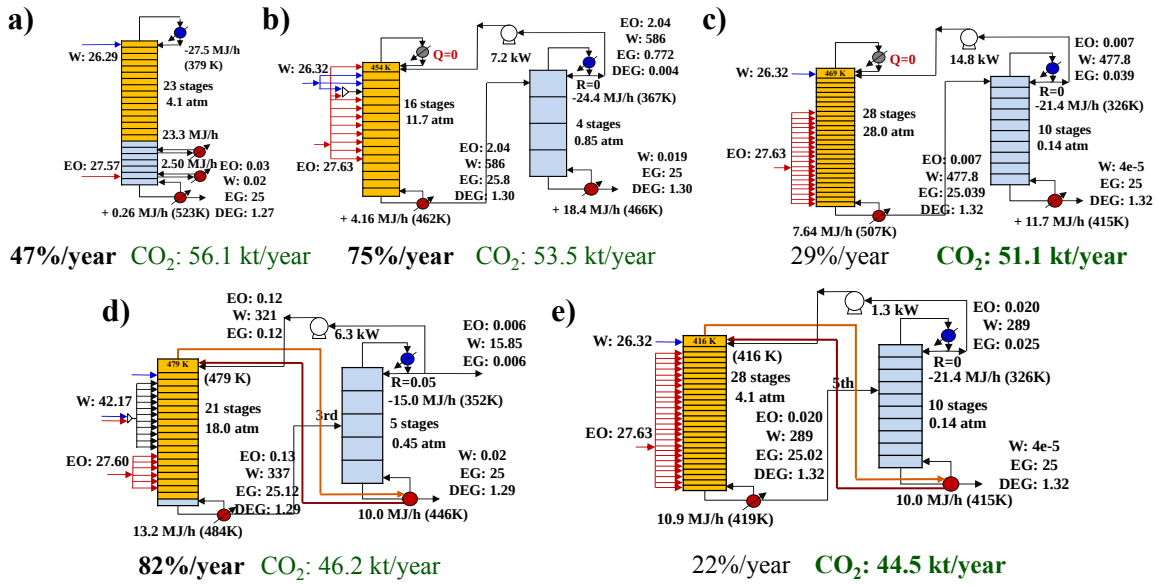

Figure 4.38: Optimal designs generated through building block superstructure. a) ROI optimal intensified RD design with two intermediate reboilers (F3), b) ROI optimal partially intensified design with two columns (F4), c) and its minimum emission counterpart, d) ROI optimal partially intensified design with heat integration (F5), e) and its minimum emission counterpart.

esting feature to note is that number of reactive and stripping stages of the intensified design F2 and the number of stages for the reactive distillation and stripping columns in F4 are nearly the same while the latter is divided into two separate columns. Also, reactive distillation columns in F4 do not include any condenser. Cooling and total reflux is facilitated by the fresh feed and the recycle stream from the second distillation column. As the second distillation column operates at vacuum conditions, its condenser temperature is low and it could be utilized as the coolant. This also provides a novel heat integration strategy. Furthermore, operating the reactive distillation columns at high pressure increases the temperatures along the reactive stages enhancing the reaction rates. This results in drastic decrease in the total reaction volume from 37.3 m^3 in ROI optimal RD (F2) to 0.9 m^3 in the ROI optimal partially intensified process F4. This also decreases the capital costs for this new process and enables much favorable economics. Heat integrated partially intensified process (F5) shown in Figures 4.38d and 4.38e also share the same characteristics with F4. Yet, to enable heat integration between the reactive and stripping columns, reactive column operates

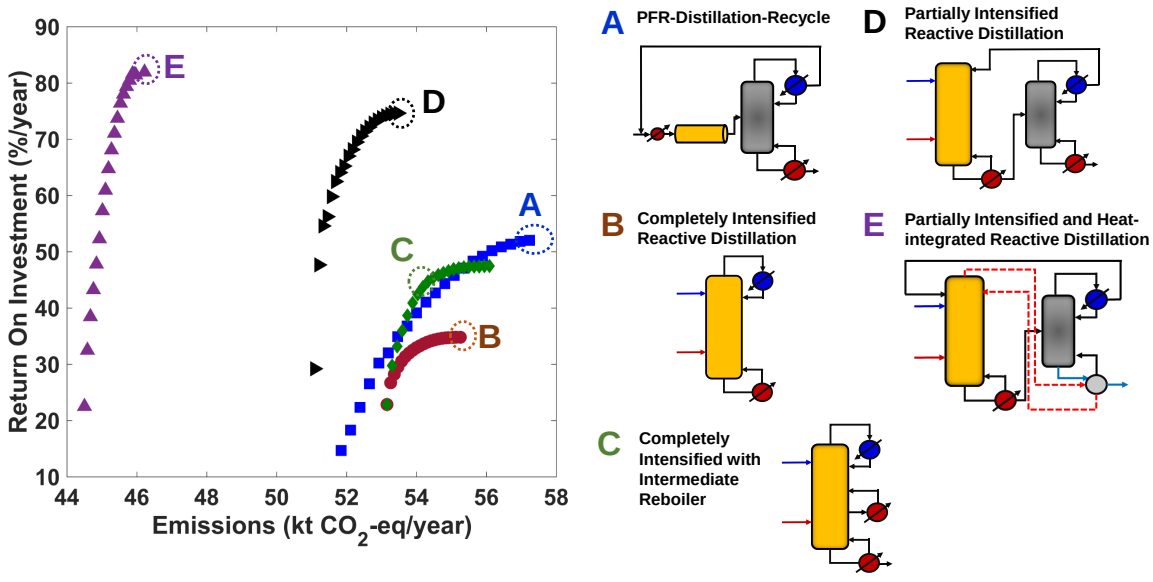

Figure 4.39: Pareto front for the new designs.

at a higher pressure than F4 and stripping column operates at a lower pressure. This increases the driving force for the heat transfer and decreases the cost for the heat exchanger between the condenser and reboiler.

To observe the effect of these designs on the pareto space, we performed multiobjective optimization on these new flowsheets (Figure 4.39). Here, the improvement in the environmental and economic objectives can be seen more clearly. Pareto curves for the RD with intermediate reboilers and non-intensified flowsheet intersect each other and intensified design performs much better within a certain range of emissions. Although it does not directly benefit in terms of environmental impact, adding intermediate reboilers make the single RD design much economical and competitive for the same level of emission levels. All points on the pareto front for F4 and F5 demonstrate superior performance than the others. With these, previously unattainable regions becomes feasible. For the same level of ROI, these new designs give the opportunity to adopt a much more environmentally benign process. This is made possible by utilizing the benefits from intensification by combing reaction and separation while at the same time eliminating the trade-offs between the two operations. Building block-based design approach provides a generic methodology where

these trade-offs can be identified and both more economical and environmental processes can be generated.

5. CONCLUSIONS

5.1 Major Contributions

This work introduced an optimization-based process design method for systematic process intensification based on building block superstructure representation. While traditional process synthesis methods operate with unit operation-based representations, building block-based representation provides a bottom-up approach towards process synthesis by emulating phenomena and tasks based on basic block design elements, building block interior and boundaries, providing a generic representation method for chemical processes. There are several major contributions of this work as listed below:

(i) A novel representation based on building blocks that allows for a bottom-up representation for chemical processes,

(ii) A novel representation for representing different phenomena, tasks and unit operations typically encountered in chemical process industry,

(iii) A novel representation providing a unified approach for process synthesis, integration and intensification using a single superstructure,

(iv) A generic MINLP-type optimization problem formulation describing the building block superstructure,

(v) An optimization-based method that allows for the identification and incorporation of intensification alternatives in process design,

(vi) An optimization-based unified method that allows for simultaneous process synthesis, integration and intensification,

(vii) An optimization-based method for automated generation of process flowsheets that can identify both traditional and intensified equipment types, and

(viii) Novel solution strategies addressing the solution of building block-based superstructure.

Hence, developed representation and optimization methodology opens up many opportunities for further research in systematic design and intensification of chemical processes.

5.2 Future Directions

The current work introduced the basic principles and capabilities of the building block superstructure representation. The full potential is yet to be explored. Further improvement can be performed within the representation and mathematical formulation to capture more process applications. For instance, applications related with pharmaceutical production or biomass processing [203] might require to incorporate new modeling elements related with solid processing.

Several solution strategies are proposed for improving the solution quality. Still, global optimality cannot be reached by the state-of-the-art global MINLP solvers. One major reason is the symmetric nature of the proposed representation and the optimization model. Furthermore, addressing the non-convexity of the model while utilizing the special structure of the proposed model can open up many more opportunities for systematic process intensification. As the method is generic in nature, if a solution algorithm can be developed for the proposed model, it can serve as a global optimization algorithm for the synthesis of a wide-range of chemical processes.

The proposed generic representation and optimization methodology makes it amenable for software applications. Incorporation of the building block superstructure in a computer-aided platform for process synthesis-intensification might result in a first-of-its-kind superstructure-based process synthesis software with automated flowsheet generation capabilities. This can also be beneficial for the chemical engineering education. Curricula of the design courses can adopt building block-based approach as a tool for introducing new unit operations, identifying un-intuitive process solutions and advancing the knowledge in process intensification. This would help exploring new design paradigms, breaking the dependency on traditional unit operation-based focus of the design courses, and fostering creativity of the chemical engineering workforce.

Van Gerzen and Stankiewicz (2009) [11] states that the PI operates at four major domains

within varying length scales: (i) spatial, (ii) thermodynamic, (iii) functional, and (iv) temporal domains. The proposed representation is generic and can capture all these domains at varying length scales. However, the current form of the optimization model addresses the identification of PI opportunities at the thermodynamic and functional domains. Further work is needed to incorporate time within the proposed mathematical formulation to capture cyclic/dynamic intensification opportunities. This requires the introduction of a new dimension within the model which would increase the model size and complexity. Surrogate modeling aided with machine learning algorithms and orthogonal collocation techniques can be explored as a remedy. Similarly, in order to capture the PI opportunities at the spatial domain, more detailed consideration of the interphase phenomena, momentum balances and energy transfer mechanisms are needed. This can enable the automated identification of micro/macro structures and alternative energy resources.

Another research domain that can be pursued is related with the dynamic behavior of the resultant designs. Controllability and flexibility of the generated designs need to be checked for physical implementation. Similarly, safety aspects can be incorporated within the multi-objective optimization framework.

A major hurdle for the advancement of PI solutions that are suggested through phenomena-based frameworks is related with the economics. There are no well-established cost functions for most of the intensified equipment. Also, it is not possible to know the resultant structures beforehand and consideration of economic objectives requires rough assumptions on the cost correlations. New approaches are needed for estimating the economics of the resulting structures. This can be achieved through considering the "building blocks" for the cost of the chemical equipment based on physical states, such as temperature, pressure, density and dimensions, e.g. molar holdup, while simultaneously capturing the economies of scale and the effect of modularity on the economics.

REFERENCES

[1] Office of Energy Efficiency and Renewable Energy, "Chemicals Industry Profile", https://www.energy.gov/eere/amo/chemicals-industry-profile, accessed on May 12, 2020.

[2] A. F. Pales, P. Levi, and T. Vass, "Tracking industry," tech. rep., International Energy Agency, Paris, 2019.

[3] F. You, L. Tao, D. J. Graziano, and S. W. Snyder, "Optimal design of sustainable cellulosic biofuel supply chains: multiobjective optimization coupled with life cycle assessment and input–output analysis," *AIChE Journal*, vol. 58, no. 4, pp. 1157–1180, 2012.

[4] B. Wang, B. H. Gebreslassie, and F. You, "Sustainable design and synthesis of hydrocarbon biorefinery via gasification pathway: Integrated life cycle assessment and technoeconomic analysis with multiobjective superstructure optimization," *Computers & Chemical Engineering*, vol. 52, pp. 55–76, 2013.

[5] M. M. El-Halwagi, "A return on investment metric for incorporating sustainability in process integration and improvement projects," *Clean Technologies and Environmental Policy*, vol. 19, no. 2, pp. 611–617, 2017.

[6] K. Guillen-Cuevas, A. P. Ortiz-Espinoza, E. Ozinan, A. Jimenez-Gutierrez, N. K. Kazantzis, and M. M. El-Halwagi, "Incorporation of safety and sustainability in conceptual design via a return on investment metric," *ACS Sustainable Chemistry & Engineering*, vol. 6, no. 1, pp. 1411–1416, 2018.

[7] C. D. Demirhan, W. W. Tso, J. B. Powell, and E. N. Pistikopoulos, "Sustainable ammonia production through process synthesis and global optimization," *AIChE Journal*, vol. 65, no. 7, p. e16498, 2019.

[8] S. E. Demirel, J. Li, and M. M. F. Hasan, "Sustainable process intensification using building blocks," *Computer Aided Chemical Engineering*, vol. 47, pp. 157–162, 2019.

[9] A. I. Stankiewicz and J. A. Moulijn, "Process intensification: transforming chemical engineering," *Chemical Engineering Progress*, vol. 96, no. 1, pp. 22–34, 2000.

[10] J. A. Moulijn, A. Stankiewicz, J. Grievink, and A. Górak, "Process intensification and process systems engineering: a friendly symbiosis," *Computers & Chemical Engineering*, vol. 32, no. 1-2, pp. 3–11, 2008.

[11] T. Van Gerven and A. Stankiewicz, "Structure, energy, synergy, time: The fundamentals of process intensification," *Industrial & Engineering Chemistry Research*, vol. 48, no. 5, pp. 2465–2474, 2009.

[12] S. E. Demirel, J. Li, and M. M. F. Hasan, "Systematic process intensification," *Current Opinion in Chemical Engineering*, vol. 22, pp. 108–113, 2019.

[13] Y. Tian, S. E. Demirel, M. M. F. Hasan, and E. N. Pistikopoulos, "An overview of process systems engineering approaches for process intensification: State of the art," *Chemical Engineering and Processing: Process Intensification*, vol. 133, pp. 160 – 210, 2018.

[14] A. Stankiewicz, "The principles and domains of process intensification," *Chemical Engineering Progress*, vol. 116, pp. 23–28, 2020.

[15] C. Ramshaw, "'higee' distillation-an example of process intensification," *The Chemical Engineer*, vol. 389, pp. 13–14, 1983.

[16] D. Reay, C. Ramshaw, and A. Harvey, *Process Intensification: Engineering for efficiency, sustainability and flexibility*. Butterworth-Heinemann, 2013.

[17] S. Becht, R. Franke, A. Geißelmann, and H. Hahn, "An industrial view of process intensification," *Chemical Engineering and Processing: Process Intensification*, vol. 48, no. 1, pp. 329–332, 2009.

[18] J. M. Ponce-Ortega, M. M. Al-Thubaiti, and M. M. El-Halwagi, "Process intensification: new understanding and systematic approach," *Chemical Engineering and Processing: Process Intensification*, vol. 53, pp. 63–75, 2012.

[19] P. Lutze, R. Gani, and J. M. Woodley, "Process intensification: a perspective on process synthesis," *Chemical Engineering and Processing: Process Intensification*, vol. 49, no. 6, pp. 547–558, 2010.

[20] S.-W. Choi, C. W. Jones, S. Nair, D. S. Sholl, J. S. Moore, Y. Liu, R. S. Dixit, and J. G. Pendergast, "Material properties and operating configurations of membrane reactors for propane dehydrogenation," *AIChE Journal*, vol. 61, no. 3, pp. 922–935, 2015.

[21] A. Arora, S. S. Iyer, I. Bajaj, and M. M. F. Hasan, "Optimal methanol production via sorption-enhanced reaction process," *Industrial & Engineering Chemistry Research*, vol. 57, no. 42, pp. 14143–14161, 2018.

[22] J. Siirola, "Synthesis of equipment with integrated functionality," in *Proc. Intensif.: Profits for the Chem. Ind., Rotterdam, Netherlands Agency for Energy and the Env., Sittard, The Netherlands*, May 1998.

[23] M. F. Malone and M. F. Doherty, "Reactive distillation," *Industrial & Engineering Chemistry Research*, vol. 39, no. 11, pp. 3953–3957, 2000.

[24] M. C. Georgiadis, M. Schenk, E. N. Pistikopoulos, and R. Gani, "The interactions of design control and operability in reactive distillation systems," *Computers & Chemical Engineering*, vol. 26, no. 4-5, pp. 735–746, 2002.

[25] G. J. Harmsen, "Reactive distillation: the front-runner of industrial process intensification: a full review of commercial applications, research, scale-up, design and operation," *Chemical Engineering and Processing: Process Intensification*, vol. 46, no. 9, pp. 774–780, 2007.

[26] I. Dejanović, L. Matijašević, and Ž. Olujić, "Dividing wall column - a breakthrough towards sustainable distilling," *Chemical Engineering and Processing: Process Intensification*, vol. 49, no. 6, pp. 559–580, 2010.

[27] N. Asprion and G. Kaibel, "Dividing wall columns: fundamentals and recent advances," *Chemical Engineering and Processing: Process Intensification*, vol. 49, no. 2, pp. 139–146, 2010.

[28] J. A. Caballero and I. E. Grossmann, "Optimal synthesis of thermally coupled distillation sequences using a novel MILP approach," *Computers & Chemical Engineering*, vol. 61, pp. 118–135, 2014.

[29] R. C. Pattison, A. M. Gupta, and M. Baldea, "Equation-oriented optimization of process flowsheets with dividing-wall columns," *AIChE Journal*, vol. 62, no. 3, pp. 704–716, 2016.

[30] J. Holtbrügge, A. K. Kunze, A. Niesbach, P. Schmidt, R. Schulz, D. Sudhoff, and M. Skiborowski, *Reactive and membrane-assisted separations*. Walter de Gruyter GmbH & Co KG, 2016.

[31] Y. Chen, E. Koumaditi, R. Gani, G. M. Kontogeorgis, and J. M. Woodley, "Computer-aided design of ionic liquids for hybrid process schemes," *Computers & Chemical Engineering*, vol. 130, p. 106556, 2019.

[32] S. S. Iyer, S. E. Demirel, and M. M. F. Hasan, "Combined natural gas separation and storage based on in silico material screening and process optimization," *Industrial & Engineering Chemistry Research*, vol. 57, no. 49, pp. 16727–16750, 2018.

[33] M. M. F. Hasan, E. L. First, and C. A. Floudas, "Discovery of novel zeolites and multi-zeolite processes for p-xylene separation using simulated moving bed (smb) chromatography," *Chemical Engineering Science*, vol. 159, pp. 3–17, 2017.

[34] R. C. Pattison and M. Baldea, "A thermal-flywheel approach to distributed temperature control in microchannel reactors," *AIChE journal*, vol. 59, no. 6, pp. 2051–2061, 2013.

[35] S. Bac, S. Keskin, and A. K. Avci, "Modeling and simulation of water-gas shift in a heat exchange integrated microchannel converter," *International Journal of Hydrogen Energy*, vol. 43, no. 2, pp. 1094–1104, 2018.

[36] Z. Qian, Q. Chen, and I. E. Grossmann, "Optimal synthesis of rotating packed bed reactor," *Computers & Chemical Engineering*, vol. 105, pp. 152–160, 2017.

[37] M. Baldea and T. F. Edgar, "Dynamic process intensification," *Current Opinion in Chemical Engineering*, vol. 22, pp. 48–53, 2018.

[38] L. Yan, T. F. Edgar, and M. Baldea, "Dynamic process intensification of binary distillation via periodic operation," *Industrial & Engineering Chemistry Research*, vol. 58, no. 15, pp. 5830–5837, 2018.

[39] V. H. Agreda, L. Partin, and W. Heise, "High-purity methyl acetate via reactive distillation," *Chemical Engineering Progress*, pp. 40–46, 1990.

[40] V. H. Agreda and L. R. Partin, "Reactive distillation process for the production of methyl acetate," Mar. 6 1984. US Patent 4,435,595.

[41] J. J. Siirola, "Industrial applications of chemical process synthesis," in *Advances in chemical engineering*, vol. 23, pp. 1–62, Elsevier, 1996.

[42] G. Harmsen, "Industrial best practices of conceptual process design," *Chemical Engineering and Processing: Process Intensification*, vol. 43, no. 5, pp. 671–675, 2004.

[43] G. Parkinson, "Dividing-wall columns find greater appeal," *Chemical Engineering Progress*, vol. 103, no. 5, pp. 8–11, 2007.

[44] Ö. Yildirim, A. A. Kiss, and E. Y. Kenig, "Dividing wall columns in chemical process industry: a review on current activities," *Separation and Purification Technology*, vol. 80, no. 3, pp. 403–417, 2011.

[45] R. Thakur, C. Vial, K. Nigam, E. Nauman, and G. Djelveh, "Static mixers in the process industries - a review," *Chemical Engineering Research and Design*, vol. 81, no. 7, pp. 787–826, 2003.

[46] J. Harmsen, "Process intensification in the petrochemicals industry: drivers and hurdles for commercial implementation," *Chemical Engineering and Processing: Process Intensification*, vol. 49, no. 1, pp. 70–73, 2010.

[47] J. B. Powell, "Application of multiphase reaction engineering and process intensification to the challenges of sustainable future energy and chemicals," *Chemical Engineering Science*, vol. 157, pp. 15–25, 2017.

[48] Y. Richardson, J. Blin, and A. Julbe, "A short overview on purification and conditioning of syngas produced by biomass gasification: catalytic strategies, process intensification and new concepts," *Progress in Energy and Combustion Science*, vol. 38, no. 6, pp. 765–781, 2012.

[49] E. Drioli, A. I. Stankiewicz, and F. Macedonio, "Membrane engineering in process intensification - an overview," *Journal of Membrane Science*, vol. 380, no. 1-2, pp. 1–8, 2011.

[50] I. E. Grossmann and I. Harjunkoski, "Process systems engineering: Academic and industrial perspectives," *Computers & Chemical Engineering*, vol. 126, pp. 474–484, 2019.

[51] S. E. Demirel, J. Li, and M. M. F. Hasan, "A general framework for process synthesis, integration, and intensification," *Industrial & Engineering Chemistry Research*, vol. 58, no. 15, pp. 5950–5967, 2019.

[52] X. Li and A. Kraslawski, "Conceptual process synthesis: past and current trends," *Chemical Engineering and Processing: Process Intensification*, vol. 43, no. 5, pp. 583–594, 2004.

[53] Q. Chen and I. Grossmann, "Recent developments and challenges in optimization-based process synthesis," *Annual Review of Chemical and Biomolecular Engineering*, vol. 86, pp. 249–283, 2017.

[54] J. J. Siirola and D. F. Rudd, "Computer-aided synthesis of chemical process designs. from reaction path data to the process task network," *Industrial & Engineering Chemistry Fundamentals*, vol. 10, no. 3, pp. 353–362, 1971.

[55] J. Seader and A. Westerberg, "A combined heuristic and evolutionary strategy for synthesis of simple separation sequences," *AIChE Journal*, vol. 23, no. 6, pp. 951–954, 1977.

[56] J. Douglas, "A hierarchical decision procedure for process synthesis," *AIChE Journal*, vol. 31, no. 3, pp. 353–362, 1985.

[57] J. M. Douglas, *Conceptual design of chemical processes*. McGraw-Hill New York, 1988.

[58] R. Smith, *Chemical process: design and integration*. John Wiley & Sons, 2005.

[59] R. Smith and B. Linnhoff, "The design of separators in the context of overall processes," *Chem. Eng. Res. Des*, vol. 66, no. 5, pp. 195–228, 1988.

[60] J. M. Commenge and L. Falk, "Methodological framework for choice of intensified equipment and development of innovative technologies," *Chemical Engineering and Processing: Process Intensification*, vol. 84, pp. 109–127, 2014.

[61] T. F. Yee and I. E. Grossmann, "Simultaneous optimization models for heat integration - II heat exchanger network synthesis," *Computers & Chemical Engineering*, vol. 14, no. 10, pp. 1165–1184, 1990.

[62] A. Ciric and C. Floudas, "Heat exchanger network synthesis without decomposition," *Computers & Chemical Engineering*, vol. 15, no. 6, pp. 385–396, 1991.

[63] A. Aggarwal and C. Floudas, "Synthesis of general distillation sequences - nonsharp separations," *Computers & Chemical Engineering*, vol. 14, no. 6, pp. 631–653, 1990.

[64] A. C. Kokossis and C. A. Floudas, "Synthesis of isothermal reactor-separator-recycle systems," *Chemical Engineering Science*, vol. 46, no. 5-6, pp. 1361–1383, 1991.

[65] L. Achenie and L. Biegler, "A superstructure based approach to chemical reactor network synthesis," *Computers & Chemical Engineering*, vol. 14, no. 1, pp. 23–40, 1990.

[66] T. F. Yee, I. E. Grossmann, and Z. Kravanja, "Simultaneous optimization models for heat integration - III. process and heat exchanger network optimization," *Computers & Chemical Engineering*, vol. 14, no. 11, pp. 1185–1200, 1990.

[67] L. Kong, V. Avadiappan, K. Huang, and C. T. Maravelias, "Simultaneous chemical process synthesis and heat integration with unclassified hot/cold process streams," *Computers & Chemical Engineering*, vol. 101, pp. 210–225, 2017.

[68] M. J. Andrecovich and A. Westerberg, "An MILP formulation for heat-integrated distillation sequence synthesis," *AIChE journal*, vol. 31, no. 9, pp. 1461–1474, 1985.

[69] R. C. Baliban, J. A. Elia, and C. A. Floudas, "Simultaneous process synthesis, heat, power, and water integration of thermochemical hybrid biomass, coal, and natural gas facilities," *Computers & Chemical Engineering*, vol. 37, pp. 297–327, 2012.

[70] O. Onel, A. M. Niziolek, J. A. Elia, R. C. Baliban, and C. A. Floudas, "Biomass and natural gas to liquid transportation fuels and olefins (BGTL+ C2_C4): process synthesis and global optimization," *Industrial & Engineering Chemistry Research*, vol. 54, no. 1, pp. 359–385, 2015.

[71] L. Mencarelli, Q. Chen, A. Pagot, and I. E. Grossmann, "A review on superstructure optimization approaches in process system engineering," *Computers & Chemical Engineering*, p. 106808, 2020.

[72] H. Yeomans and I. E. Grossmann, "A systematic modeling framework of superstructure optimization in process synthesis," *Computers & Chemical Engineering*, vol. 23, no. 6, pp. 709–731, 1999.

[73] I. E. Grossmann, P. A. Aguirre, and M. Barttfeld, "Optimal synthesis of complex distillation columns using rigorous models," *Computers & Chemical Engineering*, vol. 29, no. 6, pp. 1203–1215, 2005.

[74] F. Friedler, K. Tarjan, Y. Huang, and L. Fan, "Graph-theoretic approach to process synthesis: axioms and theorems," *Chemical Engineering Science*, vol. 47, no. 8, pp. 1973–1988, 1992.

[75] F. Friedler, K. Tarjan, Y. Huang, and L. Fan, "Graph-theoretic approach to process synthesis: polynomial algorithm for maximal structure generation," *Computers & Chemical Engineering*, vol. 17, no. 9, pp. 929–942, 1993.

[76] T. Farkas and Z. Lelkes, "Process flowsheet superstructures: Structural multiplicity and redundancy: Part I: Basic GDP and MINLP representations," *Computers & Chemical Engineering*, vol. 29, no. 10, pp. 2180–2197, 2005.

[77] T. Farkas and Z. Lelkes, "Process flowsheet superstructures: Structural multiplicity and redundancy: Part II: Ideal and binarily minimal MINLP representations," *Computers & Chemical Engineering*, vol. 29, no. 10, pp. 2198–2214, 2005.

[78] M. M. El-Halwagi and V. Manousiouthakis, "Synthesis of mass exchange networks," *AIChE Journal*, vol. 35, no. 8, pp. 1233–1244, 1989.

[79] M. J. Bagajewicz and V. Manousiouthakis, "Mass/heat-exchange network representation of distillation networks," *AIChE Journal*, vol. 38, no. 11, pp. 1769–1800, 1992.

[80] W. Wu, C. A. Henao, and C. T. Maravelias, "A superstructure representation, generation, and modeling framework for chemical process synthesis," *AIChE Journal*, vol. 62, no. 9, pp. 3199–3214, 2016.

[81] A. R. Ciric and D. Gu, "Synthesis of nonequilibrium reactive distillation processes by MINLP optimization," *AIChE Journal*, vol. 40, no. 9, pp. 1479–1487, 1994.

[82] J. R. Jackson and I. E. Grossmann, "A disjunctive programming approach for the optimal design of reactive distillation columns," *Computers & Chemical Engineering*, vol. 25, no. 11-12, pp. 1661–1673, 2001.

[83] M. M. El-Halwagi, *Pollution prevention through process integration: systematic design tools*. Elsevier, 1997.

[84] J. J. Klemeš and Z. Kravanja, "Forty years of heat integration: pinch analysis (PA) and mathematical programming (MP)," *Current Opinion in Chemical Engineering*, vol. 2, no. 4, pp. 461–474, 2013.

[85] M. M. El-Halwagi and D. C. Yee Foo, "Process synthesis and integration," *Kirk-Othmer Encyclopedia of Chemical Technology*, pp. 1–24, 2000.

[86] R. M. Khorasany and M. Fesanghary, "A novel approach for synthesis of cost-optimal heat exchanger networks," *Computers & Chemical Engineering*, vol. 33, no. 8, pp. 1363–1370, 2009.

[87] C. A. Jaksland, R. Gani, and K. M. Lien, "Separation process design and synthesis based on thermodynamic insights," *Chemical Engineering Science*, vol. 50, no. 3, pp. 511–530, 1995.

[88] W. Marquardt, S. Kossack, and K. Kraemer, "A framework for the systematic design of hybrid separation processes," *Chinese Journal of Chemical Engineering*, vol. 16, no. 3, pp. 333–342, 2008.

[89] Z. Yuan, B. Chen, and R. Gani, "Applications of process synthesis: Moving from conventional chemical processes towards biorefinery processes," *Computers & Chemical Engineering*, vol. 49, pp. 217–229, 2013.

[90] S. E. Demirel, J. Li, and M. M. F. Hasan, "Systematic process intensification using building blocks," *Computers & Chemical Engineering*, vol. 105, pp. 2–38, 2017.

[91] P. Lutze, D. K. Babi, J. M. Woodley, and R. Gani, "Phenomena based methodology for process synthesis incorporating process intensification," *Industrial & Engineering Chemistry Research*, vol. 52, no. 22, pp. 7127–7144, 2013.

[92] R. Karuppiah and I. E. Grossmann, "Global optimization for the synthesis of integrated water systems in chemical processes," *Computers & Chemical Engineering*, vol. 30, no. 4, pp. 650–673, 2006.

[93] C. A. Henao and C. T. Maravelias, "Surrogate-based superstructure optimization framework," *AIChE Journal*, vol. 57, no. 5, pp. 1216–1232, 2011.

[94] A. Cozad, N. V. Sahinidis, and D. C. Miller, "Learning surrogate models for simulation-based optimization," *AIChE Journal*, vol. 60, no. 6, pp. 2211–2227, 2014.

[95] P. Balasubramanian, I. Bajaj, and M. M. F. Hasan, "Simulation and optimization of reforming reactors for carbon dioxide utilization using both rigorous and reduced models," *Journal of CO2 Utilization*, vol. 23, pp. 80–104, 2018.

[96] M. Baldea, "From process integration to process intensification," *Computers & Chemical Engineering*, vol. 81, pp. 104–114, 2015.

[97] P. Pichardo and V. I. Manousiouthakis, "Infinite dimensional state-space as a systematic process intensification tool: Energetic intensification of hydrogen production," *Chemical Engineering Research and Design*, vol. 120, pp. 372–395, 2017.

[98] M.-O. Bertran, R. Frauzem, A.-S. Sanchez-Arcilla, L. Zhang, J. M. Woodley, and R. Gani, "A generic methodology for processing route synthesis and design based on superstructure optimization," *Computers & Chemical Engineering*, vol. 106, pp. 892–910, 2017.

[99] J. A. Arizmendi-Sánchez and P. Sharratt, "Phenomena-based modularisation of chemical process models to approach intensive options," *Chemical Engineering Journal*, vol. 135, no. 1-2, pp. 83–94, 2008.

[100] B.-G. Rong, E. Kolehmainen, and I. Turunen, "Methodology of conceptual process synthesis for process intensification," in *Computer Aided Chemical Engineering*, vol. 25, pp. 283–288, Elsevier, 2008.

[101] H. Freund and K. Sundmacher, "Towards a methodology for the systematic analysis and design of efficient chemical processes: Part 1. from unit operations to elementary process functions," *Chemical Engineering and Processing: Process Intensification*, vol. 47, no. 12, pp. 2051–2060, 2008.

[102] N. M. Kaiser, R. J. Flassig, and K. Sundmacher, "Reactor-network synthesis via flux profile analysis," *Chemical Engineering Journal*, vol. 335, pp. 1018–1030, 2018.

[103] Y. Tian and E. N. Pistikopoulos, "Synthesis of operable process intensification systems: advances and challenges," *Current Opinion in Chemical Engineering*, vol. 25, pp. 101–107, 2019.

[104] M. Skiborowski, "Process synthesis and design methods for process intensification," *Current Opinion in Chemical Engineering*, vol. 22, pp. 216–225, 2018.

[105] A. K. Tula, M. R. Eden, and R. Gani, "Computer-aided process intensification: Challenges, trends and opportunities," *AIChE Journal*, vol. 66, no. 1, p. e16819, 2020.

[106] S. Wilson and V. Manousiouthakis, "IDEAS approach to process network synthesis: Application to multicomponent MEN," *AIChE Journal*, vol. 46, no. 12, pp. 2408–2416, 2000.

[107] K. Holiastos and V. Manousiouthakis, "Infinite-dimensional state-space (IDEAS) approach to globally optimal design of distillation networks featuring heat and power integration," *Industrial & Engineering Chemistry Research*, vol. 43, no. 24, pp. 7826–7842, 2004.

[108] P. G. Ghougassian and V. Manousiouthakis, "Globally optimal networks for multipressure distillation of homogeneous azeotropic mixtures," *Industrial & Engineering Chemistry Research*, vol. 51, no. 34, pp. 11183–11200, 2012.

[109] W. Zhou and V. I. Manousiouthakis, "Non-ideal reactor network synthesis through IDEAS: Attainable region construction," *Chemical Engineering Science*, vol. 61, no. 21, pp. 6936–6945, 2006.

[110] J. F. Burri and V. I. Manousiouthakis, "Global optimization of reactive distillation networks using IDEAS," *Computers & Chemical Engineering*, vol. 28, no. 12, pp. 2509–2521, 2004.

[111] F. E. da Cruz and V. I. Manousiouthakis, "Process intensification of reactive separator networks through the IDEAS conceptual framework," *Computers & Chemical Engineering*, vol. 105, pp. 39–55, 2017.

[112] K. P. Papalexandri and E. N. Pistikopoulos, "Generalized modular representation framework for process synthesis," *AIChE Journal*, vol. 42, no. 4, pp. 1010–1032, 1996.

[113] S. R. Ismail, E. N. Pistikopoulos, and K. P. Papalexandri, "Modular representation synthesis framework for homogeneous azeotropic separation," *AIChE Journal*, vol. 45, no. 8, pp. 1701–1720, 1999.

[114] S. R. Ismail, P. Proios, and E. N. Pistikopoulos, "Modular synthesis framework for combined separation/reaction systems," *AIChE Journal*, vol. 47, no. 3, pp. 629–649, 2001.

[115] T. Y. Algusane, P. Proios, M. C. Georgiadis, and E. N. Pistikopoulos, "A framework for the synthesis of reactive absorption columns," *Chemical Engineering and Processing: Process Intensification*, vol. 45, no. 4, pp. 276–290, 2006.

[116] S. R. Ismail, E. N. Pistikopoulos, and K. P. Papalexandri, "Synthesis of reactive and combined reactor/separation systems utilizing a mass/heat exchange transfer module," *Chemical Engineering Science*, vol. 54, no. 13-14, pp. 2721–2729, 1999.

[117] P. Proios, N. F. Goula, and E. N. Pistikopoulos, "Generalized modular framework for the synthesis of heat integrated distillation column sequences," *Chemical Engineering Science*, vol. 60, no. 17, pp. 4678–4701, 2005.

[118] P. Proios and E. N. Pistikopoulos, "Generalized modular framework for the representation and synthesis of complex distillation column sequences," *Industrial & Engineering Chemistry Research*, vol. 44, no. 13, pp. 4656–4675, 2005.

[119] P. Proios and E. N. Pistikopoulos, "Hybrid generalized modular/collocation framework for distillation column synthesis," *AIChE Journal*, vol. 52, no. 3, pp. 1038–1056, 2006.

[120] Y. Tian and E. N. Pistikopoulos, "Synthesis of operable process intensification systems–steady-state design with safety and operability considerations," *Industrial & Engineering Chemistry Research*, vol. 58, no. 15, pp. 6049–6068, 2018.

[121] Y. Tian, I. Pappas, B. Burnak, J. Katz, and E. N. Pistikopoulos, "A systematic framework for the synthesis of operable process intensification systems–reactive separation systems," *Computers & Chemical Engineering*, vol. 134, p. 106675, 2020.

[122] A. Peschel, H. Freund, and K. Sundmacher, "Methodology for the design of optimal chemical reactors based on the concept of elementary process functions," *Industrial & Engineering Chemistry Research*, vol. 49, no. 21, pp. 10535–10548, 2010.

[123] A. Peschel, F. Karst, H. Freund, and K. Sundmacher, "Analysis and optimal design of an ethylene oxide reactor," *Chemical Engineering Science*, vol. 66, no. 24, pp. 6453–6469, 2011.

[124] D. K. Babi, P. Lutze, J. M. Woodley, and R. Gani, "A process synthesis-intensification framework for the development of sustainable membrane-based operations," *Chemical Engineering and Processing: Process Intensification*, vol. 86, pp. 173–195, 2014.

[125] D. K. Babi, J. Holtbruegge, P. Lutze, A. Gorak, J. M. Woodley, and R. Gani, "Sustainable process synthesis–intensification," *Computers & Chemical Engineering*, vol. 81, pp. 218–244, 2015.

[126] H. Kuhlmann, H. Veith, M. MoÌĹller, K.-P. Nguyen, A. Górak, and M. Skiborowski, "Optimization-based approach to process synthesis for process intensification: Synthesis of reaction-separation processes," *Industrial & Engineering Chemistry Research*, vol. 57, no. 10, pp. 3639–3655, 2017.

[127] H. Kuhlmann and M. Skiborowski, "Optimization-based approach to process synthesis for process intensification: General approach and application to ethanol dehydration," *Industrial & Engineering Chemistry Research*, vol. 56, no. 45, pp. 13461–13481, 2017.

[128] J. C. Carrasco and F. V. Lima, "An optimization-based operability framework for process design and intensification of modular natural gas utilization systems," *Computers and Chemical Engineering*, vol. 105, pp. 246–258, 2017.

[129] J. C. Carrasco and F. V. Lima, "Novel operability-based approach for process design and intensification: Application to a membrane reactor for direct methane aromatization," *AIChE Journal*, vol. 63, no. 3, pp. 975–983, 2017.

[130] S. Recker, M. Skiborowski, C. Redepenning, and W. Marquardt, "A unifying framework for optimization-based design of integrated reaction-separation processes," *Computers and Chemical Engineering*, vol. 81, pp. 260–271, 2015.

[131] J. A. Arizmendi-Sanchez and P. N. Sharratt, "Phenomena-based modularisation of chemical process models to approach intensive options," *Chemical Engineering Journal*, vol. 135, no. 1-2, pp. 83–94, 2008.

[132] B. G. Rong, E. Kolehmainen, and I. Turunen, "Methodology of conceptual process synthesis for process intensification," *Computer Aided Chemical Engineering*, vol. 25, pp. 283–288, 2008.

[133] R. Lakerveld, H. J. M. Kramer, A. I. Stankiewicz, and J. Grievink, "Application of generic principles of process intensification to solution crystallization enabled by a task-based design approach," *Chemical Engineering and Processing: Process Intensification*, vol. 49, no. 9, pp. 979–991, 2010.

[134] M. Gopalakrishnan, J. M. Ponce-Ortega, and M. M. El-Halwagi, "A systems approach for process simplification through process integration," *Chemical Engineering and Technology*, vol. 35, no. 7, pp. 1262–1272, 2012.

[135] A. K. Tula, M. R. Eden, and R. Gani, "Hybrid method and associated tools for synthesis of sustainable process flowsheets," *Computers & Chemical Engineering*, vol. 131, p. 106572, 2019.

[136] M. M. F. Hasan, S. E. Demirel, and J. Li, "A building block approach to process intensification," *Chemical Engineering Progress*, vol. 115, no. 3, pp. 35–43, 2019.

[137] J. Li, S. Demirel, and M. M. F. Hasan, "Building block-based synthesis and intensification of work-heat exchanger networks (whens)," *Processes*, vol. 7, no. 1, p. 23, 2019.

[138] J. D. Seader, E. J. Henley, and D. K. Roper, *Separation process principles*, vol. 25. Wiley New York, 1998.

[139] J. Li, S. E. Demirel, and M. M. F. Hasan, "Process synthesis using a block superstructure with automated flowsheet generation and optimization," *AIChE Journal*, vol. 64, no. 8, pp. 3082–3100, 2018.

[140] R. Taylor, H. Kooijman, and J.-S. Hung, "A second generation nonequilibrium model for computer simulation of multicomponent separation processes," *Computers & Chemical Engineering*, vol. 18, no. 3, pp. 205–217, 1994.

[141] R. Taylor and R. Krishna, "Modelling reactive distillation," *Chemical Engineering Science*, vol. 55, no. 22, pp. 5183–5229, 2000.

[142] S. E. Demirel, J. Li, and M. M. F. Hasan, "A general framework for process synthesis, integration and intensification," *Computer Aided Chemical Engineering*, vol. 44, pp. 445–450, 2018.

[143] S. E. Demirel, J. Li, and M. M. F. Hasan, "Simultaneous process synthesis and heat integration using a single superstructure," *Computing and Systems Technology Division 2017 - Core Programming Area at the 2017 AIChE Annual Meeting*, vol. 2017-October, pp. 199–200, 2017.

[144] M. Tawarmalani and N. V. Sahinidis, "A polyhedral branch-and-cut approach to global optimization," *Mathematical Programming*, vol. 103, no. 2, pp. 225–249, 2005.

[145] R. Misener and C. A. Floudas, "ANTIGONE: algorithms for continuous/integer global optimization of nonlinear equations," *Journal of Global Optimization*, vol. 59, no. 2-3, pp. 503–526, 2014.

[146] A. Khajavirad and N. V. Sahinidis, "A hybrid LP/NLP paradigm for global optimization relaxations," *Mathematical Programming Computation*, vol. 10, no. 3, pp. 383–421, 2018.

[147] A. G. Dixon, W. R. Moser, and Y. H. Ma, "Waste reduction and recovery using O2-permeable membrane reactors," *Industrial & Engineering Chemistry Research*, vol. 33, no. 12, pp. 3015–3024, 1994.

[148] M. M. F. Hasan, R. Baliban, J. Elia, and C. Floudas, "Modeling, simulation, and optimization of postcombustion CO2 capture for variable feed concentration and flow rate. 2. pressure swing adsorption and vacuum swing adsorption processes," *Industrial & Engineering Chemistry Research*, vol. 51, no. 48, pp. 15665–15682, 2012.

[149] W.-H. Chen, M.-R. Lin, T. L. Jiang, and M.-H. Chen, "Modeling and simulation of hydrogen generation from high-temperature and low-temperature water gas shift reactions," *International Journal of Hydrogen Energy*, vol. 33, no. 22, pp. 6644–6656, 2008.

[150] P. Gangadharan, K. C. Kanchi, and H. H. Lou, "Evaluation of the economic and environmental impact of combining dry reforming with steam reforming of methane," *Chemical Engineering Research and Design*, vol. 90, no. 11, pp. 1956–1968, 2012.

[151] G. A. Olah, A. Goeppert, M. Czaun, and G. S. Prakash, "Bi-reforming of methane from any source with steam and carbon dioxide exclusively to metgas (CO–2H2) for methanol and hydrocarbon synthesis," *Journal of the American Chemical Society*, vol. 135, no. 2, pp. 648–650, 2013.

[152] V. R. Choudhary, K. C. Mondal, and T. V. Choudhary, "Partial oxidation of methane to syngas with or without simultaneous steam or CO2 reforming over a high-temperature stable-NiCoMgCeOx supported on zirconia–hafnia catalyst," *Applied Catalysis A: General*, vol. 306, pp. 45–50, 2006.

[153] K. Roh, R. Frauzem, T. B. H. Nguyen, R. Gani, and J. H. Lee, "A methodology for the sustainable design and implementation strategy of CO2 utilization processes," *Computers & Chemical Engineering*, vol. 91, pp. 407–421, 2016.

[154] IPCC, "Climate change 2007: the physical science basis: summary for policymakers," *Geneva: Intergovernmental Panel On Climate Change*, 2007.

[155] S. Schlömer, T. Bruckner, L. Fulton, E. Hertwich, A. McKinnon, D. Perczyk, J. Roy, R. Schaeffer, R. Sims, P. Smith, *et al.*, "Annex III: Technology-specific cost and performance parameters," *Climate Change*, pp. 1329–1356, 2014.

[156] F. Tüzün, E. Kocdemir, and G. Uğuz, "Comparison of gas permeability and selectivity between alumina membrane and vycor glass at high temperatures," *Advances in Materials Physics and Chemistry*, vol. 2, no. 4, p. 237, 2012.

[157] H.-B. Xie, Y. Zhou, Y. Zhang, and J. K. Johnson, "Reaction mechanism of monoethanolamine with CO2 in aqueous solution from molecular modeling," *The Journal of Physical Chemistry A*, vol. 114, no. 43, pp. 11844–11852, 2010.

[158] A. Kothandaraman, *Carbon dioxide capture by chemical absorption: a solvent comparison study*. Ph.D. Thesis. Department of Chemical Engineering, Massachusetts Institute of Technology, 2010.

[159] A. M. Niziolek, O. Onel, and C. A. Floudas, "Production of benzene, toluene, and xylenes from natural gas via methanol: Process synthesis and global optimization," *AIChE Journal*, vol. 62, no. 5, pp. 1531–1556, 2016.

[160] A. B. Rao, E. S. Rubin, and M. B. Berkenpas, "An integrated modeling framework for carbon management technologies," tech. rep., Final Report to DOE/NETL, Center for Energy and Environmental Studies, Carnegie Mellon University, Pittsburgh, PA, 2004.

[161] F. A. Tobiesen and H. F. Svendsen, "Study of a modified amine-based regeneration unit," *Industrial & Engineering Chemistry Research*, vol. 45, no. 8, pp. 2489–2496, 2006.

[162] J. B. Holm-Nielsen, T. Al Seadi, and P. Oleskowicz-Popiel, "The future of anaerobic digestion and biogas utilization," *Bioresource technology*, vol. 100, no. 22, pp. 5478–5484, 2009.

[163] J. J. Siirola, "The impact of shale gas in the chemical industry," *AIChE Journal*, vol. 60, no. 3, pp. 810–819, 2014.

[164] A. Basile, A. Iulianelli, T. Longo, S. Liguori, and M. De Falco, "Pd-based selective membrane state-of-the-art," in *Membrane reactors for hydrogen production processes*, pp. 21–55, Springer, 2011.

[165] S. S. Iyer, I. Bajaj, P. Balasubramanian, and M. M. F. Hasan, "Integrated carbon capture and conversion to produce syngas: Novel process design, intensification, and optimization," *Industrial & Engineering Chemistry Research*, vol. 56, no. 30, pp. 8622–8648, 2017.

[166] W. L. Luyben, "Design and control of a methanol reactor/column process," *Industrial & Engineering Chemistry Research*, vol. 49, no. 13, pp. 6150–6163, 2010.

[167] D. Humbird, R. Davis, L. Tao, C. Kinchin, D. Hsu, A. Aden, P. Schoen, J. Lukas, B. Olthof, M. Worley, *et al.*, "Process design and economics for biochemical conversion of lignocellu-

losic biomass to ethanol: dilute-acid pretreatment and enzymatic hydrolysis of corn stover," tech. rep., National Renewable Energy Laboratory (NREL), Golden, CO., 2011.

[168] A. M. Niziolek, O. Onel, J. A. Elia, R. C. Baliban, and C. A. Floudas, "Coproduction of liquid transportation fuels and C6_C8 aromatics from biomass and natural gas," *AIChE Journal*, vol. ;61, no. 3, pp. 831–856, 2015.

[169] N. Park, M.-J. Park, K.-S. Ha, Y.-J. Lee, and K.-W. Jun, "Modeling and analysis of a methanol synthesis process using a mixed reforming reactor: perspective on methanol production and CO_2 utilization," *Fuel*, vol. ;129, pp. 163–172, 2014.

[170] K. Skowerski, S. J. Czarnocki, and P. Knapkiewicz, "Tube-in-tube reactor as a useful tool for homo-and heterogeneous olefin metathesis under continuous flow mode," *ChemSusChem*, vol. 7, no. 2, pp. 536–542, 2014.

[171] G. Abdulwahab and O. G. Saidat, "Estimating the optimum operating parameters of olefin metathesis reactive distillation process," *ARPN Journal of Engineering and Applied Sciences*, vol. 8, no. 8, pp. 614–624, 2013.

[172] C. W. Jung, P. E. Garrou, and G. R. Strickler, "Disproportionation of alkenes," Nov. 24 1987. US Patent 4,709,115.

[173] M. J. Okasinski and M. F. Doherty, "Design method for kinetically controlled, staged reactive distillation columns," *Industrial & Engineering Chemistry Research*, vol. 37, no. 7, pp. 2821–2834, 1998.

[174] R. S. Huss, F. Chen, M. F. Malone, and M. F. Doherty, "Reactive distillation for methyl acetate production," *Computers & Chemical Engineering*, vol. 27, no. 12, pp. 1855–1866, 2003.

[175] B. Bessling, J.-M. Löning, A. Ohligschläger, G. Schembecker, and K. Sundmacher, "Investigations on the synthesis of methyl acetate in a heterogeneous reactive distillation process," *Chemical Engineering & Technology: Industrial Chemistry-Plant Equipment-Process Engineering-Biotechnology*, vol. 21, no. 5, pp. 393–400, 1998.

[176] A. Gorak and A. Stankiewicz, "Intensified reaction and separation systems," *Annual Review of Chemical and Biomolecular Engineering*, vol. 2, pp. 431–451, 2011.

[177] R. V. Uppaluri, P. Linke, and A. C. Kokossis, "Synthesis and optimization of gas permeation membrane networks," *Industrial & Engineering Chemistry Research*, vol. 43, no. 15, pp. 4305–4322, 2004.

[178] D. S. Sholl and R. P. Lively, "Seven chemical separations to change the world," *Nature*, vol. 532, no. 7600, pp. 435–437, 2016.

[179] A. K. Tula, B. Befort, N. Garg, K. V. Camarda, and R. Gani, "Sustainable process design & analysis of hybrid separations," *Computers & Chemical Engineering*, vol. 105, pp. 96–104, 2017.

[180] W. L. Luyben, "Comparison of pressure-swing and extractive-distillation methods for methanol-recovery systems in the tame reactive-distillation process," *Industrial & Engineering Chemistry Research*, vol. 44, no. 15, pp. 5715–5725, 2005.

[181] K.-i. Okamoto, H. Kita, K. Horii, and K. T. Kondo, "Zeolite NaA membrane: preparation, single-gas permeation, and pervaporation and vapor permeation of water/organic liquid mixtures," *Industrial & Engineering Chemistry Research*, vol. 40, no. 1, pp. 163–175, 2001.

[182] H. Yue, Y. Zhao, X. Ma, and J. Gong, "Ethylene glycol: properties, synthesis, and applications," *Chemical Society Reviews*, vol. 41, no. 11, pp. 4218–4244, 2012.

[183] S. Rebsdat and D. Mayer, "Ethylene glycol," *Ullmann's Encyclopedia of Industrial Chemistry*, 2000.

[184] M. R. Altiokka and S. Akyalcin, "Kinetics of the hydration of ethylene oxide in the presence of heterogeneous catalyst," *Industrial & Engineering Chemistry Research*, vol. 48, no. 24, pp. 10840–10844, 2009.

[185] R. F. Dye, "Ethylene glycols technology," *Korean Journal of Chemical Engineering*, vol. 18, no. 5, pp. 571–579, 2001.

[186] M. H. Barecka, M. Skiborowski, and A. Górak, "Process intensification in practice: Ethylene glycol case study," in *Practical Aspects of Chemical Engineering*, pp. 17–34, Springer, 2018.

[187] W. D. Seider, J. D. Seader, and D. R. Lewin, *Product & Process Design Principles: Synthesis, analysis and evaluation*. John Wiley & Sons, 2009.

[188] M. K. A. Hamid, G. Sin, and R. Gani, "Integration of process design and controller design for chemical processes using model-based methodology," *Computers & Chemical Engineering*, vol. 34, no. 5, pp. 683–699, 2010.

[189] M. L. Luyben and W. L. Luyben, "Design and control of a complex process involving two reaction steps, three distillation columns, and two recycle streams," *Industrial & Engineering Chemistry Research*, vol. 34, no. 11, pp. 3885–3898, 1995.

[190] Q. Zhang, M. Liu, and A. Zeng, "Performance enhancement of pressure-swing distillation process by the combined use of vapor recompression and thermal integration," *Computers & Chemical Engineering*, vol. 120, pp. 30–45, 2019.

[191] S. Espatolero, L. M. Romeo, and C. Cortés, "Efficiency improvement strategies for the feedwater heaters network designing in supercritical coal-fired power plants," *Applied Thermal Engineering*, vol. 73, no. 1, pp. 449–460, 2014.

[192] H. S. Fogler, *Elements of chemical reaction engineering*. Prentice-Hall International London, 2006.

[193] J. Li, S. E. Demirel, and M. M. F. Hasan, "Process integration using block superstructure," *Industrial & Engineering Chemistry Research*, vol. 57, no. 12, pp. 4377–4398, 2018.

[194] A. R. Ciric and S. G. Huchette, "Multiobjective optimization approach to sensitivity analysis: waste treatment costs in discrete process synthesis and optimization problems," *Industrial & Engineering Chemistry Research*, vol. 32, no. 11, pp. 2636–2646, 1993.

[195] F. Zhu, K. Huang, S. Wang, L. Shan, and Q. Zhu, "Towards further internal heat integration in design of reactive distillation columns-part IV: Application to a high-purity ethy-

lene glycol reactive distillation column," *Chemical Engineering Science*, vol. 64, no. 15, pp. 3498–3509, 2009.

[196] M. H. Barecka, M. Skiborowski, and A. Górak, "A novel approach for process retrofitting through process intensification: Ethylene oxide case study," *Chemical Engineering Research and Design*, vol. 123, pp. 295–316, 2017.

[197] J. Hur and I. Moon, "A novel ethylene oxide gas recovery system via hydrolysis in the dimethyl carbonate and monoethylene glycol production process," *Industrial & Engineering Chemistry Research*, 2020.

[198] J. P. Sheets and A. Shah, "Techno-economic comparison of biogas cleaning for grid injection, compressed natural gas, and biogas-to-methanol conversion technologies," *Biofuels, Bioproducts and Biorefining*, vol. 12, no. 3, pp. 412–425, 2018.

[199] M. Bergmann, A. Schmitz, M. Hayden, and K. Kosonen, "Imposing a unilateral carbon constraint on european energy-intensive industries and its impact on their international competitiveness-data & analysis," European Commission, DG Economic and Financial Affairs, December 2007.

[200] H. J. Hasselbach, M. Koerfer, C. P. Gruener, F. H. Hanrath, J. Stock, J. Gangadwala, and H. Krull, "Method of production of a methionine salt," May 5 2015. US Patent 9,023,284.

[201] M. M. El-Halwagi, *Sustainable design through process integration: fundamentals and applications to industrial pollution prevention, resource conservation, and profitability enhancement*. Butterworth-Heinemann, 2017.

[202] A. K. Jana and A. Mane, "Heat pump assisted reactive distillation: wide boiling mixture," *AIChE Journal*, vol. 57, no. 11, pp. 3233–3237, 2011.

[203] S. Vankadari, S. E. Demirel, J. Li, and M. M. F. Hasan, "Intensification of biorefinery operations using building blocks," in *2019 AIChE Annual Meeting*, AIChE, 2019.

APPENDIX A

MINLP MODEL DETAILS*

A.1 Rigorous Phase Assignment

For each block, phase can be assigned in accordance with the pressure and temperature of the block. Hence, for each block, bubble and dew pressures are calculated by using the composition and temperature of the block and then these pressure values are related with a phase binary variable through logical relationships. The bubble and dew pressures for a block are calculated as follows:

$$P_{i,j}^{bub} = \sum_{k \in K \setminus inert} y_{i,j,k}\, P_{i,j,k}^{sat}, \quad \forall i,j \tag{A.1}$$

$$1 = P_{i,j}^{dew} \sum_{k \in K \setminus inert} \frac{y_{i,j,k}}{P_{i,j,k}^{sat}}, \quad \forall i,j \tag{A.2}$$

where $P_{i,j}^{bub}$ and $P_{i,j}^{dew}$ are the bubble and dew pressures of block $B_{i,j}$; $y_{i,j,k}$ is the exit composition of component k in block $B_{i,j}$; and $P_{i,j,k}^{sat}$ is the vapor pressure (or Henry's coefficient) of component k in block $B_{i,j}$. $P_{i,j,k}^{sat}$ is calculated either from Antoine Equation or Henry's Law as a function of block temperature $T_{i,j}$. Accordingly, we define two subsets for set k which determines which of the equations will be used in obtaining $P_{i,j,k}^{sat}$: *KA* and *KH*. Vapor pressures are calculated as follows:

$$P_{i,j,k}^{sat} = \exp\left(A_k - \frac{B_k}{C_k + T_{i,j}}\right), \quad \forall i,j,\ k \in KH \tag{A.3}$$

$$P_{i,j,k}^{sat} = \tilde{H}_k \exp\left(-\tilde{T}_k \left(\frac{1}{T_{i,j}} - \frac{1}{298}\right)\right), \quad \forall i,j,\ k \in KH \tag{A.4}$$

*Parts of this chapter were adapted with permission from (S. E. Demirel, J. Li, and M. M. F. Hasan, "Systematic process intensification using building blocks," Computers & Chemical Engineering, vol. 105, pp. 2 - 38, 2017.) Elsevier and from (S. E. Demirel, J. Li and M. M. F. Hasan, "A general framework for process synthesis, integration, and intensification," Industrial & Engineering Chemistry Research," vol. 58, no. 15, pp. 5950 - 5967, 2019.) Copyright (2019) American Chemical Society.

where A_k, B_k and C_k are the Antoine parameters for component k, $\tilde{H}_k$ is the Henry's coefficient for component k at the reference temperature, $\tilde{T}_k$ is the parameter for component k that determines the temperature dependence of the Henry's coefficient.

The phase of a block will be liquid if the pressure of the block is greater than the bubble pressure of the block. And phase of the block will be gas if the pressure of the block is lower than the dew pressure of the block. Furthermore, if the pressure of the block is in between the bubble and dew pressures, then vapor-liquid equilibrium calculations are needed in order to describe the system properly. Accordingly, following relations have to be satisfied:

$$P_{i,j} \geq P_{i,j}^{bub} - P_{i,j}^{bub,upper} \times \left\{ z_{i,j}^{phase} + \left(z_{i,j,s,m}^{F} + z_{i,j-1,s,m}^{F} + z_{i,j,s,m}^{R} + z_{i-1,j,s,m}^{R} \right) \right\}, \ \forall i,j,s = VLPC, m = null \tag{A.5}$$

$$P_{i,j} \leq P_{i,j}^{dew} + P^{max} \times \left\{ 1 - z_{i,j}^{phase} + \left(z_{i,j,s,m}^{F} + z_{i,j-1,s,m}^{F} + z_{i,j,s,m}^{R} + z_{i-1,j,s,m}^{R} \right) \right\}, \ \forall i,j,s = VLPC, m = null \tag{A.6}$$

where $P_{i,j}^{bub,upper}$ is the upper bound on bubble pressure. It should be noted that ($z_{i,j,s,m}^{F} + z_{i,j-1,s,m}^{F} + z_{i,j,s,m}^{R} + z_{i-1,j,s,m}^{R}$) can not be greater than 1. This indicates that among the boundaries surrounding block $B_{i,j}$, only one of them can be semi-restricted. Accordingly, if block $B_{i,j}$ is in liquid phase, *i.e.* $z_{i,j}^{phase}$=0, and it is not a part of a vapor-liquid equilibrium phenomenon, *i.e.* none of the boundaries surrounding block $B_{i,j}$ is assigned to a vapor-liquid equilibrium phenomenon: $z_{i,j,s,m}^{F} = 0$; $z_{i,j-1,s,m}^{F} = 0$; $z_{i,j,s,m}^{R} = 0$; $z_{i-1,j,s,m}^{R} = 0$, then the pressure of the block should be larger than the bubble pressure of the block. Similarly, if block $B_{i,j}$ is in gas phase, *i.e.* $z_{i,j}^{phase}$=1, and it is not a part of a vapor-liquid equilibrium phenomenon, *i.e.* $z_{i,j,s,m}^{F}$= 0 ; $z_{i,j-1,s,m}^{F}$= 0; $z_{i,j,s,m}^{R}$= 0; $z_{i-1,j,s,m}^{R} = 0$, then the pressure of the block should be less than the dew pressure of the block. If, on the other hand, one of the surrounding boundaries is assigned to a vapor-liquid equilibrium phenomenon, then both equations are relaxed and the equilibrium conditions are satisfied. In this case, block phase assignments become arbitrary and they only play role in determining the topol-

ogy of the resulting process. With the above formulation, although defining phase of the feed and product streams are not necessary, by doing so can increase the speed of the calculation.

Alternatively, we can use a simpler approach based on the assumptions that the overall boiling point ($T^{boil}_{i,j}$) of a mixture in block $B_{i,j}$ can be calculated using the boiling points of its components (T^{b}_{k}) as follows.

$$T^{boil}_{i,j} = \sum_{k} T^{b}_{k}\, y_{i,j,k}, \quad \forall i,j \tag{A.7}$$

$$T_{i,j} \geq T^{boil}_{i,j} - T^{b,max} \times \left\{ z^{phase}_{i,j} + \left(z^{F}_{i,j,s,m} + z^{F}_{i,j-1,s,m} + z^{R}_{i,j,s,m} + z^{R}_{i-1,j,s,m} \right) \right\},\ \forall i,j,\ s = VLPC,\ m = null \tag{A.8}$$

$$T_{i,j} \leq T^{boil}_{i,j} + T^{max} \times \left\{ 1 - z^{phase}_{i,j} + \left(z^{F}_{i,j,s,m} + z^{F}_{i,j-1,s,m} + z^{R}_{i,j,s,m} + z^{R}_{i-1,j,s,m} \right) \right\}, \forall i,j,s = VLPC, m = null \tag{A.9}$$

where, $T^{b,max}$ is the boiling point of the heaviest (least volatile) component, and $z^{F}_{i,j,s,m}$ and $z^{R}_{i,j,s,m}$ are binary variables indicating the existense of equilibrium phenomena between two adjacent blocks in the horizontal and vertical direction, respectively. Accordingly, if block $B_{i,j}$ is in liquid phase, *i.e.* $z^{phase}_{i,j}$=0, and it is not a part of a vapor-liquid equilibrium phenomenon, *i.e.* none of the boundaries surrounding block $B_{i,j}$ is assigned to a vapor-liquid equilibrium phenomenon: $z^{F}_{i,j,s,m} = 0$; $z^{F}_{i,j-1,s,m} = 0$; $z^{R}_{i,j,s,m} = 0$; $z^{R}_{i-1,j,s,m} = 0$, then the temperature of the block should be smaller than the boiling temperature of the block, *i.e.* $T^{boil}_{i,j}$. Similarly, if block $B_{i,j}$ is in gas phase, *i.e.* $z^{phase}_{i,j}$=1, and it is not a part of a vapor-liquid equilibrium phenomenon, *i.e.* $z^{F}_{i,j,s,m} = 0$; $z^{F}_{i,j-1,s,m} = 0$; $z^{R}_{i,j,s,m} = 0$; $z^{R}_{i-1,j,s,m} = 0$, then the temperature of the block should be less than the boiling temperature of the block. If, on the other hand, one of the surrounding boundaries is assigned to a vapor-liquid equilibrium phenomenon, then both equations are relaxed and the equilibrium conditions are satisfied.

A.2 Block Energy Balance in the Presence of Phase Change

For a component *k* that may undergo a phase change in the given process conditions, enthalpy will differ according to the phase of the stream. If there is phase change in the process, then it is possible that some components may transfer from gas phase to liquid phase, while some others can transfer from liquid phase to gas phase. Hence, components in a stream may flow in reverse directions. In order to account for this, we add component index *k* into the enthalpy variables and replace energy balance equation using the following:

$$\begin{aligned}\sum_k EF_{i,j-1,k} - \sum_k EF_{i,j,k} + \sum_k ER_{i-1,j,k} - \sum_k ER_{i,j,k} \\ - EP_{i,j} + EG_{i,j} + EM_{i,j} + Q_{i,j} + W_{i,j} = 0, \quad \forall i,j\end{aligned} \tag{A.10}$$

We can describe the stream enthalpy terms based on different assumptions. We first describe a simpler version with constant heat capacity assumption. Then, we describe a more general form.

A.2.1 Constant Heat Capacity Assumption

As we only allow for one phase to exist in one block, the phase of the stream is determined by the phase of the source block. For instance, if a stream is leaving a gas block and entering into a liquid block, its phase becomes gas and in calculation of the enthalpy of this stream, heat capacity should be taken as gas heat capacity and the enthalpy of vaporization should be included in the stream enthalpy. According to these general rules, for the horizontal flow from block $B_{i,j}$ to $B_{i,j+1}$, $FP_{i,j,k}$, if the $B_{i,j}$ is in gas phase, enthalpy carried by component *k* is calculated as follows:

$$EF_{i,j,k} \geq FP_{i,j,k}\left[Cp_k^{Gas}\left(T_{i,j} - T_k^{ref}\right) + \Delta H_k^{vap}\right] - \ EU\ (2 - z_{i,j,k}^{Fplus} - z_{i,j}^{phase}),\ \forall i,j,k \tag{A.11}$$

$$EF_{i,j,k} \leq FP_{i,j,k}\left[Cp_k^{Gas}\left(T_{i,j} - T_k^{ref}\right) + \Delta H_k^{vap}\right] + \ EU\ (2 - z_{i,j,k}^{Fplus} - z_{i,j}^{phase}),\ \forall i,j,k \tag{A.12}$$

Here, Cp_k^{gas} and ΔH_k^{vap} are the heat capacity and the enthalpy of vaporization of *k* at the reference temperature, and T_k^{ref} is the reference state temperature for component *k*. $z_{i,j}^{phase}$ is the binary variable determining the phase of the block $B_{i,j}$. The above equation dictates that if the flow

between block $B_{i,j}$ to $B_{i,j+1}$ is in positive direction, *i.e.,* $z_{i,j,k}^{Fplus}$ is equal to 1, and the phase of the source block, $B_{i,j}$, is gas phase, *i.e.*, $z_{i,j}^{phase}$ is 1, then the last term is deactivated and the enthalpy carried by component *k* is calculated by the given relationship. Otherwise, last term is activated and the enthalpy variable $EF_{i,j,k}$ is relaxed. Note that the temperature of the stream is equal to the source block temperature $T_{i,j}$. If the phase of the source block is in liquid phase, $z_{i,j}^{phase}$ is equal to 0, then the stream enthalpy is calculated as follows:

$$EF_{i,j,k} \geq FP_{i,j,k}\left[Cp_k^{liq}\left(T_{i,j} - T_k^{ref}\right) + \Delta H_k^{vap}\right] - EU\ (z_{i,j}^{phase} + 1 - z_{i,j,k}^{Fplus}),\ \forall i,j,k \quad \text{(A.13)}$$

$$EF_{i,j,k} \leq FP_{i,j,k}\left[Cp_k^{liq}\left(T_{i,j} - T_k^{ref}\right) + \Delta H_k^{vap}\right] + EU\ (z_{i,j}^{phase} + 1 - z_{i,j,k}^{Fplus}),\ \forall i,j,k \quad \text{(A.14)}$$

If the horizontal flow is in the negative direction, *i.e.*, $z_{i,j,k}^{Fplus}$ is equal to 0, and phase of the block $B_{i,j+1}$ is in gas phase, *i.e.*, $z_{i,j+1}^{phase}$ is equal to 1, then the equations for $EF_{i,j,k}$ becomes the following:

$$\begin{aligned} EF_{i,j,k} \geq\ & -FN_{i,j,k}\left[Cp_k^{Gas}\left(T_{i,j+1} - T_k^{ref}\right) + \Delta H_k^{vap}\right] \\ & - EU\ \left(z_{i,j,k}^{Fplus} + 1 - z_{i,j+1}^{phase}\right),\ \forall i,j,k \end{aligned} \quad \text{(A.15)}$$

$$\begin{aligned} EF_{i,j,k} \leq\ & -FN_{i,j,k}\left[Cp_k^{Gas}\left(T_{i,j+1} - T_k^{ref}\right) + \Delta H_k^{vap}\right] \\ & + EU\ \left(z_{i,j,k}^{Fplus} + 1 - z_{i,j+1}^{phase}\right),\ \forall i,j,k \end{aligned} \quad \text{(A.16)}$$

And if the horizontal flow is in the negative direction, *i.e.,* $z_{i,j,k}^{Fplus}$ is equal to 0, and block $B_{i,j+1}$ is in liquid phase, *i.e.*, $z_{i,j+1}^{phase}$ is equal to zero, then the equations for $EF_{i,j,k}$ becomes the following:

$$EF_{i,j,k} \geq\ -FN_{i,j,k}\left[Cp_k^{liq}(T_{i,j+1} - T_k^{ref})\right] - EU\ \left(z_{i,j,k}^{Fplus} + z_{i,j+1}^{phase}\right),\ \forall i,j,k \quad \text{(A.17)}$$

$$EF_{i,j,k} \leq\ -FN_{i,j,k}\left[Cp_k^{liq}(T_{i,j+1} - T_k^{ref})\right] + EU\ \left(z_{i,j,k}^{Fplus} + z_{i,j+1}^{phase}\right),\ \forall i,j,k \quad \text{(A.18)}$$

Similar equations are also written for the enthalpy carried by the vertical flow, $ER_{i,j,k}$. If the vertical flow is in the positive direction, *i.e.,*$z_{i,j,k}^{Rplus}$ is equal to 1, and block $B_{i,j}$ is in gas phase, *i.e.,*

$z_{i,j}^{phase}$ is equal to one, then the equations for $ER_{i,j,k}$ become:

$$ER_{i,j,k} \geq \ RP_{i,j,k}\left[Cp_k^{Gas}(T_{i,j} - T_k^{ref}) + \ \Delta H_k^{vap}\right] - \ EU\ (2 - z_{i,j,k}^{Rplus} - z_{i,j}^{phase}),\ \forall i,j,k \quad \text{(A.19)}$$

$$ER_{i,j,k} \leq \ RP_{i,j,k}\left[Cp_k^{Gas}(T_{i,j} - T_k^{ref}) + \ \Delta H_k^{vap}\right] + \ EU\ (2 - z_{i,j,k}^{Rplus} - z_{i,j}^{phase}),\ \forall i,j,k \quad \text{(A.20)}$$

If the vertical flow is in the positive direction, *i.e.,* $z_{i,j,k}^{Rplus}$ is equal to 1, and block $B_{i,j}$ is in liquid phase, *i.e.*, $z_{i,j}^{phase}$ is equal to zero, then the equations for $ER_{i,j,k}$ becomes:

$$ER_{i,j,k} \geq \ RP_{i,j,k}\left[Cp_k^{liq}(T_{i,j} - T_k^{ref})\right] - \ EU\ \left(z_{i,j}^{phase} + 1\ -\ z_{i,j,k}^{Rplus}\right),\ \forall i,j,k \quad \text{(A.21)}$$

$$ER_{i,j,k} \leq \ RP_{i,j,k}\left[Cp_k^{liq}(T_{i,j} - T_k^{ref})\right] + \ \ EU\ \left(z_{i,j}^{phase} + 1\ -\ z_{i,j,k}^{Rplus}\right),\ \forall i,j,k \quad \text{(A.22)}$$

If the vertical flow is in the negative direction, *i.e.,*$z_{i,j,k}^{Rplus}$ is equal to 0, and block $B_{i+1,j}$ is in gas phase, *i.e.*, $z_{i+1,j}^{phase}$ is equal to one, then the equations for $ER_{i,j,k}$ becomes:

$$\begin{aligned} ER_{i,j,k} \geq \ -RN_{i,j,k}&\left[Cp_k^{Gas}(T_{i+1,j} - T_k^{ref}) + \Delta H_k^{vap}\right] \\ &- EU(z_{i,j,k}^{Rplus} + 1 - \ z_{i+1,j}^{phase}),\ \forall i,j,k \end{aligned} \quad \text{(A.23)}$$

$$\begin{aligned} ER_{i,j,k} \leq \ -RN_{i,j,k}&\left[Cp_k^{Gas}(T_{i+1,j} - T_k^{ref}) + \Delta H_k^{vap}\right] \\ &+ EU(z_{i,j,k}^{Rplus} + 1 - \ z_{i+1,j}^{phase}),\ \forall i,j,k \end{aligned} \quad \text{(A.24)}$$

If the vertical flow is in the negative direction, *i.e.*, $z_{i,j,k}^{Rplus}$ is equal to 0, and block $B_{i+1,j}$ is in liquid phase, *i.e.*, $z_{i+1,j}^{phase}$ is equal to zero, then the equations for $ER_{i,j,k}$ becomes:

$$ER_{i,j,k} \geq \ -RN_{i,j,k}\left[Cp_k^{liq}(T_{i+1,j} - T_k^{ref})\right] - \ EU\ (z_{i,j,k}^{Rplus} + \ z_{i+1,j}^{phase}),\ \forall i,j,k \quad \text{(A.25)}$$

$$ER_{i,j,k} \leq \ -RN_{i,j,k}\left[Cp_k^{liq}(T_{i+1,j} - T_k^{ref})\right] + \ EU\ (z_{i,j,k}^{Rplus} + \ z_{i+1,j}^{phase}),\ \forall i,j,k \quad \text{(A.26)}$$

Product and feed stream enthalpies are written as follows:

$$EM_{i,j} = \sum_{k} \sum_{f} M_{i,j,k,f} \left(Cp_{k,f}^{feed} \left(T_{i,j} - T_{k}^{ref} \right) + \Delta H_{k,f}^{vap,feed} \right), \ \forall i, j \tag{A.27}$$

$$EP_{i,j} = \sum_{k} \sum_{p} P_{i,j,k,p} \left(Cp_{k,p}^{prod} \left(T_{i,j} - T_{k}^{ref} \right) + \Delta H_{k,p}^{vap,prod} \right), \ \forall i, j \tag{A.28}$$

where Cp_{k}^{feed} and $Cp_{k,p}^{prod}$ are the parameters for the heat capacity of components for feed and product streams, respectively. If feed is gas (or liquid), then they are taken as gas (or liquid) phase heat capacity. $\Delta H_{k,f}^{vap,feed}$ and $\Delta H_{k,p}^{vap,prod}$ are the heat of vaporization of the components included in the feed and product, respectively. If the feed or products are liquid, then these parameters are taken as zero.

A.2.2 A More General Formulation

Here, a more generic description of the energy balance will be provided. Enthalpy terms in the energy balance equations can be dissected into several parts based on phase and the direction of the flows. And these terms can be described as a function of the source block phase, temperature and pressure. Here, the formulation is based on a convex hull formulation rather than a Big-M as in the previous section. Also, enthalpy terms are written in a more generic form by considering temperature and pressure dependence. One can also consider composition dependence but we assumed ideal mixing throughout this work. For horizontal direction $EF_{i,j}$ can be dissected into four terms based on the direction and the phase as follows:

$$EF_{i,j} = -\sum_{k \in K} EFP_{i,j,k}^{g} - \sum_{k \in K} EFP_{i,j,k}^{l} + \sum_{k \in K} EFN_{i,j,k}^{g} + \sum_{k \in K} EFN_{i,j,k}^{l}, \ \forall i, j \tag{A.29}$$

Similarly, $ER_{i,j}$ is dissected into four terms as follows:

$$ER_{i,j} = -\sum_{k \in K} ERP_{i,j,k}^{g} - \sum_{k \in K} ERP_{i,j,k}^{l} + \sum_{k \in K} ERN_{i,j,k}^{g} + \sum_{k \in K} ERN_{i,j,k}^{l}, \ \forall i, j \tag{A.30}$$

These individual stream enthalpy terms can be then defined as a function of flow rate, temperature and pressure. This functional relationship will depend on the phase. Accordingly:

$$EFP^{l}_{i,j,k} + EFP^{ls}_{i,j,k} = f^{liq}(FP_{i,j,k}, T_{i,j}, P_{i,j}) \quad \forall i,j,k \tag{A.31}$$

$$EFP^{l}_{i,j,k} \leq EU \times (1 - z^{phase}_{i,j}) \quad \forall i,j,k \tag{A.32}$$

$$EFP^{l}_{i,j,k} \geq -EU \times (1 - z^{phase}_{i,j}) \quad \forall i,j,k \tag{A.33}$$

$$EFP^{ls}_{i,j,k} \leq EU \times z^{phase}_{i,j} \quad \forall i,j,k \tag{A.34}$$

$$EFP^{ls}_{i,j,k} \geq -EU \times z^{phase}_{i,j} \quad \forall i,j,k \tag{A.35}$$

Equation A.31 assigns the liquid enthalpy of the horizontal flow in the positive direction to either $EFP^{l}_{i,j,k}$ or $EFP^{ls}_{i,j,k}$. $EFP^{ls}_{i,j,k}$ is a slack variable which is active when the source block is in vapor phase, i.e. $z^{phase}_{i,j} = 1$. In this case, $EFP^{l}_{i,j,k} = 0$. These are satisfied with Eqs. A.31-A.35. If the enthalpy relations are written in a way that they appear as positive variables, then Eqs. A.33 and A.35 can be removed from the formulation. Similar logic applies for the vapor enthalpy terms:

$$EFP^{g}_{i,j,k} + EFP^{gs}_{i,j,k} = f^{vap}(FP_{i,j,k}, T_{i,j}, P_{i,j}) \quad \forall i,j,k \tag{A.36}$$

$$EFP^{g}_{i,j,k} \leq EU \times z^{phase}_{i,j} \quad \forall i,j,k \tag{A.37}$$

$$EFP^{g}_{i,j,k} \geq -EU \times z^{phase}_{i,j} \quad \forall i,j,k \tag{A.38}$$

$$EFP^{gs}_{i,j,k} \leq EU \times (1 - z^{phase}_{i,j}) \quad \forall i,j,k \tag{A.39}$$

$$EFP^{gs}_{i,j,k} \geq -EU \times (1 - z^{phase}_{i,j}) \quad \forall i,j,k \tag{A.40}$$

Similarly, in the negative direction:

$$EFN^{l}_{i,j,k} + EFN^{ls}_{i,j,k} = f^{liq}(FN_{i,j,k}, T_{i,j+1}, P_{i,j+1}) \quad \forall i,j,k \tag{A.41}$$

$$EFN^{l}_{i,j,k} \leq EU \times (1 - z^{phase}_{i,j+1}) \quad \forall i,j,k \tag{A.42}$$

$$EFN^{l}_{i,j,k} \geq -EU \times (1 - z^{phase}_{i,j+1}) \quad \forall i,j,k \tag{A.43}$$

$$EFN^{ls}_{i,j,k} \leq EU \times z^{phase}_{i,j+1} \quad \forall i,j,k \tag{A.44}$$

$$EFN^{ls}_{i,j,k} \geq -EU \times z^{phase}_{i,j+1} \quad \forall i,j,k \tag{A.45}$$

$$EFN^{g}_{i,j,k} + EFN^{gs}_{i,j,k} = f^{vap}(FN_{i,j,k}, T_{i,j+1}, P_{i,j+1}) \quad \forall i,j,k \tag{A.46}$$

$$EFN^{g}_{i,j,k} \leq EU \times z^{phase}_{i,j+1} \quad \forall i,j,k \tag{A.47}$$

$$EFN^{g}_{i,j,k} \geq -EU \times z^{phase}_{i,j+1} \quad \forall i,j,k \tag{A.48}$$

$$EFN^{gs}_{i,j,k} \leq EU \times (1 - z^{phase}_{i,j+1}) \quad \forall i,j,k \tag{A.49}$$

$$EFN^{gs}_{i,j,k} \geq -EU \times (1 - z^{phase}_{i,j+1}) \quad \forall i,j,k \tag{A.50}$$

Note that in the negative direction, enthalpy terms depend on the variables of the block on the left side of the boundary. Similar relations can be written in the vertical direction by defining $ERP^{g}_{i,j,k}$, $ERP^{gs}_{i,j,k}$, $ERN^{g}_{i,j,k}$, $ERN^{gs}_{i,j,k}$, $ERP^{l}_{i,j,k}$, $ERP^{ls}_{i,j,k}$, $ERN^{l}_{i,j,k}$ and $ERN^{ls}_{i,j,k}$. For the enthalpy of the jump streams, external feed and product streams, these constraints can be written as below:

$$EJ^{l}_{i,j,i',j',k} + EJ^{ls}_{i,j,i',j',k} = f^{liq}(J_{i,j,i',j',k}, T_{i,j}, P_{i,j}), \quad i,j,i',j' \in LN, k \in K \tag{A.51}$$

$$EJ^{l}_{i,j,i',j',k} \leq EU \times (1 - z^{phase}_{i,j}) \quad i,j,i',j' \in LN, k \in K \tag{A.52}$$

$$EJ^{l}_{i,j,i',j',k} \geq -EU \times (1 - z^{phase}_{i,j}) \quad i,j,i',j' \in LN, k \in K \tag{A.53}$$

$$EJ^{ls}_{i,j,i',j',k} \leq EU \times z^{phase}_{i,j} \quad i,j,i',j' \in LN, k \in K \tag{A.54}$$

$$EJ^{ls}_{i,j,i',j',k} \leq EU \times z^{phase}_{i,j} \quad i,j,i',j' \in LN, k \in K \tag{A.55}$$

$$EJ^{g}_{i,j,i',j',k} + EJ^{gs}_{i,j,i',j',k} = f^{vap}(J_{i,j,i',j',k}, T_{i,j}, P_{i,j}), \quad i,j,i',j' \in LN, k \in K \tag{A.56}$$

$$EJ^{g}_{i,j,i',j',k} \leq EU \times z^{phase}_{i,j} \quad i,j,i',j' \in LN, k \in K \tag{A.57}$$

$$EJ^{g}_{i,j,i',j',k} \geq -EU \times z^{phase}_{i,j} \quad i,j,i',j' \in LN, k \in K \tag{A.58}$$

$$EJ^{gs}_{i,j,i',j',k} \leq EU \times (1 - z^{phase}_{i,j}) \quad i,j,i',j' \in LN, k \in K \tag{A.59}$$

$$EJ^{gs}_{i,j,i',j',k} \leq EU \times (1 - z^{phase}_{i,j}) \quad i,j,i',j' \in LN, k \in K \tag{A.60}$$

$$EM_{i,j} = \sum_{k \in K} \sum_{f \in FS} f^{feed}(M_{i,j,k,f}, T^{feed}_{fs}, P^{feed}_{fs}), \quad \forall i,j,f \tag{A.61}$$

$$EP_{i,j} = \sum_{k \in K} \sum_{p \in PS} f^{product}(P_{i,j,k,p}, T_{i,j}, P_{i,j}), \quad \forall i,j,p \tag{A.62}$$

Note that for the feed and product streams phase will be known. Hence, no disjunctions are needed. By using these enthalpy terms, single block energy balance can be rewritten as follows:

$$\begin{aligned}
&\sum_{k \in K} EFP^{g}_{i,j-1,k} + \sum_{k \in K} EFP^{l}_{i,j-1,k} - \sum_{k \in K} EFN^{g}_{i,j-1,k} - \sum_{k \in K} EFN^{l}_{i,j-1,k} + \sum_{k \in K} ERP^{g}_{i-1,j,k} \\
&+ \sum_{k \in K} ERP^{l}_{i-1,j,k} - \sum_{k \in K} ERN^{g}_{i-1,j,k} - \sum_{k \in K} ERN^{l}_{i-1,j,k} - \sum_{k \in K} EFP^{g}_{i,j,k} - \sum_{k \in K} EFP^{l}_{i,j,k} \\
&+ \sum_{k \in K} EFN^{g}_{i,j,k} + \sum_{k \in K} EFN^{l}_{i,j,k} - \sum_{k \in K} ERP^{g}_{i,j,k} - \sum_{k \in K} ERP^{l}_{i,j,k} + \sum_{k \in K} ERN^{g}_{i,j,k} \\
&+ \sum_{k \in K} ERN^{l}_{i,j,k} + \sum_{i',j' \in LN} \sum_{k \in K} EJ^{g}_{i',j',i,j,k} + \sum_{i',j' \in LN} \sum_{k \in K} EJ^{l}_{i',j',i,j,k} - \sum_{i',j' \in LN} \sum_{k \in K} EJ^{g}_{i,j,i',j',k} \\
&- \sum_{i',j' \in LN} \sum_{k \in K} EJ^{l}_{i,j,i',j',k} + EM_{i,j} - EP_{i,j} + Q^{h}_{i,j} - Q^{c}_{i,j} + W_{i,j} = 0, \quad \forall i,j
\end{aligned} \tag{A.63}$$

A.3 Work Calculations

The work term $W_{i,j}$ is calculated as the summation of the energy consumed/produced for all the entering streams as in Equation 3.23. Hence, compression and expansion work terms are defined for all possible inlet streams (see Figure A.1) as positive variables and $W_{i,j}$ is written as the summation of all these variables. Accordingly,

$$W^{com}_{i,j} = W^{comp,FP}_{i,j} + W^{comp,FN}_{i,j} + W^{comp,RP}_{i,j} + W^{comp,RN}_{i,j} + \sum_{f}^{FS} W^{comp,F}_{i,j,f}, \ \forall i,j \tag{A.64}$$

$$W_{i,j}^{exp} = W_{i,j}^{exp,FP} + W_{i,j}^{exp,FN} + W_{i,j}^{exp,RP} + W_{i,j}^{exp,RN} + \sum_{f}^{FS} W_{i,j,f}^{exp,F}, \ \forall i,j \qquad \text{(A.65)}$$

When the pressure of two neighboring blocks are not same and there is a stream connection between those two blocks, work related with the transfer of this stream into a different pressure should be accounted for. For instance, if the stream is leaving a low pressure block and entering into a higher pressure block, then the energy required for compressing this stream should be calculated. When two blocks are separated by a semi-restricted boundary, the pressure difference between the two blocks is the driving force for mass transfer. Hence, there is no need to account energy related phenomena (*i.e.* expansion or compression) across a semi-restricted boundary. The only case when the energy calculations should be performed is in the case of an unrestricted boundary separating two blocks with different pressures.

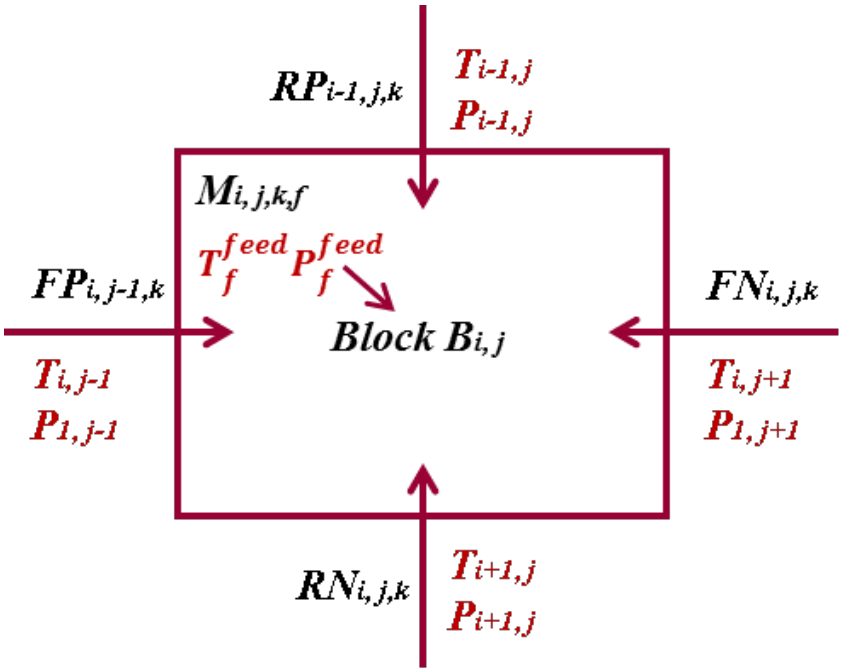

Figure A.1: Incoming streams to the block. There are two streams entering into block $B_{i,j}$ in the horizontal direction, $FP_{i,j-1,k}$ and $FN_{i,j,k}$, two entering streams in the vertical direction, $RP_{i-1,j,k}$ and $RN_{i,j,k}$. Also, there can be several incoming feed streams denoted as $M_{i,j,k,f}$. Flow rates are depicted as black and associated temperature and pressure variables are depicted as red below the flow rate variables (Reprinted with permission from [90]).

We define pressure ratio variables for each boundary separating two neighboring blocks in order to relate the pressure change with the type of the flow rate. We denote pressure ratio in the horizontal direction using $PR^F_{i,j}$ which is defined as the ratio of the pressure of the block in the right (block $B_{i,j+1}$) to the pressure of the block in the left (block $B_{i,j}$). When this pressure ratio is equal to 1, *i.e.* pressure of the two neighboring blocks are the same, then the work associated with the pressure change of this stream is equal to zero. Similarly, for the streams in the vertical direction, this ratio is defined as a separate variable, $PR^R_{i,j}$, which is the pressure ratio of the block below (block $B_{i+1,j}$) to the pressure of the block above (block $B_{i,j}$). As we stated earlier, if one stream is semi-restricted, then there is no need for any compression/expansion work calculation. Hence, pressure ratio across a semi-restricted boundary can be taken as equal to 1 and the related work term becomes zero. Moreover, if block $B_{i,j}$ is in liquid phase, then compressor and expander work terms should be zero. Accordingly, pressure ratio variables are defined as follows:

$$PR^F_{i,j} \geq \left(\frac{P_{i,j+1}}{P_{i,j}}\right) - PR^{up}(\ 2 - z^{unf}_{i,j} - z^{phase}_{i,j}),\ \forall i,j \tag{A.66}$$

$$PR^F_{i,j} \leq \left(\frac{P_{i,j+1}}{P_{i,j}}\right) + PR^{up}(\ 2 - z^{unf}_{i,j} - z^{phase}_{i,j}),\ \forall i,j \tag{A.67}$$

$$1 + \ PR^{up}\ \left(\ 1\ - z^{srf}_{i,j}\right) \geq\ PR^F_{i,j} \geq\ 1 -\ \ (\ 1\ - z^{srf}_{i,j}),\ \forall i,j \tag{A.68}$$

$$1 + \ PR^{up}\ z^{phase}_{i,j} \geq\ PR^F_{i,j} \geq\ 1 -\ \ z^{phase}_{i,j},\ \forall i,j \tag{A.69}$$

where, PR^{up} is the maximum allowed pressure ratio. When the flow is unrestricted and the block $B_{i,j}$ is in gas phase, Equations A.66-A.67 becomes active and pressure ratio is calculated as the ratio of the pressure of the block in the right to the pressure of the block in the left. On the other hand, when the flow is semi-restricted, regardless of the phase of the block, Equation A.68 becomes active and the pressure ratio becomes 1 in order to make the associated work term zero. When block is in liquid phase, Equation A.69 dictates that pressure ratio should be 1 regardless of the type of the boundary.

Similar equations are defined for the vertical direction pressure ratio, $PR^R_{i,j}$:

$$PR^R_{i,j} \geq \left(\frac{P_{i+1,j}}{P_{i,j}}\right) - PR^{up}(\ 2 - z^{unr}_{i,j} - z^{phase}_{i,j}),\ \forall i,j \tag{A.70}$$

$$PR^R_{i,j} \leq \left(\frac{P_{i+1,j}}{P_{i,j}}\right) + PR^{up}(\ 2 - z^{unr}_{i,j} - z^{phase}_{i,j}),\ \forall i,j \tag{A.71}$$

$$1 + \ PR^{up}\ \left(\ 1\ - z^{srr}_{i,j}\right) \geq\ PR^R_{i,j} \geq\ 1 -\ \ (\ 1\ - z^{srr}_{i,j}),\ \forall i,j \tag{A.72}$$

$$1 + \ PR^{up}\ z^{phase}_{i,j} \geq\ PR^R_{i,j} \geq\ 1 -\ \ z^{phase}_{i,j},\ \forall i,j \tag{A.73}$$

And in order to prevent work calculation for the feed blocks if the feed stream is in liquid phase, we define $PR^{feed}_{i,j,f}$ as the ratio of the block pressure, *i.e.* $P_{i,j}$, to the feed stream pressure P^{feed}_f and write the following formulation:

$$PR^{feed}_{i,j,f} = \left(\frac{P_{i,j}}{P^{feed}_f}\right),\ \forall i,j,\ f\ \in GFS \tag{A.74}$$

$$PR^{feed}_{i,j,f} = 1,\ \forall i,j,\ f\ \in LFS \tag{A.75}$$

With this, the isentropic work for a horizontal entering stream is calculated as follows:

$$W^{comp,FP}_{i,j} - W^{exp,FP}_{i,j} = \left(\sum_k FP_{i,j-1,k}\right) T_{i,j-1}\ R_{gas}\ \frac{\gamma}{\gamma-1}\ \left[\left(PR^F_{i,j-1}\right)^{\frac{\gamma-1}{\gamma}} - 1\right],\ \forall i,j \tag{A.76}$$

$$W^{comp,FN}_{i,j} - W^{exp,FN}_{i,j} = \left(\sum_k FN_{i,j,k}\right)\ T_{i,j+1}\ R_{gas}\ \frac{\gamma}{\gamma-1}\ \ \left[\left(\frac{1}{PR^F_{i,j}}\right)^{\frac{\gamma-1}{\gamma}} - 1\right],\ \forall i,j \tag{A.77}$$

For the vertical entering streams $RP_{i-1,j,k}$ and $RN_{i,j,k}$, work terms are defined as follows:

$$W^{comp,RP}_{i,j} - W^{exp,RP}_{i,j} = \left(\sum_k RP_{i-1,j,k}\right)\ T_{i-1,j}\ R_{gas}\ \frac{\gamma}{\gamma-1}\ \left[\left(PR^R_{i-1,j}\right)^{\frac{\gamma-1}{\gamma}} - 1\right],\ \forall i,j \tag{A.78}$$

$$W^{comp,RN}_{i,j} - W^{exp,RN}_{i,j} = \left(\sum_k RN_{i,j,k}\right)\ T_{i+1,j}\ R_{gas}\ \frac{\gamma}{\gamma-1}\ \ \left[\left(\frac{1}{PR^R_{i,j}}\right)^{\frac{\gamma-1}{\gamma}} - 1\right],\ \forall i,j \tag{A.79}$$

The work related to feed streams is also calculated in a similar fashion.

$$W_{i,j,f}^{comp,F} - W_{i,j,f}^{exp,F} = \left(\sum_{k} M_{i,j,k,f} \right) T_f^{feed} R_{gas} \frac{\gamma}{\gamma - 1} \left[\left(PR_{i,j,f}^{feed} \right)^{\frac{\gamma-1}{\gamma}} - 1 \right], \forall i, j, f \quad \text{(A.80)}$$

With the above equations, if the pressure ratio is equal to 1, then the right hand side becomes zero and the net difference between the expander and compressor work terms also becomes zero. Otherwise, the work energy required for the calculated pressure ratio is assigned to the associated work term in the left hand side determined by the sign of the calculated work energy. For instance, if the work calculated is negative, then it is equated to the expander energy term.

A.4 Multi-block Material and Energy Balances

On top of material balance around each block, a second material balance constraint around each horizontal and vertical pair of blocks can be written. While this constraint is equal to the summation of the material balances around the adjacent blocks, and redundant, it enables to reduce the model size when fixed configurations are used with phase contact phenomena. For horizontal direction, material balance around each adjacent block is written as follow:

$$\begin{aligned} & F_{i,j-1,k} + R_{i-1,j,k} - R_{i,j,k} - F_{i,j+1,k} + R_{i-1,j+1,k} - R_{i,j+1,k} + G_{i,j,k} + \sum_{f \in FS} M_{i,j,k,f} \\ & - \sum_{p \in PS} P_{i,j,k,p} + G_{i,j+1,k} + \sum_{f \in FS} M_{i,j+1,k,f} - \sum_{p \in PS} P_{i,j+1,k,p} \\ & + \sum_{(i',j') \in LN} J_{i',j',i,j,k} - \sum_{(i',j') \in LN} J_{i,j,i',j',k} \\ & + \sum_{(i',j') \in LN} J_{i',j',i,j+1,k} - \sum_{(i',j') \in LN} J_{i,j+1,i',j',k} = 0, \quad \forall\, i, j, k \end{aligned} \quad \text{(A.81)}$$

A similar constraint can be written for the vertical direction as follows:

$$
\begin{aligned}
&F_{i,j-1,k} + R_{i-1,j,k} - F_{i,j,k} - F_{i+1,j,k} + F_{i+1,j-1,k} - R_{i+1,j,k} + G_{i,j,k} + \sum_{f \in FS} M_{i,j,k,f} \\
&- \sum_{p \in PS} P_{i,j,k,p} + G_{i+1,j,k} + \sum_{f \in FS} M_{i+1,j,k,f} - \sum_{p \in PS} P_{i+1,j,k,p} \\
&+ \sum_{(i',j') \in LN} J_{i',j',i,j,k} - \sum_{(i',j') \in LN} J_{i,j,i',j',k} \\
&+ \sum_{(i',j') \in LN} J_{i',j',i+1,j,k} - \sum_{(i',j') \in LN} J_{i+1,j,i',j',k} = 0, \quad \forall\, i, j, k
\end{aligned}
\tag{A.82}
$$

When fixed configurations are used, i.e. positions of the phase contact phenomena are known, this constraint can be used instead of Eq. 3.9 which helps into reduce the number of variables via making the horizontal (or vertical) streams between the adjacent blocks, i.e. $F_{i,j,k}$ (or $R_{i,j,k}$), redundant. This is similar to, for example, using a tray material balance for a distillation column, instead of using material balance around each phase. It should be noted that, however, when no prior structural fixing is performed, and, hence, the assignment of the block boundary is not known, Eq. 3.9 is needed.

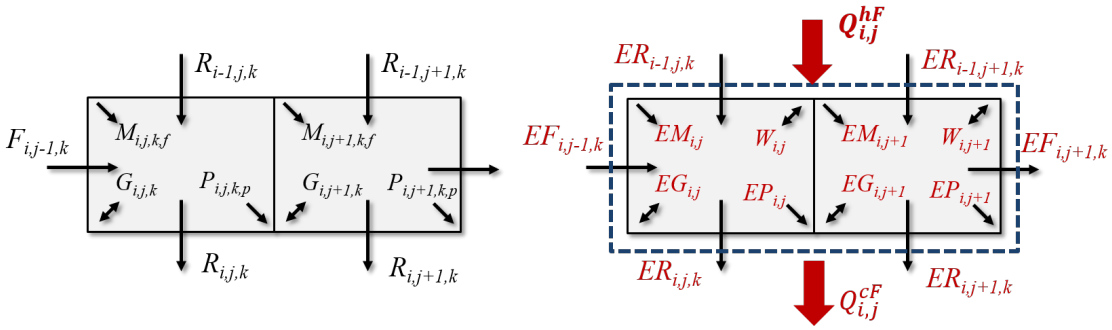

Figure A.2: Multi-block material and energy balance variables. Variables for horizontal multi-block material (left) and energy balances (right). (Jump stream variables are not shown in the figures).

Similar to material balance constraints, additional energy balance constraints between each pair of neighboring blocks can be written (See Figure A.2). These energy balance constraints can be

also used to reduce the model size when the position of the phase contact boundaries are known beforehand. Furthermore, these constraints can be also used to increase model accuracy when the conductive heat transfer at the phase boundary is neglected. Hence, unlike the multi-block material balances, these constraints are not redundant and can be utilized to increase model accuracy even if no prior fixing on the position of the phase contact phenomena is performed. For horizontal direction, multiblock energy balance is satisfied as follows:

$$\begin{aligned} &EF_{i,j-1} + ER_{i-1,j} - ER_{i,j} - EF_{i,j+1} + ER_{i-1,j+1} - ER_{i,j+1} + EG_{i,j} + EM_{i,j} \\ &- EP_{i,j} + EG_{i,j+1} + EM_{i,j+1} - EP_{i,j+1} + \sum_{(i',j')\in LN} EJ_{i',j',i,j} \\ &- \sum_{(i',j')\in LN} EJ_{i,j,i',j'} + \sum_{(i',j')\in LN} EJ_{i',j',i,j+1} - \sum_{(i',j')\in LN} EJ_{i,j+1,i',j'} \\ &+ W_{i,j} + W_{i,j+1} + Q^{hF}_{i,j} - Q^{cF}_{i,j} = 0, \quad \forall\, i,j \end{aligned} \tag{A.83}$$

In these constraints, $Q^{hF}_{i,j}$ and $Q^{cF}_{i,j}$ are the heating and cooling duties for the two neighboring blocks in the horizontal direction. These terms corrrespond to the combination of single block heat duties:

$$Q^{hF}_{i,j} - Q^{cF}_{i,j} = Q^{h}_{i,j} - Q^{c}_{i,j} + Q^{h}_{i,j+1} - Q^{c}_{i,j+1}, \quad i \in I, j \in J$$

Yet, we still define these new energy balance terms to prevent double counting the single and two-block heat duty variables if they appear in objective function. A similar energy balance constraint can be also written in the vertical direction:

$$\begin{aligned} &EF_{i,j-1} + ER_{i-1,j} - EF_{i,j} - EF_{i+1,j} + EF_{i+1,j-1} - ER_{i+1,j} + EG_{i,j} + EM_{i,j} \\ &- EP_{i,j} + EG_{i+1,j} + EM_{i+1,j} - EP_{i+1,j} + \sum_{(i',j')\in LN} EJ_{i',j',i,j} \\ &- \sum_{(i',j')\in LN} EJ_{i,j,i',j'} + \sum_{(i',j')\in LN} EJ_{i',j',i+1,j} - \sum_{(i',j')\in LN} EJ_{i+1,j,i',j'} \\ &+ W_{i,j} + W_{i+1,j} + Q^{hR}_{i,j} - Q^{cR}_{i,j} = 0, \quad \forall\, i,j \end{aligned} \tag{A.84}$$

$Q^{hR}_{i,j}$ and $Q^{cR}_{i,j}$ are the heating and cooling duties for the two neighboring blocks in the vertical direction.

If the position of the phase contact phenomena is known beforehand, then either single block energy balances or these multiblock energy balance constraints can be activated. Accordingly, positions of the $Q^{h}_{i,j}$, $Q^{c}_{i,j}$, $Q^{hF}_{i,j}$, $Q^{cF}_{i,j}$, $Q^{hR}_{i,j}$, $Q^{cR}_{i,j}$ are known and they can be directly incorporated into the objective function. An example of this is shown in Section.

If the positions are not fixed beforehand, however, then several additional constraints are needed to determine the actual heat duty terms that should appear in the objective function. This is ensured through the following constraints for the horizontal direction heating duty variables:

$$Q^{hF}_{i,j} = Q^{hFs}_{i,j} + Q^{hF1}_{i,j}, \quad i \in I, j \in J \tag{A.85}$$

$$Q^{hFs}_{i,j} = EU \times \sum_{(s,m) \in Equil(s,m)} \left(1 - z^{sF}_{i,j,s,m}\right) \qquad i \in I, j \in J \tag{A.86}$$

Here, Eq. A.85 dissects the horizontal heat duty variable into two counterparts: $Q^{hFs}_{i,j}$ and $Q^{hF1}_{i,j}$. While $Q^{hFs}_{i,j}$ is a dummy variable and activated through Eq. A.86, $Q^{hF1}_{i,j}$ denotes the actual heating duty required and incorporated into the objective function. If the horizontal boundary is assigned with a phase contact phenomenon, then $z^{sF}_{i,j,s,m}$ becomes 1 and $Q^{hFs}_{i,j}$ becomes zero according to Eq. A.86. Otherwise, $Q^{hFs}_{i,j}$ becomes active. As the objective function will include a penalty term for minimizing $Q^{hF1}_{i,j}$, no other constraint is needed. Similar constraints are also written for the cold utility term:

$$Q^{cF}_{i,j} = Q^{cFs}_{i,j} + Q^{cF1}_{i,j}, \quad i \in I, j \in J \tag{A.87}$$

$$Q^{cFs}_{i,j} = EU \times \sum_{(s,m) \in Equil(s,m)} \left(1 - z^{F}_{i,j,s,m}\right) \qquad i \in I, j \in J \tag{A.88}$$

Similar constraints can be also written in the vertical direction as follows:

$$Q^{hR}_{i,j} = Q^{hRs}_{i,j} + Q^{hR1}_{i,j}, \quad i \in I, j \in J \tag{A.89}$$

$$Q^{hRs}_{i,j} = EU \times \sum_{(s,m) \in Equil(s,m)} \left(1 - z^{R}_{i,j,s,m}\right) \qquad i \in I, j \in J \tag{A.90}$$

$$Q_{i,j}^{cR} = Q_{i,j}^{cRs} + Q_{i,j}^{cR1}, \quad i \in I, j \in J \tag{A.91}$$

$$Q_{i,j}^{cRs} = EU \times \sum_{(s,m) \in Equil(s,m)} \left(1 - z_{i,j,s,m}^{R}\right) \qquad i \in I, j \in J \tag{A.92}$$

This needs to be also performed for the single block heat duty variables:

$$Q_{i,j}^{h} = Q_{i,j}^{hs} + Q_{i,j}^{h1}, \quad \forall\, i, j \tag{A.93}$$

$$Q_{i,j}^{hs} = EU \times \sum_{(s,m) \in Equil(s,m)} \left(z_{i,j,s,m}^{F} + z_{i,j-1,s,m}^{F} + z_{i,j,s,m}^{R} + z_{i-1,j,s,m}^{R}\right), \ \forall\, i, j \tag{A.94}$$

Here Eq. A.93 dissects heating duty term into two counterparts: $Q_{i,j}^{hs}$ and $Q_{i,j}^{h1}$. While $Q_{i,j}^{hs}$ is used as a dummy variable to deactivate the heat duty term when one of the boundaries around the block is assigned with phase contact phenomena, $Q_{i,j}^{h1}$ is the real block heat duty term that is active when none of the boundaries around the block is assigned with phase contact phenomena. Similar constraints are written for the cold utility terms as follows:

$$Q_{i,j}^{c} = Q_{i,j}^{cs} + Q_{i,j}^{c1}, \quad \forall\, i, j \tag{A.95}$$

$$Q_{i,j}^{cs} = EU \times \sum_{(s,m) \in Equil(s,m)} \left(z_{i,j,s,m}^{F} + z_{i,j-1,s,m}^{F} + z_{i,j,s,m}^{R} + z_{i-1,j,s,m}^{R}\right), \ \forall\, i, j \tag{A.96}$$

When these constraints are utilized, an objective function for minimizing energy can be written as below:

$$\min \quad \sum_{i,j} Q_{i,j}^{c1} + Q_{i,j}^{h1} + Q_{i,j}^{hR1} + Q_{i,j}^{cR1} + Q_{i,j}^{hF1} + Q_{i,j}^{cF1} \tag{A.97}$$

A.5 Short-cut Models for Semi-restricted Boundary

These models are used to obtain number of trays, volume, reflux ratio, height, diameter etc of a pre-specified equipment. These design variables are obtained with short-cut models [57]. However, short-cut models generally include nonlinear and nonconvex terms and including these variable with block superstructure indices, i.e. i, j, result in highly nonlinear models. In order to address this issue, when solving process synthesis problems with known equipment types, instead

of defining each design variable to each block, we perform a reformulation and denote each of these design variables with their equipment indices only. Here, an example on distillation column design formulation is given. Similar constraints are used in the solution of the problems described in Sections 4.7.1 and 4.7.2. More details on the design of several other units and the more reformulation can be found in Li et al. (2018).

For distillation columns, several new design variables are defined. These include inlet, top and bottom flow rates: $F^{in}_{s,k}$, $F^{top}_{s,k}$, $F^{bot}_{s,k}$, respectively. Accordingly, feed, i.e. $y^{in}_{s,k}$, top, i.e. $y^{top}_{s,k}$, and bottom,i.e. $y^{bot}_{s,k}$, compositions can be calculated. Similarly, temperature variables are also defined for top and bottom: T^{top}_{s} and T^{bot}_{s}, respectively. Here, we take $\tau_{i,j,k,d,s,m}$ position independent and reduce it to $\tau_{s,k}$ which designates the fraction of k in feed to distillation column s taken out as the bottoms or distillate (See Section 3.6.2). Whether this fraction refers to bottom or distillate depends on the assignment of the semi-restricted boundary. If the stream through semi-restricted boundary refers to bottom of the column, then this designates the recovery of the component k at the bottoms. And all the other unrestricted flows, jump products or external products refer to distillate from the column. In the constraints below, we take the semirestricted boundary as the bottom of the distillation column as is also the case in Case Studies 4.7.1. and 4.7.2. With these descriptions, design of a distillation column is performed though the following constraints:

$$\phi_{i,j,k} - \phi^{up}_{i,j,k}(1 - z^{sep}_{i,j,s,m}) \leq F^{in}_{s,k} \leq \phi_{i,j,k} + \phi^{up}_{i,j,k}(1 - z^{sep}_{i,j,s,m}) \quad \forall i, j, s, m \in SM \tag{A.98}$$

$$z^{FPlus}_{i,j} + (1 - z^{F}_{i,j,s,m}) \leq z^{sep}_{i,j,s,m} \leq z^{FPlus}_{i,j} - (1 - z^{F}_{i,j,s,m}) \quad \forall i, j, s, m \in SM \tag{A.99}$$

$$z^{RPlus}_{i,j} + (1 - z^{R}_{i,j,s,m}) \leq z^{sep}_{i,j,s,m} \leq z^{RPlus}_{i,j} - (1 - z^{R}_{i,j,s,m}) \quad \forall i, j, s, m \in SM \tag{A.100}$$

$$1 - z^{FPlus}_{i,j} + (1 - z^{F}_{i,j,s,m}) \leq z^{sep}_{i,j+1,s,m} \leq 1 - z^{FPlus}_{i,j} - (1 - z^{s}_{i,j,s,m}) \quad \forall i, j, s, m \in SM \tag{A.101}$$

$$1 - z^{RPlus}_{i,j} + (1 - z^{R}_{i,j,s,m}) \leq z^{sep}_{i+1,j,s,m} \leq 1 - z^{RPlus}_{i,j} - (1 - z^{R}_{i,j,s,m}) \quad \forall i, j, s, m \in SM \tag{A.102}$$

$$F^{in}_{s,k} = F^{top}_{s,k} + F^{bot}_{s,k} \quad \forall s, k \tag{A.103}$$

$$F_{s,k}^{bot} = F_{s,k}^{in}\tau_{s,k} \quad \forall s,k \tag{A.104}$$

$$F_{s,k}^{in} = y_{s,k}^{in}\sum_{k'} F_{s,k'}^{in} \quad \forall s,k \tag{A.105}$$

$$F_{s,k}^{bot} = y_{s,k}^{bot}\sum_{k'} F_{s,k'}^{bot} \quad \forall s,k \tag{A.106}$$

$$F_{s,k}^{top} = y_{s,k}^{top}\sum_{k'} F_{s,k'}^{top} \quad \forall s,k \tag{A.107}$$

$$\sum_{k} y_{s,k}^{top} = 1; \sum_{k} y_{s,k}^{bot} = 1; \sum_{k} y_{s,k}^{in} = 1; \quad \forall s \tag{A.108}$$

$$P_{s,k}^{sat,D} = f^{sat}(T_s^{top}) \quad \forall s,k \tag{A.109}$$

$$P_{s,k}^{sat,B} = f^{sat}(T_s^{bot}) \quad \forall s,k \tag{A.110}$$

$$1 = P_s^s \sum_{k} y_{s,k}^{top}/P_{s,k}^{sat,D} \quad \forall s \tag{A.111}$$

$$P_s^s = \sum_{k} P_{s,k}^{sat,B} y_{s,k}^{bot} \quad \forall s \tag{A.112}$$

$$\alpha_{s,k} = \sqrt{(P_{s,k}^{sat,D}/P_{s,k'}^{sat,D})(P_{s,k}^{sat,B}/P_{s,k'}^{sat,B})} \quad \forall s,k \in K, k' \in HK \tag{A.113}$$

$$\alpha_{s,k}^{N_s^{stagemin}} = ((1-\tau_{s,k})/\tau_{s,k'})/((1-\tau_{s,k'})/\tau_{s,k}) \quad \forall s,k \in K, k' \in HK \tag{A.114}$$

$$\sum_{k} \frac{\alpha_{s,k} y_{s,k}^{in}}{\alpha_{s,k} - \theta_s} = 0 \quad \forall s \tag{A.115}$$

$$R_s^{min} + 1 = \sum_{k} \frac{\alpha_{s,k} y_{s,k}^{top}}{\alpha_{s,k} - \theta_s} \quad \forall s \tag{A.116}$$

$$R_s^{min} = \left(\frac{1}{\alpha_{s,k}-1}\right)\left(\frac{y_{s,k}^{top}}{y_{s,k}^{in}} - \frac{\alpha_{s,k}(1-y_{s,k}^{top})}{1-y_{s,k}^{in}}\right) \quad \forall s,k \in LK \tag{A.117}$$

$$R_s^{real} = 1.3 R_s^{min} \quad \forall s \tag{A.118}$$

$$\frac{N_s^{stage} - N_s^{stagemin}}{N_s^{stage}+1} = 0.75\left(1 - \frac{R_s^{real} - R_s^{min}}{R_s^{real}+1}\right)^{0.5688} \quad \forall s \tag{A.119}$$

$$R_s^{real1} \geq R_s^{real} + 1 - R_s^{real1up}(1 - \sum_{s,m \in SM} z_{i,j,s,m}^{sep}) \quad \forall s \tag{A.120}$$

$$P_s^s - \left(P^{max} - P^{min}\right)(1 - z_{i,j,s,m}^{sep}) \leq P_{i,j} \leq P_s^s + \left(P^{max} - P^{min}\right)(1 - z_{i,j,s,m}^{sep})\ \forall s, m \in SM \tag{A.121}$$

$$T_s^{top} - \left(T^{max} - T^{min}\right)(1 - z_{i,j,s,m}^{sep}) \leq T_{i,j} \leq T_s^{top} + \left(T^{max} - T^{min}\right)(1 - z_{i,j,s,m}^{sep})\ \forall s, m \in SM \tag{A.122}$$

$$\begin{aligned} T_{i,j}^{sF} \geq & T_s^{bot} - (T^{max} - T^{min})(1 - z_{i,j,s,m}^{F}) \quad \forall i, j, s, m \in SM \\ T_{i,j}^{sF} \leq & T_s^{bot} + (T^{max} - T^{min})(1 - z_{i,j,s,m}^{sF}) \quad \forall i, j, s, m \in SM \end{aligned} \tag{A.123}$$

$$\begin{aligned} T_{i,j}^{sR} \geq & T_s^{bot} - (T^{max} - T^{min})(1 - z_{i,j,s,m}^{R}) \quad \forall i, j, s, m \in SM \\ T_{i,j}^{sR} \leq & T_s^{bot} + (T^{max} - T^{min})(1 - z_{i,j,s,m}^{sR}) \quad \forall i, j, s, m \in SM \end{aligned} \tag{A.124}$$

$$FP_{i,j,k} \leq F_{s,k}^{bot} + FU_{i,j,k}(2 - z_{i,j,s,m}^{F} - z_{i,j}^{FPlus}) \quad \forall i, j, k, s, m \in SM \tag{A.125}$$

$$FP_{i,j,k} \geq F_{s,k}^{bot} - FU_{i,j,k}(2 - z_{i,j,s,m}^{F} - z_{i,j}^{FPlus}) \quad \forall i, j, k, s, m \in SM \tag{A.126}$$

$$RP_{i,j,k} \leq F_{s,k}^{bot} + RU_{i,j,k}(2 - z_{i,j,s,m}^{R} - z_{i,j}^{RPlus}) \quad \forall i, j, k, s, m \in SM \tag{A.127}$$

$$RP_{i,j,k} \geq F_{s,k}^{bot} - RU_{i,j,k}(2 - z_{i,j,s,m}^{R} - z_{i,j}^{RPlus}) \quad \forall i, j, k, s, m \in SM \tag{A.128}$$

$$FN_{i,j,k} \leq F_{s,k}^{bot} + FU_{i,j,k}(1 - z_{i,j,s,m}^{F} + z_{i,j}^{FPlus}) \quad \forall i, j, k, s, m \in SM \tag{A.129}$$

$$FN_{i,j,k} \geq F_{s,k}^{bot} - FU_{i,j,k}(1 - z_{i,j,s,m}^{F} + z_{i,j}^{FPlus}) \quad \forall i, j, k, s, m \in SM \tag{A.130}$$

$$RN_{i,j,k} \leq F_{s,k}^{bot} + RU_{i,j,k}(1 - z_{i,j,s,m}^{R} + z_{i,j}^{RPlus}) \quad \forall i, j, k, s, m \in SM \tag{A.131}$$

$$RN_{i,j,k} \geq F_{s,k}^{bot} - RU_{i,j,k}(1 - z_{i,j,s,m}^{R} + z_{i,j}^{RPlus}) \quad \forall i, j, k, s, m \in SM \tag{A.132}$$

$$Q_s^{reb} = Q_s^{con} = \sum_{k \in K} \Delta H_k^{vap} F_{s,k}^{top}, \quad \forall s \tag{A.133}$$

In the above constraints, Eq.A.98 assigns the inlet flow rate to the block $B_{i,j}$, i.e. $\phi_{i,j,k}$, to the distillation equipment inlet $F_{s,k}^{in}$ if $B_{i,j}$ is assigned with distillation equipment s. Note that $B_{i,j}$ represents a distillation unit if one of the boundaries of $B_{i,j}$ is assigned as distillation boundary and the flow rate through this boundary is the outlet from $B_{i,j}$. This relation is described with Eqs. A.99-A.102 via defining a 0-1 continuous separation boundary variable, $z_{i,j,s,m}^{sep}$ which takes

the value of 1 if one of the surrounding boundaries for $B_{i,j}$ is assigned with distillation boundary and flow through this boundary is outlet from $B_{i,j}$. Equations A.103-A.108 describe the material balances around distillation equipment, concentration of the inlet, top and bottom streams and flux through the semi-restricted boundary, which is in this case the bottom flow rate. Equations A.109-A.110 are to determine the vapor pressure of the components at the top, i.e. $P_{s,k}^{sat,D}$, and bottom, i.e. $P_{s,k}^{sat,B}$, of the distillation column s. Equations A.111-A.112 are for determining the bubble and dew point temperatures at the top and bottom of the column, respectively, by assuming no pressure drop across the column. Equation A.113 is to determine the average relative volatility of each component based on the heavy component included in set HK. Equation A.114 is to determine the minimum number of stages. In binary distillation columns, minimum reflux ratio can be calculated through Eq. A.117. In multicomponent distillation systems, it can be calculated through Eqs. A.115-A.116. Equations A.118-A.120 are to determine the real number of stages and reflux ratio. Equations A.121-A.122 are to assign distillation column pressure and top temperature to the block temperature and pressure. Equations A.123-A.124 are to assign bottoms temperature to the semi-restricted stream that distillation is assigned to. Equations A.125-A.132 are to map the equipment inlet and outlet variables to the semi-restricted flow. Disjunctions are written in case that distillation column position is not a priori fixed. Equation A.133 is to determine the condensor and reboiler duty as a function of distillate flow.

APPENDIX B

CASE STUDY RESULTS AND PARAMETERS*

B.1 Case Study in Section 4.7: A Hybrid Solution Approach

B.1.1 Cost parameters

In all the problems throughout this section, raw materials ethylene oxide (283 K) and water (298 K) are assumed to be available in liquid state with a maximum availability of 35 and 100 kmol/h, respectively. EO cost is taken as 43.7 $/kmol and water cost is taken as 0.002 $/kmol [187]. Hot utility (HP steam at 527 K) and cold utility costs are taken as 0.00681 $/MJ and 0.000312 $/MJ. In capital cost calculations, cost functions given in Douglass [57] are used with a capital recovery factor of 0.333 and M&S index of 1431.7 [190]. For all equipment, material of construction is selected as stainless steel as in a typical ethylene glycol plant [185]. Also, these costs take into account the pressure correction factors given in Douglass [57] for the maximum allowed pressure within the process (i.e. 36 bar). CSTR cost is approximated as three times of the cost of a pressure vessel with L/D=2 (L: Length and D: Diameter) [189]. A void space of 10% of the reaction volume is considered for the overall volume and this is restricted between 3-30 m^3 [188]. PFR cost is approximated as a multitubular heat exchanger with 1-in diameter tubes which provide fully developed turbulent flow through the reactor[185]. Reactor fixed costs are taken from Kokossis and Floudas[64] Pump costs are taken from Espatolero et al.[191]. Note that in calculating the height of the distillation columns, a tray efficiency of 0.5 is considered for non-reactive columns. Tray efficiency for the reactive columns is assumed as 0.7. Tray heights for the reactive columns are calculated based on the correlations given in Ciric and Gu[81]. All the

*Parts of this chapter were adapted with permission from (S. E. Demirel, J. Li and M. M. F. Hasan, "A general framework for process synthesis, integration, and intensification," Industrial & Engineering Chemistry Research," vol. 58, no. 15, pp. 5950 - 5967, 2019.) Copyright (2019) American Chemical Society.

capital cost functions are provided below:

$$Cost^{CSTR} = 40356 + 152588(1.1V^R(m^3))^{0.623} \tag{B.1}$$

$$Cost^{PFR} = 19964 + 488042(V(m^3))^{0.623} \tag{B.2}$$

$$Cost^{HEX} = 18207.9(A(m^2))^{0.65} \tag{B.3}$$

$$Cost^{DC} = 74258.3 + 64.89D(ft)^{1.55}H(ft) + 3011.6D(ft)^{1.066}H(ft)^{0.802} \tag{B.4}$$

$$Cost^{pump} = 18612(W(kW)/4)^{0.55} \tag{B.5}$$

B.1.2 Heat Integration Formulation

Here, we provide the formulation that is used in simultaneous process synthesis and HENS with isothermal streams and short-cut models. In this model, additional binary variables on determining the active matches, i.e. $z^{match}_{w,w}$, and classification of heat duties, i.e. z^{hot}_w and z^{cold}_w, are used. These binary variables are indexed over w which is an element of the set $w = \{w|w = 1, ..., |W|\}$ that includes all the streams and other heat duties that can be matched with each other. The binary variable $z^{hx}_{s',s}$ is defined to designate the match between the streams associated with distillation columns:

$$z^{hx}_{s,s'} = \begin{cases} 1 & \text{if the distillate stream of column } s' \text{ is supplying heat to the bottom stream of column } s \\ 0 & \text{Otherwise} \end{cases}$$

Energy balance for condensors and reboilers become:

$$Qh^{reboiler}_s + \sum_{s' \in match_{s,s'}} q_{s,s'} = Q^{reb}_s \tag{B.6}$$

$$Qc^{condensor}_s + \sum_{s' \in match_{s,s'}} q_{s,s'} = Q^{con}_s \tag{B.7}$$

where $Qh_s^{reboiler}$ and $Qc_s^{condensor}$ are external utility consumption. $q_{s,s'}^h$ and $q_{s',s}^c$ are heat duty exchanged at process heat exchangers. Set $match(s, s')$ designates the allowed pairs for integration.

The approach temperatures between distillate stream of column s' and bottom stream of column s is determined as follows:

$$dt_{s,s'}^{hx} \leq T_s^{top} - T_{s'}^{bot} + (T^{max} - T^{min})(1 - z_{s',s}^{hx}) \quad s, s' \in match(s, s') \tag{B.8}$$

Heat duty of a stream match is zero if the two streams do not exchange heat:

$$q_{s,s'}^h \leq q^{max}(1 - z_{s,s'}^{hx}) \quad s, s' \in match(s, s') \tag{B.9}$$

B.2 Case Study in Section 4.8: Sustainable Process Intensification

The general mathematical model equations given in Section 3.3 are used in this case study. Equations 3.108 and 3.109 serve as the material balance constraints for standalone and vapor-liquid phase contact block pairs, respectively. Note that one block can only belong to either SB or TB set. Using TB set eliminates the need for interblock variables when an equilibrium-based separation model is adopted as it is the case in vapor-liquid phase contact blocks. $G_{i,j,k}$ term in Eq. 3.110 describes the generation terms due to reactions. This is implemented for the ethylene glycol production as follows:

$$G_{i,j,k} = \sum_{r \in RXN} React_{i,j,k,r} \quad i, j \in RxnB, k \in K \tag{B.10}$$

$$React_{i,j,k,r} = Cons_{i,j,r}\gamma_{r,k}V_{i,j} \quad i, j \in RxnB, \gamma_{r,k} \neq 0 \tag{B.11}$$

$$Cons_{i,j,r} = f^{rxn}(T_{i,j}, C_{i,j,k}, k_r^0, E_r^A) \quad i, j \in RxnB, r \in Rxn \tag{B.12}$$

Here, the reaction set includes $r = main, side$ and reaction rates in $Cons_{i,j,r}$ term denotes the reaction rate for reaction r per unit volume and the reaction rate is calculated based on block reaction volume, $V_{i,j}$, with Eq. B.11. Set $RxnB$ determines the building blocks $B_{i,j}$ at which reaction

is allowed. Since the reaction is homogeneous liquid phase reactions, these blocks are in liquid phase. Equation B.12 is implemented through following homogeneous kinetic rate expressions obtained from Altıokka and Karayalçın (2009)[184]:

$$-r_{EO}^{main} \quad [kmol/h] = 60 \times \exp\left(13.62 - \left(\frac{8220}{T[K]}\right)\right) C_{EO}[kmol/m^3] \times C_W[kmol/m^3]$$

$$-r_{EO}^{side} \quad [kmol/h] = 60 \times \exp\left(15.57 - \left(\frac{8700}{T[K]}\right)\right) C_{EO}[kmol/m^3] \times C_{EG}[kmol/m^3]$$

Here, reactant concentrations are in molar concentration. These molar concentrations are calculated based on molar fractions and assuming a linear mixing rule which requires pure molar concentration of each species. Accordingly, following constitutive equations are used:

$$C_{i,j,k} \times \left(\sum_{k' \in K} \frac{y_{i,j,k'}}{\rho_{i,j,k'}}\right) = y_{i,j,k} \quad i,j \in RxnB, k \in K^{reactants} \tag{B.13}$$

$$\rho_{i,j,k} = \rho_k^{d1} + \rho_k^{d2} \times T_{i,j} + \rho_k^{d3} \times T_{i,j}^2 \quad i,j \in RxnB, k \in K \tag{B.14}$$

$K^{reactants}$ denotes the set of components k that act as reactants in the system, i.e. EO, EG and W. Here, $\rho_{i,j,k}$, molar concentration of pure components are obtained from ASPEN Plus and fitted to the polynomial expression given in Eq. B.14 as a function of temperature. These parameters are given below in physical parameters section. With these, extent of reaction terms become:

$$Cons_{i,j,r=Main} = 60 \times \exp\left(13.62 - \left(\frac{8220}{T_{i,j}}\right)\right) C_{i,j,k=EO} \times C_{i,j,k=W}, \quad i,j \in RxnB \tag{B.15}$$

$$Cons_{i,j,r=Side} = 60 \times \exp\left(15.57 - \left(\frac{8700}{T_{i,j}}\right)\right) C_{i,j,k=EO} \times C_{i,j,k=EG}, \quad i,j \in RxnB \tag{B.16}$$

Fresh raw materials fs can be introduced into any block included in set $FeedB$. As the feed streams are in liquid phase, these blocks also are in liquid phase. The feed availability and compositions are ensured via the following:

$$M_{i,j,k,fs} = F_{fs}^{feed} y_{k,fs}^{feed} z_{i,j,fs}^{feedfrac}, \quad i,j,fs \in FeedB; \tag{B.17}$$

$$\sum_{i,j,fs \in FeedB} z_{i,j,fs}^{feedfrac} \leq 1 \tag{B.18}$$

$$z_{i,j,fs}^{feedfrac} \leq 1, \quad i,j,fs \in FeedB \tag{B.19}$$

Here, $z_{i,j,fs}^{feedfrac}$ is a 0-1 continuous variable denoting what fraction of the total available feed stream is introduced into the block $B_{i,j}$.

Equations 3.111 denote the horizontal and vertical flow rates with respect to their directions. $F_{i,j,k}$ and $R_{i,j,k}$ denote the flow rate through a horizontal and vertical boundary, respectively. These terms are activated according to the sets $ActF$ and $ActR$. Each flow within the superstructure is allowed to flow in both directions. While HP and HN denote the active horizontal positive and negative flow components, respectively, VP and VN denote the vertical positive and negative flow components, respectively.

Equations 3.112-3.114 are for satisfying product purity and demand. Stream splitting through unrestricted boundaries, jump flows and product streams are satisfied through Eqns. 3.115-3.118. Here, total molar flow rates are used which are defined as follows:

$$FP_{i,j}^{T} = \sum_{k \in K} FP_{i,j,k}; \quad FN_{i,j}^{T} = \sum_{k \in K} FN_{i,j,k} \quad i,j \in ActF \tag{B.20}$$

$$RP_{i,j}^{T} = \sum_{k \in K} RP_{i,j,k}; \quad RN_{i,j}^{T} = \sum_{k \in K} RN_{i,j,k} \quad i,j \in ActR \tag{B.21}$$

$$J_{i,j,i',j'}^{T} = \sum_{k \in K} J_{i,j,i',j'k} \quad i,j,i',j' \in LN \tag{B.22}$$

$$P_{i,j,ps}^{p,total} = \sum_{k \in K} P_{i,j,k,ps} \quad i,j,ps \in ProdB \tag{B.23}$$

$$\sum_{k \in K} y_{i,j,k} = 1 \quad i,j \in AB \tag{B.24}$$

Equation 3.119 is to satisfy the thermodynamic equilibrium between the horizontal building block pairs when the block on the left is in liquid and the block on the right is in vapor phase. The position of these phases can be also reversed and also the orientation can be in vertical direction.

Here, we only consider horizontal direction and assign liquid phase to the block on the left. $VLPC$ set designates the blocks $B_{i,j}$ in which these phase calculations are valid. In this case study, we only consider vapor-liquid phase contact phenomena for the separation which does not require any enabling material, e.g. membrane, absorbent. Accordingly, $s = \{VL - PC\}$ and $m = \{null\}$. $Equil$ set designates an equilibrium-based separation phenomena and material. These sets might not be needed within the scope of the presented case study as we consider single type of phenomena, yet we include them for the consistency with the original model. Here, we assume ideal phase equilibrium. Then, following relations are written:

$$K^{eq}_{i,j,k,s,m} P_{i,j} = P^{sat}_{i,j,k} \quad i,j \in VLPC, k \in K, s,m \in Equil \tag{B.25}$$

$$P^{sat}_{i,j,k} = exp\left(A^{ant}_k - \frac{B^{ant}_k}{T_{i,j} + C^{ant}_k}\right) \quad i,j \in VLPC \cup LB^{check}, k \in K \tag{B.26}$$

Here, Eq. B.26 is to calculate the saturation pressure based on Antoine equation. Antoine parameters are obtained from ASPEN Plus and given in the next section. Note that although equilibrium calculations are performed for each block within the $VLPC$ set, Antoine equation is also valid for blocks where phase of the blocks are checked for feasible operation. For instance, condensers for the base case designs are assumed to be total condensers and phase of these blocks are ensured to be in liquid phase with Eqs. 3.120 Specifically, these constraints are written as follows:

$$P_{i,j} \geq \sum_{k \in K} y_{i,j,k} P^{sat}_{i,j,k} i,j \in LB^{check} \tag{B.27}$$

$$P_{i,j} \leq \frac{1}{\sum\limits_{k \in K} \frac{y_{i,j,k}}{P^{sat}_{i,j,k}}} \; i,j \in VB^{check} \tag{B.28}$$

while Eq. B.27 checks for bubble pressure, Eq. B.28 checks for dew pressure. Sets LB^{check} and VB^{check} designate the block positions where these equations are valid.

Equation 3.121 is to calculate the pump work required for increasing the pressure of a liquid stream for jump streams. We only allowed for liquid pressure increase through these jump streams

within this case study. Equations 3.122-3.123 describe the energy balances. While the former is used for single blocks, the latter is used for two block energy balances for the vapor-liquid phase contact block pairs. Enthalpy terms in these equations are implemented a described in Appendix A.2.2. These individual stream enthalpy terms are defined as follows as a function of temperature (based on ideal gas assumption):

$$EFP^{l}_{i,j,k} = FP_{i,j,k}\left(H^{a,liq}_{k} + H^{b,liq}_{k}T_{i,j}\right) \quad i,j \in HP^{liq}, k \in K \tag{B.29}$$

$$EFP^{g}_{i,j,k} = FP_{i,j,k}\left(H^{a,vap}_{k} + H^{b,vap}_{k}T_{i,j}\right) \quad i,j \in HP^{vap}, k \in K \tag{B.30}$$

$$EFN^{l}_{i,j,k} = FN_{i,j,k}\left(H^{a,liq}_{k} + H^{b,liq}_{k}T_{i,j+1}\right) \quad i,j \in HN^{liq}, k \in K \tag{B.31}$$

$$EFN^{g}_{i,j,k} = FN_{i,j,k}\left(H^{a,vap}_{k} + H^{b,vap}_{k}T_{i,j+1}\right) \quad i,j \in HN^{vap}, k \in K \tag{B.32}$$

$$ERP^{l}_{i,j,k} = RP_{i,j,k}\left(H^{a,liq}_{k} + H^{b,liq}_{k}T_{i,j}\right) \quad i,j \in VP^{liq}, k \in K \tag{B.33}$$

$$ERP^{g}_{i,j,k} = RP_{i,j,k}\left(H^{a,vap}_{k} + H^{b,vap}_{k}T_{i,j}\right) \quad i,j \in VP^{vap}, k \in K \tag{B.34}$$

$$ERN^{l}_{i,j,k} = RN_{i,j,k}\left(H^{a,liq}_{k} + H^{b,liq}_{k}T_{i+1,j}\right) \quad i,j \in VN^{liq}, k \in K \tag{B.35}$$

$$ERN^{g}_{i,j,k} = RN_{i,j,k}\left(H^{a,vap}_{k} + H^{b,vap}_{k}T_{i+1,j}\right) \quad i,j \in VN^{vap}, k \in K \tag{B.36}$$

Here, subsets are used to designate the position of the interblock streams for which these constraints active. For instance, HP^{liq} is to denote the active $FP_{i,j,k}$ streams for which the enthalpy is calculated based on Eq. B.29. Note that $HP^{liq} \subseteq HP$ which states that even a horizontal positive stream exists, enthalpy calculations might not be needed for this stream. This is allowed to simplify the model if a block is only used for material transfer with single inlet and outlet not requiring any energy balance calculations. Similar enthalpy relations are also written for the jump streams, external feed and product streams as below:

$$EJ^{l}_{i,j,i',j',k} = J_{i,j,i',j',k}\left(H^{a,liq}_{k} + H^{b,liq}_{k}T_{i,j}\right) \quad i,j,i',j' \in LN^{liq}, k \in K \tag{B.37}$$

$$EJ^{g}_{i,j,i',j',k} = J_{i,j,i',j',k}\left(H^{a,vap}_{k} + H^{b,vap}_{k}T_{i,j}\right) \quad i,j,i',j' \in LN^{vap}, k \in K \tag{B.38}$$

$$EM_{i,j} = \sum_{k\in K}\sum_{fs\in FS} M_{i,j,k,fs}\left(H^{a,liq}_{k} + H^{b,liq}_{k}T^{feed}_{fs}\right) \quad i,j \in FB \tag{B.39}$$

$$EP_{i,j} = \sum_{k\in K}\sum_{p\in PS} P_{i,j,k,ps}\left(H^{a,liq}_{k} + H^{b,liq}_{k}T_{i,j}\right) \quad i,j \in PB \tag{B.40}$$

By using these enthalpy terms, energy balance constraints Eq. 3.122 for the single block energy balance can be rewritten as follows:

$$\begin{aligned}
&\sum_{k\in K} EFP^{g}_{i,j-1,k} + \sum_{k\in K} EFP^{l}_{i,j-1,k} - \sum_{k\in K} EFN^{g}_{i,j-1,k} - \sum_{k\in K} EFN^{l}_{i,j-1,k} \\
&+ \sum_{k\in K} ERP^{g}_{i-1,j,k} + \sum_{k\in K} ERP^{l}_{i-1,j,k} - \sum_{k\in K} ERN^{g}_{i-1,j,k} - \sum_{k\in K} ERN^{l}_{i-1,j,k} \\
&- \sum_{k\in K} EFP^{g}_{i,j,k} - \sum_{k\in K} EFP^{l}_{i,j,k} + \sum_{k\in K} EFN^{g}_{i,j,k} + \sum_{k\in K} EFN^{l}_{i,j,k} \\
&- \sum_{k\in K} ERP^{g}_{i,j,k} - \sum_{k\in K} ERP^{l}_{i,j,k} + \sum_{k\in K} ERN^{g}_{i,j,k} \\
&+ \sum_{k\in K} ERN^{l}_{i,j,k} + \sum_{i',j'\in LN}\sum_{k\in K} EJ^{g}_{i',j',i,j,k} + \sum_{i',j'\in LN}\sum_{k\in K} EJ^{l}_{i',j',i,j,k} \\
&- \sum_{i',j'\in LN}\sum_{k\in K} EJ^{g}_{i,j,i',j',k} - \sum_{i',j'\in LN}\sum_{k\in K} EJ^{l}_{i,j,i',j',k} \\
&+ EM_{i,j} - EP_{i,j} + Q^{h}_{i,j} - Q^{c}_{i,j} = 0, \quad i,j \in SB
\end{aligned} \tag{B.41}$$

Similarly, two block energy balance equation Eq. 3.123 can be rewritten as follows:

$$\begin{aligned}
&\sum_{k\in K} EFP^{g}_{i,j-1,k} + \sum_{k\in K} EFP^{l}_{i,j-1,k} - \sum_{k\in K} EFN^{g}_{i,j-1,k} - \sum_{k\in K} EFN^{l}_{i,j-1,k} \\
&+ \sum_{k\in K} ERP^{g}_{i-1,j,k} + \sum_{k\in K} ERP^{l}_{i-1,j,k} - \sum_{k\in K} ERN^{g}_{i-1,j,k} - \sum_{k\in K} ERN^{l}_{i-1,j,k} \\
&- \sum_{k\in K} EFP^{g}_{i,j+1,k} - \sum_{k\in K} EFP^{l}_{i,j+1,k} + \sum_{k\in K} EFN^{g}_{i,j+1,k} + \sum_{k\in K} EFN^{l}_{i,j+1,k} \\
&- \sum_{k\in K} ERP^{g}_{i,j,k} - \sum_{k\in K} ERP^{l}_{i,j,k} + \sum_{k\in K} ERN^{g}_{i,j,k} + \sum_{k\in K} ERN^{l}_{i,j,k} \\
&- \sum_{k\in K} ERP^{g}_{i,j+1,k} - \sum_{k\in K} ERP^{l}_{i,j+1,k} + \sum_{k\in K} ERN^{g}_{i,j+1,k} + \sum_{k\in K} ERN^{l}_{i,j+1,k}
\end{aligned}$$

$$
\begin{aligned}
&+ \sum_{k\in K} ERP^{g}_{i-1,j+1,k} + \sum_{k\in K} ERP^{l}_{i-1,j+1,k} - \sum_{k\in K} ERN^{g}_{i-1,j+1,k} - \sum_{k\in K} ERN^{l}_{i-1,j+1,k} \\
&+ \sum_{i',j'\in LN} \sum_{k\in K} EJ^{g}_{i',j',i,j,k} + \sum_{i',j'\in LN} \sum_{k\in K} EJ^{l}_{i',j',i,j,k} - \sum_{i',j'\in LN} \sum_{k\in K} EJ^{g}_{i,j,i',j',k} \\
&- \sum_{i',j'\in LN} \sum_{k\in K} EJ^{l}_{i,j,i',j',k} + \sum_{i',j'\in LN} \sum_{k\in K} EJ^{g}_{i',j',i,j+1,k} + \sum_{i',j'\in LN} \sum_{k\in K} EJ^{l}_{i',j',i,j+1,k} \\
&- \sum_{i',j'\in LN} \sum_{k\in K} EJ^{g}_{i,j+1,i',j',k} - \sum_{i',j'\in LN} \sum_{k\in K} EJ^{l}_{i,j+1,i',j',k} + EM_{i,j} - EP_{i,j} + EM_{i,j+1} \\
&- EP_{i,j+1} + Q^{hF}_{i,j} - Q^{cF}_{i,j} = 0, \quad i,j \in TB
\end{aligned}
\tag{B.42}
$$

Here, $Q^{hF}_{i,j}$ $Q^{cF}_{i,j}$ are the heat duty variables for the two neighboring blocks. As mentioned earlier, a block can belong to either SB or TB set. Hence, when a block belongs to TB, single block heat duty variables are not utilized and fixed to be zero.

Some variables although appear in material and energy balances, may not be necessary. These variables are also fixed to be zero. For instance, if an interblock horizontal stream flows in positive direction, i.e. $FP_{i,j,k}$ is active, and belongs to HP set, then the negative counterpart is fixed to be zero, i.e. $FN_{i,j,k} = 0$. Similarly, all the associated energy balance variables are taken as zero. Similarly, for the reaction variables, we write the following:

$$G_{i,j,k} = 0, \quad i,j \notin RxnB, k \in K \tag{B.43}$$

$$Cons_{i,j,r} = 0, \quad i,j \notin RxnB, r \in Rxn \tag{B.44}$$

$$React_{i,j,k,r} = 0,\ i,j \notin RxnB, \gamma_{r,k} = 0, k \in K \tag{B.45}$$

These result in significant reduction in the model size.

B.2.1 Physical Parameters

Density parameters are obtained through regression on the data taken from ASPEN Plus. Vapor pressure is calculated based on Antoine equation with the parameters obtained from Aspen Plus. Temperature dependence of specific enthalpy for each species is obtained through ASPEN Plus and fitted to a linear function (Table B.3).

Table B.1: Molar concentration parameters.

	ρ_k^{d1} $[\frac{kmol}{m^3}]$	ρ_k^{d2} $[\frac{kmol}{m^3 K}]$	ρ_k^{d3} $[\frac{kmol}{m^3 K^2}]$
W	75.22	-0.06505	0
EO	1.655	0.1263	-0.0002286
EG	23.66	-0.01804	0
DEG	13.59	-0.009986	0

Table B.2: Antoine equation parameters.

	A_k^{ant}	B_k^{ant}	C_k^{ant}
EO	10.884	3152	7.667
W	11.680	3828	-45.412
EG	11.963	4764	-72.275
DEG	11.256	4655	-103.551

B.2.2 Capital Cost Functions

In Eqs. 3.129-3.138, objective function for a reactive separation column is provided. Here, we describe a more general form that we have used in implementing all the optimization problems. First we provide the general form of the objective functions as obtained from the literature. For all equipment, material of construction is selected as stainless steel as in a typical ethylene glycol plant[185]. Also, these costs take into account the pressure correction factors given in Douglass[57] for the maximum allowed pressure within the process (i.e. 36 atm).

Cost of heat exchangers are calculated based on heat exchange area [57]:

$$Cost^{HEX}(\$) = \frac{M\&S}{280} 101.3 A[ft^2]^{0.65}(2.29 + F_m(F_d + F_p)) \tag{B.46}$$

F_m, F_d and F_p are taken as 3.75, 1 and 0.39, respectively. PFR cost is approximated as a multitubular heat exchanger with 1-in diameter tubes which provide fully developed turbulent flow through the reactor[185]. Hence, this cost function is also used as a basis for the PFR. Reactive

Table B.3: Enthalpy parameters.

	$H_k^{a,vap}$	$H_k^{b,vap}$	$H_k^{a,liq}$	$H_k^{b,liq}$
EO	-74.6	0.0697	-143.8	0.2037
W	-252.3	0.0348	-320.0	0.1068
EG	-424.3	0.1030	-519.0	0.1924
DEG	-603.4	0.1823	-723.0	0.3043

and non-reactive distillation column shell cost functions are taken as[57]:

$$Cost^{Column}(\$) = \frac{M\&S}{280} 101.9 D[ft]^{1.066} H[ft]^{0.802} (2.18 + (F_m F_p)) \tag{B.47}$$

F_m and F_p are taken as 2.25 and 1.60, respectively. Column tray costs are given as[57]:

$$Cost^{trays}(\$) = \frac{M\&S}{280} 4.7 D[ft]^{1.55} H[ft](F_s + F_t + F_m) \tag{B.48}$$

F_s,F_t and F_m are taken as 1, 0 and 1.7, respectively. Pump costs are taken from Espatolero et al.[191]:

$$Cost^{pump} = C_B (W(kW)/4)^{0.55} f_M f_P f_T f_{M\&S} \tag{B.49}$$

C_B, f_M, f_P, f_T and $f_{M\&S}$ are taken as 9840, 1.0, 1.5, 1.0 and 1.261, respectively.

B.2.3 Objective Functions

Here, we provide the more detailed version of the objective functions with the variables and constraints introduced above. Economic objective for maximizing ROI is implemented as follows:

$$\text{max} \quad ROI \times ICC \times \alpha^{TCI} = ANP \tag{B.50}$$

Here ROI is the return on investment, ICC is the installed capital cost, ANP is the annual net (after-tax) profit and α^{TCI} is the total capital investment cost multiplier to obtain the total investment cost as a function of ICC. ICC is the summation of all capital investment required for the individual pieces of equipment. All cost functions are calculated as given above by assuming an

M&S index of 1431.7[190] and multipliers are modified for the flow rate, energy or volume units we used in the model.

$$
\begin{aligned}
ICC = & \sum_{e \in E^{Dist}} 64.89 (HE_e)(D_e)^{1.55} + \sum_{e \in E^{Dist}} 3011.6 (HE_e)^{0.802} (D_e)^{1.066} \\
& + 18612 \sum_{i,j,i',j' \in LN^{pump}} (J^{pump}_{i,j,i',j'}/4)^{0.55} + 488043 \sum_{e \in E^{PFR}} (V^{PFR}_e)^{0.65} \\
& + 18208 \sum_{i,j \in Reb/Reb^{hex}} \left[\frac{Q^{h2}_{i,j}}{U^{reb} \left(T^{HU} - T_{i,j} \right)} \right]^{0.65} \\
& + 18208 \sum_{i,j \in Cond/Cond^{hex}} \left[\frac{Q^{c}_{i,j}}{U^{cond} \left(\frac{\Delta T^{in,cond}_{i,j} + \Delta T^{out,cond}_{i,j}}{2} \right)} \right]^{0.65} \\
& + 18208 \sum_{i,j \in Reb^{hex}} \left[\frac{Q^{h3}_{i,j}}{U^{reb} \left(T^{HU} - T_{i,j} \right)} \right]^{0.65} \\
& + 18208 \sum_{i,j \in Cond^{hex}} \left[\frac{Q^{c3}_{i,j}}{U^{cond} \left(\frac{\Delta T^{in,cond}_{i,j} + \Delta T^{out,cond}_{i,j}}{2} \right)} \right]^{0.65} \\
& + 18208 \sum_{i,j \in BCool} \left[\frac{Q^{c}_{i,j}}{U^{BCool} \left(\frac{\Delta T^{in,cool}_{i,j} + \Delta T^{out,cool}_{i,j}}{2} \right)} \right]^{0.65} \\
& + 18208 \sum_{i,j \in BHeat} \left[\frac{Q^{h}_{i,j}}{U^{BHeat} \left(\frac{\Delta T^{in,heat}_{i,j} + \Delta T^{out,heat}_{i,j}}{2} \right)} \right]^{0.65} \\
& + 18208 \sum_{i,j,i',j' \in hex} \left[\frac{q^{hex}_{i,j,i',j'}}{U^{hex} dt^{hex}_{i,j,i',j'}} \right]^{0.65}
\end{aligned}
\tag{B.51}
$$

Here, the first and second terms are the installed capital costs (ICC) for the distillation column trays and the column shell, respectively. HE_e and D_e are the total height and diameter of the columns e, respectively, in ft. These are calculated based on Eqs. 3.135-137 as a function of the vapor flow rate, temperature, pressure and reaction volume of the individual blocks that these equipment are comprised of indicated by the set EqR.

The third term is the ICC for the pumps located on the jump streams and $J^{pump}_{i,j,i',j'}$ is the work needed in kW. The work term is calculated as follows:

$$J^{pump}_{i,j,i',j'} = \frac{10^5 \times \left(\sum_k J_{i,j,i',j',k} MW_k\right)(P_{i',j'} - P_{i,j})}{\rho^{mix}_{i,j} \times 1000 \times 3600 \times \eta^{pump} \times \eta^{motor}}, \quad i,j,i',j' \in LN^{pump} \tag{B.52}$$

Here, MW_k is the molecular weight of component k, $\rho^{mix}_{i,j}$ is the liquid density which is assumed to be 1000 kg/m^3, pressure terms are in atm, η^{pump} and η^{motor} are the pump and motor efficiencies which are taken as 0.5 and 0.9, respectively.

The forth term is the ICC for the PFR as a function of the PFR volume. Volume of the PFR unit is calculated as the summation of the individual volumes of the building blocks that represent the reactor:

$$V^{PFR}_e = \sum_{i,j \in EqR} V_{i,j}, \quad e \in E^{PFR} \tag{B.53}$$

$$V_{i,j} = V_{i',j'} \quad e \in E^{PFR}, i,j, \in EqR, i',j' \in EqR \tag{B.54}$$

$$P_{i,j} = P_{i',j'} \quad e \in E^{PFR}, i,j, \in EqR, i',j' \in EqR \tag{B.55}$$

Here, the second and third equations state that the volumes and pressures of the blocks belonging to the same PFR unit should be the same.

The fifth to eleventh terms in Eq. B.51 are for the ICC of the reboilers, condensers, block heaters, block coolers and heat exchangers. All heat duty terms are in MJ/h. The overall heat transfer coefficients U^{BHeat} and U^{reb} are taken as 5.11 MJ/h/m^2/K. U^{cond}, U^{BCool} and U^{hex} are taken as 8.176 MJ/h/m^2/K. Specifically, the fifth and sixth terms are for the reboiler and condenser blocks that are not allowed to exchange heat with the other blocks, respectively. Here, T^{HU} is the hot utility temperature, i.e. 527.2 K. For the condensers, temperature driving force is assumed to be the linear average between the inlet and outlet temperature differences. These terms are calculated as follows:

$$\Delta T^{in,cond}_{i,j} = T_{i,j} - T^{CU,in}, \quad i,j \in Cond \tag{B.56}$$

$$\Delta T_{i,j}^{out,cond} = T_{i,j} - T^{CU,out}, \quad i,j \in Cond \tag{B.57}$$

$T^{CU,in}$ and $T^{CU,out}$ are the inlet and outlet temperatures for the cooling water and taken as 305.2 and 325.2 K, respectively.

The seventh and eighth terms are the ICC for the reboilers and condensers for the residual heat required, if any, after heat integration, respectively. The ninth and tenth terms are for the block coolers and heaters, respectively. Temperature difference terms are calculated as follows:

$$\Delta T_{i,j}^{in,cool} = T_{i,j} - T^{CU,in}, \quad i,j \in Bcool \tag{B.58}$$

$$\Delta T_{i,j}^{out,cool} = T_{i',j'} - T^{CU,out}, \quad i,j,i',j' \in Bcoolmatch \tag{B.59}$$

$$\Delta T_{i,j}^{in,heat} = T^{HU} - T_{i,j}, \quad i,j \in Bheat \tag{B.60}$$

$$\Delta T_{i,j}^{out,heat} = T^{HU} - T_{i',j'}, \quad i,j,i',j' \in Bheatmatch \tag{B.61}$$

Here, $Bcool$ and $Bheat$ sets designate the block positions $B_{i,j}$ where coolers and heaters are positioned, respectively. The block temperatures, i.e. $T_{i,j}$, where these heaters/coolers are located correspond to the outlet temperatures of these units. We do not introduce any inlet temperature term for these blocks, instead we designate the inlet temperatures by specifying the source blocks for the incoming streams. These are denoted by sets $Bcoolmatch$ and $Bheatmatch$ for the coolers and heaters, respectively. These sets denote the position of the source block $B_{i',j'}$ that we use as the inlet temperature for the block heaters/coolers positioned in block $B_{i,j}$. The final term is the ICC for the heat exchangers.

Annual net (after-tax) profit, ANP, can be described as:

$$ANP = (Income - (AOC + Maintenance + Depreciation)) \times (1 - \theta) + Depreciation$$

where AOC describes the annual operating cost. Accordingly, we calculate ANP as shown below:

$$
\begin{aligned}
ANP = \Bigg\{ & n^{op} \times \left(\sum_{i,j,k,ps \in ProdB} SP_{k,p} P_{i,j,k,p} \right) - n^{op} \times \left(\sum_{i,j,k,f \in FB} UF_f M_{i,j,k,f} \right) \\
& - n^{op} \times UF^{hot} \left(\sum_{i,j \in Reb/Reb^{hex}} Q^{h2}_{i,j} + \sum_{i,j \in Reb^{hex}} Q^{h3}_{i,j} + \sum_{i,j \in BHeat} Q^{h}_{i,j} \right) \\
& - n^{op} \times UF^{cold} \left(\sum_{i,j \in Cond/Cond^{hex}} Q^{c}_{i,j} + \sum_{i,j \in Cond^{hex}} Q^{c3}_{i,j} + \sum_{i,j \in BCool} Q^{c}_{i,j} \right) \\
& - n^{op} \times UF^{El} \left(\sum_{i,j,i',j' \in LN} J^{pump}_{i,j,i',j'} \times 3600 \right) \\
& - \left(\alpha^{Maint} \times ICC \times \alpha^{FCI} \right) - \left(\alpha^{Dep} \times ICC \times \alpha^{FCI} \right) \Bigg\} \Big\{ 1 - \theta \Big\} + \Big\{ \alpha^{Dep} \times ICC \times \alpha^{FCI} \Big\}
\end{aligned}
\tag{B.62}
$$

n^{op} is the operating time and taken as 8000 hours. The first term is the revenue from the product streams. The second term is the cost of the raw materials. The third and forth terms describe the hot and cold utility costs, respectively. UF^{hot} is taken as 0.009906 \$/MJ. UF^{cold} is taken as 0.000324 \$/MJ. The fifth term is the total cost of electricity consumption and UF^{El} is taken as 1.94×10^{-7} \$/kJ. The sixth term describes the yearly maintenance cost as a function of fixed capital investment cost. α^{FCI} is the fixed capital investment cost multiplier to obtain the total investment cost as a function of ICC. α^{FCI} is taken as 1.924. Maintenance cost is assumed as 7.5% of the fixed capital investment, i.e. $\alpha^{Maint} = 0.075$. The seventh term is the depreciation cost and 10 year linear depreciation scheme is adopted. Hence, $\alpha^{Dep} = 0.10$. Seventh term includes the tax rate for which the rate is assumed to be 40%, i.e. $\theta = 0.40$.

B.2.4 Cost Breakdown of the Optimal Solutions

Here, a detailed cost breakdown for the optimal base-case flowsheets as well as the generated designs are provided. Note that results correspond to the ultimate optimal solutions obtained considering larger superstructures.

Table B.4: Cost breakdown for the base case designs for ethylene glycol production.

Flowsheet	F1	F1	F2	F2
Objective	max ROI	min CO_2	max ROI	min CO_2
Stage	7	10	19	44
Height (m)	7.3	9.1	21.6	48.3
Diameter (m)	1.9	2.2	2.6	2.8
Rxn Volume (m^3)	0.3	30	37.7	110.9
Costs				
Shell Cost ($1000)	269	376	909	1835
Tray Cost ($1000)	26.2	41.2	129	313
Reboiler ($1000)	335	261	731	508
Condenser ($1000)	257	261	277	691
Reactor ($1000)	243	4452	-	-
Heater ($1000)	94	0	-	-
Pump ($1000)	42.6	8.6	-	-
Total Installed Capital ($1000)	1267	5400	2046	3347
Hot Utility ($1000/year)	2165	1620	1971	1755
Cold Utility ($1000/year)	75	58	69	62
Fresh EO ($1000/year)	6473	6474	6472	6474
Fresh W ($1000/year)	0.42	0.42	0.42	0.42
Electricity ($1000/year)	10	0.6	-	-
Op. Cost ($1000/year)	8724	8153	8512	8291
Emissions				
Steam (kt CO_2/year)	21.14	15.81	19.24	17.13
EO (kt CO_2/year)	36.02	36.02	36.01	36.03
Electricity (kt CO_2/year)	0.08	0.004	-	-
Total (kt CO_2/year)	57.23	51.84	55.25	53.15
Economics				
Total Annualized Cost ($1000/year)	9150	9971	9201	9418
Annual Economic Prof. ($1000/year)	1493	1796	1612	1732
Total Capital Investment ($1000)	2868	12223	4631	7576
ROI(%/year)	52	14.7	34.8	22.9

Table B.5: Cost breakdown for the generated designs for ethylene glycol production.

Flowsheet	F3	F4	F4	F5	F5
Objective	max ROI	max ROI	min CO_2	max ROI	min CO_2
Stage RD	25	18	30	23	30
Stage DC	-	6	12	7	12
Height RD (m)	24.9	16.6	24.7	20.0	34.1
Height DC (m)	-	5.5	9.1	6.1	9.1
Diameter RD (m)	1.8	0.6	2.8	0.8	2.8
Diameter DC (m)	-	2.0	2.5	1.7	2.2
Reaction Volume (m^3)	19.8	0.9	27.3	2.0	84.0
Costs					
Shell Cost RD ($1000)	681	142	1069	233	1387
Shell Cost DC ($1000)	-	225	432	204	371
Tray Cost RD ($1000)	83	9	160	18	221
Tray Cost DC ($1000)	-	21	50	18	40
Condenser RD ($1000)	251	0	0	0	0
Condenser DC ($1000)	-	252	647	232	467
Reboiler RD ($1000)	445	258	130	262	129
Reboiler DC ($1000)	-	94	297	0	0
HEX ($1000)	-	-	-	193	1852
Pump ($1000)	-	26	38	24	10
Total Ins. Cap. ($1000)	1459	1027	2823	1183	4478
Hot Utility ($1000/year)	2063	1789	1536	1045	867
Cold Utility ($1000/year)	71	63	56	39	34
Fresh EO ($1000/year)	6461	6465	6475	6467	6475
Fresh W ($1000/year)	0.42	0.42	0.42	0.67	0.42
Electricity ($1000/year)	-	4.0	8.3	3.5	0.7
Op. Cost ($1000/year)	8595	8322	8074	7556	7377
Emissions					
Steam (kt CO_2/year)	20.13	17.47	14.99	10.20	8.46
EO (kt CO_2/year)	35.95	35.98	36.03	35.99	36.03
Electricity (kt CO_2/year)	0	0.03	0.07	0.03	0.01
Total (kt CO_2/year)	56.09	53.47	51.08	46.22	44.50
Economics					
Total Annual. Cost ($1000/year)	9086	8668	9025	7954	8884
Annual Ec. Prof. ($1000/year)	1568	1736	1867	2194	2270
Total Cap. Inv. ($1000)	3303	2325	6390	2678	10135
ROI(%/year)	47.5	74.7	29.2	81.9	22.4